

2012

Geochemistry and Origin of Diagenetic Fluids and Paleohydrology of Paleozoic Carbonates in Southwestern Ontario, Canada

Omid Haeri-Ardakani

Follow this and additional works at: <http://scholar.uwindsor.ca/etd>

Recommended Citation

Haeri-Ardakani, Omid, "Geochemistry and Origin of Diagenetic Fluids and Paleohydrology of Paleozoic Carbonates in Southwestern Ontario, Canada" (2012). *Electronic Theses and Dissertations*. Paper 4811.

This online database contains the full-text of PhD dissertations and Masters' theses of University of Windsor students from 1954 forward. These documents are made available for personal study and research purposes only, in accordance with the Canadian Copyright Act and the Creative Commons license—CC BY-NC-ND (Attribution, Non-Commercial, No Derivative Works). Under this license, works must always be attributed to the copyright holder (original author), cannot be used for any commercial purposes, and may not be altered. Any other use would require the permission of the copyright holder. Students may inquire about withdrawing their dissertation and/or thesis from this database. For additional inquiries, please contact the repository administrator via email (scholarship@uwindsor.ca) or by telephone at 519-253-3000ext. 3208.

**Geochemistry and Origin of Diagenetic Fluids and
Paleohydrology of Paleozoic Carbonates in
Southwestern Ontario, Canada**

by

Omid Haeri-Ardakani

A Dissertation
Submitted to the Faculty of Graduate Studies
through the Department of Earth and Environmental Sciences
in Partial Fulfillment of the Requirements for
the Degree of Doctor of Philosophy at the
University of Windsor

Windsor, Ontario, Canada
2012
© 2012 Omid Haeri-Ardakani

Geochemistry and Origin of Diagenetic Fluids and Paleohydrology of Paleozoic
Carbonates in Southwestern Ontario, Canada

by

Omid Haeri-Ardakani

APPROVED BY:

K. Azmy, External Examiner
Memorial University

K. Drouillard
Department of Biological Sciences/GLIER

M. Cioppa
Department of Earth and Environmental Sciences

J. Gagnon
Department of Earth and Environmental Sciences

I. Al-Aasm, Advisor
Department of Earth and Environmental Sciences

M. Coniglio, Co-advisor
Department of Earth and Environmental Sciences
University of Waterloo

K. Gorey, Chair of Defense
School of Social Work

31 July 2012

Declaration of Co-Authorship/previous publication

I. Co-Authorship Declaration

This thesis incorporates material that is the result of field work and laboratory analysis. Field work, laboratory analysis, data interpretation, key ideas and manuscript preparation were the responsibility of the first author. I certify that this thesis is the product of my own work but owe much to the scientific guidance, and precise editing of Dr. Ihsan Al-Aasm and Dr. Mario Coniglio, who are co-authors of the associated manuscripts. They provided me with valuable comments that led to the development of this thesis.

II. Declaration of previous publications

This thesis includes 3 original papers that have been submitted and/or are in preparation for publication in international peer-reviewed journals. The percentages given by the authors' names represent their relative scientific contribution.

Manuscript 1 (Chapter 2)

Haeri-Ardakani, O., (70%), Al-Aasm, I.S., (10%), Coniglio, M., (10%), Samson, I., (10%) 2012, Diagenetic evolution and associated mineralization of the Middle Devonian carbonates, southwestern Ontario, Canada, submitted to Bulletin of Canadian Petroleum Geology. All co-authors provided insightful criticism on early versions of this manuscript. This project was possible through Natural Science and Engineering Research Council of Canada (NSERC) grants to I.S. Al-Aasm and M. Coniglio.

Manuscript 2 (Chapter 3)

Haeri-Ardakani, O., (70%), Al-Aasm, I.S., (15%), Coniglio, M., (15%), 2012, Petrologic and geochemical attributes of fracture-related dolomitization in Ordovician carbonates and their spatial distribution in southwestern Ontario, Canada, submitted to the Journal of Marine and Petroleum Geology. Funding for this project was provided by Natural Science and Engineering Research Council of Canada (NSERC) grants to I.S. Al-Aasm and M. Coniglio.

Manuscript 3 (Chapter 4)

Haeri-Ardakani, O. (70%), Al-Aasm, I.S. (15%), Coniglio, M. (15%), 2012, Fracture mineralization and fluid flow evolution: An example From Ordovician-Devonian carbonates, southwestern Ontario, Canada (in preparation). All co-authors provided insightful criticism on early versions of this manuscript. This project was possible through a funding provided by Natural Science and Engineering Research Council of Canada (NSERC) grants to I.S. Al-Aasm and M. Coniglio.

Abstract

This study presents integrated petrography, stable carbon and oxygen isotopes, strontium isotopes and rare earth elements (REE) geochemistry as well as fluid inclusion microthermometry of diagenetic minerals from the Paleozoic carbonates succession of southwestern Ontario, Canada. These data provide new insights into the nature of fluids affecting these rocks and their spatial and temporal relationships. Fractures in the Paleozoic succession had an important role in reservoir enhancement, channelling of diagenetic fluids and migration of hydrocarbons.

The spatial patterns, extent of dolomitization and dolomite petrography indicate that different hydrologic systems were responsible for dolomitization in each of the stratigraphic intervals considered. Fine-crystalline Devonian and Silurian dolomite formed in early stages of diagenesis whereas coarse-crystalline fracture-related Ordovician dolomite formed in later stages of diagenesis in burial environment and in the presence of hydrothermal fluids.

The distinct $\delta^{18}\text{O}_{\text{fluid}}$, $\delta^{13}\text{C}$, ΣREE values, and REE_{SN} patterns of dolomite from each age interval suggest compartmentalization of diagenetic fluids. The $\delta^{18}\text{O}_{\text{fluid}}$ and $^{87}\text{Sr}/^{86}\text{Sr}$ ratios indicate diagenetic fluids in each strata originated from coeval seawater and evolved through water/rock interaction. The more positive $\delta^{18}\text{O}_{\text{fluid}}$ calculated from dolomite $\delta^{18}\text{O}$ values and the high salinity of Ordovician and Silurian brines and less radiogenic $^{87}\text{Sr}/^{86}\text{Sr}$ ratios of Ordovician dolomite relative to those of coeval seawater indicate mixing of Ordovician and Silurian connate waters with ^{18}O -enriched fluids influenced by dissolution of Silurian evaporites.

The significantly higher dolomite T_h values (75 to 120°C) from Devonian to Ordovician units relative to inferred maximum burial temperature (60 to 90°C) of these strata suggest involvement of hydrothermal fluids in the precipitation and/or recrystallization of dolomite. The presence of hydrocarbon-bearing fluid inclusions with high T_h values (>80°C) in late-stage calcite cements from Devonian to Ordovician and their negative $\delta^{13}\text{C}$ values (approaching -32‰ VPDB) implies that hydrothermal diagenetic fluids carried hydrocarbons.

A thermal anomaly along the mid-continent rift during Devonian to Mississippian (Alleghanian orogeny) time likely was the source of excess heat in the Michigan Basin. The potential thermal buoyancy of hot brines was the driving force for migration of hydrothermal fluids from the center of the basin towards its margin through regional aquifers and network of fractures.

Acknowledgements

I would like to express my gratitude to my thesis advisors, Dr. Ihsan Al-Aasm and Dr. Mario Coniglio, for their funding and guidance through the course of this study. This project was funded through a contribution of individual Natural Science and Engineering Research Council of Canada (NSERC) grants to I.S. Al-Aasm and Mario Coniglio.

I am grateful to Dr. I. Samson and Dr. M. Cioppa who always generously provided me with their valuable scientific advice. I am indebted to Dr. Fereydoun Ghazban, my mentor and M.Sc. supervisor, who always encouraged and supported me with his valuable advice.

This study was not possible without assistance of Ontario Oil, Gas and Salt Resources Library staff. I would like to express my gratitude to Mr. Richard Ostrowski for his cooperation in core sampling. I am also appreciative of the assistance provided by Melissa Price for stable isotope analysis and other lab work. My special thanks to all the faculty and staff members in the Department of Earth and Environmental Sciences for their academic and administrative support during the last 5 years.

My acknowledgements would not be complete without expressing my gratitude to my family, especially my wife. I would not have been able to finish this without her encouragement and cooperation. Last but not least I would like to thank my parents for all their love and support.

Table of Contents

Declaration of Co-Authorship/previous publication	iii
Abstract	v
Acknowledgments	vii
List of Tables	xii
List of Figures	xiii
List of Appendices	xvi
Chapter 1	1
1.1 Introduction	1
1.2 Thesis objectives	4
1.3 Outline of thesis structure	6
1.4 Geologic setting	7
1.4.1 Ordovician carbonates (Trenton Group)	9
1.4.2 Silurian carbonates (Guelph Formation)	10
1.4.3 Devonian carbonates (Lucas Formation)	11
1.5 Tectonic setting	12
1.6 References	13
Chapter 2	25
Diagenetic evolution and associated mineralization in Middle Devonian carbonates, southwestern Ontario, Canada	25
2.1 Introduction	25
2.2 Geologic setting	26
2.3 Burial history	28

2.4	Materials and methods	29
2.5	Results	30
	2.5.1 Mineralization	30
	2.5.2 Petrography	31
	2.5.3 Geochemistry	32
	2.5.4 Fluid inclusions	34
2.6	Discussion	35
	2.6.1 Dolomite texture	35
	2.6.2 Implication of geochemical data	37
	2.6.3 Rare earth elements (REE)	44
2.7	Conclusions	45
2.8	Acknowledgements	46
2.9	References	47
	Chapter 3	75
	Petrologic and geochemical attributes of fracture-related dolomitization in Ordovician carbonates and their spatial distribution in southwestern Ontario, Canada	75
3.1	Introduction	75
3.2	Geologic setting	76
	3.2.1 Faults and fractures	77
3.3	Material and methods	78
3.4	Results	80
	3.4.1 Petrography	80
	3.4.2 Geochemistry	82
	3.4.3 Fluid inclusions	84
3.5	Discussion	85
	3.5.1 Oxygen isotope geochemistry and microthermometry	85
	3.5.2 Strontium isotopes	90
	3.5.3 Rare earth elements (REE)	92
	3.5.4 Fluid flow mechanism	94

3.6	Conclusions	98
3.7	Acknowledgements	100
3.8	References	100
Chapter 4		131
Fracture mineralization and fluid flow evolution: An example from Ordovician-Devonian carbonates, southwestern Ontario, Canada		131
4.1	Introduction	131
4.2	Geologic setting	132
4.2.1	Ordovician carbonates (Black River and Trenton Groups)	133
4.2.2	Silurian carbonates (Guelph Formation)	133
4.2.3	Devonian carbonates (Lucas Formation)	134
4.3	Tectonic setting	135
4.4	Materials and methods	135
4.5	Results	137
4.5.1	Petrography	137
4.5.2	Geochemistry	139
4.5.3	Fluid inclusions	141
4.6	Discussion	144
4.6.1	Dolomitization models	144
4.6.2	Oxygen and carbon isotope geochemistry	146
4.6.3	Strontium isotopes	152
4.6.4	Rare earth elements (REE)	156
4.6.5	Fluid flow model	159
4.6.6	Timing of hydrothermal event	163
4.7	Conclusions	164
4.8	Acknowledgements	166
4.9	References	166
Chapter 5		201
Conclusions of research		201
5.1	Nature of paleohydrologic system(s)	202

5.2	Connection of the diagenetic systems	202
5.3	Source of heat and driving force of hydrothermal fluids	204
5.4	Recommendations for future studies	205
	Appendices	207
	Appendix 1	207
	Appendix 2	214
	Appendix 3	217
	Vita Auctoris	225

List of Tables

Table 2.1 Carbon and oxygen isotopic composition of replacive dolomite and fracture-filling calcite and the calcitic components of the Lucas Formation.....	71
Table 2.2 Summary statistics of rare earth elements (REE) results of selected mineral of the Lucas Formation.....	73
Table 2.3 Summary statistics of fluid inclusion microthermometry results of selected minerals of the Lucas Formation.....	74
Table 3.1 Carbon and oxygen isotopic composition of the dolomite and fracture-filling calcite of the Sherman Fall Formation.	125
Table 3.2 Summary statistics of rare earth elements (REE) of selected minerals and undolomitized host rock of the Sherman Fall Formation.....	129
Table 3.3 Summary statistics of fluid inclusion microthermometry results of selected minerals of the Sherman Fall Formation.	130
Table 4.1 Summary statistics of oxygen, carbon and strontium isotope results of dolomite and late-stage calcite from the Paleozoic succession of southwestern Ontario. ..	195
Table 4.2 Summary statistics of rare earth elements concentration of Devonian, Silurian, and Ordovician different diagenetic phases	197
Table 4.3 Summary statistics of fluid inclusion microthermometry results of selected minerals from Devonian to Ordovician.....	199
Table 4.4 Average T_h and salinity of calcite, dolomite and quartz hosted fluid inclusions of Devonian to Ordovician rocks in the center of the Michigan Basin and its margin.	200
Table 4.5 Σ REE of selected minerals from Devonian to Ordovician and $\delta^{18}O_{\text{fluid}}$, and salinity of fluids responsible for their precipitation	200

List of Figures

Figure 1.1 Generalized basement structural contours and location of structural arches and basins	19
Figure 1.2 Depositional cycles and tectonic elements of the Michigan and Appalachian sedimentary basins.	20
Figure 1.3 Cross section of Paleozoic sedimentary succession of southwestern Ontario and adjacent sedimentary basins.	21
Figure 1.4 Generalized Paleozoic stratigraphic column for southern Ontario.	22
Figure 1.5 Paleozoic tectonic cycles of Appalachian orogeny.	23
Figure 1.6 Conceptual fracture framework and mapped faults of southern Ontario.	24
Figure 2.1 Generalized Paleozoic bedrock geology map of southern Ontario.	56
Figure 2.2 Middle Devonian stratigraphy of southwestern Ontario.	57
Figure 2.3 Core photographs of Middle Devonian rocks, southwestern Ontario.	58
Figure 2.4 Burial history curve for the southern Michigan Basin	59
Figure 2.5 Sampling location map.	60
Figure 2.6 Cavities in host rock dolomite filled with different type of minerals.	61
Figure 2.7 Paragenetic sequence of the Lucas Formation in southwestern Ontario	62
Figure 2.8 Photomicrographs of Middle Devonian rocks	63
Figure 2.9 Cross plot of stable oxygen and carbon isotopic values for the Lucas Formation, southwestern Ontario	65
Figure 2.10 $^{87}\text{Sr}/^{86}\text{Sr}$ ratio vs. $\delta^{18}\text{O}$ values of fine crystalline dolomite and fracture-filling calcite	66
Figure 2.11 PAAS normalized REE pattern for average values of fine (D1) and medium (D2) crystalline dolomite and fracture-filling calcite (LC) samples	67
Figure 2.12 Ce (Ce/Ce^*) _{SN} -La (Pr/Pr^*) _{SN} anomaly cross plot of D1, D2 and fracture-filling calcite (LC) samples.	68
Figure 2.13 Photomicrograph of fluid inclusions in calcite and celestine	69
Figure 2.14 Homogenization temperatures and salinities of primary fluid inclusions in fracture-filling calcite and celestine.	70
Figure 3.1 Generalized Paleozoic bedrock geology map of southern Ontario	109
Figure 3.2 Ordovician stratigraphy of southwestern Ontario.	110

Figure 3.3 Conceptual fault framework, mapped fault location and location of Ordovician oil fields.....	111
Figure 3.4 Core photographs of Trenton Group (Sherman Fall Formation) carbonates, southwestern Ontario	112
Figure 3.5 Sample location map.	113
Figure 3.6 Paragenetic sequence of the Sherman Fall Formation in southwestern Ontario	114
Figure 3.7 Photomicrographs of Trenton Group carbonates, southwestern Ontario	115
Figure 3.8 $\delta^{18}\text{O}$ and $\delta^{13}\text{C}$ values of replacive dolomite (D2), dolomite cement (D3) and fracture-filling calcite (C3) from the Sherman Fall Formation, southwestern Ontario.....	117
Figure 3.9 Strontium isotopic composition of replacive dolomite (D2) and saddle dolomite cement (D3b) from The Sherman Fall Formation	118
Figure 3.10 PAAS normalized REE pattern for average values of matrix dolomite (D2), saddle dolomite cement (D3b) and fracture-filling calcite (C3) and whole rock (WR) samples.....	119
Figure 3.11 Ce (Ce/Ce^*) _{SN} -La (Pr/Pr^*) _{SN} anomaly cross plot of whole rock (WR), D2, D3b, and C3 samples.....	120
Figure 3.12 Photomicrographs of fluid inclusions.....	121
Figure 3.13 Homogenization temperatures and salinities of primary fluid inclusions in saddle dolomite cement (D3b) and fracture-filling calcite (C3).....	122
Figure 3.14 Temperature vs. $\delta^{18}\text{O}$ fluid for various $\delta^{18}\text{O}$ values of dolomite	123
Figure 3.15 Map of the Michigan Basin and surrounding arches and proposed fluid flow out of the Michigan Basin during the Paleozoic	124
Figure 4.1 Generalized Paleozoic bedrock geology map of southern Ontario	177
Figure 4.2 Generalized Paleozoic stratigraphic column for southern Ontario.....	178
Figure 4.3 Paragenetic sequence of the Paleozoic succession in southwestern Ontario..	179
Figure 4.4 Photomicrographs of dolomite and late-stage calcite from the Paleozoic succession of southwestern Ontario.	181
Figure 4.5A $\delta^{18}\text{O}$ and $\delta^{13}\text{C}$ values of replacive dolomite (D1 and D2) of the Paleozoic carbonate succession of southwestern Ontario.	182

Figure 4.5B $\delta^{18}\text{O}$ and $\delta^{13}\text{C}$ values of saddle dolomite cement (D3) of Silurian and Ordovician rocks.	183
Figure 4.5C $\delta^{18}\text{O}$ and $\delta^{13}\text{C}$ values of late-stage calcite cement of the Paleozoic succession of southwestern Ontario.	184
Figure 4.6A Secular $^{87}\text{Sr}/^{86}\text{Sr}$ curve of Devonian to Cambrian seawater and $^{87}\text{Sr}/^{86}\text{Sr}$ ratio of dolomite from Lucas and Guelph formations and Trenton Group	185
Figure 4.6B Secular $^{87}\text{Sr}/^{86}\text{Sr}$ curve of Devonian to Cambrian sea water and $^{87}\text{Sr}/^{86}\text{Sr}$ ratios variation of brines of sandstone and carbonate reservoirs from Cambrian to Devonian of southwestern Ontario.....	186
Figure 4.7A Average shale-normalized (PAAS) values of REE concentration in different diagenetic minerals of Devonian samples.....	187
Figure 4.7B Average shale-normalized (PAAS) values of REE concentration in different diagenetic minerals of Silurian samples.....	188
Figure 4.7C Average shale-normalized (PAAS) values of REE concentration in different diagenetic minerals of Ordovician samples	189
Figure 4.8A Ce $(\text{Ce}/\text{Ce}^*)_{\text{SN}}$ and La $(\text{Pr}/\text{Pr}^*)_{\text{SN}}$ anomaly evaluation of Devonian fine- (D1) and medium-crystalline (D2) dolomite and fracture-filling calcite	190
Figure 4.8B Ce $(\text{Ce}/\text{Ce}^*)_{\text{SN}}$ and La $(\text{Pr}/\text{Pr}^*)_{\text{SN}}$ anomaly evaluation of the Silurian fine- (D1) and medium-crystalline (D2) and saddle dolomite (D3) and vug-filling calcite	191
Figure 4.8C Ce $(\text{Ce}/\text{Ce}^*)_{\text{SN}}$ and La $(\text{Pr}/\text{Pr}^*)_{\text{SN}}$ anomaly evaluation of Trenton Group limestone host rock and corresponding diagenetic minerals.....	192
Figure 4.9 Fluid inclusion homogenization temperature and salinity of selected minerals from Paleozoic carbonate succession.....	193
Figure 4.10 The location of buried mid-continent rift under the Michigan Basin.....	194

List of Appendices

Appendix 1 Carbon, oxygen and strontium isotope results of replacive dolomite and cement and fracture-filling calcite of the Paleozoic carbonate succession of southwestern Ontario.....	207
Appendix 2 Results of REE analysis of selected minerals from the Paleozoic succession of southwestern Ontario	214
Appendix 3 Results of fluid inclusions microthermometry of selected minerals from the Paleozoic carbonate succession of southwestern Ontario.	217

Chapter 1

1.1 Introduction

Fluid movement in sedimentary basins has the potential to transfer mass and heat, which has a major impact on diagenesis, porosity and permeability, hydrocarbon migration and ore deposits formation (Kharaka and Hanor, 2004). During their migration, basinal fluids can cause chemical and thermal alteration of the sedimentary rocks and leave behind diagenetic evidence of the extent and nature of these events (Bethke and Marshak, 1990). As a result, geo-fluids studies are of great importance in understanding the origin, evolution and migration of basinal fluids and their geologic impact.

The majority of the Paleozoic oil and gas producing reservoirs in southwestern Ontario are porous, dolomitized carbonates. Faults and fractures have played an important role as conduits for dolomitizing fluids, changing some of the non-porous limestone into dolomitized oil and gas reservoirs, especially in Ordovician carbonates. However, in the Silurian and Devonian carbonates, fractures initially have no major role in dolomitization, they enhanced the reservoir quality (e.g., Hamilton, 1991; Sanford et al., 1985).

Structural and geophysical studies show that the Precambrian basement fracture trends acted as a “tectonic template” and controlled propagation of fractures into overlying Paleozoic rocks (Sanford et al., 1985; Boyce and Morris, 2002). These fractures, which propagated from the basement, are ideal conduits to channelize basinal fluids. Such basinal fluids are responsible for wholesale diagenetic changes including late stage dolomitization, MVT ore precipitation and hydrocarbon accumulation (e.g., Sanford et al., 1985; Farquhar et al., 1987; Coniglio et al., 1994; Carter et al., 1996).

Several lines of evidence point at the involvement of fault and fractures in the migration of diagenetic fluids and hydrocarbons in the Paleozoic sedimentary sequence of the Michigan Basin and southwestern Ontario including: 1) fracture-filling calcite containing hydrocarbon-bearing fluid inclusions in Devonian rocks in the center and margin of the basinal (Luczaj et al., 2006; Haeri-Ardakani et al., 2012a); 2) hydrothermal fracture-filling saddle dolomite in the central Michigan Basin in Devonian rocks (Luczaj et al., 2006); 3) fracture- and vug-filling hydrothermal saddle dolomite in Silurian rocks

in the center and margin of the basin (Barnes et al., 2008); 4) fracture-related dolomitization of Black River and Trenton groups carbonates (Middleton et al., 1993; Coniglio et al., 1994; Haeri-Ardakani et al., 2012b); and 5) selective dissolution of Silurian Salina evaporites along fractures (Sanford et al., 1985).

In addition, similarities in hydrocarbon characteristics of different ages in the Michigan Basin and southwestern Ontario led early workers to suggest upward cross-formational migration of hydrocarbons through a network of fractures (Vogler et al., 1981; Obermajer et al., 2000). Several workers also suggested that upward cross-formational fluid flow is responsible for emplacement of saline fluids in Devonian reservoirs (e.g., Wilson and Long, 1993; Weaver et al., 1995; Ma et al., 2005; Luczaj et al., 2006).

High homogenization temperatures (120 to 200°C) are obtained from the fluid inclusions hosted in minerals (calcite, saddle dolomite, matrix dolomite, fluorite, celestine, illite, and chlorite) or calculated based on $\delta^{18}\text{O}$ values of diagenetic mineral in the Devonian to Cambrian sedimentary succession in the center and margin (study area) of the Michigan Basin (e.g., Coniglio and Williams-Jones, 1992; Middleton et al., 1993, Coniglio et al., 1994; Simo et al., 1994; Girard and Barnes, 1995; Harper et al., 1995; Yoo et al., 2000; Zeigler and Longstaffe, 2000; Luczaj et al., 2006). These temperatures are significantly higher than maximum burial temperatures for individual strata (varying from 60 to 120°C) suggesting involvement of hydrothermal fluids in the precipitation and/or recrystallization of diagenetic minerals and their host carbonates.

The occurrence of hydrothermal alteration and dolomitization (Coniglio et al., 1994; Yoo et al., 2000, Luczaj, 2006) in the periphery of the Michigan Basin suggest a radially outward fluid flow from the Michigan Basin (e.g., Luczaj, 2006). The presence of secondary K-feldspar, chlorite and illite in Cambro-Ordovician rocks and similar clay alteration in underlying the Precambrian rocks suggest that fluid flow focused along Precambrian-Paleozoic unconformity boundary (Harper et al., 1995; Ziegler and Longstaffe, 2000). The high permeability Cambrian sandstone in combination with a fracture network acted as a regional aquifer facilitating the migration of diagenetic fluids from the center of the basin toward its margin.

Major studies on the diagenetic history, including dolomitization of the carbonate succession in Ordovician to Devonian strata in Michigan, southwestern Ontario, Ohio, and New York have been carried out by earlier workers.

Late stage hydrothermal fluids, precipitating saddle dolomite, calcite, sulfate and sulfide minerals mainly occurring along fault and fractures were reported from the Ordovician Trenton and Black River groups of Michigan, southwestern Ontario, and New York (Taylor and Sibley, 1986; Hurley and Budros, 1990; Budai and Wilson, 1991; Coniglio et al., 1994; Smith, 2006). In southwestern Ontario, solid hydrocarbons coating saddle dolomite and late calcite cement shows close association of these late stage precipitates with hydrocarbons migration in dolomitic reservoirs (Coniglio et al., 1994).

In a preliminary study on Paleozoic sedimentary succession in the Michigan Basin from Ordovician to Devonian carbonate and siliciclastic rocks, reservoir creation was attributed to fracture-related hydrothermal dolomitization (Barnes et al., 2008). Reactivation of basement faults facilitated vertical migration of dolomitizing fluids. In the Paleozoic succession of the central Michigan Basin diagenetic minerals precipitated at temperatures from 80 to 170°C from saline ¹⁸O-enriched fluids (Barnes et al., 2008).

Fracture-related saddle dolomite cement in the Middle Devonian Dundee Formation of central Michigan is associated with minor calcite, anhydrite, pyrite and fluorite. Based on geochemical and fluid inclusion data, the dolomitizing fluids were hot fluids that originated from deeper parts of the basin along major fractures and faults and that were connected to structures in the Precambrian basement (Luczaj et al., 2006).

Cercione and Lohmann (1987) distinguished a regionally consistent assemblage of late diagenetic phases including pyrite, pyrobitumen, dolomite cement, and equant calcite spars in Middle Silurian pinnacle reefs in northern Michigan. The presence of late-stage calcite cements contains hydrocarbon-bearing fluid inclusions with homogenization temperatures between 83 and 122°C. Late-diagenetic carbonate phases precipitated from saline basinal brines that migrated through cross-formational fluid flow.

Farquhar et al. (1987) reported the presence of non-economic MVT-type mineralization in vugs and veins in dolomites of the Middle Silurian Lockport Formation

in southwestern Ontario. They also indicated that expulsion of basinal brines due to Appalachian compressional tectonics could be considered a major cause for the occurrence of non-economic MVT mineralization in southwestern Ontario.

The presence of hydrocarbon-bearing fluid inclusions in late-stage saddle dolomite, and calcite in Ordovician (Poutry, 1988; Hurley and Budros, 1990; Budai and Wilson, 1991; Coniglio et al., 1994, Haeri-Ardakani et al., 2012), Silurian (Cercone and Lohmann, 1987) and Devonian (Luczaj et al., 2006; Haeri-Ardakani et al., 2012) strata implies that hydrocarbon-bearing fluids were capable of dolomitization of limestone. In addition, these fluids also precipitated fluorite, celestine, pyrite and sphalerite.

1.2 Thesis objectives

Based on reviews of previous work in the Michigan Basin and southwestern Ontario part of the Michigan Basin, it is now clear that the geochemical characteristics and the nature of the late stage diagenetic fluid(s) which affected the Paleozoic succession are poorly known. Due to the close connection of dolomitization and generation of economically significant secondary porosity, a broader study in scale, both geographically and stratigraphically with additional geochemical data and fluid inclusion data is needed to address major questions regarding dolomitization in the area. Previous diagenetic investigations focused on the features present in specific stratigraphic units.

While the similarity in hydrocarbon composition of different ages and high salinity of Devonian-hosted brines and Devonian saddle dolomite fluid inclusions were attributed to cross-formational fluid flow (e.g., Vogler et al., 1981; Wilson and Long, 1993; Weaver et al., 1995; Obermajer et al., 2000; Ma et al., 2005), the question concerning the importance, locally or regionally, of cross-formational fluid flow in Paleozoic sedimentary succession of the Michigan Basin still remains. These studies suggest vertical migration (cross-formational fluid flow) of basinal brines and hydrocarbons through the Paleozoic sedimentary sequence. In addition, the debate continues on whether faults and fractures in the underlying Precambrian basement could have provided conduits for fluid migration into the overlying Paleozoic sedimentary succession (Hobbs et al., 2011).

To be able to address questions concerning the cross-formational fluid flow in the Paleozoic succession of southwestern Ontario, the major reservoir rock units in Ordovician (Trenton Group), Silurian (Guelph Formation), and Devonian (Lucas Formation) strata have been selected. Stable isotopes (oxygen and carbon), Sr isotopes, rare earth elements (REE) geochemistry, and fluid inclusion analysis were used to address the following questions:

- 1) What is the nature of the paleohydrologic system(s) that led to partial dolomitization of Devonian and Ordovician sequences and pervasive dolomitization of Silurian sequences?,
- 2) Were the diagenetic systems in various rock units separate or connected?, and finally
- 3) What is the source of heat for hydrothermal fluids and the driving force for their migration?

The aim of the proposed study is to identify and fingerprint the fluids which affected the Paleozoic succession as well as to determine their temporal and spatial relationships. To achieve this aim, the following tasks were carried out:

- 1) Identification of diagenetic mineral phases, their relationship to host carbonates, and their environment of formation
- 2) Characterization of the nature of diagenetic fluids (temperature and composition) during the various stages of diagenesis
- 3) Investigation of the presence or absence of hydrocarbons and their possible role in formation of diagenetic minerals (i.e., carbonate cements)
- 4) Development of a general qualitative paleohydrologic model which explains the depth of fluid circulation and how diagenetic fluids moved through the basin

Most parts of southern Ontario are overlain by a relatively thick cover of glacial deposits. Due to the scarcity of outcrops in the western part of study area, most of the samples for this investigation were obtained from subsurface cores from numerous oil and gas wells drilled and stored in the Ontario Oil, Gas and Salt Resources Library in London, Ontario. Rock exposures and natural outcrops were examined in accessible quarries in the Lake Simcoe, Windsor and London area, and Bruce Peninsula.

Approximately four hundred thin sections were prepared and studied using conventional petrographic microscopy as well as ultraviolet and cathodoluminescence microscopy. Thirty doubly-polished, 100 µm-thick wafers of calcite, dolomite, fluorite, celestine, and sphalerite were prepared for fluid inclusion studies. Samples of selected diagenetic minerals were processed and analyzed for stable oxygen and carbon isotopes, $^{87}\text{Sr}/^{86}\text{Sr}$ isotopic ratios and rare earth elements (REE) composition.

1.3 Outline of the thesis structure

In order to be able to address the questions in the framework of the thesis objectives a thorough understanding of dolomitization models and nature of fluids involved in dolomitization and subsequent alteration of each time interval is necessary. Previous studies proposed various dolomitization mechanisms for Middle Silurian and Ordovician carbonate rocks in the study area; however, the dolomitization mechanism and subsequent alteration of Middle Devonian carbonates was not discussed in detail.

Thus, as a first step Middle Devonian carbonates have been studied in order to have a better understanding of dolomite formation and alteration as well as late-stage fracture mineralization. Subsequently, the previously proposed models for Silurian and Ordovician dolomitization were critically reviewed to refine them with employment of additional geochemical data (i.e., Sr isotopes and REE). Finally, the obtained data from field, petrography, fluid inclusion, and geochemical studies in combination with existing data on dolomitization and late-stage mineralization of each age interval were applied to suggest a conceptual paleohydrological model for migration of diagenetic fluids in carbonate succession of southwestern Ontario.

The results of this study are presented in the framework of a PhD thesis consisting of five chapters. Chapter One is the introduction for the thesis and Chapter Five presents a summary of the entire investigation. Chapters two to four are a collection of three manuscripts submitted to peer-reviewed scientific journals.

A version of chapter 2 was submitted to Bulletin of Canadian Petroleum Geology entitled: “Diagenetic evolution and associated mineralization in Middle Devonian carbonates, southwestern Ontario, Canada”. In this chapter the dolomitization mechanism

of Middle Devonian carbonate rocks (Lucas Formation) and subsequent alteration of dolomite were investigated and discussed. In addition to dolomitization, the nature of fluid(s) for late-stage fracture-filling calcite cement and celestine were investigated. The combination of stable isotope, Sr isotopes, rare earth elements (REE), and fluid inclusion data suggest involvement of hydrothermal fluids in recrystallization of dolomite and precipitation of calcite and celestine while the same fluids carried hydrocarbons.

A version of chapter 3 was submitted to the Journal of Marine and Petroleum Geology entitled: “Petrologic and geochemical attributes of fracture-related dolomitization in Ordovician carbonates and their spatial distribution in southwestern Ontario, Canada”. In this chapter the models proposed for fracture-related dolomitization of the Trenton Group (Middle Ordovician) were reviewed and critically evaluated. Additional geochemical data (i.e., Sr isotopes and REE) was generated and applied in order to better constrain the nature of dolomitizing fluids and propose a fluid flow model. A thermal anomaly over the buried mid-continent rift was suggested as the driving force for migration of diagenetic fluids.

A version of chapter 4 was accepted as an extended abstract in the GEOFLUIDS VII–International Conference entitled: “Fracture mineralization and fluid flow evolution: An example from Ordovician-Devonian carbonates, southwestern Ontario, Canada”. The complete manuscript will be submitted to the Geofluids Journal by July 2012. In order to discover a possible genetic relationships between dolomite of each age interval from Ordovician to Devonian, dolomitization mechanisms in combination with petrographic and geochemical characteristics of dolomite were investigated. Geochemical and fluid inclusions results were employed to establish a conceptual paleohydrological model for migration of diagenetic fluids and hydrocarbons in the carbonate succession of the study area. The results of this study indicate changes in pore fluid composition and compartmentalization of diagenetic fluids.

1.4 Geologic setting

During the Paleozoic Era, eastern North America was located at tropical latitudes and intermittently covered by inland seas which deposited a succession of carbonates, siliciclastics and evaporites. The Paleozoic succession of southern Ontario consists of

marine sediments from Cambrian to Mississippian age (Armstrong and Carter, 2006). The resultant sedimentary rock cover contains erosional and non-depositional gaps due to regression, which resulted in an incomplete stratigraphic record (Johnson et al. 1992).

Southern Ontario is located between two major Paleozoic sedimentary basins, the Appalachian Basin to the southeast and the Michigan Basin to the west (Fig. 1.1). These two basins are separated by the northeast-southwest trending Algonquin Arch, which extends from northeast of the Canadian shield and terminates at the southwest near the city of Chatham. This structural high again resumes near the Windsor area, where it is named the Findlay Arch, and extends to the southwest into Michigan and Ohio. The structural depression shaped between the two Arch sections is called the Chatham Sag (Brigham, 1971).

The Michigan and Appalachian basins are two different types of sedimentary basins. The Michigan Basin is a nearly circular intracratonic basin, and is carbonate-dominated and evaporite-bearing. In contrast, the Appalachian Basin is dominated by siliciclastic sediments and is an elongate foreland basin that developed as a result of collisional orogenesis along the eastern margin of North America continent during the Paleozoic (Armstrong and Carter, 2006).

Sanford et al. (1985) interpreted the Algonquin and Findlay arches to have formed in late Precambrian time and reactivated periodically during the Paleozoic. The arches formed a broad platform between the differentially subsiding Michigan Basin in the west and Appalachian Basin to the southeast (Fig. 1.2). The orogenic activity at the eastern margin of North America controlled the geometry of the basins and the separating arches. Basinal subsidence due to sedimentation and thermal contraction with movement (e.g., uplift) of the arch collectively are the main tectonic elements controlling sedimentation in the two basins (Johnson et al., 1992; Carter et al., 1996).

The Paleozoic cover that overlies the arch complex is up to 1500 m thick and consists of carbonates, shales, evaporites, and minor sandstone of Cambrian to Mississippian (Figs. 1.3 and 1.4). The Paleozoic strata along the northern part of the Algonquin Arch generally dip westward at a gradient of approximately 5.5 to 8.5 m/km

into the Michigan Basin, and southward, into the Appalachian Basin (Armstrong and Carter, 2006).

1.4.1 Ordovician carbonates (Trenton Group)

Sedimentation of Paleozoic cover in the area commenced with a transgression over the Precambrian basement. This transgression represents one of the greatest sea level rises in geological history (Coniglio et al., 1990). This transgression was responsible for the deposition of Black River and Trenton facies assemblages that characterize a succession from supratidal and tidal flat clastics/carbonates to lagoonal carbonates and offshore shallow water and deep shelf carbonates (Coniglio et al. 1990).

The strata forming these groups represent the upper part of a widespread carbonate platform developed during Middle Ordovician over a vast area of the North American craton (Wilson and Sengupta, 1985). Black River and Trenton groups unconformably overlie Upper Cambrian clastics and carbonates or lie directly on Precambrian basement rocks of the Canadian Shield. The Trenton Group in the subsurface of southwestern Ontario exhibits a sharp irregular contact with overlying shales of the Blue Mountain Formation (Armstrong and Carter, 2006).

The Trenton Group is characterized by fossiliferous carbonates, interbedded with argillaceous units, exhibiting; 1) fining upward, beginning with sharp, irregularly based grainstone and sharp upper contact, 2) grainstone interbedded with wackestone or carbonate mudstone with sharp upper and lower contacts, 3) packstone or grainstone nodules enclosed by argillaceous seams within carbonate mudstone or wackestone (Armstrong and Carter, 2006). The Trenton Group consists of the Cobourg, Sherman Fall, and Kirkfield formations, in descending stratigraphic order.

The Cobourg Formation consists of very fine- to coarse-grained, fossiliferous limestone and argillaceous limestone. Shaly partings are common and thin shale interbeds are locally common. The Sherman Fall Formation consists of a lower shaly or argillaceous unit and an upper thinner and coarse-grained bioclastic or fragmental unit. The lower argillaceous unit consists of interbedded limestone and calcareous shale, while the upper fragmental unit consists of thin- to thick-bedded, medium- to coarse-grained,

fossiliferous limestone, dominantly bioclastic and intraclastic grainstone. The Kirkfield Formation is the lowest unit of the Trenton Group and consists of thin- to thick-bedded, fossiliferous limestone with shaly partings and locally significant thin shale interbeds (Armstrong and Carter, 2006).

1.4.2 Silurian carbonates (Guelph Formation)

During late to middle Silurian southern Ontario and Michigan was flooded by warm shallow seas and laid approximately 25° south of the equator (Van der Voo, 1988). This condition was ideal for development of reefal complexes (barrier and patch reef) in the warm shallow waters and for formation of pinnacle reefs in deeper waters sloping into the Michigan Basin. These reefal carbonates are known as the Guelph Formation in southern Ontario, while they are called the Niagaran carbonates in Michigan. The Middle Silurian Guelph Formation consists of platformal and reefal dolostones and limestones. The Guelph Formation underlies the cyclic evaporite and carbonates of the Upper Silurian Salina Group and overlies platformal argillaceous carbonates of the Lockport Formation (Johnson et al. 1992).

Rapid subsidence in the center of the basin relative to the margin of the basin caused deeper water basinal facies of the Guelph formation to be deposited in the middle of the Michigan Basin, while shallower low energy restricted facies, shallow higher energy facies and reef and inter-reef facies were deposited on the margin of the basin and Algonquin Arch (Armstrong and Goodman, 1990). A northern and southern pinnacle reef belt formed a discontinuous ring around the Michigan Basin. Pinnacle reefs in southwestern Ontario occur in a lower part of the ramp or on the basin slope setting. Inter-reef facies consist of dolomitized crinoidal wackestone to packstone and mudstone, which thicken to the south and east into the reef bank/barrier complex (Carter et al., 1994). Inter-pinnacle and deeper water facies are micritic limestone and wackestone.

Massive, laminated, organic-rich and sometimes fossiliferous dolomite of the Eramosa Member of the Guelph Formation is the major back reef lagoonal facies which are developed farther to the east and north and exposed along the Niagara Escarpment in a 10–30 km wide zone. Lateral and vertical development of the reef bank/barrier reef complex ultimately formed a nearly continuous barrier and transformed the Michigan

Basin into an isolated evaporative basin, characterized by cyclical evaporite-carbonate deposits for most of the remaining Silurian (Sonnenfeld and Al-Aasm, 1991).

1.4.3 Devonian carbonates (Lucas Formation)

During the Middle Devonian the Michigan Basin experienced extreme aridity and restricted marine environmental conditions indicated by the type of fauna present and the occurrence of evaporative facies, supratidal, mud flat, shallow intertidal and subtidal lithofacies of the Detroit River Group (i.e., Amherstburg and Lucas formations) (Gardner, 1974; Birchard et al., 2004). The Devonian succession in southwestern Ontario consists mainly of limestones and shales with dolostone and sandstones (Uyeno et al., 1982). With continuation of transgression, the Algonquin Arch was flooded and the Detroit River Group was disconformably overlain by the Dundee Formation (Sanford, 1993).

Throughout most of the region, the Lucas Formation sharply and conformably overlies the Amherstburg Formation. The Amherstburg Formation consists of fossiliferous, bituminous, commonly cherty limestones and dolostone (Johnson et al. 1992). In Ontario the Amherstburg Formation conformably and gradationally overlies cherty fossiliferous limestones of the Lower Devonian Bois Blanc Formation. In the subsurface the Amherstburg Formation conformably overlies orthoquartzitic sandstone of the Sylvania Formation (Armstrong and Carter, 2006), which is also considered part of the Detroit River Group (Uyeno et al. 1982). The Sylvania sandstones are thicker and more extensive in central Michigan.

The Lucas Formation is the uppermost formation in the Detroit River Group and consists of limestones, dolostones, anhydritic beds and local sandy limestones. The Lucas Formation of the Michigan Basin in the study area is characterized as a low-energy, shallow-water evaporitic system (Hamilton, 1991; Birchard et al., 2004), while in the Appalachian Basin a more open marine, higher energy depositional environment prevailed during deposition of the Lucas Formation (Birchard et al., 2004). In the Michigan Basin, to the north of Algonquin Arch in general, the Lucas Formation consists fine crystalline dolostone with anhydrite interbeds, while south of Algonquin Arch, in the Appalachian Basin, it is limestone (Birchard et al., 2004). Anhydrite and anhydritic dolostone interbeds are common lithofacies of the Lucas Formation in the Michigan

Basin part of the study area. In deeper drilled wells up to 7 cycles of dolomite capped by anhydrite were reported (Birchard et al., 2004).

1.5 Tectonic setting

Following the formation of the Proterozoic metamorphic basement (Grenville Orogen), the region experienced three pulses of tectonic activities (Fig. 1.4; Sanford, 1993): 1) Taconic (Ordovician), 2) Acadian/Caledonian (Devonian), and 3) Alleghanian (Carboniferous). The major phases of basin subsidence and uplift coincide with peaks of these orogenic cycles (Fig. 1.5) and significantly affected sedimentary input into the region (Sanford et al., 1985). The resulting stresses were substantial to produce local reactivation of basement structures and regional development of fractures in the Paleozoic cover. These basins and their prevailing arches were active over an extended period of time, from Cambrian to Carboniferous. The basement is believed to have a well-developed pattern of joints and faults, similar to the highly fractured Canadian Shield (Sanford et al., 1985; Boyce and Morris, 2002). The systematic relationship between the regional basement magnetic trends in southern Ontario and fracture patterns within the overlying Paleozoic sedimentary rocks supports upward propagation of basement fractures and faults into the overlying Paleozoic sedimentary cover strata (Boyce and Morris, 2002).

A conceptual fracture framework for southern Ontario (Fig. 1.6) based on structure mapping of Paleozoic stratigraphic marker horizons was proposed by Sanford et al. (1985). They defined two principal fracture domains for southern Ontario, the Bruce and Niagara megablocks (Fig. 1.6). The Bruce megablock exhibit a simple pattern of west-east fractures, while Niagara megablock has a more complicated fracture pattern with northwest, northeast and west-east trends. The basement magnetic trends provide general support for the conceptual fracture framework proposed by Sanford et al. (1985), where there is a general correspondence between fracture orientations, basement magnetic trends (Boyce and Morris, 2002), and location of mapped faults (Carter et al., 1996) especially in southwestern Ontario (Fig. 1.6). However, there is no correspondence between basement magnetic trends and location of mapped faults in the Paleozoic

sedimentary cover and inferred fracture network of the Bruce megablock (Boyce and Morris, 2002).

Regardless of coincidence of the actual fracture network with the conceptual fracture framework many oil and gas reservoirs in southwestern Ontario either are bounded by Paleozoic fault systems that originate in and displace the underlying Precambrian basement, or are elongated parallel with the local direction of magnetic strike (Carter et al., 1996). This indicates that fractures have a major role in reservoir creation and hydrocarbon migration in the study area. Reactivation of the fracture framework in the Paleozoic sedimentary rocks of the Michigan Basin and southern Ontario is interpreted to have controlled the movement of diagenetic fluids, distribution of hydrocarbon reservoirs and hydrocarbon migration, and salt dissolution features (Brigham, 1971; Sanford et al. 1985, Budai and Wilson, 1991; Coniglio et al. 1994, Carter et al. 1996).

1.6 References

- Armstrong, D. K., Carter, T. R., 2006. An Updated Guide to the Subsurface Paleozoic Stratigraphy of Southern Ontario. Ontario Geological survey Open File Report 6191, 214 p.
- Armstrong, D. K., Goodman, W. R., 1990. Stratigraphy and depositional environments of Niagaran carbonates, Bruce Peninsula, Ontario. American Association of Petroleum Geologists, 1990 Eastern Section Meeting, Ontario Petroleum Institute, Field Trip Guidebook 2, 59 p.
- Barnes, D. A., Parris, T. M., Grammer, G. M., 2008. Hydrothermal Dolomitization of Fluid Reservoirs in the Michigan Basin, USA. Search and Discovery Article #50087, Adapted from oral presentation at AAPG Annual Convention, San Antonio, Texas.
- Bethke, C. M., Marshak, S., 1990. Brine migrations across North America – The plate tectonics of groundwater. Annual Review of Earth and Planetary Science 18, 287-315.

- Birchard, M. C., Rutka, M. A., Brunton, F. R., 2004. Lithofacies and geochemistry of the Lucas Formation in the subsurface of Southwestern Ontario: A high purity limestone and Potential high purity dolostone resource. Ontario Geological Survey Open file report 6137, 180 p.
- Boyce, J. I., Morris, W. A., 2002. Basement-controlled faulting of Paleozoic strata in southern Ontario, Canada: new evidence from geophysical lineament mapping, *Tectonophysics*, 353, 151-171.
- Brigham, R. J. 1971. Structural geology of southwestern Ontario and southeastern Michigan; Ontario Department of Mines and Northern Affairs, Paper 71-2, 110 p.
- Budai, J. M., Wilson, J. L., 1991. Diagenetic history of Trenton and Black River Formations in the Michigan Basin. In: Catacosinos, P. A., Daniels, Jr., P. A. (Eds.), Early sedimentary evolution of the Michigan Basin, Geological Society of America Special Paper 256, 73-88.
- Carter, T. R., Trevail, R. A. and Smith, L. 1994. Core workshop: Niagaran reef and inter-reef relationships in the subsurface of southwestern Ontario. Geological Association of Canada, Mineralogical Association of Canada Joint Annual Meeting, Waterloo 1994, Field Trip A5, Guidebook, 38 p.
- Carter, T. R., Trevail, R. A., Easton, R. M., 1996. Basement controls on some hydrocarbon traps in southern Ontario, Canada. In: Van der Pluijm, B.A., Catacosinos, P.A. (Eds.), Basement and Basins of Eastern North America. Geological Society of America Special Paper 308, 95-107.
- Cercone, K. R., Lohmann, K. C., 1987. Late burial diagenesis of Niagaran (Middle Silurian) pinnacle reefs in Michigan Basin, *American Association of Geologist Bulletin* 71, 156-166.
- Coniglio, M., Melchin, M. J., Brookfield, M. E., 1990. Stratigraphy, sedimentology and biostratigraphy of Ordovician rocks of the Peterborough–Lake Simcoe area of southern Ontario; American Association of Petroleum Geologists Eastern Section Meeting, Ontario Petroleum Institute, Field Trip Guidebook 3, 82 p.

- Coniglio, M., Sherlock, R., William-Jones, A. E., Middleton, K., Frapé, S. K., 1994. Burial and hydrothermal diagenesis of Ordovician carbonates from the Michigan Basin, Ontario, Canada. In: Purser, B., Tucker, M., Zenger, D. (Eds.), *Dolomites – A volume in honour of Dolomieu*, Special publication of IAS 21, 231-254.
- Coniglio, M., Williams-Jones, A. E., 1992. Diagenesis of Ordovician carbonates from north-east Michigan Basin, Manitoulin Island area, Ontario: evidence from petrography, stable isotopes and fluid inclusion. *Sedimentology* 39, 813-836.
- Farquhar, R. M., Haynes, S. J., Mostaghel, M. A., Tward, A. G., Macqueen, R. W., Fletcher, I. R., 1987. Lead isotopes ratios in Niagara Escarpment rocks and galenas: implications for primary and secondary sulfide deposition, *Canadian Journal of Earth Science* 24, 1625-1633.
- Frizzell, R., Cotesta, L., Usher, S., 2008. Phase I Regional Geology, Southern Ontario. Nuclear Waste Management Organization Report, 142 p.
- Gardner, W. C., 1974. Middle Devonian stratigraphy and depositional environments in the Michigan Basin. *Michigan Basin Geological Society Special Papers* 1, 138 p.
- Girard, J. P., Barnes, D. A., 1995. Illitization and paleothermal regimes in the middle Ordovician St. Peter sandstone, central Michigan Basin: K–Ar, oxygen isotope, and fluid inclusion data. *American Association of Petroleum Geologists Bulletin* 79, 49–69.
- Haeri-Ardakani, O., Al-Aasm, I., Coniglio, M., 2012a. (In review) Diagenetic evolution and associated mineralization in Middle Devonian carbonates, southwestern Ontario, Canada. Submitted to the *Bulletin of Canadian Petroleum Geology*.
- Haeri-Ardakani, O., Al-Aasm, I., Coniglio, M., 2012b. (In review) Petrologic and geochemical attributes of fracture-related dolomitization in Ordovician carbonates and their spatial distribution in southwestern Ontario, Canada. Submitted to the *Journal of Marine and Petroleum Geology*.

- Hamilton, G. D., 1991. Styles of reservoir development in Middle Devonian carbonates of southwestern Ontario. Unpublished MSc thesis.
- Harper D. A., Longstaffe F. J., Wadleigh M. A. McNutt R. H., 1995. Secondary K-feldspar at the Precambrian-Paleozoic unconformity, southwestern Ontario. *Canadian Journal of Earth Science* 32, 1432-1450.
- Hobbs, M. Y., Frape, S. K., Shouakar-Stash, O., Kennell, L. R., 2011. Regional hydrogeochemistry- Southern Ontario. Nuclear Waste Management Organization Report, 157 p.
- Hurley, N. F., and Budros, R., 1990. Albion-Scipio and Stoney Point Fields – USA, Michigan Basin, In: Beaumont, E.A., Foster, N. H. (Eds.) *Stratigraphic Traps I, Treatise of Petroleum Geology Atlas of Oil and Gas Fields*, AAPG, 1-37.
- Johnson, M. D., Armstrong, D. K., Sanford, B. V., Telford, P. G., Rutka, M. A., 1992. Paleozoic and Mesozoic geology of Ontario. In: *Geology of Ontario*, Ontario Geological Survey Special Volume 4, Part 2, 907-1008.
- Kharaka, Y. K., and Hanor, J. S., 2004. Deep fluids in the continents: I. Sedimentary Basins, *Treatise on Geochemistry*, 5, 499-540.
- Luczaj, J. A., 2006. Evidence against the Dorag (mixing-zone) model for dolomitization along the Wisconsin arch-A case for hydrothermal diagenesis. *American Association of Petroleum Geologists Bulletin* 90, 1719-1738.
- Luczaj, J. A., Harrison III, W. B., and Williams, N. S., 2006. Fractured hydrothermal dolomite reservoirs in the Devonian Dundee Formation of the central Michigan Basin. *AAPG Bulletin* 90, 1787-1801.
- Ma, L., Castro, M. C., Hall, C. M., Walter, L. M., 2005. Cross-formational flow and salinity sources inferred from a combined study of helium concentrations, isotopic ratios, and major elements in the Marshall aquifer, southern Michigan. *Geochemistry Geophysics Geosystems* 6, 1-21.

- Middleton, K., Coniglio, M., Sherlock, R., Frappe, S. K., 1993. Dolomitization of Middle Ordovician carbonate reservoirs, southwestern Ontario, *Bulletin of Canadian Petroleum Geology* 41, 150-163.
- Obermajer, M., Fowler, M. G., Snowdon, L.P. Macqueen, R. W., 2000. Compositional variability of crude oils and source kerogen in the Silurian carbonate-evaporite sequences of the eastern Michigan Basin, Ontario, Canada. *Bulletin of Canadian Petroleum Geology*, 48, 307-322.
- Prouty, C. E., 1988. Trenton exploration and wrenching tectonics – Michigan Basin and environs, In: Keith, B. D. (Ed.), *The Trenton Group (Upper Ordovician Series) of eastern North America. American Association of Petroleum Geologists Studies in Geology* 29, 207-237.
- Sanford, B. V., 1993. St. Lawrence Platform: geology; In: Stott, D.F. and Aitken, J.D. (Eds.), *Sedimentary Cover of the Craton in Canada, Geological Survey of Canada, Geology of Canada Series*, 5, 723-786.
- Sanford, B. V., Thompson, F. J., McFall, G. H., 1985. Plate tectonics – A possible controlling mechanism in the development of hydrocarbon traps in southwestern Ontario, *Bulletin of Canadian Petroleum Geology* 33, 52-71.
- Simo, J. A., Johnson, C. M., Vandrey, M. R., Brown, P. E., Castro Giovanni, E., Drzewiecki, P. E., Valley, J. W., Boyer, J. 1994. Burial dolomitization of the Middle Ordovician Glenwood Formation by evaporitic brines, Michigan Basin. In: Purser, B., Tucker, M., Zenger, D. (Eds.), *Dolomites – A volume in honour of Dolomieu, Special Publication IAS* 21, 169-186.
- Smith, L. B., 2006. Origin and reservoir characteristics of Upper Ordovician Trenton-Black River hydrothermal dolomite reservoirs in New York. *AAPG Bulletin* 90, 1691-1718.
- Sonnenfeld, P. and Al-Aasm, I. 1991. The Salina evaporites in the Michigan Basin. In: Catocinos, P. A., Daniels, Jr., P. A. (Eds.), *Early sedimentary evolution of the Michigan Basin. Geological Society of America, Special Paper* 256, 139-153.

- Taylor, T. R., Sibley, D. F., 1986. Petrographic and geochemical characteristics of dolomite types and the origin of ferroan dolomite in the Trenton Formation, Ordovician, Michigan Basin, U.S.A. *Sedimentology* 33, 61-86.
- Uyeno, T. T., Telford, P. G., Sanford, B. V. 1982. Devonian conodonts and stratigraphy of southwestern Ontario. *Geological Survey of Canada Bulletin* 332, 55 p.
- Van der Voo, R., 1988. Paleozoic paleogeography of North America, Gondwana, and intervening displaced terranes: Comparisons of paleomagnetism with paleoclimatology and biogeographical patterns. *Geological Society of America Bulletin* 100, 311-324.
- Vogler, E. A., Meyers, P. A., Moore, W. A., 1981. Comparison of Michigan Basin crude oils. *Geochimica et Geochimica Acta* 45, 2287-2293.
- Weaver, T. R., Frape, S. K., Cherry, J. A., 1995. Recent cross-formational fluid flow and mixing in the shallow Michigan Basin. *GSA Bulletin* 107, 697-707.
- Wilson, J. A., and Sengupta, A., 1985. The Trenton Formation in the Michigan Basin and environs: pertinent questions about its stratigraphy and diagenesis, In: Cercone, K. R., Budai, J. M. (Eds.), *Ordovician and Silurian rocks of the Michigan Basin: Michigan Basin Geological Society Special Paper* 4, 1-13.
- Wilson, T. P., Long, D. T., 1993. Geochemistry and isotope chemistry of Michigan Basin brines: Devonian formations. *Applied Geochemistry* 8, 81-100.
- Yoo, C. M., Gregg, J. M., Shelton K. L., 2000. Dolomitization and dolomite neomorphism: Trenton and Black River limestone (Middle Ordovician) Northern Indiana, U.S.A. *Journal of Sedimentary Research* 70, 265-274.
- Ziegler, K., and Longstaffe, F. J., 2001. Clay mineral authigenesis along a mid-continental scale fluid conduit in Palaeozoic sedimentary rocks from southern Ontario, Canada. *Clay Minerals* 59, 239-260.

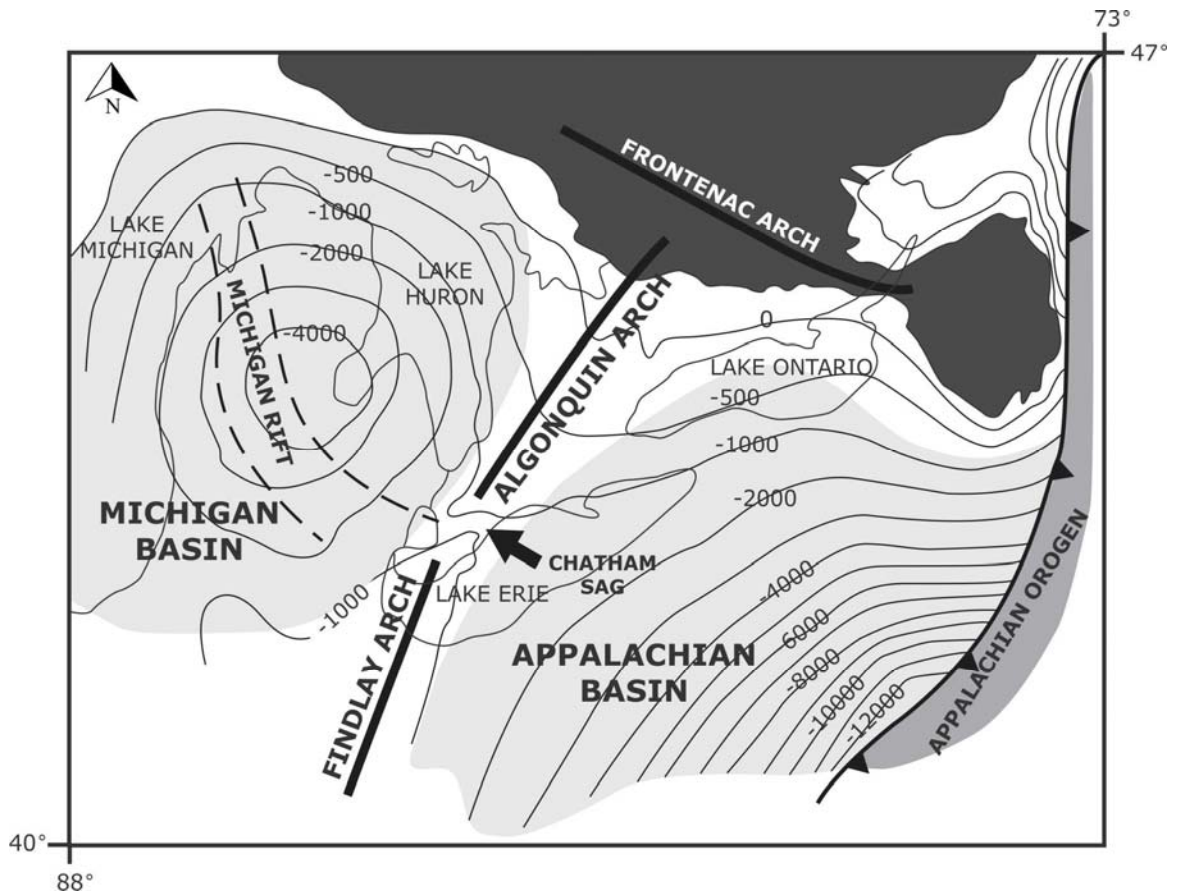


Figure 1.1 Generalized basement structural contours (meters relative to sea level datum) and location of structural arches and basins (adapted from Johnson et al. 1992).

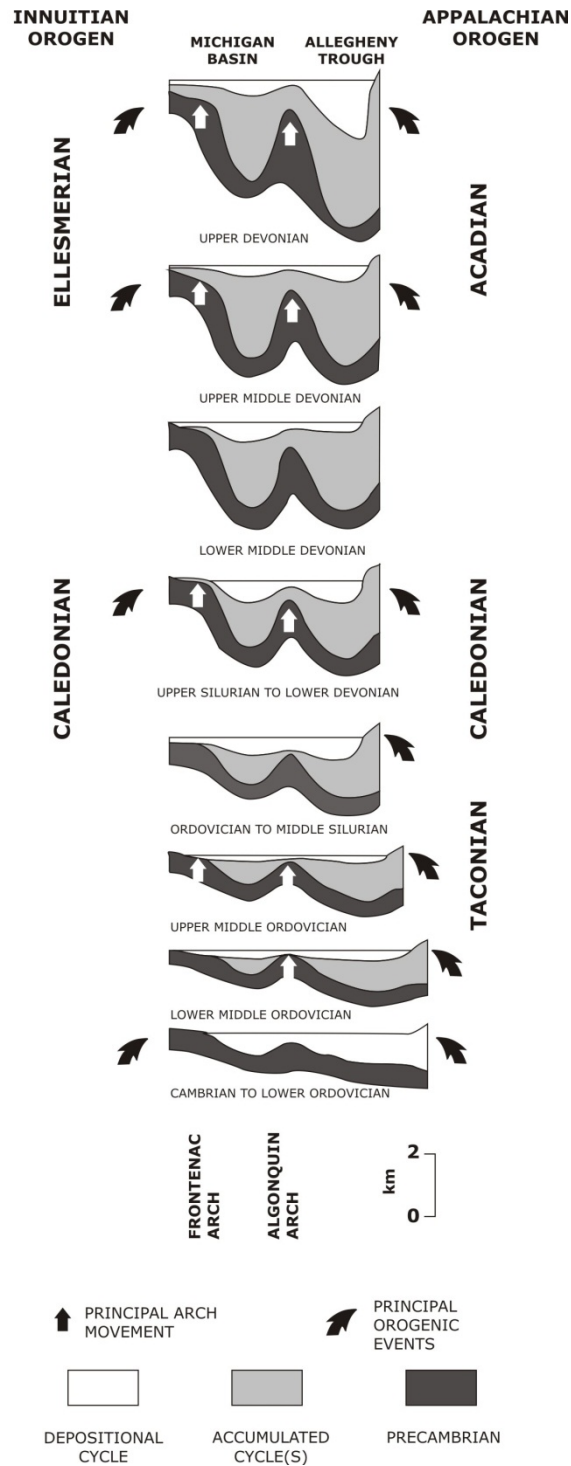


Figure 1.2 Depositional cycles and tectonic elements of the Michigan and Appalachian sedimentary basins (adapted Sanford et al., 1985).

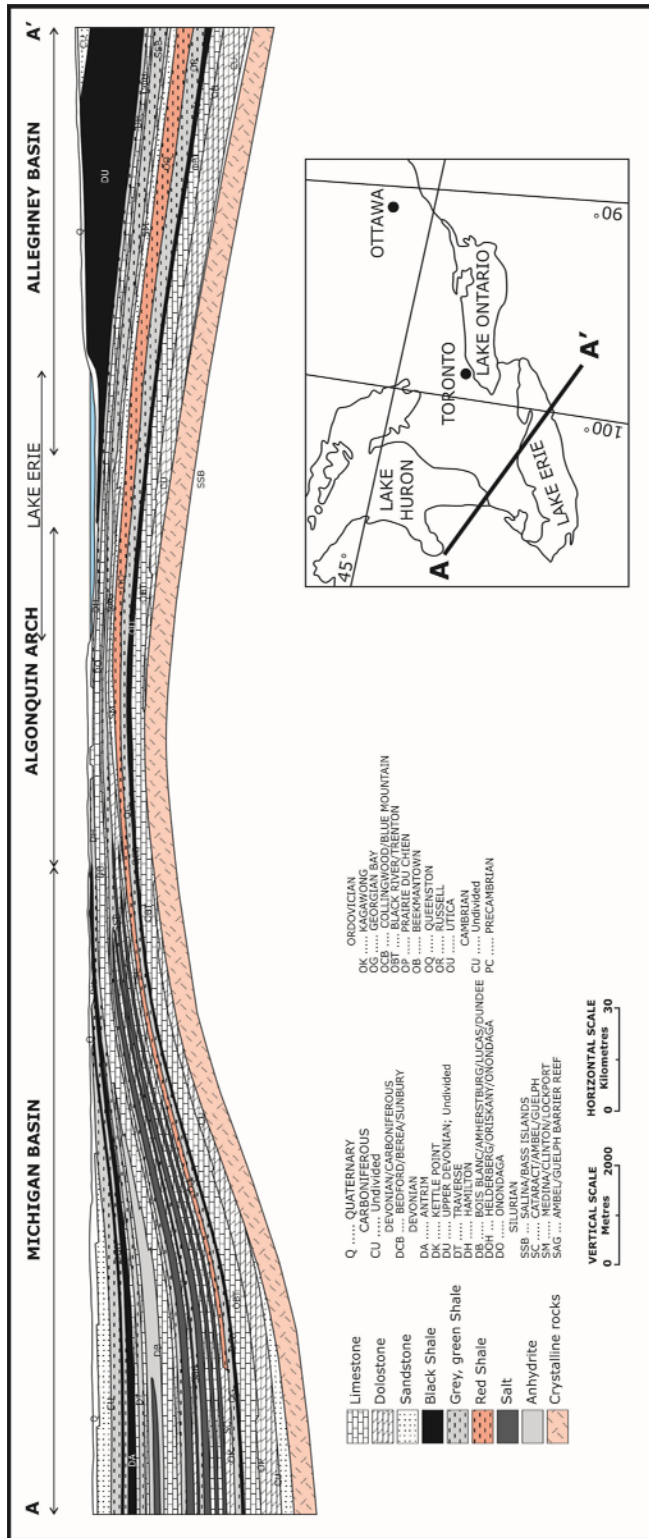


Figure 1.3 Cross section of Paleozoic sedimentary succession of southwestern Ontario and adjacent sedimentary basins. Cross section line showed on the inset map (adapted from Sanford, 1993).

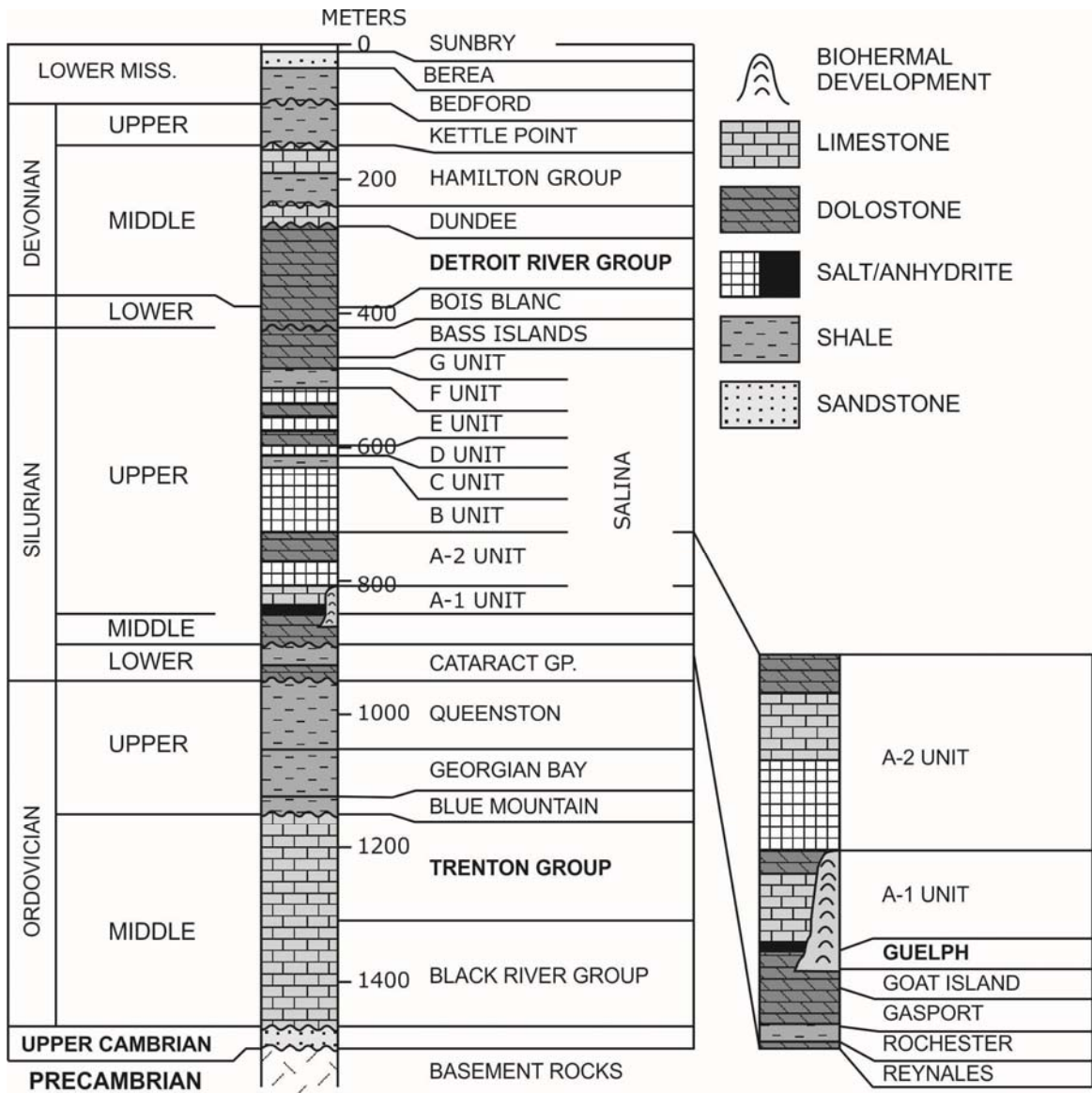


Figure 1.4 Generalized Paleozoic stratigraphic column for southern Ontario (adapted from Sanford et al., 1985). Stratigraphic units in bold font are the focus of this study.

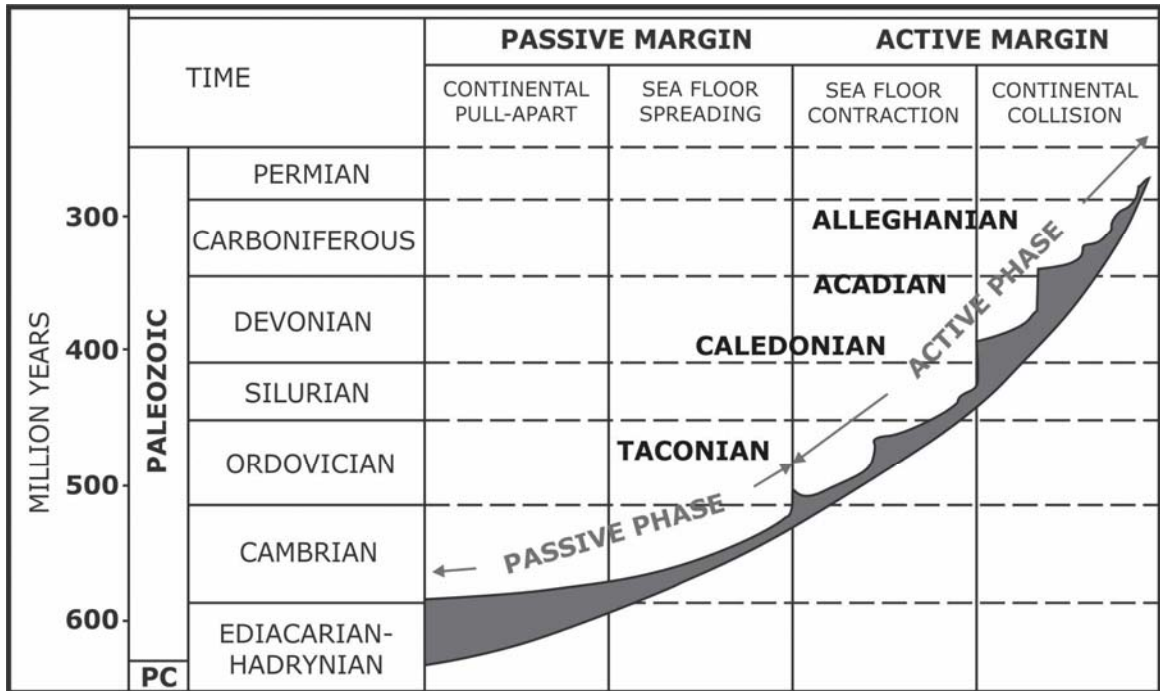


Figure 1.5 Paleozoic tectonic cycles of Appalachian orogeny (adapted from Sanford et al., 1985).

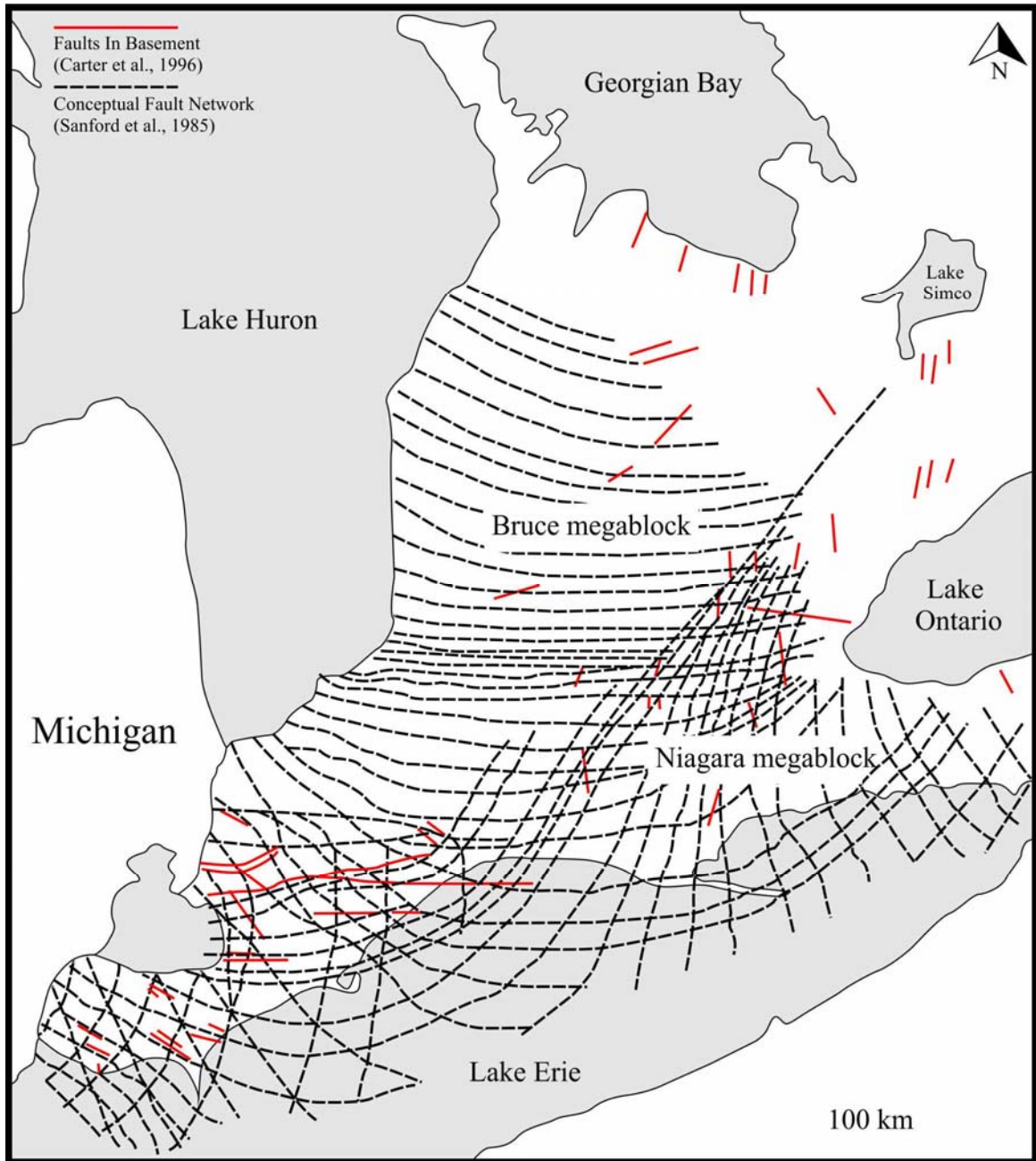


Figure 1.6 Conceptual fracture framework (adapted from Sanford et al., 1985) and mapped faults of southern Ontario (adapted from Carter et al., 1996) that displace the Paleozoic-Precambrian surface unconformity (adapted from Frizzell et al., 2008).

Chapter 2

Diagenetic evolution and associated mineralization in Middle Devonian carbonates, southwestern Ontario, Canada

2.1 Introduction

Middle Devonian carbonate rocks near Oil Springs in southwestern Ontario were the first commercial oil reservoirs discovered in North America (Hamilton 1991, 2004). By the end of 2006, the total cumulative oil production from Middle Devonian reservoirs was more than 44.3 MMbbl, and oil still continues to be produced from six active pools (Lazorek and Carter, 2008). More than 50% of oil production in Ontario has been recovered from the dolomitized zones within the Middle Devonian Lucas and Dundee formations (Powell et al., 1984; Hamilton, 2004). Diagenetic processes, most importantly dolomitization, appear to have played a major role in the reservoir development and porosity enhancement in these carbonates. Thus, a better understanding of the origin and distribution of dolomite in Middle Devonian carbonates in southwestern Ontario is of great interest for the petroleum industry.

The Middle Devonian Lucas and Dundee formations of the Michigan Basin have been the subject of several studies (Dutton, 1985; Birchard, 1990; Hamilton, 1991; Birchard et al., 2004). Although dolomitization has been responsible for creation of the reservoir quality in dolomitized facies in these formations, few studies have dealt with dolomitization (Hamilton, 1991) but the focus was mostly on stratigraphy and facies analysis.

Based on petrographic studies, facies analysis and limited geochemical data, Hamilton (1991) classified the hydrocarbon reservoirs in the Lucas and Dundee formations into different types. Two of these facies are dolomitized facies. He advocated reflux of evaporative brines to be responsible for forming fine crystalline dolomite, whereas the medium crystalline variety was postulated to have formed in a burial

environment. The sabkha model was also suggested as a possible mechanism for dolomitization of the Lucas Formation of the Detroit River Group (Fargerstorm, 1983).

The main focus of the present investigation is better understanding of the mechanism for dolomitization of the host rocks and later mineralized fractures in the Middle Devonian Lucas Formation, using petrography, stable oxygen and carbon isotopes, strontium isotopes and fluid inclusion data. Late-stage mineralization is also examined in order to understand the possible timing of hydrocarbon migration and the nature of the fluids involved.

2.2 Geologic setting

During the Palaeozoic Era, southwestern Ontario was located at tropical latitudes (Van der Voo, 1988) and intermittently covered by inland seas that deposited a succession of carbonates, siliciclastics and evaporites. The Palaeozoic succession in the region consists of marine sediments ranging in age from Cambrian to Mississippian (Armstrong and Carter, 2006). The succession contains erosional and/or non-depositional gaps mainly due to regression, resulting in an incomplete stratigraphic record (Johnson et al. 1992).

Southwestern Ontario is located between two major Palaeozoic sedimentary basins, the Appalachian Basin to the southeast, and the Michigan Basin to the west (Fig. 2.1). The Michigan Basin is a nearly circular intracratonic basin, and is carbonate-dominated with some evaporite successions. In contrast, the Appalachian Basin, which is dominated by siliciclastics, is an elongate foreland basin that developed as a result of collisional tectonics along the eastern margin of the North American continent (Armstrong and Carter, 2006). During late Lower to early Middle Devonian time, the Michigan and Appalachian basins formed two large epicontinental seas, separated by the Algonquin Arch.

The Algonquin Arch extends from the southeastern part of the Canadian Shield and terminates to the southwest near the city of Chatham. This structural high resumes in the Windsor area, as the Findlay Arch, and extends to the southwest into Michigan and Ohio. The structural depression between the two arch sections is the Chatham Sag

(Brigham, 1971). According to Sanford et al. (1985), the Algonquin and Findlay arches formed a broad platform between the differentially subsiding Michigan Basin to the west and the Appalachian Basin to the southeast. These arches were affected by periodic epeirogenic movements throughout the Palaeozoic in response to the Appalachian orogeny (Bradly, 1983; Quinlan and Beaumont, 1984).

A widespread marine transgression occurred during the Early Middle Devonian (Emsian–Eifelian) and a succession of minor craton-derived clastic sediments, basin-centered evaporites, and extensive carbonate sediments were deposited (Johnson et al., 1992). At this time, southwestern Ontario was covered by a shallow sea that was characterized by restricted marine conditions, as indicated by absence of marine fauna, evaporative facies, supratidal, mud flat, and shallow intertidal and subtidal lithofacies of the Lucas Formation (Gardner, 1974; Hamilton, 1991; Johnson et al., 1992; Birchard et al., 2004). Throughout most of region, the Lucas Formation sharply and conformably overlies the Amherstburg Formation (Fig. 2.2). The Lucas Formation in the central part of the Michigan Basin consists of limestone and dolostone alternating with anhydrite and halite. The salt and anhydrite units that dominate in the central part of the basin wedge out to over the Algonquin Arch eastward toward the basin margin, and are replaced by fine-crystalline dolostone with interbeds of anhydrite (Johnson et al., 1992; Sanford, 1993). Interlayers of anhydrite and pore spaces resulting from dissolution of evaporite minerals exist in the core samples in the studied area (Figs. 2.3A and B).

Hamilton (1991) identified six lithofacies in the Lucas Formation. They are: (1) Laminated peloidal mudstone, which is common in the upper part of the Lucas Formation and generally underlies the Dundee Formation; (2) Stromatoporoid floatstone facies; this facies includes stromatoporoid fragments and lesser amounts of rugose corals and echinoderm particles; (3) Peloidal packstone to grainstone facies containing very diverse bioclasts (e.g., stromatoporoid, brachiopod, coral and bryozoan fragments), intraclasts, and also contain medium- to coarse-grained, well-rounded quartz grains; (4) Dolomitic mudstone, which is a conspicuous thin unit (0.3–0.7 m) in cores and outcrop, and comprises micritic to fine crystalline dolomite; (5) Microcrystalline dolostone, which is the reservoir for the Oil Springs field, and is dominantly composed of fine-crystalline

dolomite (75–80%) and a less common medium-crystalline dolomite (20–25%); and (6) Calcareous sandstone consisting of variable amount of micritized carbonate grains and bioclasts with medium-grained, well-sorted quartz grains. Stromatolitic domes (Fig. 2.3C) and anhydrite interbeds are commonly associated with this facies, which has been interpreted to indicate deposition in a shallow evaporitic environment similar to supratidal environment of the Trucial coast in the Persian Gulf (Gardner, 1974; Hamilton, 1991; Birchard, 1993; Birchard et al., 2004).

2.3 Burial history

A number of investigations of the thermal history of the Michigan Basin (Legall et al., 1981; Cercone, 1984; Vugrinovich, 1988; Cercone and Pollack, 1991; Coniglio et al., 1994; Luczaj et al., 2006) based on a variety of proxies (e.g., organic maturity data, stable isotopes, fluid inclusions) point to the occurrence of high temperatures (up to 200°C) in the past (Ma et al., 2009). Uncertainties in the thickness of eroded sediments, the timing of thermal maturation, and the magnitude of the past geothermal gradient, make the burial history and thermal evolution of the Michigan Basin a controversial issue (e.g., Legall et al., 1981; Cercone, 1984; Nunn et al., 1984; Vugrinovich, 1988; Cercone and Pollack, 1991; Crowley, 1991).

A wide range of paleo-geothermal gradients (20–65°C/km) has been proposed to satisfy maturation of Devonian age source rocks and Pennsylvanian coals in the Michigan Basin (e.g., Legall et al., 1981; Cercone, 1984; Vugrinovich, 1988). Based on burial curve reconstruction, Middle Devonian rocks in the northern and southern Michigan Basin (i.e., margins of the basin) reached a maximum depth of 1500 m (Fig. 2.4), assuming erosion of 1000 m of Carboniferous sediments (Cercone, 1984).

From conodont and acritarch colour alteration studies, Legall et al. (1981) estimated a maximum paleotemperature of 60°C for the top of the Middle Devonian interval in southwestern Ontario, which corresponds to burial depths of 1300 m for a geothermal gradient of 30°C/km and a surface temperature of 20°C. The thermal window for generation of oil is between 60 and 90°C (Tissot and Welte, 1984). The organic maturity of Devonian source rocks (i.e., Marcellus and Kettle Point formations) in

southwestern Ontario indicates that organic matter in these formations is immature to marginally mature and did not produce oil (Powell et al., 1984; Obermajer et al., 1997), which indicates that the maximum paleotemperature for Middle Devonian rocks in southwestern Ontario was approximately equal or slightly higher than 60°C.

2.4 Materials and methods

Samples for this study were taken from both surface outcrops and subsurface cores. Surface samples were collected from the McGregor and Amherstburg quarries near Windsor, and the Saint Mary's Quarry north of London, Ontario (Fig. 2.5). Core samples were obtained from the core collections at the Ontario Oil, Gas and Salt Library, in London, Ontario. One hundred thin sections were prepared and stained with Alizarin red S and potassium ferricyanide and examined using optical, ultra-violet and cathodoluminescence microscopy.

For oxygen and carbon stable isotope analysis, approximately 5 mg of selected micro-drilled host rocks and their diagenetic phases were reacted with 100% pure phosphoric acid at 25°C for calcite and 50°C for dolomite, respectively. Mixed calcite and dolomite samples were treated using a sequential extraction technique (Al-Aasm et al., 1990). Isotopic values are presented in δ -notation and reported relative to the VPDB standard. Repeatability of isotopic measurements is better than $\pm 0.05\%$.

Six doubly-polished wafers of calcite and celestine were prepared for fluid inclusion studies. To avoid re-equilibration of fluid inclusions a liquid-cooled diamond rotary saw was used for cutting of samples (Goldstein, 2003) and cold epoxy utilized during sample mounting. Detailed fluid inclusion petrography was carried in order to determine fluid inclusion origin (i.e. primary or secondary/pseudosecondary) using an Olympus BX51 microscope. To assess the presence of gases and hydrocarbons in inclusions, and characterize solid phases, Raman spectroscopy was carried out using a 514 nm Ar ion laser with a 50 \times objective at the University of Windsor.

Fluid inclusion microthermometry measurements were carried out using a Linkam THMG 600 heating-freezing stage at the University of Windsor. Calibration with

precision of $\pm 1^\circ\text{C}$ at 300°C and $\pm 0.1^\circ\text{C}$ at -56.6°C was conducted using synthetic H_2O and CO_2 fluid inclusion standards. To reduce the risk of stretching or decrepitation during freezing of inclusions, the fluid inclusion heating experiments were conducted prior to cooling experiments.

The $^{87}\text{Sr}/^{86}\text{Sr}$ isotope ratios were analyzed for few selected calcite cements and matrix dolomites using an automated Finnigan 261 mass spectrometer equipped with nine Faraday collectors. Correction for isotopic fractionation was made by normalization to $^{86}\text{Sr}/^{88}\text{Sr} = 0.1194$. The mean standard error of mass spectrometer performance was ± 0.00003 for standard NBS-987.

Rare Earth Element (REE) concentrations were measured using an X series II Thermo Fisher ICP-MS, subsequent to a general leach and digestion procedure. Each sample powder was weighed, reacted with 1% HNO_3 acid, and then diluted with approximately 50 mg laboratory internal standards. Precision is in the range of 3.3% to 17%, and accuracy is in the range of 1.0% to 6.4%. Measured values were normalized to Post-Archean Australian average Shale (PAAS). The REE and strontium isotope analysis were carried out in Commonwealth Scientific and Industrial Research Organisation (CSIRO) of Australia.

2.5 Results

2.5.1 Mineralization

A belt of Mississippi Valley-Type (MVT) mineralization, hosted by Middle Silurian to Middle Devonian carbonate rocks extends from northeastern Indiana, through southeastern Michigan and southwestern Ontario. The main minerals in the mineralized areas are calcite, celestine, dolomite, fluorite, pyrite and sphalerite with minor amounts of barite, galena, quartz and native sulfur (Carlson, 1983).

In the McGregor and Amherstburg quarries in southwestern Ontario, minor mineralization is present, and consists of celestine, fluorite, and calcite (Figs. 2.6A, B) filling vugs and fractures. Minor amounts of sphalerite, pyrite and native sulfur (Fig. 2.6C) also occur, however there is no evidence of mineralization in Saint Mary's quarry

in the eastern part of the study area (Fig. 2.5). Dissolution vugs (10–40 cm wide) and honeycomb structures are common. The honeycomb structures are filled with celestine and fluorite (Fig. 2.6D), with lesser native sulfur and traces of pyrite and sphalerite. Fluorite also occurs in fractures, along with calcite (Fig. 2.7).

2.5.2 Petrography

2.5.2.1 *Matrix carbonates and fossils*

The carbonate host rock consists of mudstone, grainstone, and peloidal grainstone. Mudstone generally comprises non-ferroan microspar. Allochems in the grainstone are stromatoporoids, brachiopods, echinoderms and rugose corals. Calcitic allochems are generally preserved, and have in some cases been replaced by chalcedony.

2.5.2.2 *Calcite*

Four types of calcite cement have been identified: (1) fibrous calcite of 20 μm crystals that have mainly grown on brachiopod fragments; (2) syntaxial calcite; 3) equant calcite crystals ranging in size from 200–500 μm (Fig. 2.8A); and 4) blocky calcite, mainly filling fractures. All calcite cements are non-ferroan. Calcite cements, with the exception of fracture-filling calcite, commonly fill the interparticle, intra-skeletal and biomoldic pore spaces, and exhibit a uniform dull orange CL.

Blocky, fracture-filling calcite (type 4 above) is the most ubiquitous form of calcite cement in the studied samples. Fracture widths range from 0.01 mm to 3 cm, and, depending on the fracture width, crystal size varies from 100–500 μm . In wide fractures, coarser crystal cements engulf fragments of host rock, and smaller fractures are occluded by calcite, with crystal sizes ranging from 100–200 μm . Calcite cement in fractures shows concentric zonation of bright and dark orange under CL (Fig. 2.8B).

2.5.2.3 *Dolomite*

Two main types of replacive dolomite have been distinguished based on petrographic observations. The first D1, is a fine-grained, crystalline, matrix dolomite with non-planar to planar-s crystals ranging in size from 5–20 μm that has mainly replaced mudstone facies, and in some samples replaced peloids; it occurs throughout the

study area (Figs. 2.8C and D). The extent of fine-crystalline (D1) dolomitization varies from 5%–100% of rock volume. The second is a medium-grained crystalline (50–150 μm , average size of 100 μm) planar-e dolomite with cloudy cores and clear rims that has limited distribution (Figs. 2.8E and F). Medium-crystalline dolomite (D2) replaced bioclasts and calcite cement (Fig. 2.8D) and in some samples is associated with solution seams (Fig. 2.8E). Both dolomite types exhibit homogeneous dull-red cathodoluminescence.

Small (1 by 4 mm), elongated dissolution pores occur in fine-crystalline dolomite (Fig. 2.3A). High-amplitude stylolites appear to cross cut D1 dolomite (Fig. 2.8G). SEM examination of the fine-crystalline dolomite shows ragged, corroded surfaces, solution pits, and inter-crystalline porosity (Fig. 2.8H).

2.5.2.4 *Celestine and Fluorite*

Bladed crystals of celestine are mainly found in vugs of variable size, which range from 100 μm to 50 cm. In addition, in some samples, celestine fills micro-fractures. Small crystals of fluorite mainly formed in solution vugs and breccias with celestine and calcite. Fluorite crystals generally show growth zonation and range in size from 20–40 μm .

2.5.3 *Geochemistry*

2.5.3.1 *Oxygen and carbon isotopes*

Matrix calcite, D1 and D2 dolomite, and fracture-filling calcite from the Lucas Formation were analysed for oxygen and carbon stable isotopes (Fig. 2.9, Table 2.1). Matrix and stromatoporoid calcite have similar isotopic compositions. Matrix calcite (n = 3) show $\delta^{18}\text{O}$ values ranging from -6.4 to -5.1‰ VPDB, and $\delta^{13}\text{C}$ values ranging from 0.4 to 1.8‰ VPDB. Stromatoporoid calcite (n=4) show $\delta^{18}\text{O}$ values ranging from -6 to -5.5‰ VPDB, and $\delta^{13}\text{C}$ values ranging from 0.6 to 1.8‰ VPDB. In comparison, replacement dolomite exhibits a wider range of $\delta^{18}\text{O}$, from slightly more enriched (up to -3.9‰) to significantly depleted (-9.4‰), and generally heavier $\delta^{13}\text{C}$ values (0.4 to 1.8‰).

The two types of dolomite have similar ranges of $\delta^{18}\text{O}$ and $\delta^{13}\text{C}$, although the fine-crystalline dolomite (D1) extends to heavier values (Fig. 2.9). D1 dolomite (n = 26)

has $\delta^{18}\text{O}$ values ranging from -9.4 to -3.9‰ VPDB and $\delta^{13}\text{C}$ values from 0.9 to 3.3‰ VPDB. D2 dolomite ($n=8$) $\delta^{18}\text{O}$ values vary from -9.3 to -5.8‰ VPDB and $\delta^{13}\text{C}$ values from 0.80 to 3‰ VPDB. Fracture-filling calcite ($n = 13$) has $\delta^{18}\text{O}$ values ranging from -9.4 to -5.5‰ VPDB, which are similar to the range exhibited by the other carbonates (Fig. 2.9), however, the $\delta^{13}\text{C}$ values are all depleted, with values ranging from 0 to -7.7‰ VPDB.

2.5.3.2 *Strontium isotopes*

The Sr isotopic composition of fracture-filling calcite ($n = 3$) and fine-crystalline dolomite ($n = 6$) was determined (Table 2.1). Due to the disseminated nature of medium crystalline dolomite separation of this phase was not possible. Fine crystalline dolomite samples yielded $^{87}\text{Sr}/^{86}\text{Sr}$ ratios of 0.70797 – 0.70838 . Samples of fracture-filling calcite have $^{87}\text{Sr}/^{86}\text{Sr}$ ratios ranging from 0.70798 – 0.70838 (Fig. 2.10).

2.5.3.3 *Rare earth elements (REE)*

Samples of fine- and medium-crystalline replacive dolomite and fracture-filling calcite from the Lucas Formation were analysed for REE content. Ce_{SN} $[(\text{Ce}/\text{Ce}^*)_{\text{SN}}=\text{Ce}_{\text{SN}}/(0.5\text{La}_{\text{SN}}+0.5\text{Pr}_{\text{SN}})]$, La_{SN} $[(\text{Pr}/\text{Pr}^*)_{\text{SN}}=\text{Pr}_{\text{SN}}/0.5\text{Ce}_{\text{SN}}+0.5\text{Nd}_{\text{SN}}]$, anomalies were calculated with the equations of Bau and Dulski (1996).

The fine-crystalline dolomite yields lower ΣREE than medium-crystalline dolomite, but lower than those of fracture-filling calcite (Table 2.2). The REE_{SN} content of fine-crystalline dolomite is one order of magnitude higher than modern warm water brachiopods (Azmy et al., 2011) and one order of magnitude lower than Devonian microbialites (Nothdurft et al., 2004). The REE_{SN} content of fracture-filling calcite is one order of magnitude higher than fine-crystalline dolomite and comparable with Devonian microbialites (Fig. 2.11). All samples show a pronounced positive La anomaly and predominantly negative Ce anomaly (Fig. 2.12). REE_{SN} pattern of all Devonian dolomite and calcite are subparallel to those of modern warm water brachiopods (Azmy et al., 2011) and Devonian microbialites with slight HREE depletion (Fig. 2.11).

2.5.4 Fluid inclusions

Fracture-filling calcite cement and celestine samples were selected for fluid inclusion studies. The medium crystalline dolomite contains small inclusions ($<3\mu\text{m}$) that are unsuitable for microthermometry, and the two samples of fluorite examined do not contain any fluid inclusions. Primary fluid inclusions in calcite are located along growth zones (Fig. 2.13A); however, no such growth zones were observed in celestine. These contain two-phase, liquid-rich (LV) inclusions. Relatively large (20–40 μm), isolated, two phase, liquid-rich, liquid-vapor (LV) fluid inclusions in celestine are possibly primary. These do not appear to be related to fractures; secondary inclusions, located along healed fractures, are smaller (2–5 μm) (Fig. 2.13D). In addition, some small (3–5 μm) one-phase liquid inclusions were also observed in celestine (Fig. 2.13E).

In general, fluid inclusions in both calcite and celestine have consistent liquid/vapour (L/V) ratios in same assemblages. Some inclusions in calcite fluoresce under UV light, whereas celestine fluid inclusions show no fluorescence (Fig. 2.13C). The L/V ratio of hydrocarbon-bearing fluid inclusions in calcite is higher than the associated non-fluorescing (aqueous-rich) inclusions (Fig. 2.13B). Some fluid inclusions in celestine appear to have necked down (Fig. 2.13F). The hydrocarbon-bearing inclusions neither homogenized nor froze under high (350°C) and low (–170°C) temperatures, respectively, without change in L/V ratio.

The summary statistics of fluid inclusion microthermometry results are presented in Table 2.3 (complete fluid inclusion results in appendix 3). Homogenization (T_h) temperatures of non-hydrocarbon bearing fluid inclusions in calcite range from 87.1°C to 171.9°C ($126 \pm 24.5^\circ\text{C}$, $n = 17$). Homogenization temperatures in calcite-hosted fluid inclusion assemblages are consistent (e.g., 91–104°C). Ice melting temperatures range from –15.1 °C to –17.7 °C, indicating a salinity range from 18.5 to 21.1 eq. wt. % NaCl (19.7 ± 0.8 eq. wt. % NaCl, $n = 17$). Homogenization temperatures of large isolated inclusions in celestine vary over a wide range of temperatures, from 118.2 °C to 321.8°C ($219.5 \pm 51^\circ\text{C}$, $n = 74$). In the majority of fluid inclusion assemblages in celestine homogenization temperature varies in a wide range (e.g., 175 to 320°C). The salinity of

these inclusions in celestine is slightly less than those in calcite (Fig. 2.14). Ice melting temperatures of inclusions in celestine range from -6.1°C to -16.1°C , averaging -10.4°C , indicating a salinity of 10.3 to 18.4 eq. wt. % NaCl (14.4 ± 1.8 eq. wt. % NaCl, $n = 83$).

Raman spectra obtained from the liquid phase of fluorescent calcite-hosted inclusions yielded three peaks at 858, 2254 and 2950 cm^{-1} . The latter two peaks indicate the presence of saturated hydrocarbons (cf. Zhang et al., 2007). One-phase liquid inclusions in celestine were also analyzed; their spectra contain peaks at 2616 cm^{-1} , and 2919 cm^{-1} , consistent with the presence of H_2S and CH_4 (Burke, 2001).

2.6 Discussion

2.6.1 Dolomite texture

The texture of precursor limestone commonly controls dolomite crystal size. Coarse-crystalline dolomite fabrics reflect replacement of coarse-grained sedimentary rocks, such as oolitic grainstone or possibly recrystallization of matrix dolomite, whereas fine-crystalline dolomite indicates replacement of fine-grained sedimentary rocks, such as laminated mudstones (Gao and Land, 1991). Such relationships are also seen in the Lucas Formation dolomitic facies, 95 % of which is fine-crystalline dolomite, which has resulted from the replacement of lime-mudstone. It forms dense, unimodal mosaics of very fine- to fine-crystalline planar-s dolomite that preserve fine laminations of the precursor mudstone (Figs. 2.8C and D). Lithofacies analysis indicates that the precursor mudstone/wackestone facies of the Lucas Formation was deposited in intertidal to supratidal settings (Hamilton, 1991).

The presence of D1, stromatolites/algal mats (Fig. 2.3C), and interlayers of anhydrite (Fig. 2.3B), as well as the absence of a normal marine fossil assemblage in dolomitized facies (Hamilton, 1991), suggests that the dolomite of the Lucas Formation formed in an evaporative setting (cf. Adams and Rhodes, 1960). Dolomite formed through an evaporative reflux and/or sabkha mechanism is commonly fine- to medium-grained (5–20 μm), crystalline, and matrix-selective, and may be inter-grown with abundant evaporites (Figs. 2.3A, and B).

D1 in the Lucas Formation is non-planar to planar-s in texture and crystal size ranges from 5–20 μm . Such fine crystalline dolomite is normally formed in near-surface, low-temperature, and saline environments with abundant nucleation sites (Gregg and Sibley, 1984; Gregg and Shelton, 1990). Therefore, based on the size and morphology of the fine crystalline dolomite, and its association with evaporite sediments, it can be concluded that this dolomite formed in a near surface hypersaline realm in the early stages of diagenesis. Post dolomitization stylolites (Fig. 2.8G) further support an early diagenetic origin for the fine-grained dolomite.

D2 in the Lucas Formation is less abundant (< 5%) and limited to grainstone and sandy limestone facies, with the larger crystal size could be related to the coarse-grained nature of the precursor limestone (Fig. 2.8E) and possibly precipitation at lower degrees of supersaturation (Tucker and Wright, 1990, p. 168). The association of D2 with solution seams and stylolites (Fig. 2.8F), however, suggests that D2 possibly formed in a higher temperature during burial.

To interpret the genesis of dolomite, it is important to determine whether the dolomite preserved its original texture and composition or it has been subjected to recrystallization processes (Machel, 1997). Generally speaking, petrographic and textural evidence of dolomite recrystallization are (e.g., Montanez and Read, 1992; Kupezs and Land, 1994; Machel, 2004): (1) non-planar crystal boundaries, (2) coarsening of crystal sizes in a fine-grained matrix, and (3) lack of zonation shown by CL. Replacement dolomite of the Lucas Formation displays a homogeneous red cathodoluminescence with no zonation, possibly suggestive of recrystallization (Mazzullo, 1992; Machel 2004), although such characteristics could also reflect crystallization from a homogeneous (unchanging) dolomitizing fluid during dolomitization (Machel, 2004).

The ragged crystal surfaces and solution pits (Fig. 2.8H), however, favour recrystallization of a precursor dolomite (Mazzullo, 1992; Al-Aasm, 2000). The other textural characteristics of recrystallization (e.g., non-planar crystal boundaries and crystal size coarsening) in D1 and D2 are, however, absent in the currently investigated rocks. On the other hand, the petrographic recrystallization criteria defined by Machel (1997)

suggest that the Lucas Formation dolomite (D1 and D2) have been “insignificantly recrystallized” (Machel, 2004), and to some extent preserve the texture of early-formed dolomite particularly because it has been proven that early formed dolomite from seawater can preserve its original textural and geochemical characteristics after several kilometers (about 4 km) of burial and hundreds of millions of years (e.g., Al-Aasm and Packard, 2000).

2.6.2 Implications of geochemical data

2.6.2.1 Dolomite

The $\delta^{18}\text{O}$ values of the dolomite (fine- and medium-crystalline) show a wide range, from -9.4 to -3.9‰ VPDB, with an average of $-6.4 \pm 1.2\text{‰}$ VPDB. Dolomite depleted in ^{18}O may have (1) precipitated initially in a regional mixing zone, (2) precipitated at elevated temperatures during later diagenesis, or (3) recrystallized from an earlier generation of dolomite during later shallow to deep burial diagenesis (Smith and Dorobek, 1993).

Lithofacies evidence indicates that Lucas Formation was deposited in an evaporative setting under an arid climate (Gardner, 1974; Hamilton, 1991, Birchard et al., 2004). Results of studies from Florida and Yucatan shows that dominant diagenetic process in most typical freshwater–seawater mixing zones is extensive dissolution of carbonate rocks, and karstification (Machel, 2004 and references therein). Lack of evidence for subaerial exposure or karstification and associated meteoric diagenesis in Lucas Formation indicates that dolomite precipitation in a mixing zone setting is unlikely.

The coarse crystal size, non-planar texture, presence of saddle dolomite cement, negative $\delta^{18}\text{O}$ values are evidences of dolomitization in higher temperature conditions during burial (Gregg and Sibley, 1984; Taylor and Sibley, 1986; Machel, 2004). Fine crystal size, lack of non-planar texture and saddle dolomite indicates that precipitation of Lucas Formation dolomite at higher temperature is unlikely.

Given the textural evidence for dolomite formation in an evaporative setting, interpretation of the stable isotope data from Lucas Formation dolomite needs to be done

in the context of the estimated range of $\delta^{18}\text{O}$ values for Middle Devonian dolomite precipitating from seawater in such a setting. The $\delta^{13}\text{C}$ and $\delta^{18}\text{O}$ values of the Lucas Formation limestone ($\delta^{18}\text{O} = -5.7 \pm 0.5\text{‰}$ VPDB, $\delta^{13}\text{C} = 1.24 \pm 0.6\text{‰}$ VPDB) is within the estimated ranges of $\delta^{13}\text{C}$ (from -2.0 to $+3.0\text{‰}$ VPDB) and $\delta^{18}\text{O}$ (from -2.0 to -9.0‰ VPDB) for Middle Devonian marine calcite (Veizer et al., 1999; Geldern et al., 2006).

Many studies have indicated that dolomite is commonly enriched in ^{18}O relative to co-existing calcite by a factor of 3 ± 1 (e.g. Land 1980; Major et al. 1992). The $\delta^{18}\text{O}$ values of undolomitized limestone of the Lucas Formation range from -5.1 to -6.4‰ VPDB. If the fine-crystalline dolomite of the Lucas Formation precipitated from Middle Devonian seawater, the original values for dolomite would be between -1.1 and -2.4‰ VPDB with an average of $-1.7 \pm 0.5\text{‰}$ VPDB. These values are in the range of those determined for Middle Devonian fine-crystalline dolomite from Pine Point (-1.6 to -3.8‰ VPDB; Qing, 1998) and the Elk Point Basin (-0.6 to -4‰ VPDB; Fu et al., 2006) that was interpreted have precipitated contemporaneously from seawater (Fig. 2.9).

The alternative is that the dolomitizing fluid was evaporated Middle Devonian seawater. Evaporated seawater at or near gypsum saturation would be $3 \pm 1\text{‰}$ (i.e., 2 to 4‰) enriched in ^{18}O relative to contemporaneous seawater (Sofer and Gat 1975; Gonfiantini 1986). Assuming a $\delta^{18}\text{O}$ value of -2‰ (VSMOW) for Middle Devonian seawater (Veizer et al., 1999), the $\delta^{18}\text{O}$ value of evaporated seawater value would range from 0 to $+2\text{‰}$ (VSMOW). A dolomite precipitated from such evaporated seawater at temperatures typical of a sabkha setting (30 to 40°C, McKenzie, 1981) would have a $\delta^{18}\text{O}$ value in the range -2.3 to $+1.4\text{‰}$ (VPDB) (Fig. 2.9), using the fractionation equation of Fritz and Smith (1970) for protodolomite ($10^3 \ln \alpha_{\text{dolomite-water}} = (2.78 \times 10^6/T^2) + 0.11$).

In either scenarios precipitation from normal or evaporated seawater, the Lucas Formation dolomite ($\delta^{18}\text{O} = -6.4 \pm 1.2\text{‰}$ VPDB) displays a 4.7 to 6.4‰ negative shift compared to the predicted values. This indicates that the oxygen isotopic composition of the fine-crystalline dolomite has been significantly modified after initial formation (Fig. 2.9). However, the precipitation of dolomite was from seawater is supported by the

$^{87}\text{Sr}/^{86}\text{Sr}$ value of one sample, which is in the range expected for Middle Devonian seawater (Fig. 2.10).

Modification of the composition of early-formed dolomite is not unexpected and has been documented elsewhere. As early diagenetic dolomite is fine-grained and poorly ordered, they are reactive and susceptible to recrystallization processes (see, McKenzie, 1981; Carballo et al., 1987; Hardie, 1987; Mazzullo, 1992; Machel, 2004). Numerous studies have suggested that recrystallization of early-formed dolomite is a common process during progressive burial and can occur in several steps (e.g. Al-Aasm, 2000 and references therein; Fu et al., 2006). Such modified dolomite is generally characterized by stoichiometric major element ratios, negative shifts in $\delta^{18}\text{O}$, and enrichment in ^{87}Sr .

Lucas Formation dolomite displays such negative shifts in $\delta^{18}\text{O}$ values and the majority of samples have more radiogenic $^{87}\text{Sr}/^{86}\text{Sr}$ values (0.70797 to 0.70838) (Fig. 2.10) in comparison to expected values for Mid-Devonian seawater ($^{87}\text{Sr}/^{86}\text{Sr} = 0.7078\text{--}0.7079$; Diener et al., 1996; Denison et al., 1997; Veizer et al., 1999). Enrichment in ^{87}Sr indicates addition of radiogenic Sr from external sources such as basinal brines or meteoric waters.

The $\delta^{18}\text{O}$ values of the dolomite (D1 and D2) show a wide range, from -9.4 to -3.9‰ VPDB. The $\delta^{18}\text{O}$ value of any mineral precipitated from, or modified by, a fluid is a function of the temperature and oxygen isotope value of the fluid ($\delta^{18}\text{O}_{\text{fluid}}$). In the absence of fluid inclusion data, other means of temperature estimation must be used. The total burial experienced by the Middle Devonian sequence in southwestern Ontario is uncertain, however based on extrapolation of better constrained data from elsewhere in the Michigan Basin (Legall et al., 1981; Cercone, 1984) is estimated to be 1300 m. Maximum temperatures at peak burial, assuming a $25^\circ\text{C}/\text{km}$ geothermal gradient and a surface temperature of 20°C , would have been 53°C , a figure which is consistent with estimates from conodont and acritarch colour alteration studies (Legall et al., 1981) and Devonian source rock maturation which shows organic matter in these rock are immature or marginally mature (Powell et al., 1984; Obermajer et al., 1997).

Paleotemperature based on fine- and medium-crystalline dolomite $\delta^{18}\text{O}$ values, using Middle Devonian evaporated seawater (avg. = 1‰ VSMOW) as the dolomitizing fluid, would range from 60 to 98°C with an average of $76.6 \pm 8.2^\circ\text{C}$, which is higher than estimated range of burial temperature ($\sim 53^\circ\text{C}$) and values extracted from acritarch and conodont alteration indices ($\sim 60^\circ\text{C}$; Legall et al, 1981). Given that the original dolomite was precipitated in a sabkha environment, the wide range of depleted values can only be explained by modification of the isotopic values as a result of fluid-rock interaction with ^{18}O -depleted fluid(s). Therefore, Lucas Formation dolomite must have been recrystallized at higher temperatures than the estimated maximum burial temperature.

The $\delta^{13}\text{C}$ values of the fine- and medium-crystalline dolomite plot within the estimated range of Middle Devonian marine carbonates (-2 to $+3\%$ VPDB, Veizer et al., 1999; Geldren et al., 2006). Consequently, the initial composition of $\delta^{13}\text{C}$ of dolomite likely did not change drastically during recrystallization. This suggests that the fluids responsible for recrystallization of the precursor dolomite had a similar $\delta^{13}\text{C}$ composition to Middle Devonian marine carbonates or were buffered by these carbonates.

Increasing $^{87}\text{Sr}/^{86}\text{Sr}$ values of dolomite relative to coeval seawater is another criteria for recrystallization of dolomite (e.g., Al-Aasm, 2000 and references therein). The radiogenic $^{87}\text{Sr}/^{86}\text{Sr}$ values of the majority of fine-crystalline dolomite (Fig. 2.10) further support recrystallization of dolomite during interaction with basinal brines. Basinal brines commonly have high $^{87}\text{Sr}/^{86}\text{Sr}$ values relative to marine values of the same age. The potential sources of ^{87}Sr in sedimentary basin brines are; illitization of smectite and dissolution of ^{87}Sr -enriched evaporite minerals, alkali feldspar, and also of detrital mica in the deep subsurface (Chaudhuri and Claur, 1992).

The $^{87}\text{Sr}/^{86}\text{Sr}$ ratios of Late Devonian Berea sandstone range from 0.70807 to 0.70915 (Hobbs et al., 2011) which is significantly higher than Devonian seawater $^{87}\text{Sr}/^{86}\text{Sr}$ ratio (0.7078–0.7079). The interaction of fluids with overlying Upper Devonian shale ($^{87}\text{Sr}/^{86}\text{Sr} = 0.7102\text{--}0.7129$, Steuber et al., 1987) or those from interaction with overlying sandstone could have shifted the $^{87}\text{Sr}/^{86}\text{Sr}$ ratios of dolomite toward more

radiogenic values. However, rising hot basinal brine from central parts of the basin could be another potential source of ^{87}Sr -enriched fluids.

2.6.2.2 Fracture-Filling Calcite

Fracture-filling calcite with depleted $\delta^{18}\text{O}$ and $\delta^{13}\text{C}$ values (Fig. 2.9) may have formed from the influx of meteoric water (at varying temperatures) or basinal brines that have undergone varying degrees of water/rock interaction. Possible sources for fluid (s) with depleted $\delta^{13}\text{C}$ values are light carbon from hydrocarbon in oil field brines, or fluids derived from soil-derived CO_2 . Assuming average $\delta^{18}\text{O}$ of fracture-filling calcite, at 126°C (average calcite T_h) $\delta^{18}\text{O}_{\text{fluid}}$ would be $+9\text{‰}$ VSMOW, using calcite-water fractionation equation of Friedman and O'Neil (1977). From this calculation appears that fracture-filling calcite precipitated from ^{18}O enriched, hot, saline fluids with a salinity of about 18.6 wt. % equivalent NaCl. Enriched ^{18}O values of water and the high salinity of calcite fluid inclusions rule out any significant role for meteoric water and light carbon derived from soil CO_2 as a source of negative $\delta^{13}\text{C}$ in precipitation of fracture-filling calcite.

Common sources of ^{18}O -enriched waters are basinal brines, waters from gypsum dehydration, waters from salt dissolution, isotopic exchange reactions between waters and associated carbonate minerals, or mixtures of the above (e.g., Hitchon and Friedman, 1969; Knauth and Beeunas, 1986). The $\delta^{18}\text{O}$ values of basinal brine shift toward more positive values (up to $+10\text{‰}$ VSMOW) as temperature and salinity increase (Sheppard, 1986; Taylor, 1987).

Raman analysis of the fluid phase in hydrocarbon-bearing inclusions indicates the presence of saturated hydrocarbons, which is supported by fluorescence of these inclusions under UV light (Fig. 2.13C). The low $\delta^{13}\text{C}$ values ($<-10\text{‰}$) for oil field brines most likely result from sulfate reduction during bacterial or thermal degradation of organic matter (Carothers and Kharaka, 1980; Franks et al., 2001). The negative $\delta^{13}\text{C}$ values of fracture-filling calcite are interpreted to indicate the incorporation of carbon that was produced by the oxidation of hydrocarbons. In such a model, hydrocarbon oxidation

via thermal sulfate reduction (TSR) resulted in production of CO₂ that was incorporated into calcite characterized by low δ¹³C values.

The presence of native sulfur (Fig. 2.6C) and H₂S is consistent with this model as these are by-products of the oxidation process (Machel, 2001). Raman spectrometry of one phase (L) inclusions in celestine (Fig. 2.13E) indicates the presence of H₂S, reflecting derivation from thermal sulfate reduction, and TSR commonly occurs at temperature of about 100–140°C (Machel, 2001), consistent with the fluid inclusion estimates. If metals are present in the system, sulfide minerals could precipitate using the reduced sulfur derived from TSR. Small amounts of fine sphalerite and pyrite crystals in the host rock were likely formed by this mechanism.

The trapping temperature of fracture-filling calcite fluid inclusions (126 ± 24.5°C, n = 17) is significantly higher than the maximum estimated burial temperature (60°C) for Middle Devonian strata in southwestern Ontario. It suggests that hydrothermal fluids that carried hydrocarbons were responsible for precipitation of the fracture-filling calcite. Late stage fracture-filling calcite in the central part of the Michigan Basin also contains hydrocarbon bearing fluid inclusions (Luczaj et al., 2006). Fracture-filling saddle dolomite is also reported from the Dundee Formation in the central Michigan Basin (Luczaj et al., 2006). Fluid inclusion studies of this dolomite indicate that it precipitated from hot (about 135°C) and saline (31.6 wt. % NaCl) fluids (Luczaj et al., 2006).

If we consider an outward fluid flow from the deeper part of the basin, it is possible that the absence of saddle dolomite in fractures in the study area reflects loss of Mg during migration to the margin of the basin. This type of flow pattern is supported by studies that suggest that hydrocarbons from Devonian source rocks in the central part of the basin migrated toward the basin margin (Powell et al., 1984; Obermajer et al., 1997). Oil field brines commonly have high ⁸⁷Sr/⁸⁶Sr values relative to marine values of the same age (Barnaby et al., 2004). Radiogenic ⁸⁷Sr/⁸⁶Sr values of fracture-filling calcite (Fig. 2.10) further suggests a role for oil field brines in the precipitation of calcite. The lower salinity of calcite-hosted (19.7 ± 0.8 wt. % NaCl) relative to saddle dolomite-hosted

fluid inclusions in the center of the basin (31.6 wt. % NaCl) is possibly due to a higher proportion of meteoric water in brines towards the basin margin.

2.6.2.3 Significance of Celestine formation

Two principal mechanisms have been proposed for the origin of celestine deposits: (1) syngenetic precipitation of celestine from evaporating sea water, and (2) epigenetic replacement of carbonates and calcium sulfates by celestine (Hanor, 2004). Although the Lucas Formation sediments were deposited in an evaporative setting, occurrence of celestine in dissolution vugs associated with fluorite and native sulfur (Fig. 2.6C) and two phase fluid inclusions suggest an epigenetic origin for celestine.

The concentration of Sr in gypsum and anhydrite precipitated in marine environments varies from 2000–5000 ppm, respectively (Warren, 2006). Dissolution of gypsum or anhydrite can therefore create Sr-rich waters (Warren, 2006), and the Sr concentration of basinal brines significantly increases with salinity (Hanor, 2004). Evaporite dissolution also supplies SO_4 , which can combine with Sr to precipitate celestine, usually in a mixing zone between hypersaline brine and meteoric water (Kesler and Jones, 1981; Scholle et al., 1990; Warren, 2006, and references therein). As the solubility of celestine decreases with decreasing salinity (Reardon and Armstrong, 1987), celestine precipitates from fluids when dilution occurs. Dissolution of Middle Devonian evaporites is a potential source of sulfate and Sr for celestine precipitation.

Fluid inclusion homogenization temperatures for celestine-hosted inclusions are high, ranging from 118.2–321.8°C ($219.5 \pm 51^\circ\text{C}$, $n = 74$). These data represent a wide range of temperatures compared to those from fracture-filling calcite (Fig. 2.14) and are significantly higher than the estimated peak burial (60–80°C).

A fluid inclusion can potentially provide trapping temperature information when it is primary where three criteria are met: (1) it should be trapped as a homogeneous phase; (2) the inclusion volume must not have changed since trapping (other than normal thermal contraction of the host phase); and (3) no mass has been added or removed from the inclusion after trapping; if conditions 2 and 3 are violated, the inclusion is considered to

have re-equilibrated and will not provide PTX information that reflects the trapping conditions (Bodnar, 2003). With change in fluid inclusion volume, microthermometric behaviour of fluid inclusion will change. For example increase in volume without fluid loss results in lower density and increase in homogenization temperature (Bodnar, 2003).

A wide range in homogenization temperatures in a fluid inclusion assemblage (FIA) is an indication of fluid inclusion stretching (Bodnar, 2003). Although the range of variation in homogenization temperature in some fluid inclusion assemblages is low (121-135°C), the majority of FIAs show a wide range of homogenization temperatures (175-320°C). In addition, some celestine-hosted fluid inclusions appear to neck down and have experienced volume change (Fig. 2.13F). FIAs with lower homogenization temperature (121-135°C) overlap with homogenization temperatures from fracture-filling calcite (Fig. 2.14) and appear to show a reasonable range of trapping temperatures, which is significantly higher than peak burial temperature (60°C) and suggest involvement hydrothermal fluids in precipitation of celestine.

The mean salinity value of fluid inclusions hosted by celestine is 14.4 ± 1.8 eq. wt. % NaCl (n = 83), which is distinctly lower than the values for inclusions in fracture-filling calcite (Fig. 2.14). Given the fact that celestine postdates calcite in the paragenetic sequence (Fig. 2.7), these lower salinity values suggest that basinal brines were diluted with meteoric water and celestine precipitation as a result. Most modern basinal brines have depleted $\delta^{18}\text{O}$ values that represent the mixing of meteoric water with connate, seawater-derived brines (Kharaka and Hanor, 2005). The occurrence of celestine in dissolution vugs (Fig. 2.6) further supports the role of meteoric water in dilution of basinal brine and celestine precipitation. The occurrence of liquid H_2S in fluid inclusions of celestine suggests that the evolution of the mineralizing fluids was associated with the migration and maturation of hydrocarbons. Elemental sulfur usually forms when the system runs out of reactive hydrocarbons (Machel, 2001).

2.6.3 Rare earth elements (REE)

The rare earth element (REE) pattern of modern marine carbonates, including scleractinian corals (Wyndham et al., 2004) and microbialites (Webb and Kamber, 2000) resemble those of their ambient sea water (Webb et al., 2009). Numerous studies suggest

that carbonates preserve their REE composition during diagenesis, specifically dolomitization except in an open diagenetic system and/or a high water/rock ratio (Banner et al., 1988; Bau and Alexander, 2006; Webb et al., 2009; Allwood et al., 2010). However, the results of several recent studies indicates that diagenetic alteration may change these REE patterns and concentrations (Shields and Stille, 2001; Azmy et al., 2011), and therefore REE can be used as potential indicators of diagenetic redistribution of REE in carbonates (Azmy et al., 2011) and potentially the REE concentration of diagenetic mineral reflect the REE composition of diagenetic fluid (e.g., Azmy et al., 2011).

All samples exhibit seawater like REE_{SN} trend similar to those of modern warm water brachiopods and Devonian microbialites. This similar trend suggests that D1 and D2 and fracture-filling calcite have preserved their original seawater REE signature and had formed from basinal fluids that had a seawater precursor and were likely circulated in the crust.

The D1 and D2 have yielded higher average ΣREE (2.6 ± 2 and 6.7 ± 7.9 ppm, respectively) than those of the modern warm water brachiopods (0.3 ± 0.2 ppm; Azmy et al., 2011) but significantly lower than those of Devonian microbialites (Fig. 2.11) (20.1 ± 8.5 ppm, Nothdurft et al., 2004). It indicates that REE composition of fluid potentially control the REE composition of diagenetic minerals. The progressive enrichment in average ΣREE of diagenetic minerals (dolomite and calcite) and their similar REE_{SN} patterns suggest a common source of diagenetic fluid with increase in water/rock interaction ratio with progressive burial.

2.7 Conclusions

By combining of detailed field and core examination with petrographic, geochemical, and fluid inclusion analyses, several conclusions can be made regarding the diagenesis and mineralization of the Lucas Formation, as follows:

- 1) Petrographic and field evidence suggest that fine-crystalline dolomite (D1) of the Lucas Formation formed by an evaporative reflux mechanism and were modified diagenetically during later burial.

- 2) Calculated temperatures based on $\delta^{18}\text{O}$ values of dolomite (D1 and D2) suggest dolomite recrystallization took place at temperatures (67 to 98°C) higher than maximum burial temperature (60°C) in the presence of hydrothermal fluids. This resulted in their isotopic re-equilibration and modification at higher temperatures. The $^{87}\text{Sr}/^{86}\text{Sr}$ ratios of the dolomite also support the suggested recrystallization of dolomite.
- 3) The association of medium-crystalline (D2) dolomite with solution seams and stylolites suggests that D2 possibly formed in an intermediate burial setting at temperatures higher than those of near-surface conditions.
- 4) The fracture-filling late calcite precipitated from hydrothermal hydrocarbon-bearing fluids, with negative $\delta^{13}\text{C}$ values originated from TSR. Fluid inclusion data indicate that oil emplacement took place concurrently with the precipitation of late-stage calcite cement from hydrothermal fluids having moderate salinity (19.7 wt. % NaCl).
- 5) Hot fluids with lower salinity (14.5 wt. % NaCl) precipitated celestine which originated from thermochemical sulfate reduction and from mixing of saline, Sr- and sulfate-bearing brines with meteoric waters.
- 6) Variations of average ΣREE among diagenetic minerals and similarity of their REE_{SN} pattern suggest a common source of fluids with different degrees of water/rock interaction.
- 7) The diagenetic fluids could have originated from deeper parts of the basin and invaded Devonian carbonates through fractures and faults.

2.8 Acknowledgements

This work was supported by Natural Sciences and Engineering Research Council of Canada (NSERC) grants to I. Al-Aasm and Mario Coniglio. Special thanks to M. Price for running the samples for stable isotope ratios. Review comments and constructive suggestions by Professor F. Ghazban of the University of Tehran are acknowledged with thanks.

2.9 References

- Adams, J. E. and Rhodes, M. L., 1960. Dolomitization by seepage refluxion. American Association of Petroleum Geologists Bulletin 44, 1912-1920.
- Al-Aasm, I. S., 2000. Chemical and isotopic constrains for recrystallization of sedimentary dolomites from the Western Canadian Sedimentary Basin. Aquatic geochemistry 6, 227-248.
- Al-Aasm, I. S., Packard, J. J., 2000. Stabilization of early-formed dolomite: a tale of divergence from two Mississippian dolomites. Sedimentary Geology 131, 97-108.
- Al-Aasm, I. S., Taylor, B. E., South, B., 1990. Stable isotope analysis of multiple carbonate samples using selective acid extraction. Chemical Geology 80, 119-125.
- Allwood, A. C., Kamber, B. S., Walter, M. R., Burch, I. W., Kanik, I., 2010. Trace elements record depositional history of an Early Archean stromatolitic carbonate platform. Chemical Geology 270, 148–163.
- Armstrong, D. K., Carter, T. R. 2006. An updated guide to subsurface Paleozoic stratigraphy of southern Ontario. Ontario Geological Survey, Open File Report 6191, 214 p.
- Azmy, K., Brand, U., Sylvester, P., Gleeson, S. A., Logan, A., Bitner, M. A., 2011. Biogenic and abiogenic low-Mg calcite (bLMC and aLMC): Evaluation of seawater-REE composition, water masses and carbonate diagenesis. Chemical Geology, 280, 180–190.
- Banner, J. L., Hanson, G. N., Meyers, W. J., 1988. Rare earth element and Nd isotopic variations in regionally extensive dolomites from the Burlington–Keokuk Formation (Mississippian): implications for REE mobility during carbonate diagenesis. Journal of Sedimentary Petrology 58, 415–432.
- Barnaby, R. J., Oetting, G. C., Gao, G., 2004. Strontium isotopic signatures of oil-field waters: Applications for reservoir characterization. American Association of Petroleum Geologists Bulletin 88, 1677–1704.
- Bau, M., Alexander, M., 2006. Preservation of primary REE patterns without Ce anomaly during dolomitization of Mid-Paleoproterozoic limestone and the potential re-

- establishment of marine anoxia immediately after the “Great Oxidation Event”.
South African Journal of Geology, 109, 81-86.
- Bau, M., Dulski, P., 1996. Distribution of yttrium and rare-earth elements in the Penge and Kuruman iron-formations, Transvaal Supergroup, South Africa. Precambrian Research 79, 37–55.
- Birchard, M. C., 1990. Stratigraphy and Facies of the Middle Devonian Dundee Formation, S.W Ontario, unpublished MSc thesis.
- Birchard, M. C., 1993. Stratigraphy and facies of the Middle Devonian Dundee Formation. OGRG 340, Ontario Geological Survey, Open File Report 5848, 156 p.
- Birchard, M. C., Rutka, M. A., Brunton, F. R., 2004. Lithofacies and geochemistry of the Lucas Formation in the subsurface of Southwestern Ontario: A high purity limestone and Potential high purity dolostone resource. Ontario Geological Survey Open file report 6137, 180 p.
- Bodnar, R. J., 2003. Reequilibration of fluid inclusions. In: Fluid inclusions, Analysis and Interpretation. Samson, I., Anderson, A., Marshall, D. (Eds.) Mineralogical Association of Canada, Short course series 32, 213-231.
- Bradly, D. C., 1983. Tectonics of the Acadian orogeny in New England and adjacent Canada. Journal of Geology 91, 381-400.
- Brigham, R. J., 1971. Structural geology of southwestern Ontario and southeastern Michigan; Ontario Department of Mines and Northern Affairs, Paper 71-2, 110 p.
- Burke, E. A. J., 2001. Raman microspectrometry of fluid inclusions. Lithos 55, 139-158.
- Carballo, J. D., Land, L. S., Miser, D. E., 1987. Holocene dolomitization of supratidal sediments by active tidal pumping, Sugarloaf Key Florida. Journal of Sedimentary Petrology 57, 153-165.
- Carlson, E. H., 1983. The occurrence of Mississippi Valley Type mineralization in northwestern Ohio. In: International conference on Mississippi Valley Type Lead-Zinc deposits, University of Missouri-Rolla, 424-435.
- Carothers, W. W., Kharaka, Y. K., 1980. Stable carbon isotopes of HCO₃ in oil-field waters-implication for origin of CO₂. Geochimica et Cosmochimica Acta, 44, 323-332.

- Cercone, K. R., 1984. Thermal history of Michigan Basin, The American Association of Petroleum Geologists Bulletin 68, 130-136.
- Cercone, K. R., Pollack, H. N., 1991. Thermal maturity of the Michigan Basin. In: Early sedimentary evolution of the Michigan Basin. Catacosinos, P. A., Daniels Jr. P.A. (Eds.), Geological Society of America, Special Paper 256, 1–11.
- Chaudhuri, S., Clauer, N., 1992. In: Clauer, N., Chaudhuri, S. (Eds.), Isotopic Signatures and Sedimentary Records. Lecture Notes in Earth Sciences 43, 497-529.
- Coniglio, M., R. Sherlock, Williams-Jones, A. E., Middleton, K., Frape, S. K., 1994. Burial and hydrothermal diagenesis of Ordovician carbonates from the Michigan Basin, Ontario, Canada. In: Purser, B., Tucker, M., Zenger, D. (Eds.). Dolomites a volume in honour of Dolomieu. Special Publications of the International Association of Sedimentologists 21, 231-254.
- Crowley, K. D., 1991. Thermal history of Michigan Basin and southern Canadian Shield from apatite fission track analysis. Journal of Geophysical Research 96, 697–711.
- Denison, R. E., Koepnick, R.B., Burke, W.H., Hetherington, E.A., Fletcher, A., 1997. Construction of the Silurian and Devonian $^{87}\text{Sr}/^{86}\text{Sr}$ curve. Chemical Geology 140, 109-121.
- Diener, A., Ebner, S., Veizer, J., Buhl, D., 1996. Strontium stratigraphy of Middle Devonian: Brachiopods and conodonts. Geochimica et Cosmochimica Acta 60, 639-652.
- Dutton, B. C., 1985. Sedimentology and Diagenesis of the Middle Devonian Dundee Formation in South Lambton and West Middlesex Counties, Southwestern Ontario, Canada. Unpublished MSc thesis.
- Fargerstrom, J. A., 1983. Petrology and regional significance of a Devonian carbonate/evaporate complex, eastern Michigan Basin. Journal of Sedimentary Petrology 53, 295-317.
- Franks, S. G., Dias, R. F., Freeman, K. H., Boles, J. R., Holba, A., Fincannon, A. L., Jordan, E. D., 2001. Carbon isotopic composition of organic acids in oil field waters, San Joaquin Basin, California, USA. Geochimica et Cosmochimica Acta 65, 1301-1310.

- Friedman, I., O'Neil, J. R., 1977. Compilation of stable isotope fractionation factors of geochemical interest: U.S. Geological Survey Professional Paper 440-kk, 108 p.
- Fritz, P., Smith, D. C. W., 1970. The isotopic composition of secondary dolomites: *Geochimica et Cosmochimica Acta* 34, 1161-1173.
- Fu, Q., Qing, H., Bergman, K. M., 2006. Early dolomitization and recrystallization of carbonate in an evaporite basin: the Middle Devonian Ratner laminite in southern Saskatchewan, Canada. *Journal of the Geological Society London* 163, 937-948.
- Gao, G., Land, L. S., 1991. Early Ordovician cool creek dolomite, middle arbuckle group, Slick Hills, SW Oklahoma, U.S.A.: origin and modification. *Journal of Sedimentary Petrology* 61, 161-173.
- Gardner, W. C., 1974. Middle Devonian stratigraphy and depositional environments in the Michigan Basin. Michigan Basin Geological Society, Special Papers 1, 138 p.
- Geldern, R. a, Joachimski, M. M., Day, J., Jansen, U., Alvarez, F., Yolkin, E. A., Ma, X. P., 2006. Carbon, oxygen and strontium isotope records of Devonian brachiopod shell calcite. *Paleogeography, Paleoclimatology, Paleoecology* 240, 47-67.
- Goldstein, R. H., 2003, Petrographic analysis of fluid inclusions, In: Samson, I., Anderson, A., Marshall, D. (Eds.) *Fluid inclusions, Analysis and Interpretation*. Mineralogical Association of Canada, Short course series 32, 9-53.
- Gonfiantini, R. 1986. Environmental isotopes in lake studies. In: Fritz, P., Fontes, J. C. (Eds.) *Handbook of Environmental Isotope Geochemistry*. Amsterdam, Elsevier, p. 113-168.
- Gregg, J. M., Shelton, K. L., 1990. Dolomitization and dolomite neomorphism in the back reef facies of the Bonneterre and Davis formations Cambrian, Southeastern Missouri. *Journal of Sedimentary Petrology* 60, 549-562.
- Gregg, J. M., Sibley, D. F., 1984. Epigenetic dolomitization and the origin of xenotopic dolomite texture. *Journal of Sedimentary petrology* 54, 908-931.
- Hamilton, G. D., 1991. Styles of reservoir development in Middle Devonian carbonates of southwestern Ontario. Unpublished MSc thesis.
- Hamilton, G. D., 2004. Middle Devonian Reservoirs of Ontario. Ontario oil and gas, OPI publication, p. 5-7.

- Hanor, J.S., 2004. A Model for the origin of large Carbonate- and Evaporite-Hosted celestine (SrSO_4) deposits. *Journal of Sedimentary Research* 74, 168-175.
- Hardie, L.A., 1987. Dolomitization: A critical view of some current views: *Journal of Sedimentary Research* 57, 166-183.
- Hitchon, B., Friedman, L., 1969. Geochemistry and origin of formation waters in the western Canadian sedimentary basin. I. Stable isotopes of hydrogen and oxygen. *Geochimica Cosmochimica Acta* 33, 1321-1349.
- Hobbs, M. Y., Frapce, S. K., Shouakar-Stash, O., Kennell, L. R., 2011. Regional hydrogeochemistry- Southern Ontario. Nuclear Waste Management Organization Report, 157.
- Johnson, M. D., Armstrong, D. K., Sanford, B. V., Telford, P. G., Rutka, M. A., 1992. Paleozoic and Mesozoic geology of Ontario. In: *Geology of Ontario*, Ontario Geological Survey, Special Volume 4, Part 2, 907-1008.
- Kesler, S. E., Jones, L. M., 1981. Sulfur and strontium geochemistry of celestine, barite and gypsum from the Mesozoic basins of northern Mexico. *Chemical Geology* 31, 211-224.
- Kharaka, Y. K., Hanor, J. S., 2005. Deep fluids in the Continents: 1. Sedimentary Basins. In: Drever, J. I. (Ed.), *Treatise on Geochemistry, Surface and Groundwater, Weathering, and Soils* 5, 499-540.
- Knauth, L. P., Beeunas, M. A., 1986. Isotope geochemistry of fluid inclusions in Permian halite with implications for the isotopic history of ocean water and origin of saline formation waters. *Geochimica et Cosmochimica Acta* 50, 419-433.
- Kupez, J. A., Land, L. S., 1994. Progressive recrystallization and stabilization of early-stage dolomite: Lower Ordovician El-lenburger Group, West Texas. In: Purser, B., Tucker, M., Zenger, D. (Eds.), *Dolomites a volume in honour of Dolomieu*. International Association of Sedimentology Special Publication 21, 255-279.
- Land, L. S., 1980, The isotopic and trace element geochemistry of dolomite: The state of the art. In: Zenger, D. H., Dunham, J. B., Ethington., R. L. (Eds.), *Concepts and*
- Lazorek, M., Carter, T., 2008. The oil and gas plays of Ontario. *Ontario Oil and Gas Journal*, June, 18-23.

- Legall, F. D., Barnes, C. R., Macqueen, R. W., 1981. Thermal maturation, burial history and hotspot development, Paleozoic strata of southern Ontario-Quebec, from conodont and acritarch colour alteration index. *Bulletin of Canadian Petroleum Geology* 29, 492-539.
- Luczaj, J. A., Harrison III, W. B., Williams, N. S., 2006, Fractured hydrothermal dolomite reservoirs in the Devonian Dundee Formation of the central Michigan Basin. *American Association of Petroleum Geologists Bulletin* 90, 1787–1801.
- Ma, L., Castro, M. C., Hall, C. M., 2009. Atmospheric noble gas signatures in deep Michigan Basin brines as indicators of a past thermal event. *Earth and Planetary Science Letters* 277, 137-147.
- Machel, H. G., 1997. Recrystallization versus neomorphism, and the concept of “significant recrystallization” in dolomite research. *Sedimentary Geology* 113, 161-168.
- Machel, H. G., 2001. Bacterial and thermochemical sulfate reduction in diagenetic setting – old and new insights. *Sedimentary Geology* 140, 143-175.
- Machel, H.G., 2004. Concepts and models of dolomitization: a critical reappraisal. In: Braithwaite, C.J.R., Rizzi, G., Darke, G. (Eds.), *The geometry and petrogenesis of dolomite hydrocarbon reservoirs*. Geological Society Special Publication 245, 7-63.
- Major, R. P., Lloyd, R. M., Lucia, F. J., 1992. Oxygen isotope composition of Holocene dolomite formed in a humid hypersaline setting. *Geology* 20, 586-588.
- Mazzullo, S. J., 1992, Geochemical and neomorphic alteration of dolomite: A review. *Carbonates and Evaporites* 7, 21-37.
- McKenzie, J. A., 1981, Holocene dolomitization of calcium carbonate sediments from the coastal sabkhas of Abu Dhabi, UAE: a stable isotope study. *The Journal of Geology* 89, 185-198.
- Montanez, I. P., Read, J. F., 1992. Fluid-rock interaction history during stabilization of early dolomites, upper Knox Group (Lower Ordovician), U.S. Appalachians. *Journal of Sedimentary Petrology* 62, 753-778.
- Nothdurft, L. D., Webb, G. E., Kamber, B. S., 2004. Rare earth element geochemistry of Late Devonian reefal carbonates, Canning Basin, Western Australia: confirmation

- of a seawater REE proxy in ancient limestones. *Geochimica et Cosmochimica Acta*, 68, 263-283.
- Nunn, J. A., Sleep, N. H., Moore, W. E., 1984. Thermal subsidence and generation of hydrocarbons in Michigan Basin. *The American Association of Petroleum Geologists Bulletin* 68, 296-315.
- Obermajer, M., Fowler, M. G., Goodarzi, F., Snowdon, L. R., 1997. Organic petrology and organic geochemistry of Devonian black shales in southwestern Ontario, Canada. *Organic Geochemistry* 26, 229-246.
- Powell, T. G., Macqueen, R. W., Barker, J. F., Bree, D. G., 1984. Geochemical character and origin of Ontario oils. *Bulletin of Canadian Petroleum Geology* 32, 289-312.
- Qing, H., 1998. Petrography and geochemistry of early-stage, fine- and medium-crystalline dolomites in the Middle Devonian Presqu'ile Barrier at Pine Point, Canada. *Sedimentology* 45, 433-446.
- Quinlan, G. M., Beaumont, C., 1984. Appalachian thrusting, lithospheric flexure, and the Paleozoic stratigraphy of eastern interior on North America. *Canadian Journal of Earth Sciences* 21, 973-996.
- Reardon, E. J., Armstrong, D. K., 1987. Celestine (SrSO₄) solubility in water, seawater and NaCl solution. *Geochimica et Cosmochimica Acta* 51, 63-72.
- Sanford, B. V., 1993. St. Lawrence Platform: geology; In: Scott, D. F., Aitken, J.D. (Eds.), *Sedimentary Cover of the Craton in Canada*. Geological Survey of Canada, *Geology of Canada Series* 5, 723-786.
- Sanford, B. V., Thomson, F. J., McFall, G. H., 1985. Plate tectonics – a possible controlling mechanism in the development of hydrocarbon traps in southwestern Ontario. *Bulletin of Canadian Petroleum Geology* 33, 52-71.
- Scholle, P. A., Stemmerik, L., Harpoth, O., 1990. Origin of major karst-associated celestine mineralization in Karstrynggen, Central East Greenland. *Journal of Sedimentary Petrology* 60, 397-410.
- Sheppard, S. M. F., 1986, Characterization and isotopic variations in natural waters. In: Valley, J. W., Taylor, H. P., O'Neil, J. R. (Eds.), *Stable Isotopes in High Temperature Geochemical Processes*. *Reviews in Mineralogy* 16, 165-183.

- Shields, G., Stille, P., 2001. Diagenetic constraints on the use of cerium anomalies as paleoseawater redox proxies: an isotopic and REE study of Cambrian phosphorites. *Chemical Geology* 175, 29–48.
- Smith, T. M., Dorobek, S.L., 1993. Alteration of early-formed dolomite during shallow to deep burial: Mississippian Mission Canyon Formation, central to southwestern Montana. *Geological Society of America Bulletin* 105, 1389–1399.
- Sofer, Z., Gat, J. R., 1975. The isotope composition of evaporating brines: effect of the isotopic activity ratio in saline solutions. *Earth and Planetary Science Letters*, 26, 179-186.
- Stueber, A. M. Pushkar, P., Hetherington, E. A., 1987. A strontium isotopic study of formation waters from Illinois Basin, USA. *Applied Geochemistry* 2, 477-494.
- Taylor, B. E., 1987. Stable isotope geochemistry of ore-forming fluids. In: Kyser, T. K. (Ed.), *Short Course in Stable Isotope Geochemistry of Low Temperature Fluids* 13. Mineralogical Association of Canada, 337-418.
- Taylor, T. R., Sibley D. E., 1986. Petrography and origin of ferroan dolomite in the Trenton Formation, Ordovician, Michigan Basin, U.S.A. *Sedimentology* 33, 61-86.
- Tissot, B. P., Welte, D. H., 1984. *Petroleum Formation and Occurrence, A New Approach to Oil and Gas Exploration*: New York, Springer-Verlag, 538p.
- Van der Voo, R., 1988. Paleozoic paleogeography of North America, Gondwana, and intervening displaced terranes: Comparisons of paleomagnetism with paleoclimatology and biogeographical patterns. *Geological Society of America Bulletin* 100, 311-324.
- Veizer, J., Ala, D., Azmy, K., Bruckschen, P., Buhl, D., Bruhn, F., Carden, G. A. F., Diener, A., Ebner, S., Godderis, Y., Jasper, T., Korte, C., Pawellek, F., Podlaha, O. G., Strauss, H., 1999. $^{87}\text{Sr}/^{86}\text{Sr}$ and $\delta^{13}\text{C}$ and $\delta^{18}\text{O}$ evolution of Phanerozoic seawater. *Chemical Geology* 161, 59-88.
- Vugrinovich, R., 1988. Shale compaction in the Michigan Basin: estimates of former depth of burial and implications for paleogeothermal gradients. *Bulletin of Canadian Petroleum Geology* 36, 1-8.
- Warren, J. K., 2006. *Evaporites, sediments, resources and hydrocarbons*, Springer-Verlag, 1035 p.

- Webb, G. E., Kamber, B. S., 2000. Rare earth elements in Holocene reefal microbialites: a new shallow seawater proxy. *Geochimica et Cosmochimica Acta* 64, 1557–1565.
- Webb, G. E., Nothdurft, L. D., Kamber, B. S., Kloprogge, J. T., Zhao, J.-X., 2009. Rare earth element geochemistry of scleractinian coral skeleton during meteoric diagenesis: a before and-after sequence through neomorphism of aragonite to calcite. *Sedimentology* 56, 1433–1463.
- Wyndham, T., McCulloch, M., Fallon, S., Alibert, C., 2004. High-resolution coral records of rare earth elements in coastal seawater: biogeochemical cycling and a new environmental proxy. *Geochimica et Cosmochimica Acta* 68, 2067–2080.
- Zhang, N., Tian, Z., Leng, Y. Y., Wang, H., Song, F., Meng, J., 2007. Raman characteristics of hydrocarbon and hydrocarbon inclusions. *Science in China D series* 50, 1171-1178.

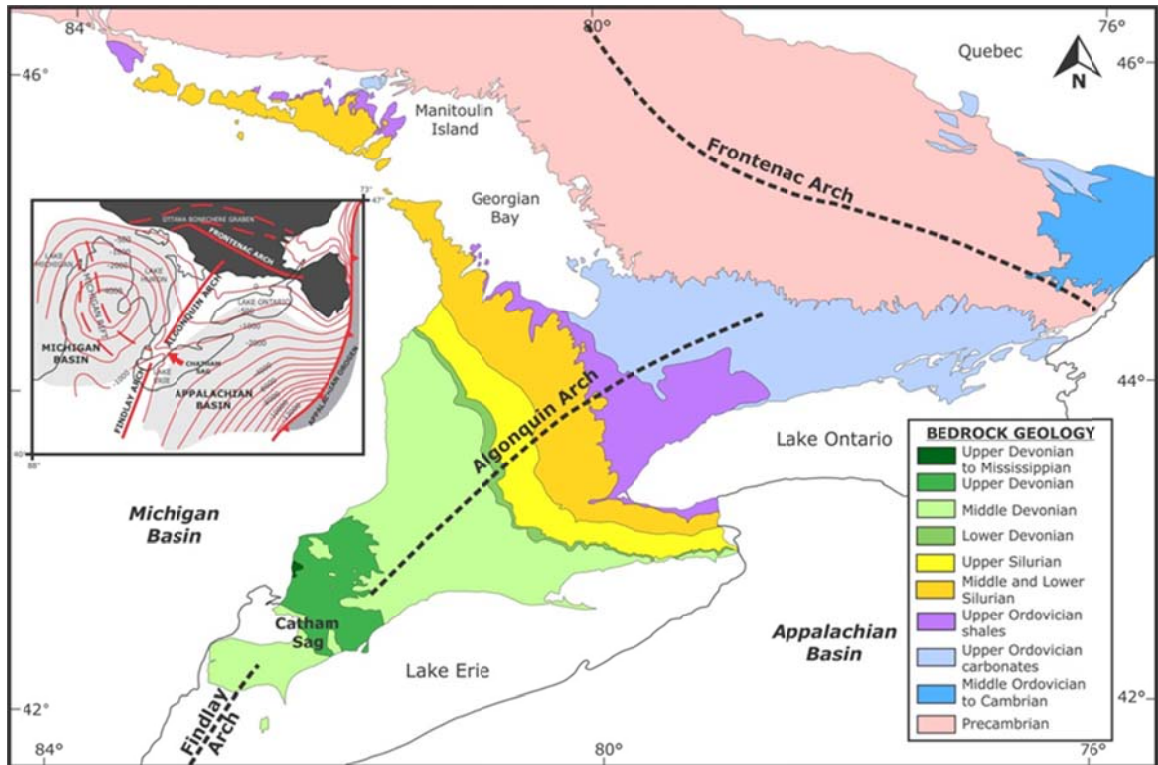


Figure 2.1 Generalized Paleozoic bedrock geology map of southern Ontario (adapted from Armstrong and Carter, 2006). Inset shows generalized basement structural contours (meters above sea level datum) and location of structural arches and basins (adapted from Johnson et al., 1992).

Geologic Time		Stratigraphic Nomenclature	
Period	Epoch	Group	Formation
Devonian	Middle	Traverse Group	Arkona
			Rockport Quarry
			Bell
		Detroit River Group	Marcellus
			Dundee
			LUCAS
	Lower	Detroit River Group	Amherstburg
			Sylvania
			Bois Blanc

Figure 2.2 Middle Devonian stratigraphy of southwestern Ontario (adapted from Birchard et al., 2004).

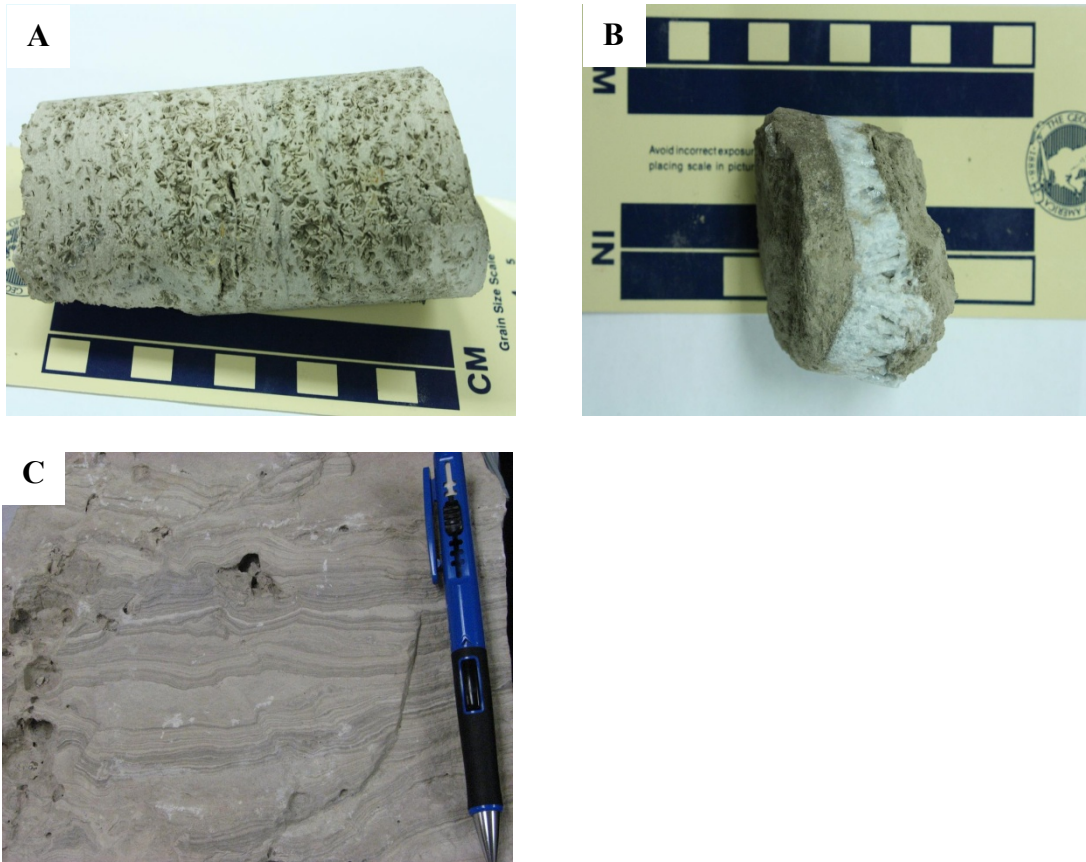


Figure 2.3 Core photographs of Middle Devonian rocks, southwestern Ontario, (A) Needle-shaped dissolution molds of evaporate minerals in groundmass of dolomite, (B) Anhydrite interlayer in dolomite, Domtar Goderich, St. 1, (C) Stromatolitic laminations in Lucas Formation, McGregor quarry.

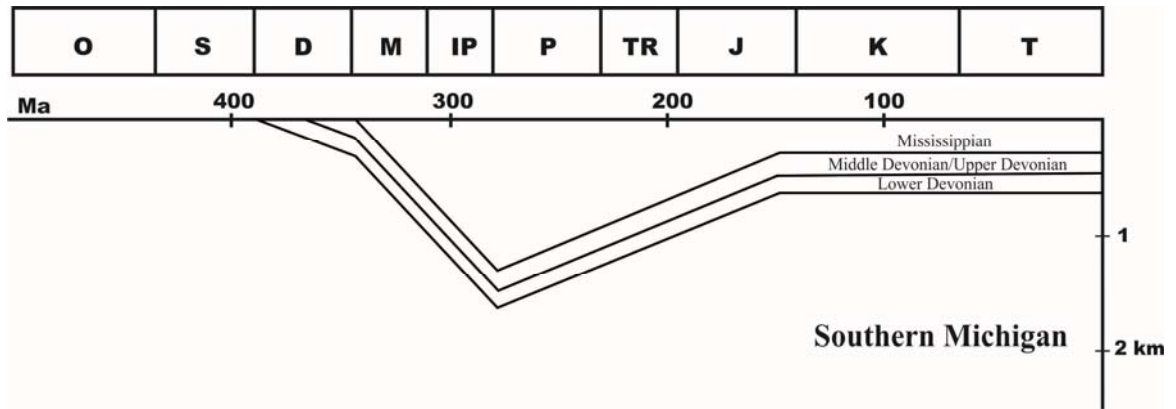


Figure 2.4 Burial history curve for the southern Michigan Basin (adapted from Cercone, 1984).

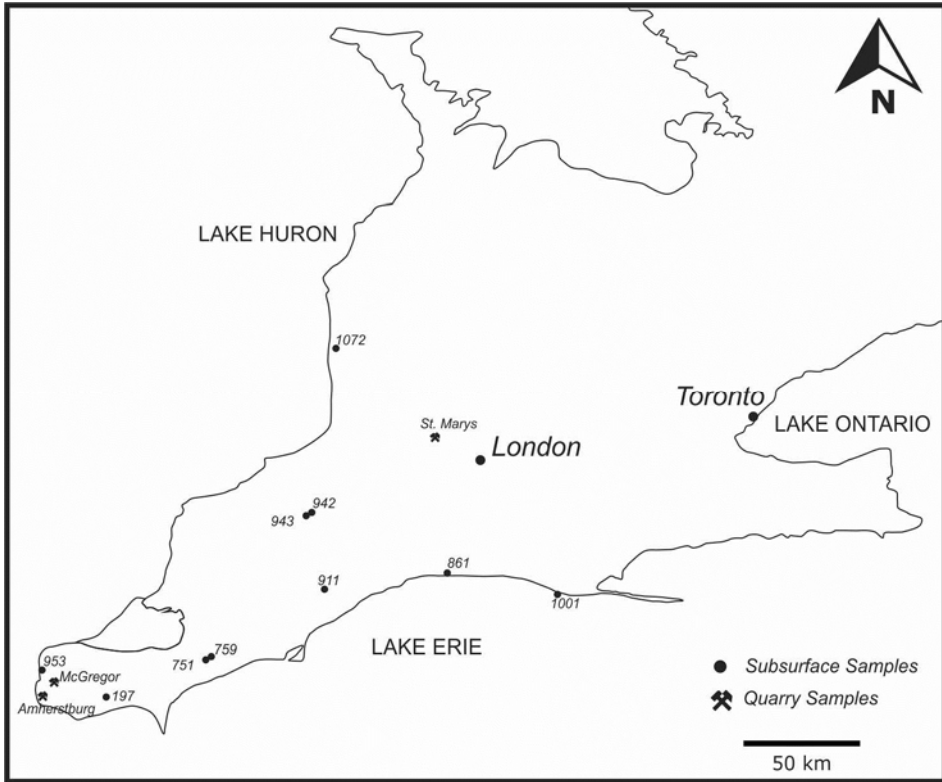


Figure 2.5 Sample location map.

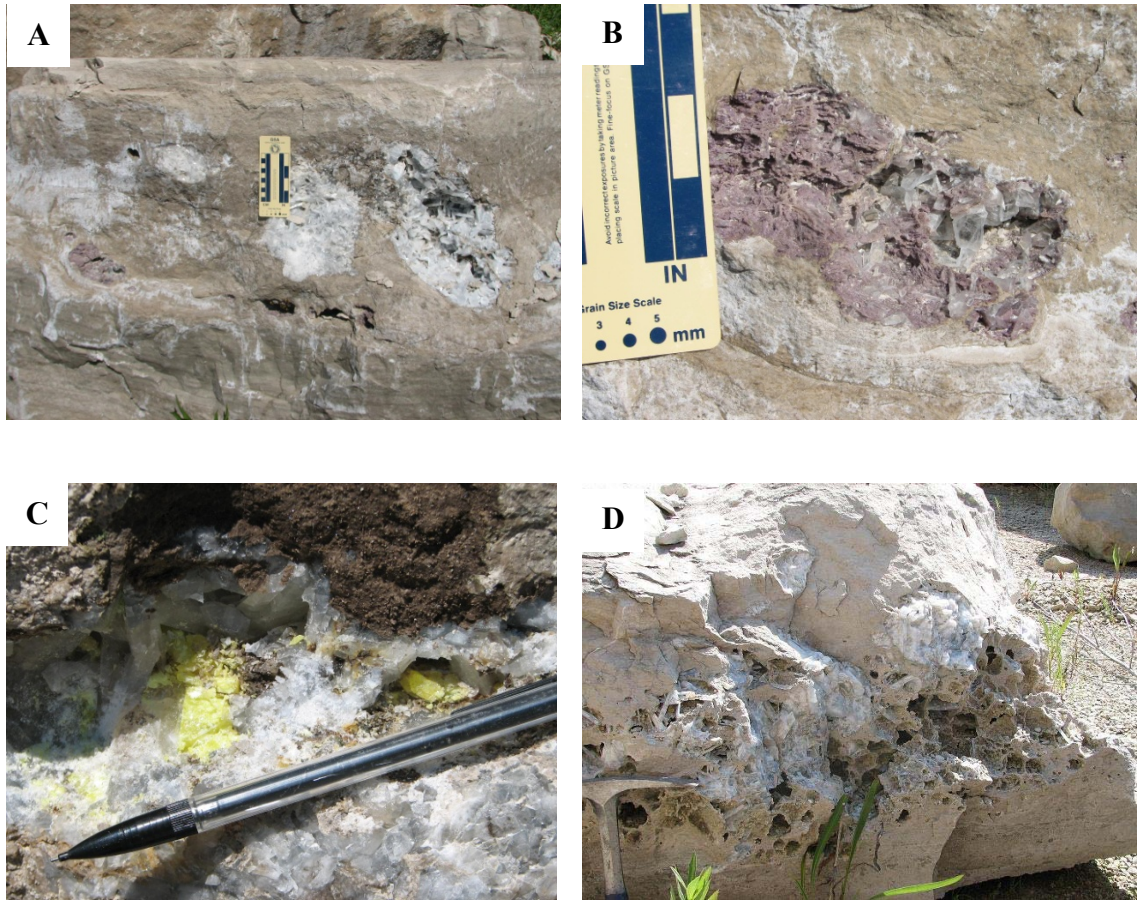


Figure 2.6 Cavities in host rock dolomite filled with (A) bladed crystals of celestine, (B) bladed crystals of celestine and fine crystalline fluorite, (C) Celestine and native sulfur, and (D) bladed celestine.

Diagenetic events	Early (Marine)	Late (Burial)
Fibrous calcite cement	Early (Marine)	
Syntaxial calcite cement	Early (Marine)	
Equant calcite cement	Early (Marine)	
Fine-crystalline dolomite (D1)	Early (Marine)	
Stylolites	Early (Marine)	
Medium-crystalline dolomite (D2)	Early (Marine)	
Fracturing	Early (Marine)	
Dissolution	Early (Marine)	
Fracture-filling calcite	Early (Marine)	
Hydrocarbon migration	Early (Marine)	
Sulfide mineralization	Early (Marine)	
Celestine	Early (Marine)	
Sulfur	Early (Marine)	
Fluorite	Early (Marine)	

Figure 2.7 Paragenetic sequence of the Lucas Formation in southwestern Ontario.

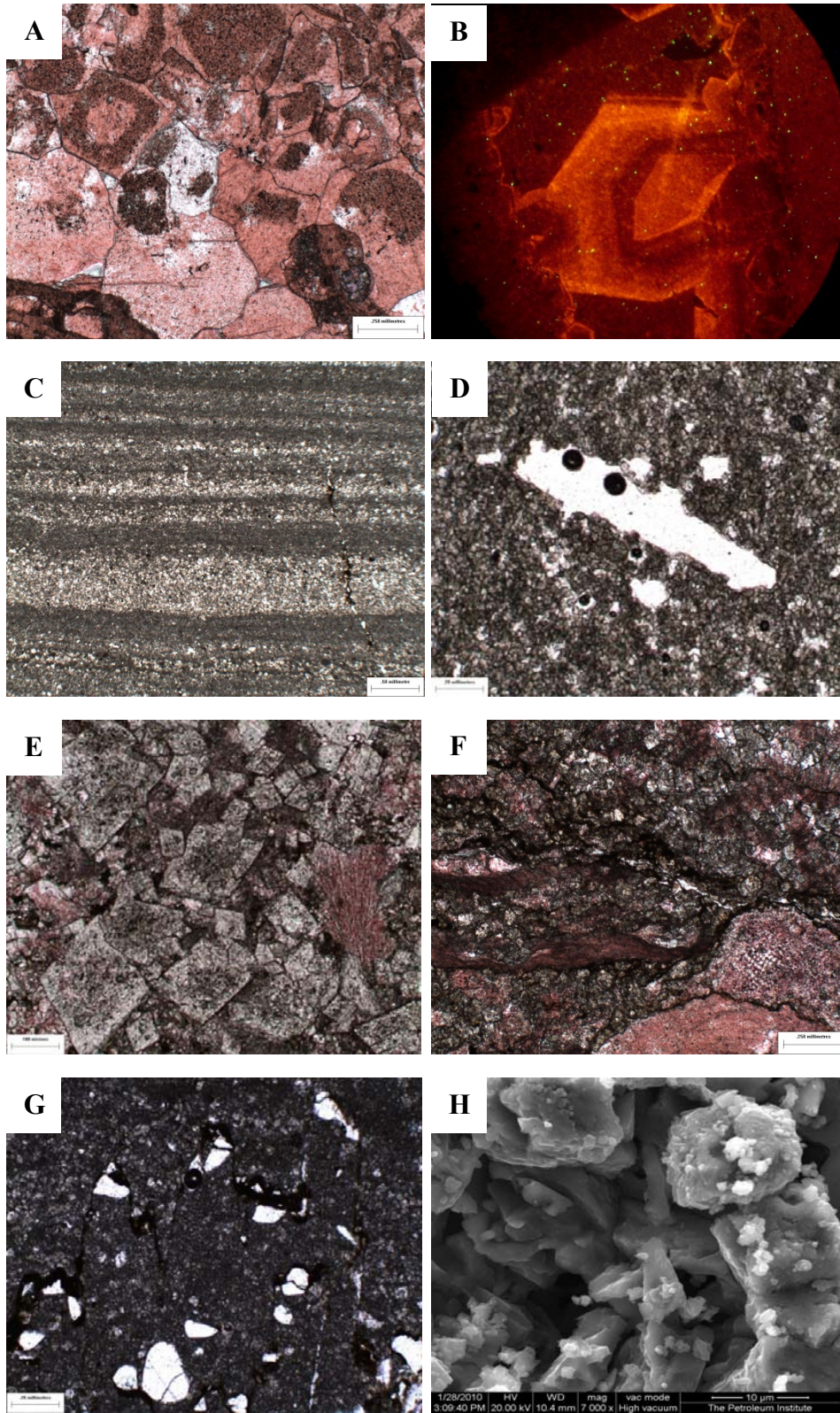


Figure 2.8 Photomicrographs of Middle Devonian rocks (A) Syntaxial and equant calcite cement, Consumers 33407, depth 98 m, scale bar 500 μm , (B) Calcite filled fracture, cathodoluminescence image, showing different generations of calcite cement, OGS 82-3,

depth 132.8 m, scale bar 100 μm , (C) Fine crystalline dolomite and preserved fine lamination of precursor lime mudstone, scale bar 500 μm , (D) Fine crystalline dolomite, with an elongated mold of an evaporite mineral, Domtar Goderich St. #1, depth 120.4 m, scale bar, 200 μm (E) Medium crystalline dolomite with cloudy center and clear rim, McGregor quarry, scale bar, 100 μm , (F) Medium crystalline, associated with solution seams in a Stromatoporoid floatstone, McGregor quarry, scale bar 250 μm , (G) High amplitude stylolites cross cut fine crystalline dolomite, McGregor quarry, scale bar 200 μm , (H) SEM photomicrograph of fine crystalline dolomite. The inter-crystalline microporosity developed as a result of dolomitization.

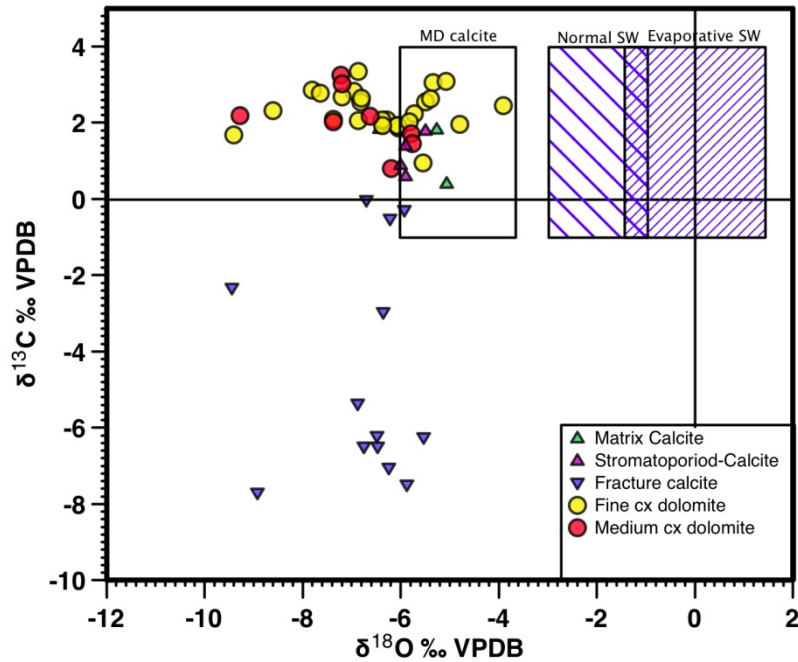


Figure 2.9 Cross plot of stable oxygen and carbon isotopic values for the Lucas Formation, southwestern Ontario. Boxes show the range of $\delta^{18}\text{O}$ and $\delta^{13}\text{C}$ for Middle Devonian marine calcite (Veizer et al., 1999), estimated $\delta^{18}\text{O}$ and $\delta^{13}\text{C}$ values for dolomite precipitated from Middle Devonian seawater (Qing, 1998; Fu et al., 2006), and estimated $\delta^{18}\text{O}$ and $\delta^{13}\text{C}$ values for dolomite precipitated from evaporated Middle Devonian sea water.

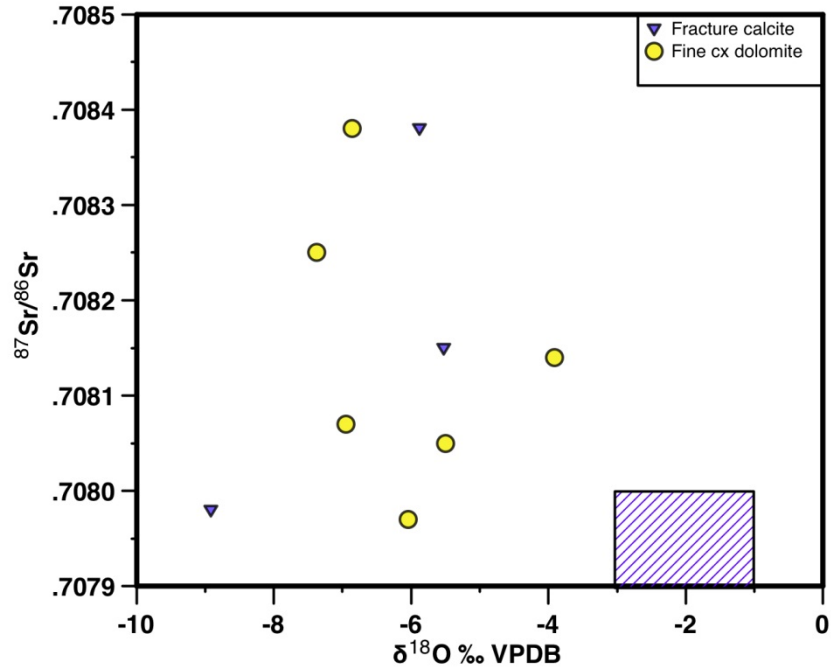


Figure 2.10 $^{87}\text{Sr}/^{86}\text{Sr}$ ratio vs. $\delta^{18}\text{O}$ values of fine crystalline dolomite and fracture-filling calcite. Hatched box encloses the estimated strontium isotope value of Middle Devonian seawater (Denison et al., 1996; Veizer et al., 1999; Geldren et al., 2006) and the estimated $\delta^{18}\text{O}$ value of dolomite precipitated from Middle Devonian seawater (Qing, 1998; Fu et al., 2006).

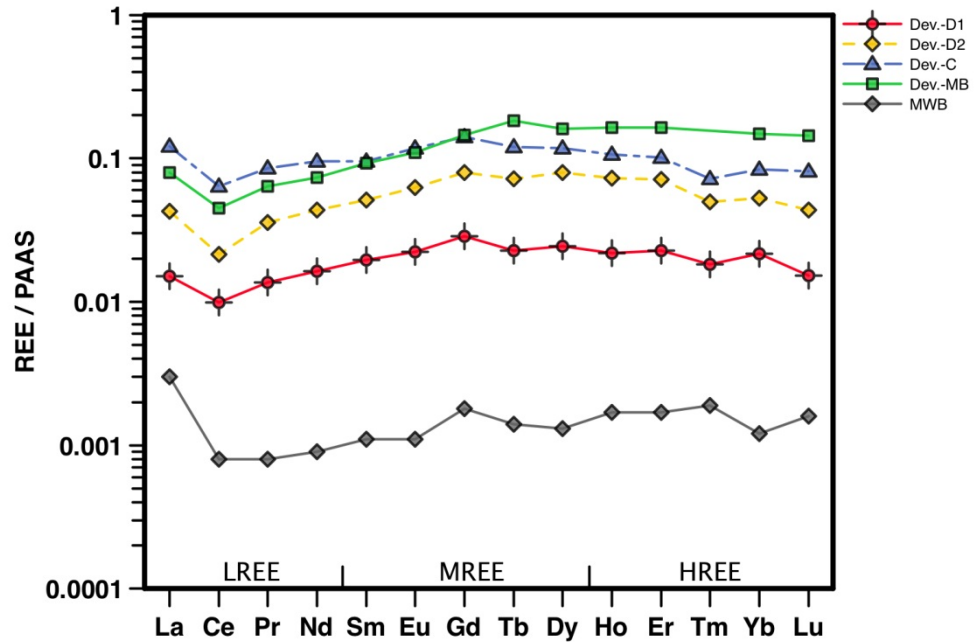


Figure 2.11 PAAS normalized REE pattern for average values of fine (D1) and medium (D2) crystalline dolomite and fracture-filling calcite (LC) samples. Average PAAS normalized REE pattern of modern warm water brachiopods (MWB; Azmy et al., 2011), and Devonian microbialites (Dev.-MB; Nothdurft et al., 2004) shown for comparison.

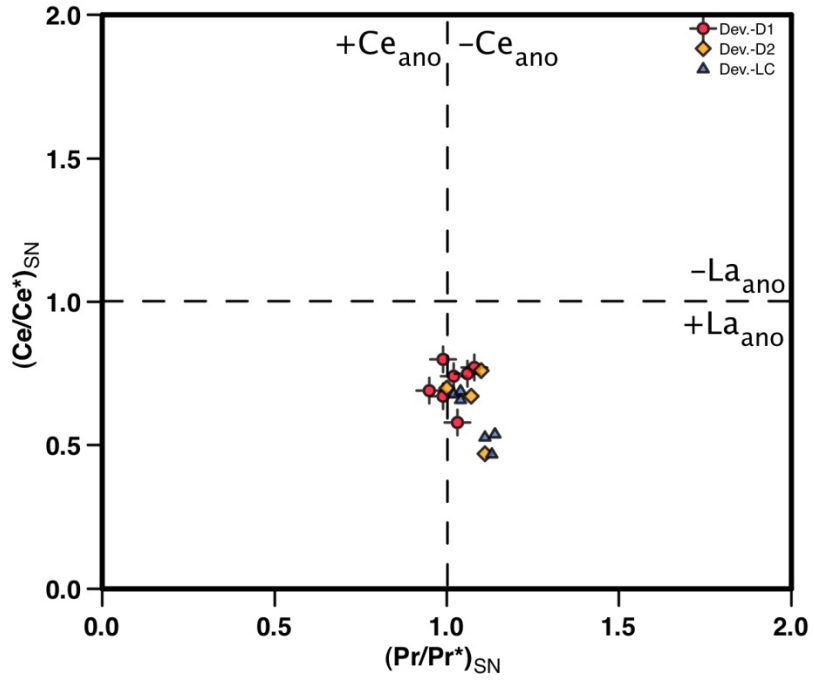


Figure 2.12 Ce $(Ce/Ce^*)_{SN}$ -La $(Pr/Pr^*)_{SN}$ anomaly cross plot of D1, D2 and fracture-filling calcite (LC) samples.

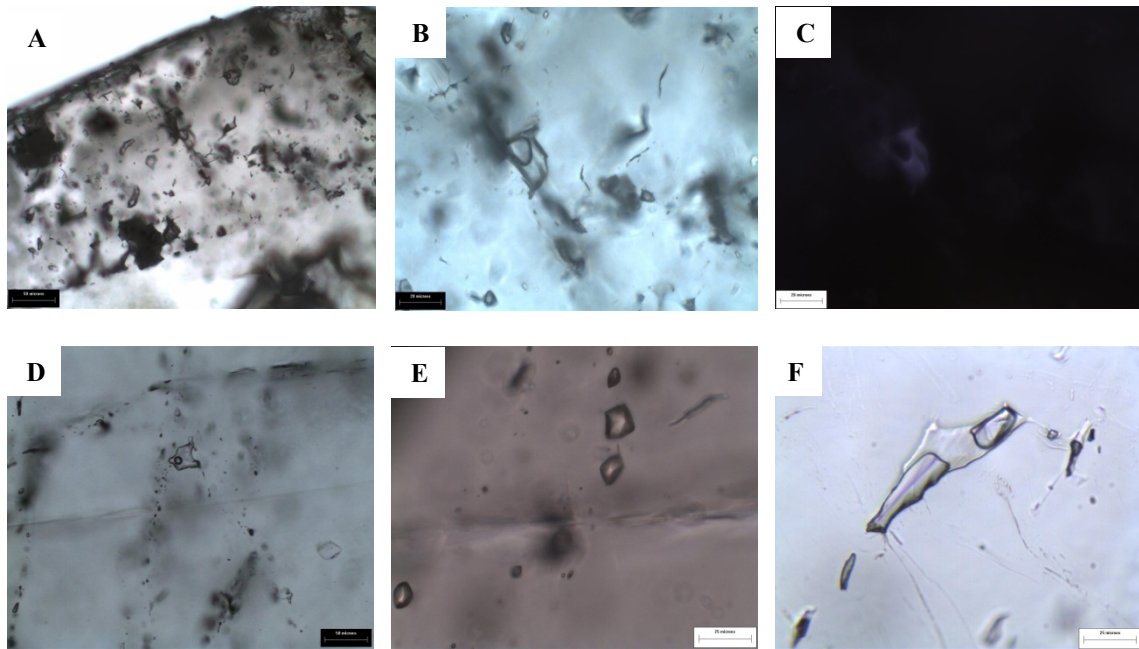


Figure 2.13 Photomicrograph of fluid inclusions in calcite and celestine; (A) Primary two phase (liquid vapour) fluid inclusions aligned along growth band in calcite, scale bar, 50 μm , (B) Closer view of A, scale bar 20 μm , (C) The same fluid inclusion under ultra violet light (UV), the liquid part of fluid inclusion fluoresce under UV light, (D) Isolated primary fluid inclusion in celestine surrounded by smaller secondary inclusions, scale bar 50 μm , (E) One phase (L) fluid inclusions in celestine, scale bar 25 μm , (F) Stretched fluid inclusion in celestine, scale bar 25 μm .

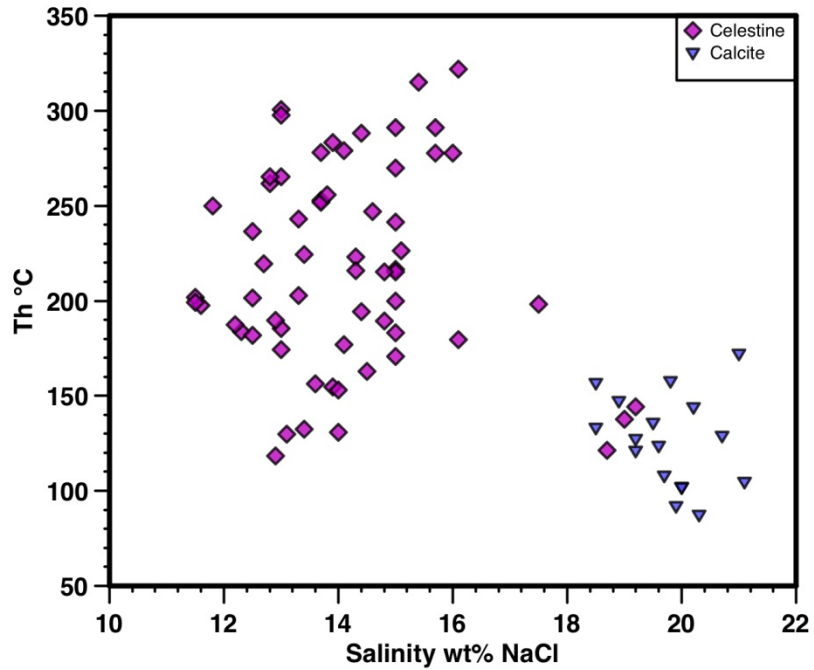


Figure 2.14 Homogenization temperatures and salinities of primary fluid inclusions in fracture-filling calcite and celestine. Celestine fluid-inclusion homogenization temperatures display a wide range of temperatures including very high temperature which is an indication of re-equilibration. There is a decreasing trend in salinity from calcite to celestine.

Table 2.1 Carbon and oxygen isotopic composition of replacive dolomite and fracture-filling calcite and the calcitic components of the Lucas Formation.

Lab ID	Sample ID	Age	Mineral	$\delta^{13}\text{C}\text{‰ VPDB}$	$\delta^{18}\text{O}\text{‰ VPDB}$	$^{87}\text{Sr}/^{86}\text{Sr}$	Reference
09-583	1010	Devonian	D1	2.5	-5.5	0.70805	
09-580	1011	Devonian	D1	3.1	-5.3		
09-581	1018	Devonian	D1	2.3	-8.6		
09-570	1023	Devonian	D1	2.9	-7.8		
09-582	1024	Devonian	D1	2.6	-5.4		
09-586	1054	Devonian	D1	2.8	-6.9	0.70807	
09-574	1016-1	Devonian	D1	2.2	-5.7		
09-079	AM010	Devonian	D1	2.8	-7.6		
09-080	AM013	Devonian	D1	2.5	-6.8		
09-272	AM014	Devonian	D1	3.3	-6.9		
09-081	AM015-2	Devonian	D1	1.7	-9.4		
09-095	AM016	Devonian	D1	3.1	-5.1		
09-082	AM018	Devonian	D1	2.7	-7.2		
09-270	AM024-1	Devonian	D1	2.6	-6.8		
09-281	AM025-2	Devonian	D1	1.9	-6.0	0.70797	
09-271	MG007	Devonian	D1	2.4	-3.9	0.70814	
09-226	MG017-2	Devonian	D1	2.1	-6.9	0.70838	
09-280	MG021-1	Devonian	D1	2.1	-6.3		
09-273	MG022	Devonian	D1	1.9	-6.1		
09-277	MG023	Devonian	D1	2.0	-4.8		
09-282	MG026	Devonian	D1	2.1	-6.4		
09-279	MG027	Devonian	D1	2.1	-7.4	0.70825	
09-225	MG044	Devonian	D1	1.9	-6.1		
09-278	MG024-2	Devonian	D1	2.0	-5.8		
09-585	SM-2	Devonian	D1	0.9	-5.5		
09-084	AM030-1	Devonian	D1	1.9	-6.4		
09-227	MG032-1	Devonian	D2	1.7	-5.8		
09-576	1056	Devonian	D2	3.2	-7.2		
09-584	1004	Devonian	D2	2.2	-9.3		
09-578	1029	Devonian	D2	1.4	-5.8		
09-269	AM007-1	Devonian	D2	3.0	-7.2		
09-276	MG013	Devonian	D2	2.0	-7.4		
09-275	MG035-2	Devonian	D2	2.2	-6.6		
09-219	MG042-2	Devonian	D2	0.8	-6.2		
09-092	AM014-VUG-6	Devonian	Late Calcite	-6.2	-6.5		
09-074	AM015-1	Devonian	Late Calcite	-2.9	-6.4		

Lab ID	Sample ID	Age	Mineral	$\delta^{13}\text{C}\text{‰ VPDB}$	$\delta^{18}\text{O}\text{‰ VPDB}$	$^{87}\text{Sr}/^{86}\text{Sr}$	Reference
09-077	AM030-3	Devonian	Late Calcite	-7.1	-6.3		
09-090	AM030-2	Devonian	Late Calcite	-7.5	-5.9		
09-558	1012-2	Devonian	Late Calcite	-2.3	-9.4		
09-560	1025-1	Devonian	Late Calcite	-0.5	-6.2		
09-561	1026-1	Devonian	Late Calcite	-0.3	-5.9		
09-565	1053-1	Devonian	Late Calcite	-0.1	-6.7		
09-241	AM002	Devonian	Late Calcite	-6.3	-5.5	0.70815	
09-217	MG032-2	Devonian	Late Calcite	-7.7	-8.9	0.70798	
09-242	MG-100	Devonian	Late Calcite	-6.5	-6.5		
09-243	MG-102	Devonian	Late Calcite	-6.5	-6.7		
09-555	SM-1	Devonian	Late Calcite	-5.4	-6.9		

Table 2.2 Summary statistics of rare earth elements (REE) results of selected minerals of the Lucas Formation.

Mineral	La (ppm)	Ce (ppm)	Pr (ppm)	Nd (ppm)	Sm (ppm)	Eu (ppm)	Gd (ppm)	Tb (ppm)	Dy (ppm)	Ho (ppm)	Er (ppm)	Tm (ppm)	Yb (ppm)	Lu (ppm)	ΣREE
D1															
n	7	7	7	7	7	7	7	7	7	7	7	7	7	7	7
Avg.	0.573	0.795	0.121	0.521	0.110	0.024	0.135	0.018	0.108	0.022	0.066	0.009	0.061	0.007	2.568
Stdev.	0.475	0.638	0.097	0.409	0.077	0.020	0.100	0.013	0.077	0.017	0.051	0.006	0.042	0.005	1.981
Max.	1.221	1.883	0.273	1.096	0.209	0.053	0.286	0.034	0.229	0.052	0.153	0.018	0.115	0.015	5.345
Min.	0.077	0.129	0.018	0.077	0.015	0.000	0.026	0.001	0.011	0.003	0.011	0.001	0.011	0.001	0.383
D2															
n	4	4	4	4	4	4	4	4	4	4	4	4	4	4	4
Avg.	1.620	1.723	0.319	1.391	0.286	0.069	0.374	0.055	0.352	0.073	0.208	0.025	0.148	0.019	6.662
Stdev.	2.045	1.719	0.374	1.719	0.333	0.095	0.475	0.079	0.498	0.100	0.276	0.034	0.184	0.021	7.918
Max.	4.651	4.172	0.868	3.936	0.781	0.211	1.084	0.174	1.098	0.223	0.622	0.076	0.424	0.050	18.370
Min.	0.345	0.446	0.062	0.268	0.068	0.014	0.102	0.013	0.085	0.019	0.056	0.007	0.051	0.007	1.578
Late calcite															
n	6	6	6	6	6	6	6	6	6	6	6	6	6	6	6
Avg.	4.609	5.129	0.757	3.057	0.537	0.129	0.660	0.093	0.517	0.106	0.295	0.036	0.234	0.035	16.195
Stdev.	4.499	5.480	0.743	2.986	0.514	0.117	0.634	0.085	0.415	0.073	0.176	0.020	0.138	0.022	15.794
Max.	13.031	15.519	2.183	8.828	1.532	0.355	1.884	0.254	1.281	0.234	0.575	0.068	0.463	0.067	46.272
Min.	0.448	0.653	0.106	0.467	0.091	0.026	0.117	0.017	0.133	0.030	0.089	0.012	0.086	0.011	2.285

Table 2.3 Summary statistics of fluid inclusion microthermometry results of selected minerals of the Lucas Formation. The complete set of data is presented in Appendix 3.

Age	Mineral	Th °C	Tm °C	Salinity
Devonian	Calcite			
Devonian	n	17	17	17
Devonian	Avg.	126.0	-17.1	19.7
Devonian	Stdev.	24.5	1.3	0.8
Devonian	Max.	171.9	-15.1	21.1
Devonian	Min.	87.1	-19.3	18.5
Devonian	Celestine			
Devonian	n	85	85	85
Devonian	Avg.	218.0	-10.4	14.4
Devonian	Stdev.	52.8	2.1	1.9
Devonian	Max.	321.8	-6.1	19.2
Devonian	Min.	118.2	-16.1	9.7

Chapter 3

Petrologic and geochemical attributes of fracture-related dolomitization in Ordovician carbonates and their spatial distribution in southwestern Ontario, Canada

3.1 Introduction

Middle Ordovician Trenton and Black River carbonates in southwestern Ontario and neighbouring regions form one of the most important hydrocarbon exploration targets and oil production reservoirs in Lower Paleozoic strata of North America (e.g., Davies and Smith 2006). Laterally equivalent carbonates in New York, Ohio, Indiana, and Wisconsin have also produced large amounts of hydrocarbons and some are host to lead-zinc-fluorite mineralization.

Hydrocarbons are produced where these carbonates have been fractured and dolomitized and laterally sealed by tight, undolomitized limestone (e.g., Taylor and Sibley, 1986; Prouty, 1988; Hurley and Budros, 1990; Middleton et al., 1993; Coniglio et al., 1994; Yoo et al., 2000, Smith 2006). Numerous studies have focused on diagenetic aspects of carbonates including hydrothermal dolomites in the Lower Palaeozoic rocks of eastern Canada and the United States (e.g., Hurley and Budros, 1990; Coniglio et al., 1994; Smith, 2006; Yoo et al., 2000; Luczaj, 2006; Conliffe et al., 2010).

Some of these studies suggested that patchy dolomitization in the vicinity of fractures formed from hydrothermal fluids that flowed up through basement-rooted faults and associated fractures (Taylor and Sibley, 1986; Coniglio et al., 1994; Smith, 2006). Faults and associated fractures appear to have acted as conduits for migration of hydrocarbons and mineralizing fluids, including dolomitizing fluids (Sanford et al., 1985; Carter et al., 1996).

The formation of replacive and saddle dolomites in the fractured zones appears to have exerted a major control on hydrocarbon occurrence and MVT mineralization and,

thus warrants detailed investigation. Therefore, an understanding of the origin and the mechanisms of precipitation of the dolomite has important implications for hydrocarbon and lead-zinc-fluorite exploration and exploitation in the regions.

The purpose of the present work is to critically review and refine the current fluid flow model to document the diagenetic processes, in particular dolomitization of the Trenton carbonates, by detailed petrography, stable isotope and strontium isotope analysis, fluid inclusion microthermometry and rare earth elements (REE) geochemistry. The objectives of this work are to determine: 1) the spatial distribution of dolomite, 2) the nature of the fluid (s) responsible for dolomitization, and 3) the fluid migration pathway(s).

3.2 Geologic setting

The study area is located between the Michigan and Appalachian basins. A broad platform formed between these two differentially subsiding basins, the Michigan Basin in the west and the Appalachian Basin to the southeast (Fig. 3.1) separated by the Algonquin and Findlay arches. The arches formed in the Late Precambrian and remained intermittently active throughout the Palaeozoic and they had a controlling effect on patterns of sedimentation during Paleozoic time (Sanford et al., 1985).

The NE-SW trending Algonquin Arch extends from the southeastern part of the Canadian Shield and terminates to the southwest near the city of Chatham. This structural high continues near Windsor, where it is called the Findlay Arch, extending southwest into Michigan and Ohio. The structural depression between the two arch sections is the Chatham Sag (Fig. 3.1).

The region is underlain by an essentially undisturbed Phanerozoic sedimentary succession resting unconformably on Precambrian basement rocks. The Appalachian Basin, dominated by siliciclastic sediments, is an elongate foreland basin that developed as a result of collisional tectonics along the eastern margin of North American continent during the Palaeozoic. The Michigan Basin is an intracratonic basin dominated by carbonates and evaporites (Armstrong and Carter, 2006). The sedimentary units thicken towards the depocenter of the Michigan Basin.

From Cambrian to Mississippian times, the region was located at tropical latitudes (Van der Voo, 1988) and intermittently covered by inland seas. Erosional and non-depositional gaps occur within the succession mainly due to regression events, resulting in an incomplete stratigraphic record (Johnson et al., 1992).

Sedimentation of Paleozoic cover in the area commenced with transgression over the Precambrian basement. The Middle Ordovician sequence consists of the Black River and Trenton groups, which together range up to 280 m in thickness. The Black River and Trenton groups consist of fossiliferous carbonates underlying the deeper-water shales of the Blue Mountain Formation (Armstrong and Carter, 2006).

The Trenton Group includes the Cobourg, Sherman Fall (the focus of this investigation) and Kirkfield formations, in descending stratigraphic order (Fig. 3.2). These strata represent the upper part of a widespread carbonate platform developed during the Middle Ordovician over a vast area of the North American craton (Wilson and Segupta, 1985). The Trenton Group in the subsurface of southwestern Ontario exhibits a sharp irregular contact with overlying shales of the Blue Mountain Formation.

The Sherman Fall Formation consists of a lower shaly or argillaceous member and an upper, thinner, coarser grained, bioclastic limestone. The lower member consists of interbedded limestone and calcareous shale ranging up to 60 m thick in the outcrop area (Melchin et al. 1994). In the subsurface, the Sherman Fall Formation ranges from about 16 m thick on Manitoulin Island to 43.8 m in Lake Erie, south of Essex County. The upper member consists of bioclastic and intraclastic grainstone. This unit ranges up to 10 m thick in outcrops near Lake Simcoe, and is interpreted to represent deposition in a shallow shoal environment (Brookfield and Brett, 1988).

3.2.1 Faults and fractures

Sanford et al. (1985) interpreted the Algonquin and Findlay arches formed in late Precambrian time and were reactivated periodically during the Paleozoic. The Algonquin Arch experienced several episodes of uplift that were coincident with subsidence in the Michigan and Appalachian basins, resulting in the present structural configuration (Carter et al., 1996).

Reactivation and corresponding readjustment of the fault blocks resulted from stresses generated at distant plate boundaries (Boyce and Morris, 2002), and these provided the structural control for the formation and further development of hydrocarbon traps in the region. Sedimentary facies distribution was attributed to the effect of the fault blocks created during collision of the Middle Ordovician shelf with an island arc (Brookfield and Brett, 1988).

Most of the faults in southern Ontario are basement faults extending upward into the overlying strata. They are normal faults with displacements from few meters up to 100 m. Displacement along these faults formed the required channelways for fluid movement, resulting in dissolution of Silurian evaporites and Middle Ordovician dolomitization of the reservoir rocks (Sanford et al., 1985).

The majority of Ordovician hydrocarbon reservoirs in southwestern Ontario are located along fractures (Fig. 3.3). These are aligned along linear structures trending approximately northwest-southeast to east-west and are located at intersecting fracture systems on the down-dropped side of fault blocks (Sanford et al., 1985).

Dolostones in the area have been subjected to some degree of brecciation (Fig. 3.4). Breccia types include chaotic and to some extent mosaic breccias. In some cases, crackle breccia is also observed (see Morrow, 1982). The inter-breccia space is completely or partially filled with white saddle dolomite and late stage calcite.

3.3 Materials and methods

Most parts of southern Ontario are overlain by a relatively thick cover of glacial deposits. Due to the scarcity of outcrops in the western part of study area, most of the samples for this investigation were obtained from subsurface cores from numerous oil and gas wells drilled and stored in the Ontario Oil, Gas and Salt Resources Library in London, Ontario. Core location and surface sampling locations are shown in Figure 3.5. Rock exposures and natural outcrops were examined in accessible quarries in the Lake Simcoe area. Surface samples were collected from the Picton quarry near Belleville. Approximately one hundred thin sections were prepared and stained with Alizarin red S

and potassium ferricyanide and studied using regular conventional petrographic microscopy as well as ultraviolet and cathodoluminescence microscopy.

For $\delta^{18}\text{O}$ and $\delta^{13}\text{C}$ analysis, approximately 5 mg of selected calcite and dolomite were micro-drilled and reacted with 100% pure phosphoric acid at 25°C for calcite and 50°C for dolomite, respectively (Al-Aasm et al., 1990) and the resultant CO_2 was measured for its oxygen and carbon isotopic ratios on a Delta plus mass spectrometer. Isotopic values are given in δ -notation and reported relative to the VPDB standard. Repeatability of isotopic measurements is better than $\pm 0.05\%$.

Ten doubly-polished, 100 μm -thick wafers of calcite and dolomite were prepared for fluid inclusion studies. To avoid reequilibration of fluid inclusions a liquid cooled diamond rotary saw was used to cut samples (Goldstein, 2003). Based on the criteria by Roedder (1984) detailed petrography was carried to determine the type of inclusion (i.e. primary or secondary/pseudosecondary) using an Olympus BX51 microscope.

Fluid inclusion microthermometry measurements were carried out using a Linkam THMG 600 heating-freezing stage at the University of Windsor. Calibration with precision of $\pm 1^\circ\text{C}$ at 300°C and $\pm 0.1^\circ\text{C}$ at -56.6°C was conducted using synthetic H_2O and CO_2 fluid inclusion standards. To reduce the risk of stretching or decrepitation during freezing of inclusions, the fluid inclusion heating experiments were conducted prior to cooling experiments.

The $^{87}\text{Sr}/^{86}\text{Sr}$ isotope ratios were determined for selected matrix dolomite ($n = 7$) and saddle dolomite cement ($n = 5$) using an automated Finnigan 261 mass spectrometer equipped with Faraday collectors. Correction for isotopic fractionation during the analyses was made by normalization to $^{86}\text{Sr}/^{88}\text{Sr}=0.1194$. The mean standard error of mass spectrometer performance was ± 0.00003 for standard NBS-987.

Rare Earth Element (REE) concentrations were measured using an X series II ThermoFisher ICP-MS, subsequent to a general leach and digestion procedure. Each sample powder was weighed, reacted with 1% HNO_3 acid, and then diluted with approximately 50 mg laboratory internal standards. Precision is in the range of 3.26% to 17%, and accuracy is in the range of 1.0% to 6.38%. Measured values were normalized to

Post-Archean Australian average Shale (PAAS). The REE and strontium isotope analysis were carried out in Commonwealth Scientific and Industrial Research Organisation (CSIRO) of Australia.

3.4 Results

3.4.1 Petrography

Petrographic study resulted in recognition of various diagenetic minerals including calcite, dolomite, anhydrite, and sulfides (Fig. 3.6). The main diagenetic features identified include compaction, dissolution and brecciation. Both matrix dolomite and void-filling saddle dolomite cement are present. More than 90% of the dolomite is medium to coarse crystalline (150–500 μm) matrix replacive dolomite. Much of the matrix dolomitization is fabric destructive, anhedral, and nonplanar.

Limestone is mainly wackestone and grainstone. Micritic limestone generally consists of non-ferroan microspar. Skeletal grains include echinoderms, brachiopods, bryozoans, and trilobites. Calcitic grains are generally well preserved with echinoderms rarely replaced by chalcedony. Sutured surfaces are observed at the contacts of grains indicating chemical compaction.

3.4.1.1 Calcite Cement

Three types of calcite cement are present in pores and fractures, including: 1) non-ferroan syntaxial calcite overgrowth around echinoderms and varying in size based on the size of echinoderm (C1), 2) ferroan equant calcite (C2), which commonly fills interparticle, intraskeletal and biomoldic pore spaces (Fig. 3.7A), and ranges in size from 50 to 200 μm , and 3) non-ferroan translucent, coarse blocky calcite cement (C3) filling secondary pores and fractures postdating saddle dolomite and ranging in size from 500 μm to 5 mm. The C3 cement occludes remaining fracture porosity and shows a uniform bright orange luminescence (Fig. 3.7F), while C1 and C2 display a homogeneous orange luminescence. The C1 and C2 cements are commonly replaced by dolomite (Fig. 3.7B).

3.4.1.2 Dolomite

Three principal types of dolomite are recognized: 1) fine crystalline dolomite with crystal size ranging from 25 to 50 μm (D1), replacing skeletal grains, calcite cement (C1 and C2) and microspar. D1 dolomite consists of tightly packed planar-e to planar-s, non-

luminescent ferroan rhombs (Fig. 3.7B). Volumetrically, this type of dolomite is less (< 5%) than the other types of dolomite and is not related to fractured host rock. It mainly occurs in cores and surface exposures when pervasive fracture dolomitization is missing and limestone is the dominant lithology.

2) Replacive matrix dolomite (D2) is fabric destructive and replaces skeletal grains, micrite and calcite cements (C1 and C2). The only recognizable replaced bioclasts are echinoderms. D2 dolomite is volumetrically more abundant (> 80%) than other types and is predominantly fracture-related. It includes two sub-populations of replacement (D2a and D2b) dolomite (Fig. 3.7C). D2a forms coarse planar-s to nonplanar crystals (300-700 μm) and is crosscut by solution seams. D2b forms planar-s to nonplanar crystals ranging in size from 50 to 100 μm . Both D2a and D2b are non-luminescent. The D2b crystals shows sweeping extinction similar to saddle dolomite (e.g., Middleton et al., 1993; Coniglio et al., 1994). There is a general tendency for an iron-rich rim to follow an earlier non-ferroan core.

3) Two types of dolomite cement are present. D3a that fills open pore spaces as cement, with planar-e rhombs ranging in size from 250 to 750 μm , showing strong zonation with cloudy centers and clear rims (Fig. 3.7D). The other dolomite cement is vug and fracture-filling saddle dolomite (D3b). Saddle dolomite cement is the most abundant porosity occluding phase and it postdates matrix dolomite (D2). It is zoned with cloudy centers and clear rims and has curved crystal faces. Saddle dolomite crystals range in size from 500 μm up to 3 mm in diameter and also occurs as ferroan cement in limestone (Fig. 3.7E). Microscopic examination indicates that the dolomite is inclusion-rich and under CL, exhibits a dull red luminescence faint zonation. In fractures, it shows corroded rims (Fig. 3.7F). Most of open spaces including fractures and vugs in the Sherman Fall Formation is lined with saddle dolomite (D3b). Saddle dolomite is the most abundant cement between the angular clasts of matrix dolomite breccia. The remaining open spaces are filled with latest calcite (C3) and occasionally anhydrite. Some pyrobitumen (commonly associated with pyrite) predates saddle dolomite (Fig. 3.7F). Fracture-related dolomite is more abundant in the western part of study area in the Chatham Sag where most of the oil fields are located along fractures.

3.4.1.3 Sulfur-bearing diagenetic minerals

Several other late diagenetic minerals occur in the Sherman Fall Formation, although their abundance is less than 1% based on visual estimates. Anhydrite is the most common sulfur-bearing late stage mineral in samples and occurs as lath-like crystals, ranging in size from 200 to 700 μm . It commonly occurs in fractures postdating fracture-filling calcite and saddle dolomite. Sulfide mineralization consists of pyrite and marcasite commonly occurring in fractures and these sulfides were precipitated following saddle dolomite. Therefore, sulfide mineralization is relatively late in the paragenetic sequence (Fig. 3.6).

3.4.2 Geochemistry

3.4.2.1 Oxygen and carbon isotopes

The $\delta^{18}\text{O}$ and $\delta^{13}\text{C}$ results for host limestone, fracture-filling calcite, replacement dolomite and saddle dolomite are presented in Figure 3.8 and Table 3.1. Due of their size, C1 and C2 were inseparable by conventional microdrilling and therefore care had to be taken in interpreting the results obtained from these phases. Twenty seven analyses of C1 and C2 calcite from the Trenton Group yielded $\delta^{18}\text{O}$ values of -4.3‰ to -7.3‰ and $\delta^{13}\text{C}$ values from -0.4‰ to 1.4‰ VPDB, respectively.

The $\delta^{18}\text{O}$ and $\delta^{13}\text{C}$ values of the limestones are consistent with postulated Middle Ordovician marine values ($\delta^{18}\text{O}$ from -5 to -8‰ and $\delta^{13}\text{C}$ from $+1.5$ to -2‰ VPDB, see Shields et al., 2003). Nine samples of the C3 cement were analyzed and yielded $\delta^{13}\text{C}$ values of 0.4‰ to -1.2‰ VPDB and $\delta^{18}\text{O}$ values of -7.3‰ to -11.5‰ VPDB.

Nine samples of D1 were microsampled from dolomitic limestone and display $\delta^{18}\text{O}$ values ranging from -2.6‰ to -8.6‰ and $\delta^{13}\text{C}$ values of 1.3‰ to -0.2‰ VPDB. Twenty three D2a samples were analyzed giving $\delta^{13}\text{C}$ values of -1.0‰ to 0.8‰ and $\delta^{18}\text{O}$ values of -11.5‰ to -8.0‰ VPDB. Thirteen samples of D2b were analyzed giving $\delta^{13}\text{C}$ values of -0.5‰ to 0.4‰ and $\delta^{18}\text{O}$ values of -10.4‰ to -7.8‰ VPDB. In addition, 12 samples were obtained from D3a yielding $\delta^{13}\text{C}$ values of -0.9‰ to 1.3‰ and $\delta^{18}\text{O}$ values of -11.8‰ to -7.1‰ VPDB.

Twenty four analyses of D3b dolomite gave $\delta^{13}\text{C}$ and $\delta^{18}\text{O}$ values ranging from 1.3‰ to -0.8‰ , and -7.3‰ to -11.5‰ VPDB, respectively. The replacement dolomites

display similar $\delta^{13}\text{C}$ values to the limestone, however, they have more negative $\delta^{18}\text{O}$ values. Saddle dolomite $\delta^{18}\text{O}$ values are shifted to more negative $\delta^{18}\text{O}$ values, while $\delta^{13}\text{C}$ values of all three types of dolomite are comparable to the $\delta^{13}\text{C}$ signature of Middle Ordovician marine carbonates.

3.4.2.2 *Strontium isotopes*

Due to small amounts of D1, separate sampling of this phase for strontium isotope analysis was not possible. Six samples of D2 yielded $^{87}\text{Sr}/^{86}\text{Sr}$ ratios ranging from 0.70830 to 0.70918. The range of $^{87}\text{Sr}/^{86}\text{Sr}$ for D3 (saddle dolomite) is from 0.70872 to 0.70907 (Fig. 3.9, Table 3.1).

3.4.2.3 *Rare earth elements (REE) results*

Samples of host limestone, replacive dolomite (D2) and saddle dolomite cement (D3b), and fracture-filling calcite (C3) from the Sherman Fall Formation were analysed for REE content. $\text{Ce}_{\text{SN}} = [(\text{Ce}/\text{Ce}^*)_{\text{SN}} = \text{Ce}_{\text{SN}} / (0.5\text{La}_{\text{SN}} + 0.5\text{Pr}_{\text{SN}})]$, $\text{La}_{\text{SN}} = [(\text{Pr}/\text{Pr}^*)_{\text{SN}} = \text{Pr}_{\text{SN}} / (0.5\text{Ce}_{\text{SN}} + 0.5\text{Nd}_{\text{SN}})]$, $\text{Eu}_{\text{SN}} = [(\text{Eu}/\text{Eu}^*)_{\text{SN}} = \text{Eu}_{\text{SN}} / (0.5\text{Sm}_{\text{SN}} + 0.5\text{Gd}_{\text{SN}})]$, and $\text{Gd}_{\text{SN}} = [(\text{Gd}/\text{Gd}^*)_{\text{SN}} = \text{Gd}_{\text{SN}} / (0.33\text{Sm}_{\text{SN}} + 0.67\text{Tb}_{\text{SN}})]$ anomalies were calculated with the equations of Bau and Dulski (1996). LREE (La-Nd) depletion over HREE (Ho-Lu) was calculated using $(\text{La}/\text{Yb})_{\text{SN}}$ ratios (Kucera et al., 2009). MREE (Sm-Dy) enrichment was calculated using $(\text{Sm}/\text{La})_{\text{SN}}$ and $(\text{Sm}/\text{Yb})_{\text{SN}}$ ratios (Felitsyn and Morad, 2002).

Whole rock undolomitized Trenton Group limestone yielded higher mean ΣREE content (17.76 ± 7.46 ppm, Table 3.2) than those of modern microbialites (1.99 ± 0.5 ppm; Webb and Kamber, 2000) and modern warm water brachiopods (Fig. 3.10) (0.3 ± 0.2 ppm; Azmy et al., 2011). Limestone shows slight depletion of LREE ($\text{La}_{\text{SN}}/\text{Yb}_{\text{SN}} = 0.9 \pm 0.16$), predominantly negative $(\text{Ce}/\text{Ce}^*)_{\text{SN}}$ and positive $(\text{Pr}/\text{Pr}^*)_{\text{SN}}$ anomalies (Fig. 3.11), slight positive Gd anomaly of 1.14 ± 0.09 , $(\text{La}/\text{Nd})_{\text{SN}}$ ratio of 0.87 ± 0.16 , and $(\text{Eu}/\text{Eu}^*)_{\text{SN}}$ positive anomaly (1.05 ± 0.09).

D2, D3b, and C3 yield significantly higher ΣREE contents than limestone (Table 3.2). Their REE_{SN} is one order of magnitude higher than undolomitized limestone (Fig. 3.10). All D2, D3b, and C3 samples show a predominantly negative Ce anomaly and positive La anomaly with few exceptions (Fig. 3.11). All samples show positive Gd

anomaly and their $(La/Nd)_{SN}$ ratio are in the range of seawater ratio (0.8 to 2). D2, D3, and C3 show consistent negative Eu anomaly.

3.4.3 Fluid inclusions

Microthermometric measurements were made on 111 primary fluid inclusions in carbonate samples including D2 dolomite (n = 30), D3b dolomite (n = 37), and C3 calcite (n = 44). The inclusions are two-phase (liquid-rich with vapor bubble) with irregular shapes. The summary statistics of fluid inclusion results are presented in Table 3.3 and the complete data set are presented in Appendix 3.

Fluid inclusions observed in D2 dolomite are very small, ranging from 2 to 8 μm , and contain small vapor bubbles constituting less than 20 vol% of the inclusion (Fig. 3.12A). This dolomite (D2) shows a narrow range of T_h values from 67.6° to 98.9°C ($81.9 \pm 9.5^\circ\text{C}$, n = 30). It was not possible to measure the last ice melting temperature due to the small size of the inclusions.

Fluid inclusions in D3b (saddle dolomite) range from 15 to 30 μm and contain vapor bubbles constituting 10 vol% of the inclusions. Fluid inclusions aligned along growth zones are considered primary in origin (Goldstein, 2003) (Fig. 3.12A). Homogenization temperatures (T_h) in D3 cement show a wider range than D2 from 96.7° to 143.5° ($121.1 \pm 13.3^\circ\text{C}$, n = 36), with the last ice-melting temperatures (T_m) ranging from -28.8° to -21.9°C ($-25.6 \pm 1.8^\circ\text{C}$, n = 23). These values correspond to salinities of 24.4 to 21.5 wt.% (NaCl+CaCl₂) equivalent (23.1 ± 0.7 , n = 24).

Fluid inclusions in C3 range from 10 to 40 μm and contain vapor bubbles constituting less than 20 vol% of the inclusions (Fig. 3.12C). Thermometric measurements of C3 show a wide range of T_h values from 60.2° to 131.1°C ($82.6 \pm 17.5^\circ\text{C}$, n = 37) with the last ice-melting temperatures range from -24.8° to -18.5°C ($-21.5 \pm 2.3^\circ\text{C}$, n = 24), indicating salinities in the range of 19.8 to 22.8 wt.% NaCl+CaCl₂ equivalent (21.2 ± 1 , n = 24).

Liquid hydrocarbons were detected in inclusions in D3b and C3 in a few samples. These inclusions display a slight bright greenish-yellow fluorescence under ultraviolet

light and commonly homogenize to a liquid phase (Figs. 3.12B, D). The inclusions containing hydrocarbons are mainly colourless under transmitted light and did not freeze.

It is important to note that the salinity values slightly decrease from saddle dolomite (D3b) to late stage calcite (C3), with a covarying decrease in homogenization temperatures (Fig. 3.13). Salinity values obtained from fluid inclusions show similar ranges in different mineral phases, mainly between 21 and 24 wt.% NaCl+CaCl₂ equivalent. There is also a general decreasing trend in average homogenization temperatures of both D3b and C3 from west (center of the basin) to east (margin of the basin).

3.5 Discussion

3.5.1 Oxygen isotope geochemistry and microthermometry

Almost all the $\delta^{13}\text{C}$ and $\delta^{18}\text{O}$ values of the undolomitized limestone samples of the Sherman Fall Formation fall within the estimated ranges of carbon isotopic composition ($\delta^{13}\text{C}$ values from -2.0 to $+2.0\text{‰}$ VPDB) and oxygen isotopic composition ($\delta^{18}\text{O}$ values from -8.0 to -4.0‰ VPDB) for Middle Ordovician marine calcite (Fig. 3.8; Shields et al., 2003). The $\delta^{13}\text{C}$ values of the D1, D2 and D3 (-0.2 to $+1.3\text{‰}$ VPDB) are interpreted to reflect the carbon isotopic composition of the precursor limestone (-0.2 to $+1.4\text{‰}$ VPDB). Dolomite carbon isotopic composition is generally buffered by the precursor limestone (Warren, 2000).

Numerous studies have indicated that dolomite is generally enriched in ^{18}O relative to coexisting calcite by $3 \pm 1\text{‰}$ (e.g. Land, 1980, 1983; Major et al., 1992). Undolomitized lime mudstones samples have $\delta^{18}\text{O}$ values ranging from -7.4 to -4.3‰ VPDB. If the Middle Ordovician seawater is considered as the source of dolomitizing fluid for fine crystalline dolomite (D1), then the $\delta^{18}\text{O}$ values of dolomite precipitated from seawater should be between -4.4 and -1.3‰ VPDB with an average of -2.9‰ . Two measured $\delta^{18}\text{O}$ values of D1 dolomite fall inside the range for estimated Middle Ordovician dolomite (Fig. 3.8). The finely crystalline nature, planar texture, and $\delta^{18}\text{O}$ values of D1 suggest an early-stage replacement of marine carbonates. A similar early-stage replacement was invoked for planar dolomites in Trenton carbonates in northern Indiana (Yoo et al., 2000).

The average $\delta^{18}\text{O}$ values of D1 dolomite (-6.9‰), however, display a negative shift by ca. 4‰ compared with the expected average $\delta^{18}\text{O}$ values for Middle Ordovician dolomite (-2.9‰). A common process during progressive burial of early formed dolomite is recrystallization and subsequent geochemical changes (Al-Aasm, 2000 and references therein). During recrystallization, dolomite may retain some of the precursor dolomite properties while others change significantly (Machel, 2004). The negative shift in $\delta^{18}\text{O}$ values of D1 can be attributed to the effect of recrystallization during burial although, petrographically, it is still fine-crystalline with planar texture. The observed shift in D1 dolomite $\delta^{18}\text{O}$ values toward more negative values compared to Middle Ordovician dolomite is interpreted to be from recrystallization during burial or later hydrothermal events (e.g., Al-Aasm, 2000).

The occurrence of replacive matrix (D2) and saddle dolomite (D3) in the vicinity of fractures implies fractures were a conduit for dolomitizing fluids. The more depleted $\delta^{18}\text{O}$ values of D2 and D3 relative to D1 reflect their different origins. The overlap in isotopic ratios for matrix dolomite (D2) and saddle dolomite (D3b) suggests some degree of recrystallization of replacive dolomite during precipitation of the saddle dolomite.

The coarse crystal size, non-planar texture, presence of saddle dolomite cement (Fig. 3.7F), negative $\delta^{18}\text{O}$ values of D2 and D3, and high homogenization temperature ($82 \pm 9.5^\circ\text{C}$, $n = 30$ and $121 \pm 13.3^\circ\text{C}$, $n = 36$, respectively) are a strong evidence of dolomitization at higher temperature conditions (Machel, 2004) either during burial or from hydrothermal fluids. There are two possibilities for the origin and resulting isotopic values of fracture-related dolomite (D2): 1) D2 formed during intermediate burial from modified seawater/brines and recrystallized during late saddle dolomite formation being partially replaced by the saddle dolomite and therefore yielding similar isotope values; and 2) matrix dolomite (D2) and saddle dolomite (D3b) precipitated at same time.

Microthermometry of fluid inclusions in diagenetic minerals found in the Middle Ordovician carbonates was used to estimate the precipitation temperature of calcite and dolomite as well as the salinity of the fluid(s) responsible for their precipitation. D2 dolomite precipitated from hot fluids ranging in temperature from 67.6 to 98.9°C ($81.9 \pm 9.5^\circ\text{C}$), however, due to very small size of D2-hosted fluid inclusions salinity

measurements were not possible. Fluid inclusions hosted in D3b saddle dolomite cement indicate precipitation from saline brines (23.1 ± 0.7 wt. % NaCl+CaCl₂, n = 23) at temperatures ranging between 96.7 and 143.5°C (121 ± 13.3 °C, n = 36). Fluid inclusion data from C3 samples suggests precipitation from hot (60.2 to 131.1°C, avg. = 82.6 ± 17.5 °C, n = 37) and saline fluids (21.2 ± 1 wt. % NaCl+CaCl₂, n = 24).

Integration of dolomite (D2 and D3b) $\delta^{18}\text{O}$ values with measured microthermometry data (estimate of minimum entrapment temperatures) has been employed to determine the $\delta^{18}\text{O}_{\text{fluid}}$ responsible for dolomitization of Middle Ordovician Trenton Group carbonates (Fig. 3.14). The $\delta^{18}\text{O}_{\text{fluid}}$ for D2 ranges from -6 to $+2$ ‰ VSMOW, and for D3 range from -2 to $+5$ ‰ VSMOW. Calculated $\delta^{18}\text{O}_{\text{fluid}}$ for D2 varies from values similar to Middle Ordovician seawater (-6.3 ‰ VSMOW; Shields et al., 2003) to values more positive ($+2$ ‰ VSMOW) than estimated Middle Ordovician seawater.

Common sources of ^{18}O -enriched waters are basinal brines, waters from gypsum dehydration, waters from salt dissolution, reactions between waters and associated carbonate minerals or mixtures of the above (e.g., Hitchon and Friedman, 1969; Knauth and Beeunas, 1986). The $\delta^{18}\text{O}$ values of basinal brine shift toward more positive values (up to $+10$ ‰ VSMOW) as temperature and salinity increase (Sheppard, 1986).

Silurian seawater (-3.5 ‰ VSMOW, Azmy et al., 1998) or Devonian seawater (-1 ‰ VSMOW, Joachimsky et al., 2009) could be considered as sources of ^{18}O -enriched waters relative to Middle Ordovician seawater, assuming cross formational fluid flow through network of fractures. Reflux of Mg-bearing (Silurian and/or Devonian) seawater or seawater derived brines or formation waters are likely to have been involved in precipitation of D2 and D3 dolomite. However, the thickness of sediments at the end of Silurian was not enough to explain the high trapping temperature of D2-hosted fluid inclusions.

Thus, by the end of the Devonian a thicker sedimentary cover existed over the region and higher burial temperatures likely reached. Influx of late Devonian seawater caused dissolution of Devonian and Silurian evaporites where dense saline fluids became

warm during downward fluid flow. Progressive mixing of warm saline fluids resulted from dissolution of evaporites from younger seawater (Devonian and/or Silurian) and in situ Middle Ordovician connate waters resulted in fluids with more positive $\delta^{18}\text{O}$ values. The lower range of D2 $\delta^{18}\text{O}_{\text{fluid}}$ (-6‰ VSMOW) values supports the suggested scenario.

A recent geochemical study of formation waters of different ages in southern Ontario and northern Michigan (Hobbs et al., 2011) indicates that formation waters in intermediate to deep reservoirs (depth greater than 200 m) originated from evaporated of seawater past halite saturation. However, excess of Cl over Br in these waters is an indication of halite dissolution (Hobbs et al., 2011). Pinti et al. (2011) suggest that infiltration and penetration of Devonian seawater dissolved halite in Devonian and Silurian evaporites, resulting in high salinity brines in Cambrian and Ordovician aquifers in the St-Lawrence Lowlands.

Based on low $\delta^{18}\text{O}$ values and higher homogenization temperatures, it is envisaged that the saddle dolomite was precipitated from hot brines during deep burial of the Trenton limestone, while the range in $\delta^{18}\text{O}$ values of the saddle dolomites can be explained by precipitation from a single fluid at variable temperatures. Middleton et al. (1993) reported a decreasing trend in fluid inclusion temperatures in a single crystal of saddle dolomite from the core to the margin of crystals which supports this interpretation that D3 precipitated from a cooling fluid. The similar $\delta^{18}\text{O}$ values of replacive dolomite (D2) and saddle dolomite (D3b) and sweeping extinction that is observed in most of the matrix dolomite suggest that the matrix dolomite (D2) has been subjected to recrystallization in the presence of high temperature fluids that precipitated late stage saddle dolomite.

Reconstruction of burial depths for the Middle Ordovician sequence using stratigraphic data resulted in a maximum burial depth of 1500 m for this sequence on Manitoulin Island (Coniglio and Williams-Jones, 1992). However, the total burial depth for Middle Ordovician rocks in southwestern Ontario is uncertain, but extrapolation of stratigraphic data from elsewhere in the Michigan Basin suggested 2000 m burial depth for southwestern Ontario (Cercone, 1984).

Assuming a normal intracratonic geothermal gradient (23°C/km) suggested by Hogarth and Sibley (1985) and a 20°C surface temperature, the maximum burial temperature at 2000 m depth for southwestern Ontario would be 66°C. Higher paleo-geothermal gradients (35 to 50°C/km; Cercone, 1984; Vugrinovich, 1988) have been proposed for the central part of the Michigan Basin to satisfy the organic maturity of Middle Devonian and Lower Pennsylvanian strata. However, conodont alteration index values (Legall et al., 1981) indicate maximum burial temperatures of 60 to 90°C for Lower Ordovician strata in southwestern Ontario.

The average homogenization temperature of D3b (121.1°C) is significantly higher than the estimated maximum burial temperature for southwestern Ontario (90°C) which is an indication of involvement of hydrothermal fluids in precipitation of saddle dolomite cement. The pronounced decrease in T_h values from D3b to C3 (Fig. 3.13) indicates a gradual cooling of a hot fluid.

Using Friedman and O'Neil's (1977) calcite-water fractionation equation, in order to achieve the average measured homogenization temperature (82.6°C) for C3 with average $\delta^{18}\text{O}_{\text{calcite}}$ (-10‰ VPDB), the $\delta^{18}\text{O}_{\text{fluid}}$ would have to be +1.5‰ VSMOW. This value is in the range of $\delta^{18}\text{O}_{\text{fluid}}$ for D3b and suggests a similar parent fluid for precipitation of D3b and C3. The $\delta^{18}\text{O}$ values of C3 calcite (-7.3 to -11.5‰ VPDB) are variable, and overlap (Fig. 3.8) with those of D3 (-8.9 to -11.8‰ VPDB). The significant overlap between C3 calcite and D3b dolomite $\delta^{18}\text{O}$ values indicates that C3 precipitating fluid were cooler than the D3b precipitating fluid during precipitation of the C3, assuming a common fluid for precipitation.

For example, for the same $\delta^{18}\text{O}$ value for both dolomite and calcite (assuming, -10‰ VPDB) if precipitated from a single fluid (assuming -3‰ VSMOW), the resulting precipitation temperatures for dolomite and calcite would be 72 and 51°C, respectively. This hypothesis is supported by the lower T_h values recorded by fluid inclusions in the C3 calcite ($82.6 \pm 17.5^\circ\text{C}$) relative to precipitation temperature for D3b dolomite ($121.1 \pm 13.3^\circ\text{C}$). It indicates that fracture-filling calcite must have been precipitated from fluids that formed saddle dolomite after they lost their Mg-content and temperature decreased

after saddle dolomite precipitation. The similarity in salinity values in D3b and C3 possibly indicates involvement of a single fluid during precipitation of D3b and C3.

C3 and saddle dolomite (D3b) host hydrocarbon-bearing fluid inclusions (Figs. 3.12C and E); further supporting the idea that both D3b and C3 precipitated from one fluid during oil migration. Bitumen coating replacive dolomite (D2) and pre-dating saddle dolomite (D3b), and hydrocarbon-bearing inclusions in saddle dolomite (D3b) and late stage calcite (C3) suggest that hydrocarbon migration to the reservoir rocks took place concurrent with precipitation of saddle dolomite and late stage fracture-filling calcite, a conclusion also reached by other workers elsewhere in the Michigan Basin (Budai and Wilson, 1991; Coniglio et al., 1994).

The precipitation of the C3 phase likely occurred after tectonically-controlled uplift of the Michigan Basin. The Algonquin Arch experienced several episodes of uplift in response to collisional tectonic events (e.g., Caledonian, Acadian, Alleghanian orogenies) that occurred along the eastern edge of North America during the Paleozoic (Sanford et al., 1985; Johnson et al., 1992). Uplift followed by subaerial erosion marked by regional unconformities took place during the Paleozoic in the Michigan Basin (Johnson et al., 1992).

3.5.2 Strontium isotopes

$^{87}\text{Sr}/^{86}\text{Sr}$ ratios could provide significant information with respect to the type of fluids involved in the formation of calcite and dolomite cements. In addition, they could indicate changes in fluid chemistry, degree and extent of water-rock interaction, and act as a tracer for basinal fluid movement (Barnaby et al., 2004). The potential sources of ^{87}Sr in sedimentary basin brines are: illitization of smectite and dissolution of ^{87}Sr -enriched evaporite minerals, alkali feldspar, and also of detrital mica in the deep subsurface (Chaudhuri and Claur, 1992).

Dolomites that precipitate from basinal brines commonly have $^{87}\text{Sr}/^{86}\text{Sr}$ ratios that are more radiogenic than coeval seawater (Allan and Wiggins, 1993). Although slightly radiogenic with respect to seawater, dolomite that plots outside the range of seawater at the time of formation suggests that the fluid responsible for dolomite precipitation

interacted to some degree with siliciclastic rocks prior to precipitating the dolomite (Allan and Wiggins, 1993).

Formation waters commonly have high $^{87}\text{Sr}/^{86}\text{Sr}$ ratios relative to marine values. The $^{87}\text{Sr}/^{86}\text{Sr}$ compositions of Trenton Group brines from carbonate reservoirs (Fig. 3.9) display a well-defined distribution, with $^{87}\text{Sr}/^{86}\text{Sr}$ ratios up to 0.7104 (avg. = 0.7099; McNutt et al., 1987). The postulated range of $^{87}\text{Sr}/^{86}\text{Sr}$ ratios of the Middle Ordovician seawater is from 0.7086 to 0.7088 (Shields et al., 2003), while the $^{87}\text{Sr}/^{86}\text{Sr}$ ratio of the Silurian Sea water ranges from 0.7079 to 0.7088 (Azmy et al., 1999; Cramer et al., 2011). Devonian seawater $^{87}\text{Sr}/^{86}\text{Sr}$ ratios vary from 0.7078 to 0.7088 (Veizer et al., 1999). Thus, based on these ratios, it appears that there is significant overlap in the range of $^{87}\text{Sr}/^{86}\text{Sr}$ ratios of Middle Ordovician, Silurian and Devonian seawater (Fig. 3.9).

The $^{87}\text{Sr}/^{86}\text{Sr}$ ratios of matrix dolomite (D2) and saddle dolomite (D3b) cluster into three distinct groups. Three samples of D2 have $^{87}\text{Sr}/^{86}\text{Sr}$ ratios (0.70830 to 0.70842) lower than Middle Ordovician seawater that fall in the range of Upper Ordovician, Silurian and Devonian seawater. Two samples of D2 and three samples of D3b display $^{87}\text{Sr}/^{86}\text{Sr}$ ratios in the range of Middle Ordovician seawater (0.70864 to 0.70867). The rest of samples (D2 and D3b) display $^{87}\text{Sr}/^{86}\text{Sr}$ ratios (0.70902 to 0.70918) more radiogenic than Middle Ordovician and younger seawater values (i.e., Upper Ordovician to Devonian) (Fig. 3.9).

Lower $^{87}\text{Sr}/^{86}\text{Sr}$ ratios of matrix dolomite (D2) relative to Middle Ordovician seawater suggest possible involvement of younger seawater (Upper Ordovician to Devonian) perhaps through cross formational fluid flow. As discussed earlier by the end of Devonian the thickness of sedimentary cover was enough to produce temperatures in the range of D2 homogenization temperatures. Consequently the lower $^{87}\text{Sr}/^{86}\text{Sr}$ ratios of D2 than Middle Ordovician seawater could be the result of influx of Devonian seawater. High salinity fluid inclusion values measured in D3 also imply the role of fluids derived from dissolution of Salina Group evaporites by younger seawater.

The alternative reason for the least radiogenic values of Ordovician replacive dolomite (D2) (Fig. 3.9) is possible water/rock interaction with ultramafic rocks of the

buried mid-continent rift (MCR) beneath the Michigan Basin. The mid-continent rift (MCR) of North America comprises ultramafic and intrusive rocks emplaced during Mesoproterozoic (Hollings et al., 2011). The $^{87}\text{Sr}/^{86}\text{Sr}$ ratio of these rocks varies from 0.7037 to 0.7064 (Hollings et al., 2011). Circulation of diagenetic fluids through highly fractured basement rocks in the center of the basin is another possible source of less radiogenic values of replacive dolomite in comparison to Middle Ordovician seawater (e.g., Brand et al., 2010).

Similar $^{87}\text{Sr}/^{86}\text{Sr}$ ratios of some of D2 and D3b which are in the range of Middle Ordovician values, suggest mixing of younger brines with Middle Ordovician connate waters or equilibration of brines with host carbonates. The lower range of $\delta^{18}\text{O}_{\text{fluid}}$ responsible for precipitation of D2 also supports mixing of younger brines with in situ connate waters. Our data is in agreement with $^{87}\text{Sr}/^{86}\text{Sr}$ ratios of matrix dolomite reported from the Trenton carbonates from southwestern Ontario (avg. = 0.70858; McNutt et al. 1987).

The $^{87}\text{Sr}/^{86}\text{Sr}$ ratios of matrix dolomite (McNutt et al., 1987) and some of D2 and D3b samples (avg. = 0.70872 ± 0.00005) are distinctly different from present-day Trenton Group brines (avg. = 0.7099 ± 0.00039). This indicates that strontium isotopes of D2 and D3 equilibrated with host rock and later with Middle Ordovician and/or late Silurian seawater. However, some of D2 and D3b (saddle dolomite), show $^{87}\text{Sr}/^{86}\text{Sr}$ ratios (0.70902 to 0.70918) more radiogenic than Ordovician and Silurian seawater and in the range of $^{87}\text{Sr}/^{86}\text{Sr}$ ratios of the Trenton Group brines (McNutt et al., 1987; Hobbs et al., 2011). Highly depleted $\delta^{18}\text{O}$ values of D2 and D3b phases in conjunction with $^{87}\text{Sr}/^{86}\text{Sr}$ ratios suggest that hydrothermal fluids were involved in precipitation of saddle dolomite and recrystallization of matrix dolomite (D2).

3.5.3 Rare earth elements (REE)

The rare earth element pattern of modern marine carbonates, including scleractinian corals (Wyndham et al., 2004) and microbialites (Webb and Kamber, 2000) resemble those of their ambient sea water (Webb et al., 2009). However, subsequent diagenetic alteration may change these REE patterns and concentrations (Shields and Stille, 2001; Azmy et al., 2011), and therefore REE can be utilized as sensitive indicators

of diagenetic redistribution of REE contents in carbonates (Azmy et al., 2011). Nonetheless, many workers suggest that carbonates preserve their REE composition and/or pattern during diagenesis (Webb et al., 2009; Allwood et al., 2010), specifically dolomitization (Banner et al., 1988; Bau and Alexander, 2006), except in high water/rock ratio diagenetic systems.

The typical characteristics of REE shale-normalized pattern of marine carbonates are (Webb and Kamber, 2000): 1) relative depletion of LREE over HREE ($(La/Yb)_{SN} < 1$); 2) negative Ce and positive La anomalies; 3) a slight Gd anomaly; and (La_{SN}/Nd_{SN} between 0.8 and 2; Shields and Stille, 2001). However, undolomitized host rock REE_{SN} pattern is slightly different from a typical seawater pattern with a nearly flat REE_{SN} pattern and slight MREE enrichment. Furthermore, dolomite and calcite samples in this study do not exhibit the typical seawater pattern and show a significant MREE enrichment and negative $(Eu/Eu^*)_{SN}$ anomaly (Fig. 3.11). This indicates that REE concentration of diagenetic minerals could have changed during dolomitization and should not necessarily preserve the precursor rock REE signature.

ΣREE of dolomite (matrix and saddle) and fracture-filling calcite relative to undolomitized host rocks indicates that dolomitizing fluids contain higher concentrations of REE. Higher concentration of REE is possible where fluids interact with rocks with elevated REE content. Two possible sources for higher REE content in the Michigan Basin are the Upper Ordovician Blue Mountain shale and Precambrian basement rocks. Whole rock and organic matter fraction of the Blue Mountain shale ΣREE content are 202.7 ± 86.5 and 343.1 ± 436.6 ppm (Abanda and Hannigan, 2006), respectively, whereas those of matrix and saddle dolomite and fracture-filling calcite are 206.6 ± 185.6 , 352.5 ± 303.4 , and 557.2 ± 430.8 ppm, respectively.

Average ΣREE of Precambrian basement is 164.9 ppm (Wedepohl, 1995). Comparable ΣREE and REE_{SN} pattern (Fig. 3.10) of Upper Ordovician shale and those of dolomite and calcite in this study suggest that water/rock interaction with overlying shale likely elevated the REE contents of fluid(s), assuming downward migration of dolomitizing fluids. However, interaction with basement rocks could not be discounted as

there is similarity in LREE pattern of dolomite and calcite and those of Precambrian basement rocks.

Numerous studies suggest that REE are mobile during black shale diagenesis (Lev et al., 2008; and references therein). During early diagenesis and breakdown of sediment organic matter, LREE associated with clay mineral surfaces have the potential to migrate from the sediments into pore waters (Hannigan and Basu, 1998). High organic matter contents indicate highly reducing conditions, which is consistent with the production of a negative Eu anomaly in D2, D3 and C3 (Fig. 3.10).

The increasing trend in Σ REE from D2 to C3 also suggests that mineralizing fluids evolved during process of organic maturation. The REE_{SN} pattern obtained from replacive dolomite (D2), saddle dolomite (D3b), and fracture-filling calcite (C3) samples and the similarity of their pattern indicates involvement of a single fluid in mineralization.

3.5.4 Fluid flow mechanism

In this section the fluid flow model proposed by Coniglio et al. (1994) will be reviewed to refine the model based on geochemical evidence. Luczaj (2006), based on the distribution of hydrothermal dolomitization in the periphery of the Michigan Basin, suggested a radially symmetrical outward fluid flow for migration of dolomitizing fluids from the center of the Michigan Basin (Fig. 3.15).

The occurrence of hydrothermal dolomite in fractured zones associated with hydrocarbon, MVT mineralization, and the similar fluid inclusion compositions of Middle Ordovician strata on the margin of the Michigan Basin (Budai and Wilson 1991), southwestern Ontario and Manitoulin Island (Coniglio et al. 1994), northern Indiana (Yoo et al., 2000) and eastern Wisconsin (Luczaj, 2006), support this idea.

Coniglio et al. (1994) suggested compaction-driven fluids as a possible fluid source for fracture-related dolomitization. Upward and lateral movement of Mg-bearing fluids resulting from transformation of clay minerals, originating from younger, older or correlative argillaceous sediments from deeper in the Michigan and Appalachian basins towards the basin margin was considered as a mechanism for migration of dolomitizing fluids (Coniglio and Williams-Jones, 1992; Middleton et al., 1993; Coniglio et al., 1994).

Yoo et al. (2000) also considered compaction-driven flow as a working mechanism to carry mass and heat from the Michigan Basin.

Clay mineral transformations have been invoked as supply of magnesium for dolomitization in the burial environment, where illitization of smectite releases magnesium into basinal brines (Warren, 2000). Hower et al. (1976) demonstrated that loss of calcium is six times more than magnesium in compacting shales of Gulf Coast. In fact, formation of illite and chlorite from smectite consumes magnesium rather than releases magnesium to basinal brines, therefore this mechanism could not supply enough magnesium for dolomitization (Land, 1985). At best, small volumes of magnesium could be produced in a subsiding and compacting shale basin (Land, 1985; Warren, 2000). In addition, it is unlikely that large volumes of brine could be expelled by compaction-driven flow in a sedimentary basin with a low subsidence rate (0.0024 cm/yr, see Fischer, 1975, p. 68) like the Michigan Basin.

Results of fluid flow modelling (Bethke, 1986; Kaufman, 1994) show that compaction-driven fluid flow in intracratonic basins is characterized by fluid velocities of 0.1 mm/yr to 1 mm/yr and very small excess hydraulic potentials. In addition slow movement of fluids expelled from the deep basin from compaction-driven flow causes conductive cooling of fluid to the surface before reaching host rocks at the basin margin (Bethke, 1986; Bjorlykke, 1993; Deming, 1994; Kaufman, 1994). Therefore, clay transformation and compaction-driven flow are not viable mechanisms for supplying magnesium and dolomitizing fluid.

Buoyancy-driven fluid flow resulting from temperature or density gradients could transport mass and heat over large distances significantly shorter time scales than compaction-driven flow (Bethke, 1986; Garven, 1995). Depending on aquifer thickness, permeability and fluid density gradient, flow rates in convection cells approach 1 m/yr (Garven, 1995). Numerical modelling of the Illinois Basin showed density-driven fluids responsible for formation of Upper Mississippi Valley Pb-Zn deposits had fluid velocities up to several m/yr (Bethke, 1986).

Density-driven free convection cells were also proposed by Coniglio et al. (1994) as an alternative mechanism for circulation of Mg-bearing Silurian seawater in Middle Ordovician rocks through network of fractures over the Algonquin Arch. However, the heat sources for maintaining convection cells were not identified. Here we present evidence that suggests these convection cells formed in the central part of the basin instead of over the Algonquin Arch and hot fluids migrated through permeable beds at the Precambrian-Palaeozoic unconformity toward the margin of the basin.

A thermal anomaly over the buried mid-continent rift (MCR) in the center of the Michigan Basin (Fig. 3.15) is attributed to reactivation of MCR (Girard and Barnes, 1995). K-Ar dating of authigenic illite yielded ages ranging from Late Devonian to Mississippian (367 to 322 Ma). The youngest (322 Ma) illite samples have more depleted $\delta^{18}\text{O}$ values and the highest estimated precipitation temperatures ($\sim 170^\circ\text{C}$) in the vicinity of the rift (Girard and Barnes, 1995). This also could be an indication of increasing heat flux with time. Furthermore, the maximum homogenization temperature (170°C) of quartz overgrowth cements that postdate illite were recorded from samples located over the buried mid-continent rift (MCR).

Simo et al. (1994) also reported high homogenization temperatures ($175 \pm 25^\circ\text{C}$) for late stage saddle dolomite in the Middle Ordovician Glenwood Formation in the central part of the Michigan Basin. In addition, results of numerical modeling have also shown that hydrothermal process could originate from buried mid-continent rift through circulation of fluids in highly fractured basement rocks at the base of sedimentary sequence and could be responsible for the high basin temperatures (Nunn, 1994; Schoofs et al., 2000).

Infiltration and penetration of Devonian seawater dissolved halite in Devonian and Silurian evaporites at the center of the basin, resulting in high salinity brines. Dense brines became warm while descending and reactivation of the MCR during Late Devonian-Mississippian provided an additional heat source for the establishment of thermally-driven convection cells. The cooling rate of brines in midcontinent sedimentary basins is estimated to be $0.1^\circ\text{C}/\text{km}$ (Bethke and Marshak, 1990). Assuming a maximum fluid temperature of 170°C in the central part of the basin (Girard and Barnes, 1995; Simo

et al., 1994) and a cooling rate of 0.1°C/km, total fluid heat loss would be 20°C for upward and lateral migration of hot brines from the center of the basin toward the basin margin 200 km away. It is important to note that we observed a decreasing trend in average homogenization temperature of saddle dolomite (D3b) from samples closer to the center of the basin (128°C) to samples (121°C) farther from the basin center.

In sedimentary basins characterized by alternating sedimentary rocks with variable permeabilities, faults and fractures can facilitate cross-formational fluid flow (Bjorlykke, 1994). They effectively provide a continuous void space that acts as a conduit for fluid flow. Intermittent reactivation of basement structures was suggested to control the location of Paleozoic fault and fracture systems in the Paleozoic sedimentary cover of southern Ontario (Sanford et al., 1985, Boyce and Morris, 2002).

Cambrian rocks in the subsurface of southwestern Ontario are dominated by quartzose sandstones of the Eau Claire and Mount Simon formations. These units unconformably overlie the Precambrian basement and wedge out towards the east (Armstrong and Carter, 2006). These high permeability sandstones could have acted as a regional aquifer throughout the basin for ascending hot brines from the center of the basin toward its margin (Harper et al., 1995; Ziegler and Longstaffe, 2000) with much higher fluid flow rates and less heat loss relative to compaction-driven fluid flow proposed by Coniglio et al. (1994). In addition, interaction of brines with plagioclase-rich sandstones of Eau Clair and Mount Simon formations (Armstrong and Carter, 2006) could explain more radiogenic $^{87}\text{Sr}/^{86}\text{Sr}$ ratios in saddle dolomite (D3b).

The least radiogenic $^{87}\text{Sr}/^{86}\text{Sr}$ ratios of matrix dolomite (D2) relative to Middle Ordovician seawater is in the range of $^{87}\text{Sr}/^{86}\text{Sr}$ ratios of younger seawater (Devonian and/or Silurian) suggest possible involvement of Devonian and/or Silurian seawater in dolomitization. On the other hand interaction and circulation of dolomitizing fluids in highly fractured ultramafic rocks of the buried mid-continent rift could be an alternative scenario for lower $^{87}\text{Sr}/^{86}\text{Sr}$ ratios of D2. The progressive increase in $\delta^{18}\text{O}_{\text{fluid}}$ from D2 (–6 to +2‰ VSMOW) to D3 (–2 to +5‰ VSMOW) suggest mixing of ^{18}O -enriched younger seawater (–3.5 to –1‰ VSMOW) with *in situ* formation waters. Progressive REE enrichment from D2 to D3b and similar REE pattern of dolomite (D2 and D3b) and the

overlying shale also support downward migration of seawater-derived brines. The increasing trend in T_h values from D2 to D3b could be due to a gradual temperature increase over the MCR which was previously suggested based on a decrease in the $\delta^{18}\text{O}$ values of illite in St. Peter and Glenwood sandstone over the time period from 370 to 322 Ma (Girard and Barnes, 1995).

Thermally-driven outward fluid flow from the center of the basin also explains the absence of fracture-related dolomitization and gradual decreasing temperature trend in D3-hosted fluid inclusions towards the east and away from the Michigan Basin. The occurrence of fracture-related dolomite in the periphery of the Michigan Basin further supports that dolomitizing fluids originated from the Michigan Basin rather than Appalachian Basin. Basin-wide buoyancy-driven fluid flow and heat transfer in the Michigan Basin was controlled by an active fault framework during Paleozoic and basal sandstone aquifer systems. A fracture system in the center of the basin was the main locus of seawater recharge into the basin, while another fracture network at the basin margin acted to focus discharge of basinal brines to the surface.

The homogenization temperatures measured in saddle dolomites in different parts of the Michigan Basin and neighbouring states (Coniglio and Williams-Jones, 1992; Middleton et al., 1993; Yoo et al., 2000; Luczaj, 2006; this study) are considerably higher than those that could arise from burial alone. This could be an indication of the presence of a regional hydrothermal system with a radial outward flow from the center of the Michigan Basin (Fig. 3.15).

3.6 Conclusions

Based on detailed field and core examination with petrographic, geochemical, and fluid inclusion analyses, several conclusions can be made regarding the diagenesis and mineralization of the Trenton Group, as follows:

- 1) Petrographic, fluid-inclusion, and stable isotope data indicate that there are several types of dolomite in the Trenton Group, ranging from early diagenetic to late hydrothermal. From the oldest to the youngest, these are: fine crystalline dolomite (D1); subhedral, replacive matrix dolomite (D2); and anhedral, fracture-filling saddle

dolomite (D3b). D1 is rare and limited to cores and outcrops where fracture dolomitization is absent. D2 is the most abundant dolomite and D3b predominantly filled fractures. Late-stage calcites (C3) postdate saddle dolomite.

- 2) Petrographic and oxygen isotopic composition suggest that D1 dolomite formed in early stages of diagenesis from Middle Ordovician seawater and recrystallized during the early stages of burial. Replacive matrix dolomite (D2) is inferred to have precipitated during progressive burial from a warm fluid (67.6° to 98.9°C) that had $^{87}\text{Sr}/^{86}\text{Sr}$ ratios in the range of Devonian seawater.
- 3) High homogenization temperature (96.7 to 143.5°C) and salinity (21.5 to 24.4 wt. % NaCl+CaCl₂) of D3b suggest a hydrothermal origin. Similar $\delta^{18}\text{O}$ and $^{87}\text{Sr}/^{86}\text{Sr}$ ratios of D2 and D3b suggest recrystallization of D2 during precipitation of D3. The slightly radiogenic $^{87}\text{Sr}/^{86}\text{Sr}$ ratios of D2 and D3b can be attributed to involvement of oil field brines during dolomitization of the precursor sediments.
- 4) C3 precipitated from the same fluid at lower temperature (60.2 to 131.1°C) and lower salinity (19.8 to 22.8 wt. % NaCl+CaCl₂), most likely when the fluid lost its Mg content. The occurrence of hydrocarbon-bearing fluid inclusions in C3 and D3b indicates a common fluid source and hydrocarbon migration during and after saddle dolomite formation.
- 5) ΣREE enrichment relative to undolomitized limestone and the similar REE_{SN} pattern of D2, D3b, and C3 and the overlying shale suggest a common fluid source with progressive water/rock interaction of dolomitizing fluids with shale. However, water/rock interaction with basement rocks also could be an alternative source of REE.
- 6) REE results shows that diagenetic minerals did not essentially preserve the host rock REE signature and fluid REE content could control the diagenetic mineral REE concentration and pattern.
- 7) Integration of petrography, stable isotope, Sr isotope, and REE results indicates that reflux of seawater younger than Ordovician (i.e., Silurian and/or Devonian) dissolved

Devonian and Silurian evaporites and moved downward through the fracture network by density driven fluid flow and circulated in highly fractured basement rocks. Hot brines in the central part of the basin migrated through basal Cambrian sandstone and ascended through the fracture network and precipitated dolomite and late stage calcite while carrying hydrocarbons. A radially outward fluid flow in the Michigan Basin is consistent with occurrence of Middle Ordovician hydrothermal dolomitization in the periphery of the Michigan Basin.

3.7 Acknowledgments

This work was supported by Natural Sciences and Engineering Research Council of Canada (NSERC) grants to I. Al-Aasm and M. Coniglio. Special thanks to M. Price for running the samples for stable isotope ratios. An early draft of this manuscript benefited from an in-depth review and constructive comments by Professor Fereydoun Ghazban.

3.8 References

- Abanda, P. A., Hannigan, R. E., 2006. Effect of diagenesis on trace element partitioning in shales. *Chemical Geology* 230, 42–59.
- Al-Aasm, I. S., Taylor, B. E., South, B., 1990. Stable isotope analysis of multiple carbonate samples using selective acid extraction. *Chemical Geology* 80, 119-125.
- Al-Aasm, I. S., 2000. Chemical and Isotopic Constraints for Recrystallization of Sedimentary Dolomites from the Western Canada Sedimentary Basin. *Aquatic Geochemistry* 6, 229-250.
- Allan, J. R., Wiggins, W. D., 1993. Dolomite reservoirs: geochemical techniques for evaluating origin and distribution. AAPG Continuing Education Course Note Series 36, 129.
- Allwood, A. C., Kamber, B. S., Walter, M. R., Burch, I. W., Kanik, I., 2010. Trace elements record depositional history of an Early Archean stromatolitic carbonate platform. *Chemical Geology* 270, 148–163.
- Armstrong, D. K., Carter, T. R., 2006. An updated guide to subsurface Paleozoic stratigraphy of southern Ontario. Ontario Geological Survey, Open File Report 6191, 214.

- Azmy, K., Veizer, J., Bassett, M. G., Copper, P., 1998. Oxygen and carbon isotopic composition of Silurian brachiopods: Implications for coeval seawater and glaciations. *Geological Society of America Bulletin* 110, 1499-1512.
- Azmy, K., Veizer, J., Wenzel, B., Bassett, M. G. Copper, P. 1999. Silurian strontium isotope stratigraphy. *Geological Society of America Bulletin* 111, 475-483.
- Azmy, K., Brand, U., Sylvester, P., Gleeson, S. A., Logan, A., Bitner, M. A., 2011. Biogenic and abiogenic low-Mg calcite (bLMC and aLMC): Evaluation of seawater-REE composition, water masses and carbonate diagenesis. *Chemical Geology*, 280, 180–190.
- Banner, J. L., Hanson, G. N., Meyers, W. J., 1988. Rare earth element and Nd isotopic variations in regionally extensive dolomites from the Burlington–Keokuk Formation (Mississippian): implications for REE mobility during carbonate diagenesis. *Journal of Sedimentary Petrology* 58, 415–432.
- Barnaby, R. J., Oetting, G. C., Gao, G., 2004. Strontium isotopic signatures of oil-field waters: Applications for reservoir characterization. *American Association of Petroleum Geologists Bulletin* 88, 1677–1704.
- Bau, M., Alexander, M., 2006. Preservation of primary REE patterns without Ce anomaly during dolomitization of Mid-Paleoproterozoic limestone and the potential re-establishment of marine anoxia immediately after the “Great Oxidation Event”. *South African Journal of Geology*, 109, 81-86.
- Bau, M., Dulski, P., 1996. Distribution of yttrium and rare-earth elements in the Penge and Kuruman iron-formations, Transvaal Supergroup, South Africa. *Precambrian Research* 79, 37–55.
- Bethke, C. M., 1986. Hydrologic Constraints on the Genesis of the Upper Mississippi Valley Mineral District from Illinois Basin Brines. *Economic Geology* 81, 233-249.
- Bethke, C. M., Marshak, S., 1990. Brine migrations across North America the plate tectonics of groundwater. *Annual Review of Earth and Planetary Science* 18, 287-315.
- Bjorlykke, K., 1993. Fluid flow in sedimentary basins. *Sedimentary Geology* 86, 137-158.

- Bjorlykke, K., 1994. Fluid-flow processes and diagenesis in sedimentary basins. In: Parnell, J. (Ed.), *Geofluids: Origin, migration and evolution of fluids in sedimentary basins*. Geological Society special publication 87, 127-140.
- Boyce, J. J., Morris, W. A., 2002. Basement-controlled faulting of Paleozoic strata in southern Ontario, Canada: New evidence from geophysical lineament mapping. *Tectonophysics* 353, 151-171.
- Brand, U., Azmy, K., Tazawa, J., Sano, H., Buhl, D., 2010. Hydrothermal diagenesis of Paleozoic seamount carbonate components. *Chemical Geology* 278, 173-185.
- Brookfield, M. E., Brett, C. E., 1988. Paleoenvironments of Mid-Ordovician (Upper Caradocian) Trenton limestones of southern Ontario, Canada: Storm sedimentation on a shoal-basin shelf model. *Sedimentary Geology* 57, 75-105.
- Budai, J. M., Wilson, W. L. 1991. Diagenetic history of the Trenton and Black River formations in the Michigan Basin. Geological Society of America, Special Paper 256, 73-88.
- Carter, T. R., Trevail, R. A., Easton, R. M., 1996. Basement controls on some hydrocarbon traps in southern Ontario, Canada. In: Van der Pluijm, B.A., Catacosinos, P.A. (Eds.), *Basement and Basins of Eastern North America*. Geological Society of America Special Paper 308, 95-107.
- Cercone, K. R., 1984. Thermal history of Michigan Basin. *American Association of Petroleum Geologists Bulletin* 68, 130–136.
- Chaudhuri, S., Clauer, N., 1992. In: Clauer, N., Chaudhuri, S. (Eds.), *Isotopic Signatures and Sedimentary Records*. Lecture Notes in Earth Sciences 43, 497-529.
- Coniglio, M., Williams-Jones, A. E., 1992. Diagenesis of Ordovician carbonates from the northeast Michigan Basin, Manitoulin Island area, Ontario: evidence from petrography, stable isotopes and fluid inclusions. *Sedimentology* 39, 813-836.
- Coniglio, M., R. Sherlock, Williams-Jones, A. E., Middleton, K., Frape, S. K., 1994. Burial and hydrothermal diagenesis of Ordovician carbonates from the Michigan Basin, Ontario, Canada. In: Purser, B., Tucker, M., Zenger, D. (Eds.), *Dolomites a volume in honour of Dolomieu*. Special Publications of the International Association of Sedimentologists 21, 231-254.

- Conliffe, J., Azmy, K., Gleeson, S. A., Lavoie, D., 2010. Fluids associated with hydrothermal dolomitization in St. George Group, western Newfoundland, Canada. *Geofluids* 10, 422–437.
- Cramer, B. D., Munnecke, A., Schofield, D. I., Haase, K. M., Hasse-Schramm, A., 2011. A revised $^{87}\text{Sr}/^{86}\text{Sr}$ curve for Silurian; Implication for global ocean chemistry and Silurian Time Scale. *The Journal of Geology* 119, 335-349.
- Davies, G. R., Smith, L. B., Jr., 2006. Structurally controlled hydrothermal dolomite reservoir facies: An overview. *American Association of Petroleum Geologists Bulletin* 90, 1641–1690.
- Deming, D., 1994. Fluid flow and heat transport in the upper continental crust. In: Parnell, J. (Ed.), *Geofluids: Origin, migration and evolution of fluids in sedimentary basins*. Geological Society special publication 87, 27-42.
- Felitsyn, S., Morad, S., 2002. REE patterns in latest Neoproterozoic–early Cambrian phosphate concretions and associated organic matter. *Chemical Geology* 187, 257–265.
- Fischer, A. G., 1975, Origin and growth of basins, In: Fischer, A. G., Judson, S. (Eds.), *Petroleum and global tectonics*. Princeton University Press 47-79.
- Friedman, I., O’Neil, J. R., 1977. Compilation of stable isotope fractionation factors of geochemical interest. U.S. Geological Survey Professional Paper 440-kk, 108.
- Garven, G., 1995. Continental-Scale Groundwater Flow and Geologic Processes. *Annual Review of Earth and Planetary Science* 23, 89-117.
- Girard, J. P., Barnes, D. A., 1995. Illitization and paleothermal regimes in the middle Ordovician St. Peter sandstone, central Michigan Basin: K–Ar, oxygen isotope, and fluid inclusion data. *American Association of Petroleum Geologists Bulletin* 79, 49–69.
- Goldstein, R. H., 2003. Petrographic analysis of fluid inclusions, In: Samson, I., Anderson A., and Marshall, D. (Eds.), *Fluid inclusions Analysis and interpretation*. Mineralogical Association of Canada Short Course Series 32, 9–53.
- Hannigan, R. E., Basu, A., 1998. Late diagenetic trace element remobilization in organic-rich black shales of the Taconic foreland basin of Quebec, Ontario and New York.

- In: Schieber, J., Zimmerle, W., Parvinder S. (Eds.), *Shales and Mudstones II, Petrography, petrophysics, geochemistry, and economic geology*, 209-233.
- Harper D. A., Longstaffe F. J., Wadleigh M. A. McNutt R. H., 1995. Secondary K-feldspar at the Precambrian-Paleozoic unconformity, southwestern Ontario. *Canadian Journal of Earth Science* 32, 1432-1450.
- Hitchon, B., Friedman, L., 1969. Geochemistry and origin of formation waters in the western Canadian sedimentary basin. I. Stable isotopes of hydrogen and oxygen. *Geochimica et Cosmochimica Acta* 33, 1321–1349.
- Hobbs, M. Y., Frape, S. K., Shouakar-Stash, O., Kennell, L. R., 2011. Regional hydrogeochemistry - Southern Ontario. Nuclear Waste Management Organization Report, 157.
- Hogarth, C. G., Sibley, D. F., 1985. Thermal history of the Michigan Basin: evidence from conodont coloration index. In: Cercone, K. R., Budai, M. (Eds.), *Middle Ordovician and Silurian Rocks of the Michigan Basin and its Margins*. Michigan Basin Geological Society Special Paper 4, 45-58.
- Hollings, P., Smyk, M., Cousens, B., 2011. The radiogenic isotope characteristics of dikes and sills associated with the Mesoproterozoic Midcontinent Rift near Thunder Bay, Ontario, Canada. *Precambrian Res.* (2011), doi:10.1016/j.precamres.2011.11.006.
- Hower, J., Eslinger, E. V., Hower, M. E., Perry E. A., 1976. Mechanism of burial metamorphism of argillaceous sediments: 1-Mineralogical and chemical evidence. *Geological Society of America Bulletin* 87, 725-737.
- Hurley, N.F., Budros, R., 1990. Albion-Scipio and Stoney Point Fields - USA. Michigan Basin. In: Beaumont, E. A., Foster, N. H., (Eds.), *Stratigraphic Traps I. Treatise of Petroleum Geology Atlas of Oil and Gas Fields*. American Association of Petroleum Geologists 1-37.
- Joachimski, M. M., Breisig, S., Buggisch, W., Talent, J. A., Mawson, R., Gereke, M., Morrow, J.R., Day, J., Weddig, K., 2009. Devonian climate and reef evolution: Insights from oxygen isotopes in apatite. *Earth and Planetary Science Letters* 284, 599–609.

- Johnson, M. D., Armstrong, D. K., Sanford, B. V., Telford, P. G., Rutka, M. A., 1992. Paleozoic and Mesozoic geology of Ontario. In: *Geology of Ontario*, Ontario Geological Survey Special Volume 4, Part 2, 907-1008.
- Kaufman, J., 1994. Numerical models of fluid flow in carbonate platforms: Implications for Dolomitization. *Journal of Sedimentary Research* 64, 128-139.
- Knauth, L. P., Beeunas, M. A., 1986. Isotope geochemistry of fluid inclusions in Permian halite with implications for the isotopic history of ocean water and origin of saline formation waters. *Geochimica et Cosmochimica Acta* 50, 419-433.
- Kucera, J., Cempirek, J., Dolnicek, Z., Mucize, P., Prochaska, W., 2009. Rare earth elements and yttrium geochemistry of dolomite from post-Variscan vein-type mineralization of the NížkýJeseník and Upper Silesian Basins, Czech Republic. *Journal of Geochemical Exploration* 103, 69-79.
- Land, L. S., 1980. The isotopic and trace element geochemistry of dolomite: The state of the art. In: Zenger, D. H., Dunham, J. B., Ethington, R. L. (Eds.) *Concepts and models of dolomitization*. SEPM Special Publication 28, 87-110.
- Land, L.S., 1985. The origin of massive dolomite. *Journal of Geological Education* 33, 112-125.
- Legall, F. D., Barnes, C. R., Macqueen, R. W., 1981. Thermal maturation, burial history and hotspot development, Paleozoic strata of southern Ontario-Quebec, from conodont and acritarch colour alteration index. *Bulletin of Canadian Petroleum Geology* 29, 492-539.
- Lev, S. M., Filer, J. K., Tomascak, P., 2008. Orogenesis vs. diagenesis: Can we use organic-rich shales to interpret the tectonic evolution of a depositional basin? *Earth-Science Reviews* 86, 1-14.
- Luczaj, J. A., 2006. Evidence against the Dorag (mixing-zone) model for dolomitization along the Wisconsin arch-A case for hydrothermal diagenesis. *American Association of Petroleum Geologists Bulletin* 90, 1719-1738.
- Machel, H. G., 2004. Concepts and models of dolomitization: a critical reappraisal. In: *The geometry and petrogenesis of dolomite hydrocarbon reservoirs*. In: Braithwaite, C. J. R., Rizzi, G., Darke, G. (Eds.), *Geological Society Special Publication* 245, 7-63.

- Major, R. P., Lloyd, R. M., Lucia, F. J., 1992. Oxygen isotope composition of Holocene dolomite formed in a humid hypersaline setting. *Geology* 20, 586–588.
- McNutt, R. H., Frape, S. K., Dollar, P., 1987. A strontium, oxygen and hydrogen isotopic composition of brines, Michigan and Appalachian Basins, Ontario and Michigan. *Applied Geochemistry* 2, 495-505.
- Melchin, M. J., Brookfield, M. E., Armstrong, D. K., Coniglio, M., 1994. Stratigraphy, sedimentology and biostratigraphy of the Ordovician rocks of the Lake Simcoe area, south-central Ontario. Geological Association of Canada–Mineralogical Association of Canada, Joint Annual Meeting, Waterloo, Ontario, Guidebook for Field Trip A4, 101.
- Middleton, K., Coniglio, M., Sherlock, R., Frape, S. K., 1993. Dolomitization of Middle Ordovician carbonate reservoirs, southwestern Ontario. *Bulletin of Canadian Petroleum Geology* 41, 150-163.
- Middleton, K. 1990. Dolomitization and porosity development in Middle Ordovician carbonate reservoirs, southwestern Ontario. In: Carter, T.R. (Ed., *Subsurface Geology of Southwestern Ontario; a Core Workshop*, American Association of Petroleum Geologists, 1990 Eastern Section Meeting, 51-68.
- Morrow, D. W., 1982. Descriptive field classification of sedimentary and diagenetic breccia fabrics in carbonate rocks. *Bulletin of Canadian Petroleum Geology* 30, 227-229.
- Nunn, J. A., 1994. Free thermal convection beneath intracratonic basins: thermal and subsidence effects. *Basin Research* 6, 115–130.
- Pinti, D. L., Beland-Otis, C., Tremblay, A., Castro, M. C., Hall, C. M., Marcil, J. S., Lavoie, J. Y., Lapointe, R., 2011. Fossil brines preserved in the St-Lawrence Lowlands, Quebec, Canada as revealed by their chemistry and noble gas isotopes. *Geochimica et Cosmochimica Acta* 75, 4228–4243.
- Prouty, C. E., 1988. Trenton exploration and wrenching tectonics – Michigan Basin and environs. In: Keith, B. D. (Ed.), *The Trenton Group (Upper Ordovician Series) of Eastern North America*. American Association of Petroleum Geologists Studies in Geology 29, 207-236.

- Roedder, E., 1984. Fluid inclusions. Mineralogical Society of America, Review in Mineralogy 12, 646.
- Sanford, B. V., Thomson, F. J., McFall, G. H., 1985. Plate tectonics – a possible controlling mechanism in the development of hydrocarbon traps in southwestern Ontario. Bulletin of Canadian Petroleum Geology 33, 52-71.
- Schoofs, S., Trompert, R.A., Hansen, U., 2000. Thermochemical convection in and beneath intracratonic basins: onset and effects. Journal of Geophysical Research 105, 25567–25585.
- Sheppard, S. M. F., 1986. Characterization and isotopic variations in natural waters. In: Valley, J.W., Taylor, H.P. Jr., O’Neil, J.R. (Eds.) Stable Isotopes in High Temperature Geochemical Processes, Reviews in Mineralogy 16, 165-183.
- Shields, G. A., Carden, G. A. F., Veizer, J., Meidla, T., Rong, J., Li, R. 2003. Sr, C, and O isotope geochemistry of Ordovician brachiopods: A major isotopic event around the Middle-Late Ordovician transition, Geochimica et Cosmochimica Acta 67, 2005-2025.
- Shields, G., Stille, P., 2001. Diagenetic constraints on the use of cerium anomalies as paleoseawater redox proxies: an isotopic and REE study of Cambrian phosphorites. Chemical Geology 175, 29–48.
- Simo, J. A., Johnson, C. M., Vandrey, M. R., Brown, P. E., Castro Giovanni, E., Drzewiecki, P. E., Valley, J. W., Boyer, J. 1994. Burial dolomitization of the Middle Ordovician Glenwood Formation by evaporitic brines, Michigan Basin. Special Publication IAS 21, 169-186.
- Smith, L. B., 2006. Origin and reservoir characteristics of Upper Ordovician Trenton-Black River hydrothermal dolomite reservoirs in New York. American Association of Petroleum Geologists Bulletin 90, 1691-1718.
- Taylor, T. R., Sibley D. E., 1986. Petrography and origin of ferroan dolomite in the Trenton Formation, Ordovician, Michigan Basin, U.S.A. Sedimentology 33, 61-86.
- Van der Voo, R., 1988. Paleozoic paleogeography of North America, Gondwana, and intervening displaced terranes: Comparisons of paleomagnetism with paleoclimatology and biogeographical patterns. Geological Society of America Bulletin 100, 311-324.

- Veizer, J., Ala, D., Azmy, K., Bruckschen, P., Buhl, D., Bruhn, F., Carden, G.A.F., Diener, A., Ebner, S., Godderis, Y., Jasper, T., Korte, C., Pawellek, F., Podlaha, O. G., Strauss, H., 1999. $^{87}\text{Sr}/^{86}\text{Sr}$ and $\delta^{13}\text{C}$ and $\delta^{18}\text{O}$ evolution of Phanerozoic seawater. *Chemical Geology* 161, 59-88.
- Vugrinovich, R., 1988. Shale compaction in the Michigan Basin: estimates of former depth of burial and implications for paleogeothermal gradients. *Bulletin of Canadian Petroleum Geology* 36, 1-8.
- Warren, J. K., 2000. Dolomite: occurrence, evolution and economically important associations. *Earth-Science Reviews* 52, 1–81.
- Webb, G. E., Kamber, B. S., 2000. Rare earth elements in Holocene reefal microbialites: a new shallow seawater proxy. *Geochimica et Cosmochimica Acta* 64, 1557–1565.
- Webb, G. E., Nothdurft, L. D., Kamber, B. S., Kloprogge, J. T., Zhao, J.-X., 2009. Rare earth element geochemistry of scleractinian coral skeleton during meteoric diagenesis: a before and-after sequence through neomorphism of aragonite to calcite. *Sedimentology* 56, 1433–1463.
- Wedepohl, K. H., 1995. The composition of continental crust. *Geochimica et Cosmochimica Acta* 59, 1217-1232.
- Wilson, J. A., and Sengupta, A., 1985. The Trenton Formation in the Michigan Basin and environs: pertinent questions about its stratigraphy and diagenesis, In: Cercone, K. R., Budai, J. M. (Eds.), *Ordovician and Silurian rocks of Michigan Basin: Michigan Basin Geological Society Special Paper* 4, 1-13.
- Wyndham, T., McCulloch, M., Fallon, S., Alibert, C., 2004. High-resolution coral records of rare earth elements in coastal seawater: biogeochemical cycling and a new environmental proxy. *Geochimica et Cosmochimica Acta* 68, 2067–2080.
- Yoo, C. M., Gregg, J. M., Shelton K. L., 2000. Dolomitization and dolomite neomorphism: Trenton and Black River limestone (Middle Ordovician) Northern Indiana, U.S.A. *Journal of Sedimentary Research* 70, 265-274.
- Ziegler, K., and Longstaffe, F. J., 2001. Clay mineral authigenesis along a mid-continent scale fluid conduit in Palaeozoic sedimentary rocks from southern Ontario, Canada. *Clay Minerals* 59, 239-260.

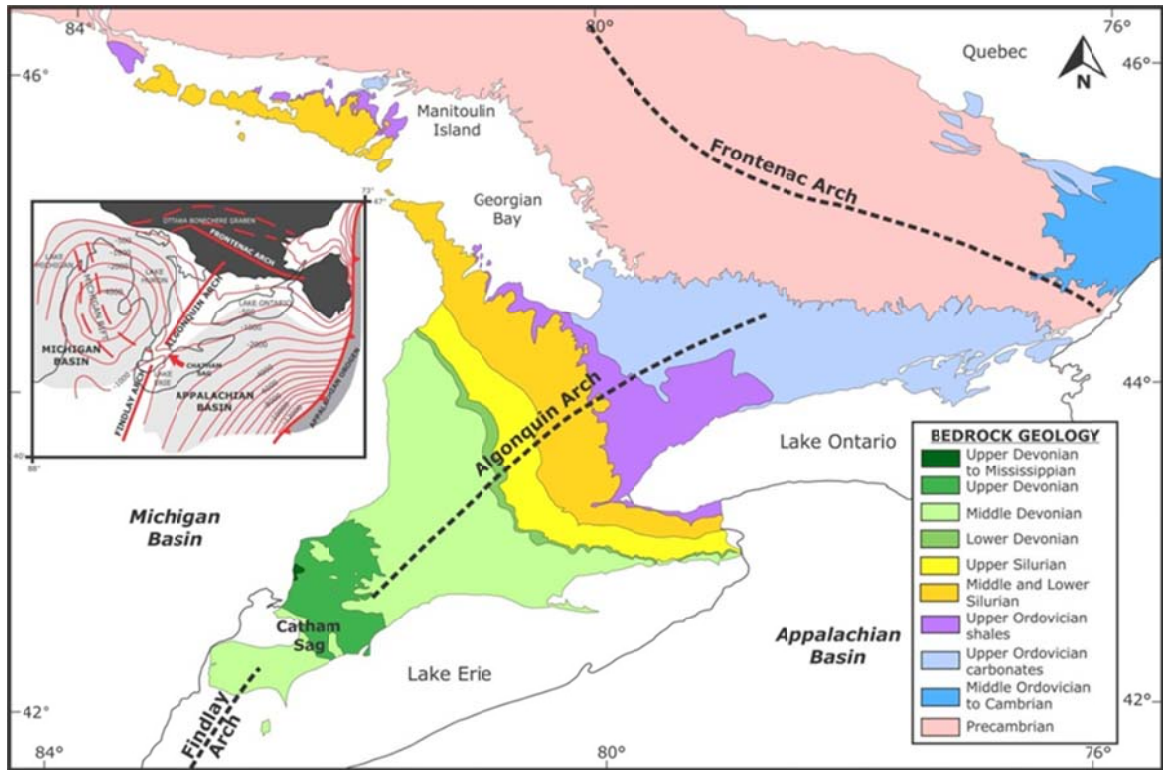


Figure 3.1 Generalized Paleozoic bedrock geology map of southern Ontario (adapted from Armstrong and Carter, 2006). Inset shows generalized basement structural contours (meters above sea level datum) and location of structural arches and basins (adapted from Johnson et al., 1992).

Geologic Time		Stratigraphic Nomenclature		
Period	Epoch	Group	Formation	
Ordovician	Upper	Queenston		
		Georgian Bay - Blue Mountain		
	Middle	Trenton	Cobourg	Collingwood
			Sherman Fall	
			Kirkfield	
		Black River	Coboconk	
			Gull River	
			Shadow Lake	

Figure 3.2 Ordovician stratigraphy of southwestern Ontario (adapted from Armstrong and Carter, 2006).

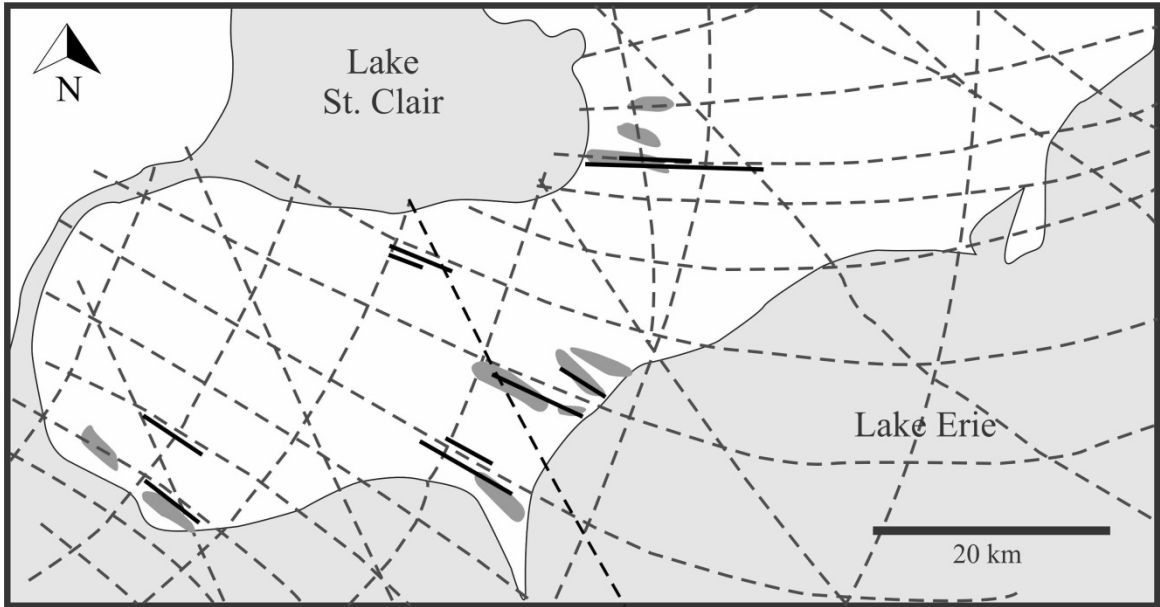


Figure 3.3 Conceptual fault framework (broken grey lines; adapted from Sanford et al. 1985), mapped fault location (solid black lines; adapted from Carter et al., 1996) and location of Ordovician oil fields (adapted from Middleton et al., 1993). Most oil fields are located along major mapped faults.

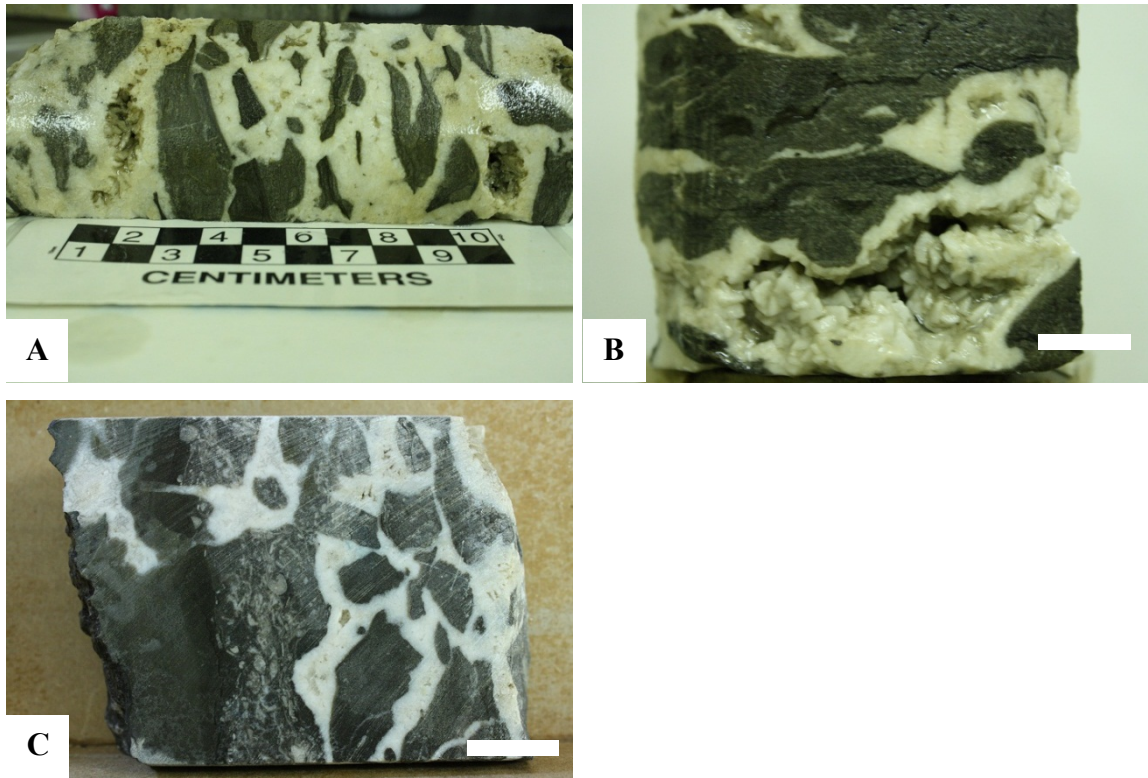


Figure 3.4 Core photographs of Trenton Group (Sherman Fall Formation) carbonates, southwestern Ontario, (A) Chaotic breccia, interparticle space filled with white saddle dolomite (D3), Cons et al 33821, 875 m, (B) Mosaic breccia, interparticle porosity partially occluded by white saddle dolomite (D3), Cons et al 33821, 862 m, scale bar 2 cm, (C) Mosaic breccia, interparticle porosity completely occluded by white saddle dolomite (D3), non-porous argillaceous limestone and packstone are extensively dolomitized and display preservation of original depositional facies, Ram BP No. 17, 756.2 m, scale bar 2 cm.

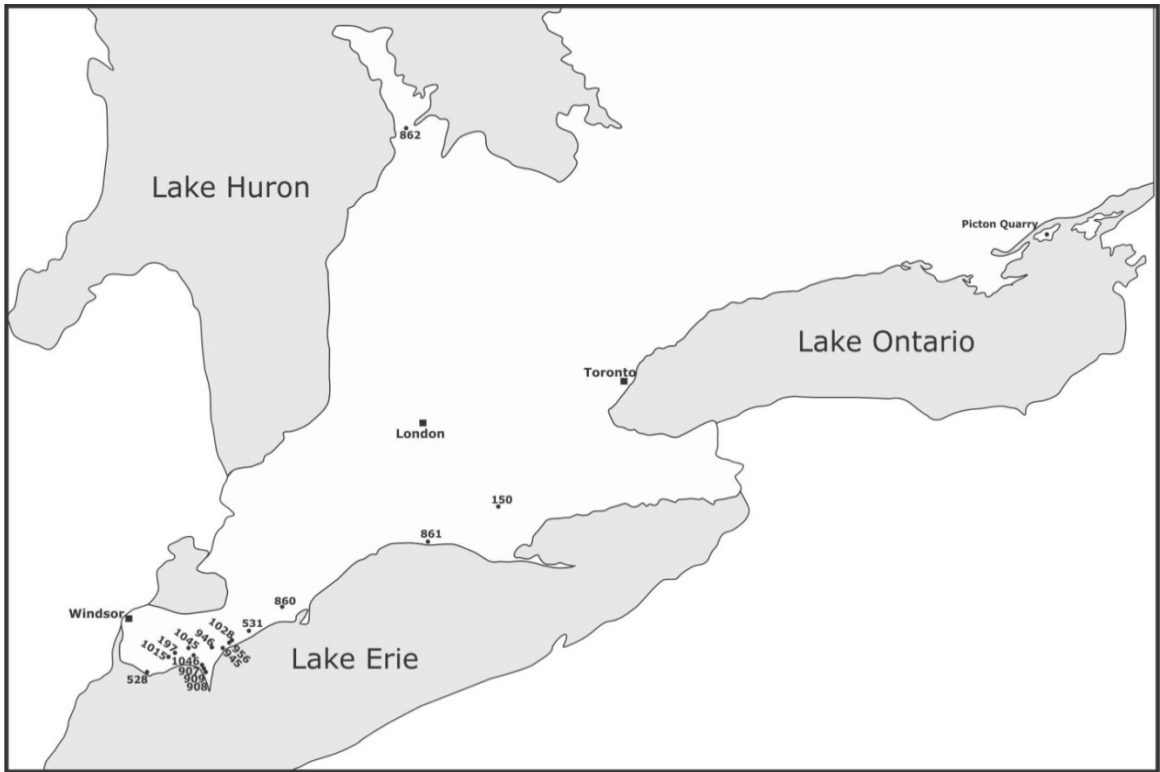


Figure 3.5 Sample location map.

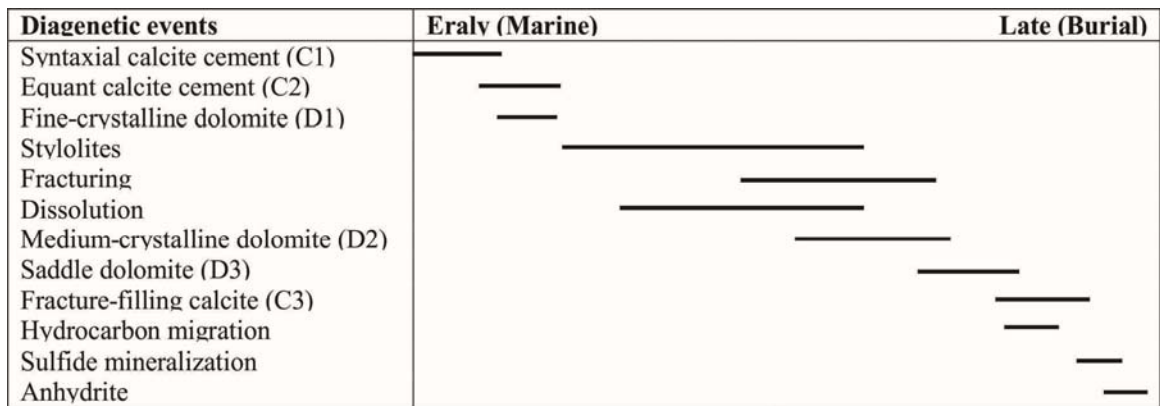


Figure 3.6 Paragenetic sequence of the Sherman Fall Formation in southwestern Ontario, modified after Middleton (1990).

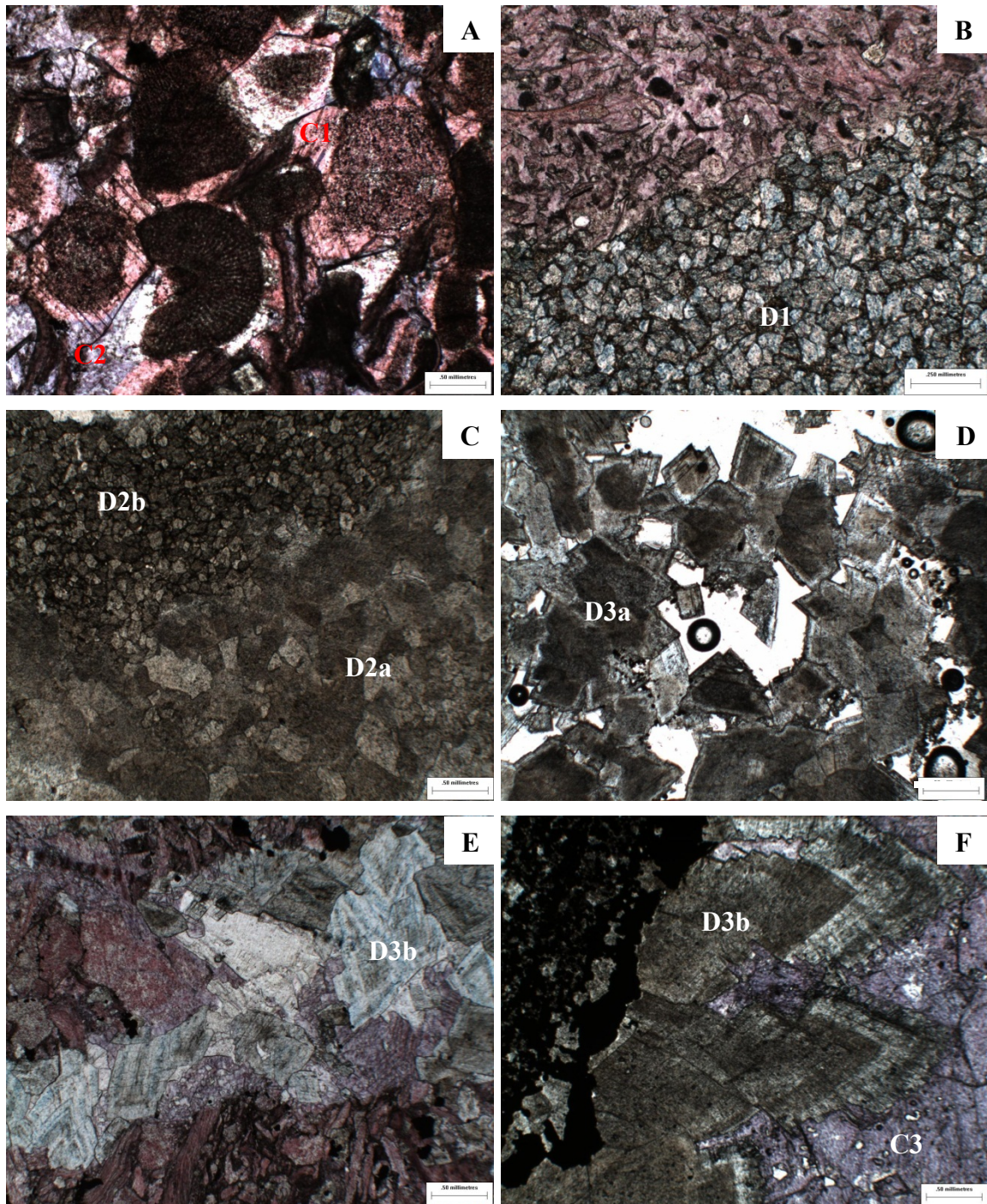


Figure 3.7 Photomicrographs of Trenton Group carbonates, southwestern Ontario; (A) Stained thin section of crinoidal grainstone facies, non-ferroan syntaxial calcite cement (C1) and ferroan blocky calcite cement (C2), Pembina et al, depth 779 m, scale bar 500 μm , (B) Ferroan planar-e to planar-s replacive dolomite (D1) replaced precursor grainstone, Picton quarry, scale bar 250 μm , (C) Coarse planar-s to non-planar, cloudy center crystals of D2a dolomite and finer crystals of planar-s D2b, dolomite, Cons et al 34151, depth 835.1 m, scale bar 500 μm , (D) Planar-e to planar-s crystals of D3a

dolomite. Crystals have a cloudy center and clear rim, in some cases the outer rim is ferroan, D2c displays undulose extinction, Telesis et al 34336, depth 861.3 m, scale bar 500 μm , (E) Saddle dolomite formed in a fracture in a grainstone. Internal parts of saddle crystals are inclusion-rich, outer zones of crystals are ferroan, Imperial et al. 813-Reimer No. 1, depth 757.5 m, scale bar 500 μm , (F) Saddle dolomite (D3b) filled fracture followed by late stage calcite (C3). Pyrite and pyrobitumen predate saddle dolomite. Core of saddle dolomite is inclusion-rich, the rim is slightly ferroan and clear. Corroded outer boundary of saddle crystals indicates minor dedolomitization, Ram BP No. 17, depth 735.2 m scale bar 500 μm

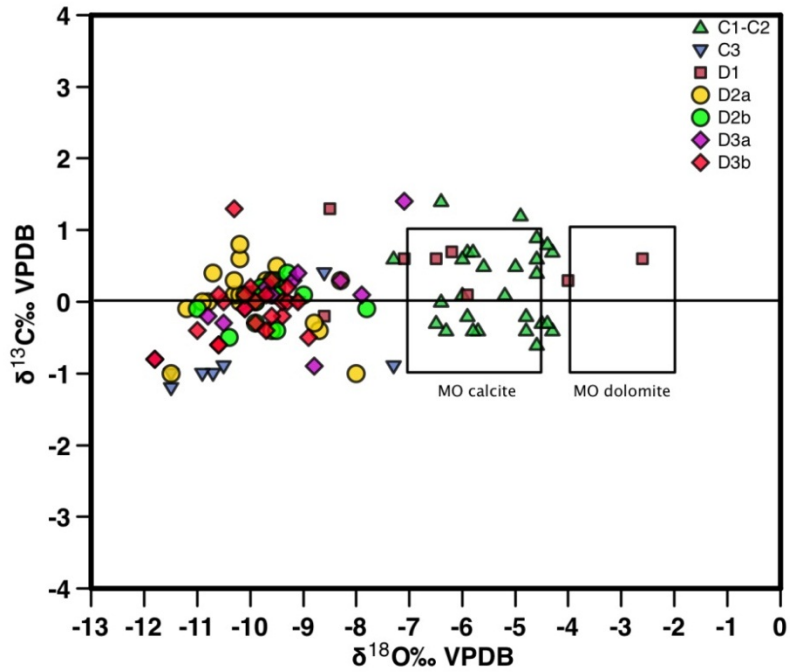


Figure 3.8 $\delta^{18}\text{O}$ and $\delta^{13}\text{C}$ values of replacive dolomite (D2), dolomite cement (D3) and fracture-filling calcite (C3) from the Sherman Fall Formation, southwestern Ontario. The two rectangles show the estimated values for marine calcite and dolomite precipitated from Middle Ordovician (MO) seawater (Shields et al., 2003).

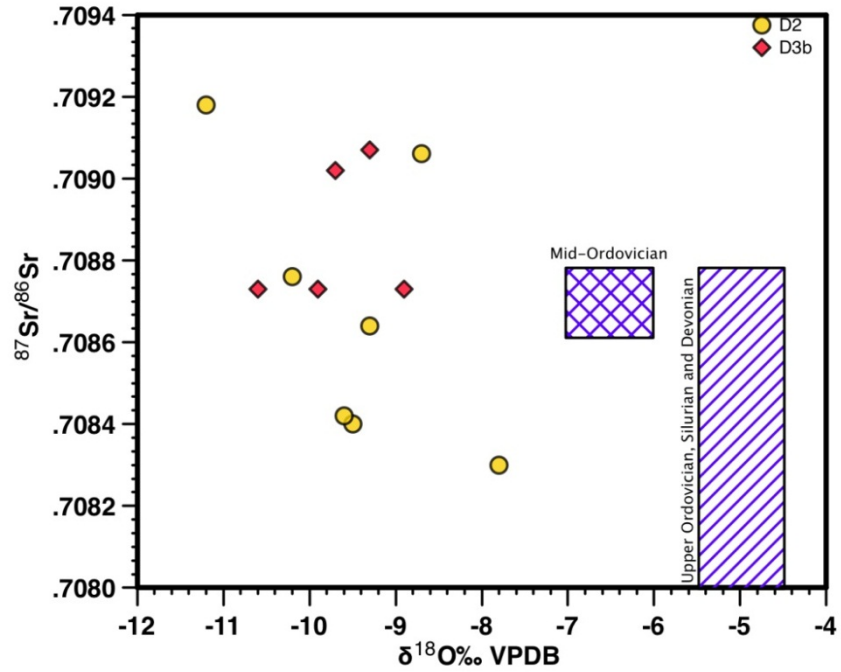


Figure 3.9 Strontium isotopic composition of replacive dolomite (D2) and saddle dolomite cement (D3b) from The Sherman Fall Formation. Boxes show $^{87}\text{Sr}/^{86}\text{Sr}$ ratio of Middle Ordovician carbonates (Shields et al., 2003) and Upper Ordovician and Silurian, Devonian (Veizer et al., 1999; Denison et al., 1997).

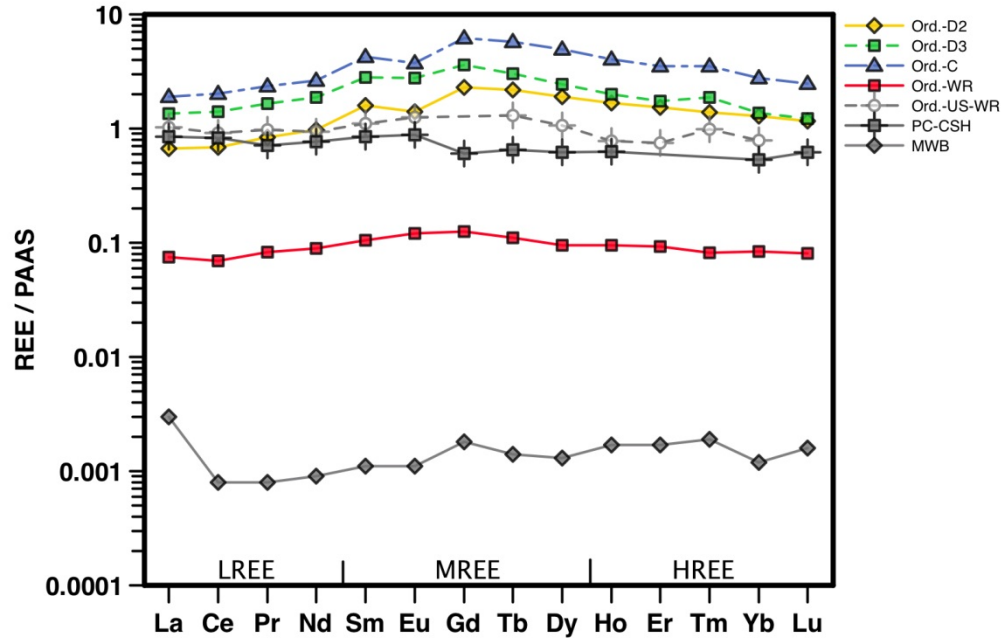


Figure 3.10 PAAS normalized REE pattern for average values of matrix dolomite (D2), saddle dolomite cement (D3b) and fracture-filling calcite (C3) and whole rock (WR) samples. Average PAAS normalized REE pattern of modern warm water brachiopods (MWB; Azmy et al., 2011), Utica shale whole rock (US-WR; Abanda and Hannigan, 2006), and Precambrian Canadian Shield (Wedpohl, 1995) shown for comparison.

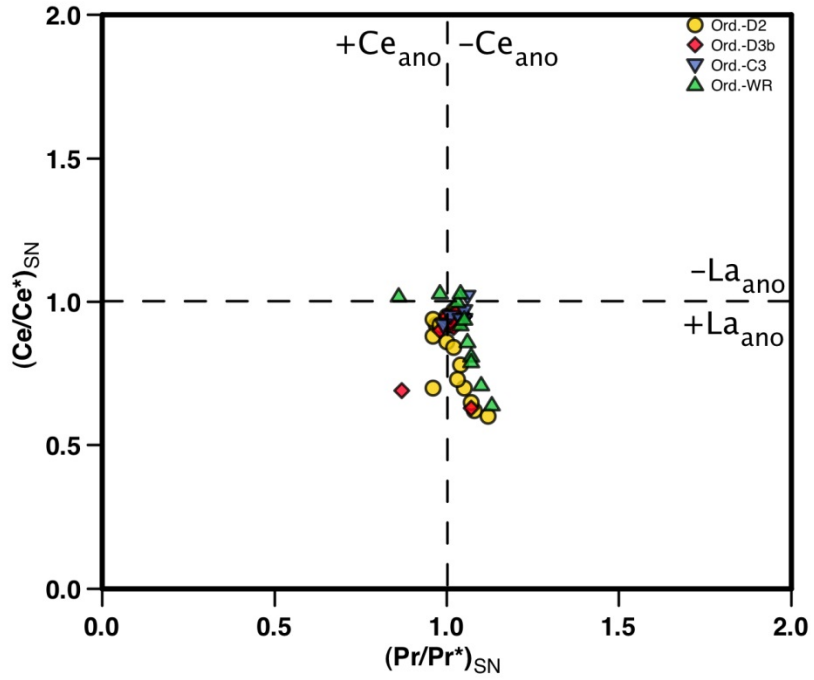


Figure 3.11 Ce $(Ce/Ce^*)_{SN}$ -La $(Pr/Pr^*)_{SN}$ anomaly cross plot of whole rock (WR), D2, D3b, and C3 samples.

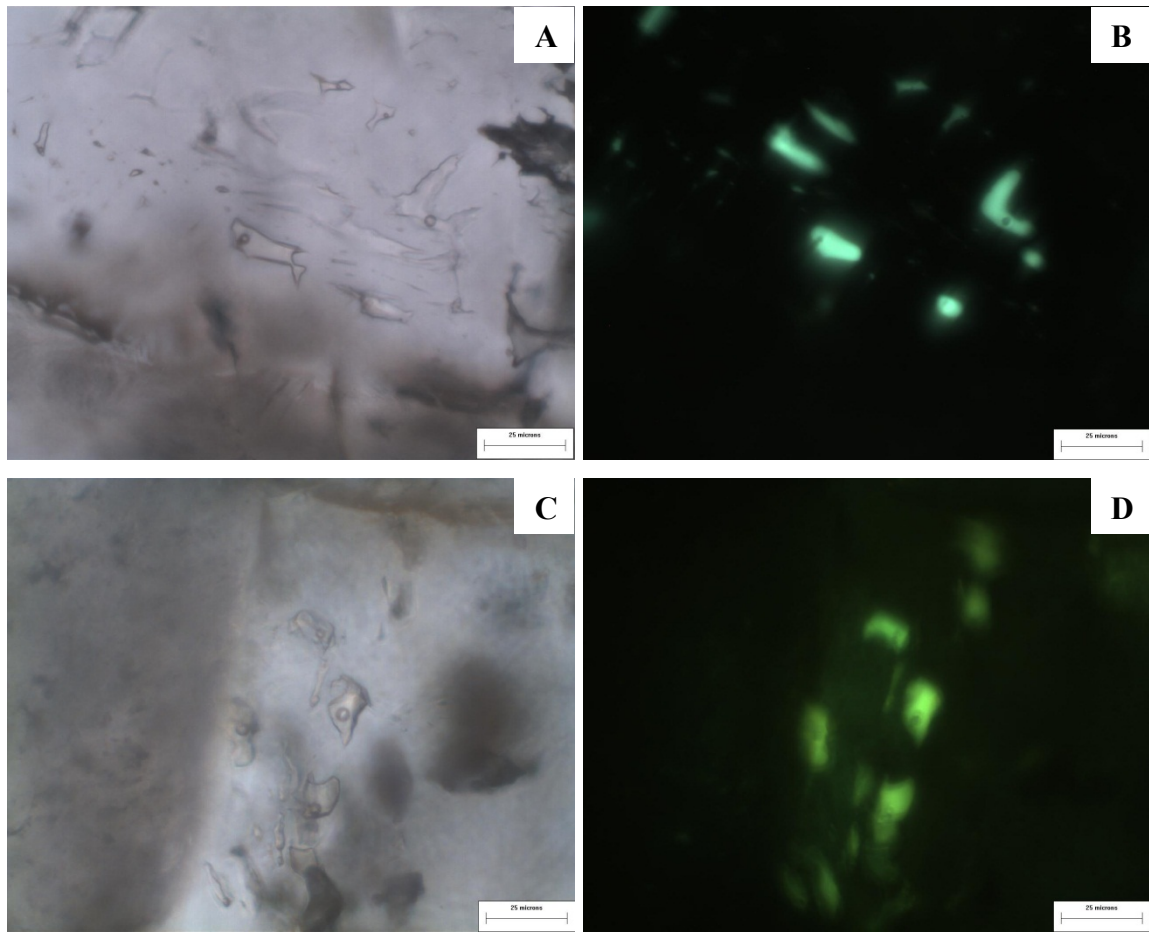


Figure 3.12 Photomicrographs of fluid inclusions. (A) Large fluid inclusion (center) and several small inclusions in saddle dolomite cement (D3b) showing various sizes ranging from 10 to 25 μm . scale bar 25 μm , (B) Same field as in Part A, using fluorescence. The petroleum-bearing inclusion displays bright greenish fluorescence under ultraviolet light, scale bar 25 μm , (C) Fluid inclusions in late stage calcite cement (C3), scale bar 25 μm , (D) Same field as in Part C, under ultraviolet light showing bright greenish yellow colour, scale bar 25 μm .

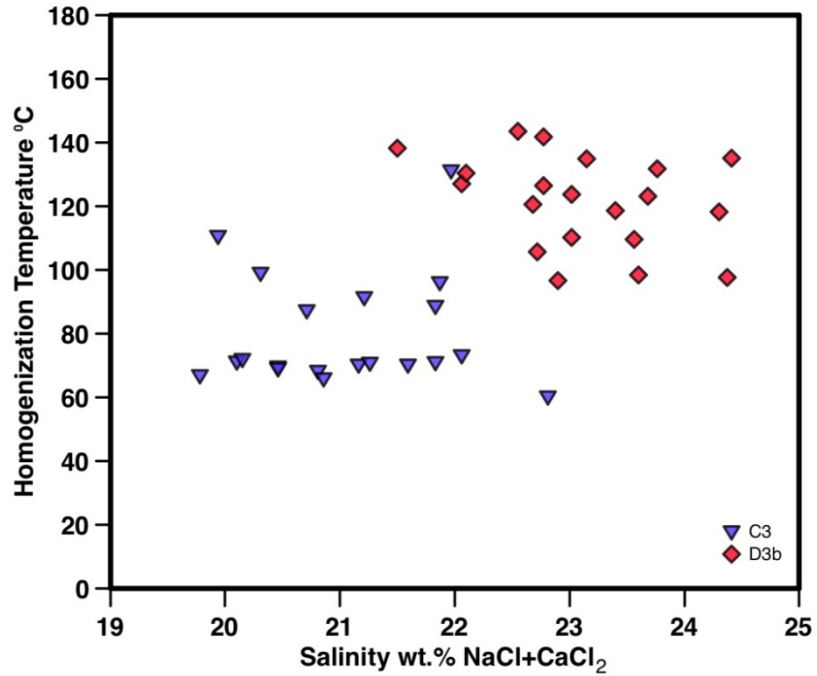


Figure 3.13 Homogenization temperatures and salinities of primary fluid inclusions in saddle dolomite cement (D3b) and fracture-filling calcite (C3). There is a decreasing trend in homogenization temperatures and salinities from D3b to C3.

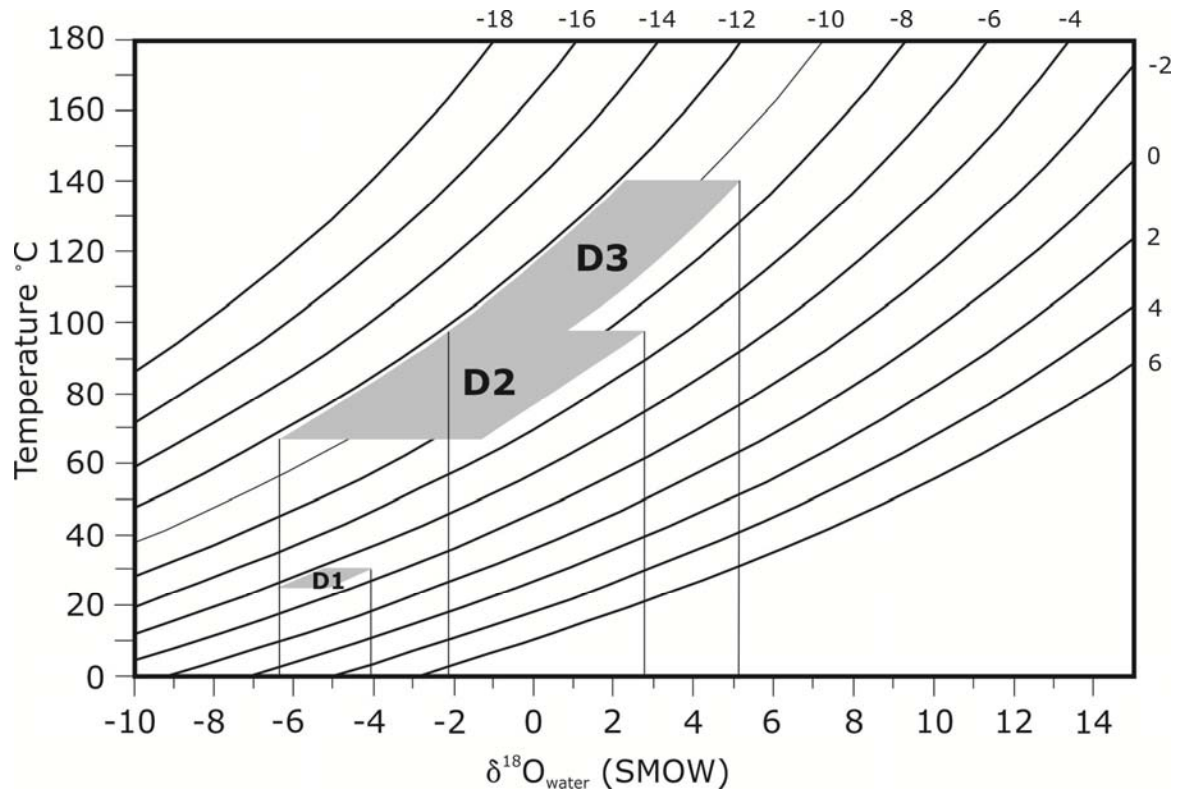


Figure 3.14 Temperature vs. $\delta^{18}\text{O}$ fluid for various $\delta^{18}\text{O}$ values of dolomite derived from the fractionation equation: $10^3 \ln \alpha_{\text{dolomite} - \text{water}} = 3.2 \times 10^6 T^{-2} - 3.3$ (Land 1983). Shaded areas represent range of homogenization temperatures and $\delta^{18}\text{O}$ for various dolomite generations (D1, D2, and D3b).

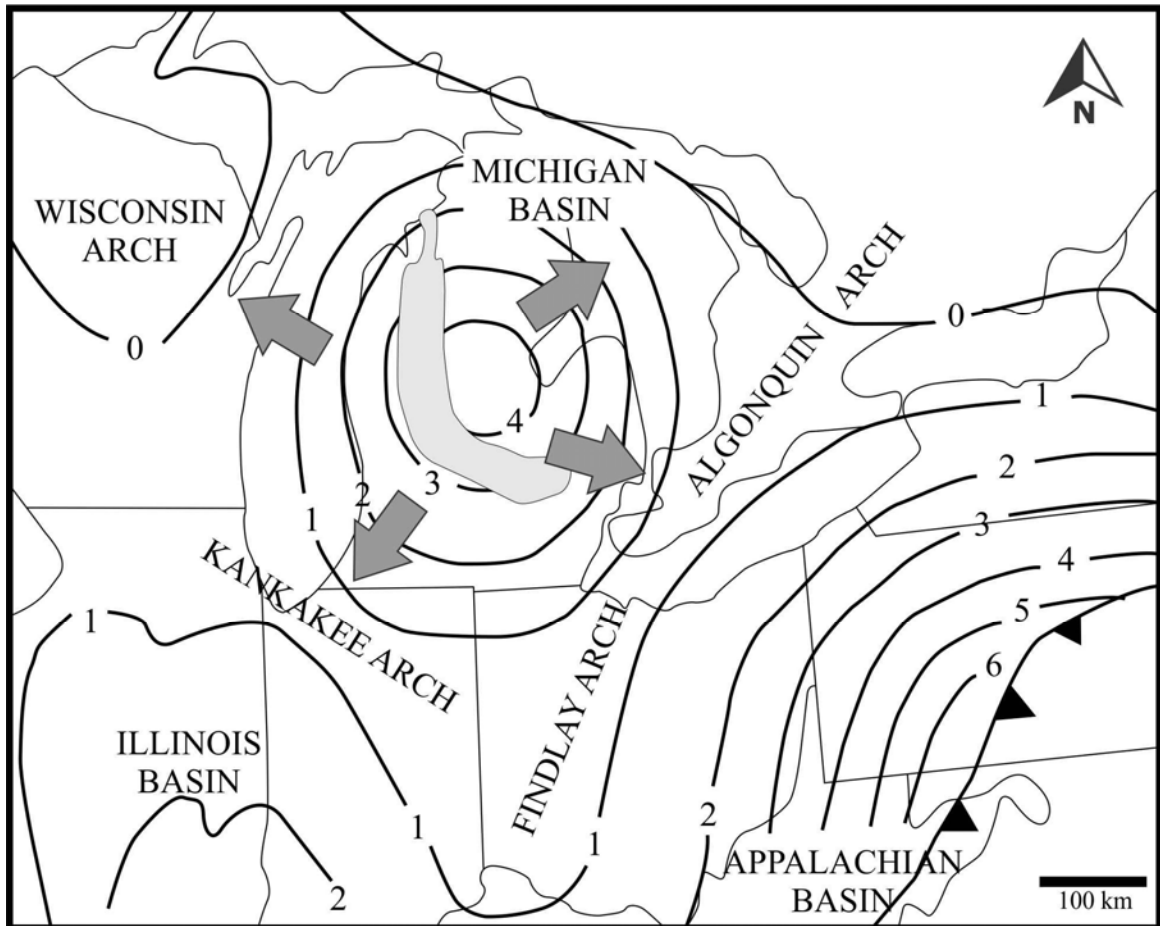


Figure 3.15 Map of the Michigan Basin and surrounding arches and proposed fluid flow out of the Michigan Basin during the Paleozoic (Luczaj, 2006). Evidence of hydrothermal dolomitization of Middle Ordovician carbonates exists around the margins of the Michigan Basin (Coniglio and Williams-Jones, 1992; Coniglio et al., 1994; Yoo et al., 2000; Luczaj, 2006), suggesting that fluid flow was directed radially outward from the center of the basin. The eastern segment of the mid-continent rift (MCR) is shown in gray.

Table 3.1 Carbon and oxygen isotopic composition of the dolomite and fracture-filling calcite of the Sherman Fall Formation.

Lab ID	Sample ID	Age	Mineral	$\delta^{13}\text{C}\text{‰ VPDB}$	$\delta^{18}\text{O}\text{‰ VPDB}$	$^{87}\text{Sr}/^{86}\text{Sr}$	Reference
10-307	3103	Ordovician	D1	1.3	-8.5		
10-302	3084-1	Ordovician	D1	0.5	-5.3		
10-304	3030	Ordovician	D1	0.6	-7.1		
10-308	3075-1	Ordovician	D1	0.6	-2.6		
10-306	3105	Ordovician	D1	0.6	-6.5		
11-084	3091	Ordovician	D1	0.1	-5.9		
11-085	3070	Ordovician	D1	0.7	-6.2		
11-086	3084	Ordovician	D1	0.3	-4.0		
11-088	3072	Ordovician	D1	-0.2	-8.6		
10-179	3061	Ordovician	D2a	-1.0	-8.0		
10-183	3134-1	Ordovician	D2a	-0.1	-11.2	0.70918	
10-184	3034-1	Ordovician	D2a	-0.4	-8.7	0.70906	
10-185	3046	Ordovician	D2a	-0.3	-8.8		
10-187	3122-1	Ordovician	D2a	-1.0	-11.5		
10-194	3130	Ordovician	D2a	0.6	-10.2		
10-196	3011-1	Ordovician	D2a	0.0	-10.2		
10-198	3128	Ordovician	D2a	0.0	-9.9		
10-200	3007	Ordovician	D2a	0.1	-10.3		
10-202	3161	Ordovician	D2a	0.5	-9.5	0.70840	
10-221	3153	Ordovician	D2a	0.0	-10.8		
10-222	3022-1	Ordovician	D2a	0.3	-9.7		
10-223	3141-1	Ordovician	D2a	0.1	-10.0		
10-225	3002-1	Ordovician	D2a	0.1	-10.2	0.70876	
10-230	3011-2	Ordovician	D2a	0.3	-9.5		
10-262	3157-1	Ordovician	D2a	0.0	-10.9		
10-263	3108	Ordovician	D2a	0.3	-8.3		
10-266	3025	Ordovician	D2a	0.8	-10.2		
10-268	3141-1	Ordovician	D2a	-0.1	-11.0		
10-271	3152	Ordovician	D2a	-0.4	-9.6		
10-273	3124-1	Ordovician	D2a	0.1	-9.6		
10-280	3129	Ordovician	D2a	0.3	-10.3		
10-285	3149-1	Ordovician	D2a	0.4	-10.7		
10-178	3106-1	Ordovician	D2b	-0.4	-9.5		
10-182	3111	Ordovician	D2b	0.1	-9.0		
10-193	3118-1	Ordovician	D2b	0.4	-9.3	0.70864	
10-195	3123-1	Ordovician	D2b	0.0	-9.9		
10-197	3006-1	Ordovician	D2b	0.2	-9.5		
10-201	3120-1	Ordovician	D2b	-0.3	-9.9		

Lab ID	Sample ID	Age	Mineral	$\delta^{13}\text{C}\text{‰ VPDB}$	$\delta^{18}\text{O}\text{‰ VPDB}$	$^{87}\text{Sr}/^{86}\text{Sr}$	Reference
10-218	3004-1	Ordovician	D2b	0.1	-9.5		
10-220	3131	Ordovician	D2b	0.3	-9.6		
10-224	3116	Ordovician	D2b	0.1	-10.1		
10-269	3014-1	Ordovician	D2b	0.2	-9.7		
10-278	3151	Ordovician	D2b	-0.5	-10.4		
10-146	3054	Ordovician	D2b	-0.1	-7.8	0.70830	
10-279	3016-1	Ordovician	D2b	0.2	-9.8		
		Ordovician	Matrix dolomite			0.708580	McNutt et al., 1987
		Ordovician	Matrix dolomite			0.708530	McNutt et al., 1987
		Ordovician	Matrix dolomite			0.708510	McNutt et al., 1987
		Ordovician	Matrix dolomite			0.708890	McNutt et al., 1987
		Ordovician	Matrix dolomite			0.708380	McNutt et al., 1987
10-175	3110	Ordovician	D3a	0.3	-8.3		
10-176	3038-1	Ordovician	D3a	0.2	-9.7		
10-188	3037-1	Ordovician	D3a	0.1	-7.9		
10-199	3136	Ordovician	D3a	-0.2	-10.8		
10-219	3029	Ordovician	D3a	0.3	-9.2		
10-228	3121	Ordovician	D3a	-0.9	-8.8		
10-229	3019	Ordovician	D3a	0.4	-9.1		
10-144	3127-1	Ordovician	D3a	-0.1	-10.1		
10-270	3020	Ordovician	D3a	0.1	-9.6	0.70842	
10-277	3135	Ordovician	D3a	-0.8	-11.8		
10-283	3140	Ordovician	D3a	-0.3	-10.5		
10-293	3103	Ordovician	D3a	1.4	-7.1		
10-177	3114	Ordovician	D3b	1.3	-10.3		
10-286	3141-2	Ordovician	D3b	-0.8	-11.8		
10-180	3123-2	Ordovician	D3b	0.3	-9.6		
10-181	3034-2	Ordovician	D3b	-0.5	-8.9	0.708726	
10-186	3011-3	Ordovician	D3b	0.2	-10.0		
10-189	3118-2	Ordovician	D3b	0.0	-9.9	0.708734	
10-190	3004-2	Ordovician	D3b	-0.2	-9.4		
10-191	3116-2	Ordovician	D3b	-0.1	-10.1		
10-192	3006-2	Ordovician	D3b	0.0	-9.4		
10-217	3122-2	Ordovician	D3b	0.1	-9.7		
10-226	3120-2	Ordovician	D3b	-0.2	-9.6		
10-227	3022-2	Ordovician	D3b	0.0	-10.5		
10-264	3002-2	Ordovician	D3b	0.0	-9.3	0.709074	
10-267	3016-2	Ordovician	D3b	0.1	-10.1		
10-272	3124-2	Ordovician	D3b	0.2	-9.3		
10-274	3149-2	Ordovician	D3b	-0.3	-9.9		

Lab ID	Sample ID	Age	Mineral	$\delta^{13}\text{C}\text{‰ VPDB}$	$\delta^{18}\text{O}\text{‰ VPDB}$	$^{87}\text{Sr}/^{86}\text{Sr}$	Reference
10-275	3014-2	Ordovician	D3b	-0.6	-10.6		
10-281	3154	Ordovician	D3b	-0.6	-10.6		
10-282	3131-2	Ordovician	D3b	-0.4	-11.0		
10-284	3157-2	Ordovician	D3b	-0.4	-9.7	0.709019	
10-145	3134-2	Ordovician	D3b	0.1	-10.6	0.708726	
10-276	3141-2	Ordovician	D3b	-0.4	-10.3		
10-261	3333	Ordovician	D3b	0.0	-9.1		
	87-69	Ordovician	Saddle dolomite	0.5	-10		Coniglio and Williams-Jones, 1992
	87-83A	Ordovician	Saddle dolomite	1.3	-9.9		Coniglio and Williams-Jones, 1992
	87-106	Ordovician	Saddle dolomite	-0.1	-9.2		Coniglio and Williams-Jones, 1992
	87-233BB	Ordovician	Saddle dolomite	0.5	-7.9		Coniglio and Williams-Jones, 1992
	87-233BB	Ordovician	Saddle dolomite	0.5	-8.1		Coniglio and Williams-Jones, 1992
	87-K-5B	Ordovician	Saddle dolomite	0.7	-8.3		Coniglio and Williams-Jones, 1992
	88-32A	Ordovician	Saddle dolomite	0.8	-9.4		Coniglio and Williams-Jones, 1992
	87-85	Ordovician	Saddle dolomite	1.3	-9.5		Coniglio and Williams-Jones, 1992
	89-17A	Ordovician	Saddle dolomite	-0.9	-8.8		Coniglio and Williams-Jones, 1992
	89-36B	Ordovician	Saddle dolomite	1.1	-9.6		Coniglio and Williams-Jones, 1992
		Ordovician	Saddle dolomite			0.70861	McNutt et al., 1987
		Ordovician	Saddle dolomite			0.71066	McNutt et al., 1987
		Ordovician	Saddle dolomite			0.71029	McNutt et al., 1987
10-156	3123-3	Ordovician	Late Calcite	0.0	-9.1		
10-157	3116-3	Ordovician	Late Calcite	0.4	-8.6		
10-158	3037-2	Ordovician	Late Calcite	-1.2	-11.5		
10-159	3126	Ordovician	Late Calcite	-0.9	-11.5		
10-216	3150-2	Ordovician	Late Calcite	-1.1	-10.7		
10-150	3014-3	Ordovician	Late Calcite	-1.0	-10.9		
10-151	3127-2	Ordovician	Late Calcite	-0.9	-10.5		
10-155	3002-3	Ordovician	Late Calcite	-0.9	-7.3		
	87-66	Ordovician	Late Calcite	-6.8	-8.0		Coniglio and Williams-Jones, 1992
	87-76	Ordovician	Late Calcite	-3.3	-8.6		Coniglio and Williams-Jones, 1992
	87-78	Ordovician	Late Calcite	1.6	-7.8		Coniglio and Williams-Jones, 1992
	88-10	Ordovician	Late Calcite	-2.5	-9.8		Coniglio and Williams-Jones, 1992
	89-5	Ordovician	Late Calcite	-0.1	-11.2		Coniglio and Williams-Jones, 1992
	89-7	Ordovician	Late Calcite	2.6	-9.4		Coniglio and Williams-Jones, 1992
	89-10	Ordovician	Late Calcite	-5.4	-9.3		Coniglio and Williams-Jones, 1992
	89-17B	Ordovician	Late Calcite	-4.3	-7.2		Coniglio and Williams-Jones, 1992
	89-21	Ordovician	Late Calcite	-13.1	-6.9		Coniglio and Williams-Jones, 1992
	89-25	Ordovician	Late Calcite	-31.2	-6.3		Coniglio and Williams-Jones, 1992
	89-36A	Ordovician	Late Calcite	-1.3	-8.3		Coniglio and Williams-Jones, 1992
	89-37	Ordovician	Late Calcite	-6.2	-8.2		Coniglio and Williams-Jones, 1992

Lab ID	Sample ID	Age	Mineral	$\delta^{13}\text{C}\text{‰ VPDB}$	$\delta^{18}\text{O}\text{‰ VPDB}$	$^{87}\text{Sr}/^{86}\text{Sr}$	Reference
	90-1	Ordovician	Late Calcite	-6.6	-6.4		Coniglio and Williams-Jones, 1992
		Ordovician	Late Calcite			0.70884	McNutt et al., 1987
		Ordovician	Late Calcite			0.70858	McNutt et al., 1987
		Ordovician	Late Calcite			0.70884	McNutt et al., 1987
		Ordovician	Late Calcite			0.70829	McNutt et al., 1987

Table 3.2 Summary statistics of rare earth elements (REE) of selected minerals and undolomitized host rock of the Sherman Fall Formation.

Mineral	La (ppm)	Ce (ppm)	Pr (ppm)	Nd (ppm)	Sm (ppm)	Eu (ppm)	Gd (ppm)	Tb (ppm)	Dy (ppm)	Ho (ppm)	Er (ppm)	Tm (ppm)	Yb (ppm)	Lu (ppm)	ΣREE (ppm)
D2															
n	24	24	24	24	24	24	24	24	24	24	24	24	24	24	24
Avg.	25.54	54.89	7.39	32.97	8.86	1.52	10.68	1.68	8.85	1.65	4.38	0.56	3.63	0.50	206.61
Stdev.	23.92	51.73	6.69	29.60	8.04	1.33	9.79	1.57	8.47	1.58	4.32	0.61	4.06	0.55	185.56
Max.	93.08	179.79	22.07	97.31	23.09	4.03	29.94	4.38	25.60	5.10	14.70	2.23	15.28	1.99	592.94
Min.	2.12	3.05	0.38	1.69	0.35	0.07	0.58	0.07	0.44	0.09	0.26	0.03	0.20	0.02	13.43
D3															
n	10	10	10	10	10	10	10	10	10	10	10	10	10	10	10
Avg.	51.40	111.62	14.68	63.47	15.59	3.01	16.75	2.33	11.46	1.99	4.97	0.76	3.84	0.53	352.50
Stdev.	44.51	99.59	13.38	59.13	15.03	2.02	13.89	1.96	9.36	1.54	3.76	0.45	3.18	0.44	303.37
Max.	147.81	326.75	43.95	194.71	49.57	7.07	44.19	6.28	29.07	4.77	11.67	1.61	9.98	1.30	991.33
Min.	1.43	1.54	0.22	0.88	0.07	0.71	0.30	0.05	0.11	0.04	0.14	0.20	0.12	0.01	6.70
Late															
n	6	6	6	6	6	6	6	6	6	6	6	6	6	6	6
Avg.	72.41	160.14	20.87	89.78	23.66	4.05	28.88	4.45	23.25	4.03	9.98	1.23	7.81	1.07	557.21
Stdev.	70.71	135.67	16.76	74.88	17.75	2.94	23.38	3.39	16.55	2.74	6.47	0.71	4.11	0.53	430.83
Max.	212.28	422.99	52.70	230.52	53.31	8.29	60.18	8.98	47.51	8.47	20.92	2.32	12.69	1.72	1352.12
Min.	21.40	50.92	7.02	29.59	9.46	1.60	10.65	1.44	7.96	1.55	3.96	0.51	3.11	0.44	217.11
WR															
n	11	11	11	11	11	11	11	11	11	11	11	11	11	11	11
Avg.	2.85	5.50	0.73	3.02	0.58	0.13	0.58	0.08	0.44	0.09	0.26	0.03	0.24	0.03	17.76
Stdev.	1.20	2.30	0.32	1.36	0.27	0.06	0.28	0.04	0.21	0.05	0.12	0.01	0.11	0.01	7.47
Max.	5.40	8.30	1.25	5.32	1.04	0.26	1.15	0.17	0.85	0.18	0.51	0.06	0.48	0.06	31.20
Min.	1.30	2.37	0.26	1.20	0.18	0.04	0.20	0.04	0.13	0.03	0.08	0.02	0.11	0.02	7.02

Table 3.3 Summary statistics of fluid inclusion microthermometry results of selected minerals of the Sherman Fall Formation. The complete set of data is presented in Appendix 3.

Age	Mineral	Th °C	Tm °C	Salinity
Ordovician	D2			
Ordovician	n	30		
Ordovician	Avg.	81.8		
Ordovician	Stdev.	9.5		
Ordovician	Max.	98.9		
Ordovician	Min.	67.6		
Ordovician	D3			
Ordovician	n	36	23	23
Ordovician	Avg.	121.1	-25.6	23.9
Ordovician	Stdev.	13.3	1.8	0.7
Ordovician	Max.	143.5	-21.9	25.1
Ordovician	Min.	96.7	-28.8	22.4
Ordovician	Calcite			
Ordovician	n	37	24	24
Ordovician	Avg.	82.6	-21.5	22.1
Ordovician	Stdev.	17.5	2.3	1.0
Ordovician	Max.	131.1	-18.5	24.8
Ordovician	Min.	60.2	-27.9	20.6

Chapter 4

Fracture mineralization and fluid flow evolution: An example from Ordovician-Devonian carbonates, southwestern Ontario, Canada

4.1 Introduction

Fractures are often the primary conduits for pore fluids, and thus have important impact on the diagenetic and evolution of host rocks for hydrocarbon reservoirs. Therefore, understanding fluid flow is essential in order to develop conceptual models that explain the spatial and temporal distribution and connectivity of reservoir porosity and permeability on regional and basinal scales. In the intracratonic Michigan Basin, faults and fractures have played an important role in modifying host limestones and channeling dolomitizing fluids in the basin (Sanford et al., 1985; Coniglio et al., 1994; Carter et al., 1996; Boyce and Morris, 2002).

Regardless of age, most Paleozoic carbonate oil and gas producing reservoirs in the southwestern Ontario part of the Michigan Basin are porous, fractured dolostones. However, there have been no systematic investigations that focus on the temporal and spatial distribution of fracture-related mineralization and the characteristics of the fluid system(s) that channeled throughout Ordovician to Devonian carbonate strata in southwestern Ontario.

Similarities of Ordovician and Devonian hydrocarbons led early workers to suggest upward cross-formational migration of hydrocarbons (Vogler et al., 1981; Obermajer et al., 1999). Several workers also suggested that upward cross-formational fluid flow is responsible for emplacement of saline fluids in Devonian reservoirs (e.g., Wilson and Long, 1993; Weaver et al., 1995; Ma et al., 2005; Luczaj et al., 2006). Debate continues on whether faults and fractures in the underlying Precambrian basement could have provided conduits for fluid migration into the overlying Paleozoic sedimentary succession (Hobbs et al., 2011). In the present study the possible genetic relationship

between dolomitization of Paleozoic carbonates in different formations, using stable isotope geochemistry, Sr isotopes, and rare earth elements will be examined.

4.2 Geologic Setting

During the Paleozoic, southern Ontario was located at tropical latitudes (Van der Voo, 1988) and intermittently covered by inland seas. Erosional and non-depositional gaps occurred within the succession mainly due to regression, resulting in an incomplete stratigraphic record (Johnson et al., 1992). Southwestern Ontario and Michigan are underlain by an essentially undisturbed Paleozoic sedimentary succession resting unconformably on Precambrian basement rocks. Sedimentary rocks in the study area range in age from Upper Cambrian to Upper Devonian.

The study area is located between two major Palaeozoic sedimentary basins, the Appalachian Basin to the southeast and the Michigan Basin to the west (Fig. 4.1). The Michigan and Appalachian basins are two different types of sedimentary basins. The Michigan Basin is a nearly circular intracratonic basin, and is carbonate-dominated and evaporite-bearing. In contrast, the Appalachian Basin is dominated by siliciclastic sediments and is an elongate foreland basin that developed as a result of collisional orogenesis along the eastern margin of North America continent during the Paleozoic (Armstrong and Carter, 2006). The Findlay and Algonquin arches in the Precambrian basement form the boundary between the Paleozoic sedimentary rocks of the Appalachian and Michigan basins (Fig. 4.1).

The NE-SW trending Algonquin Arch extends from northeast of the Canadian shield and terminates to the southwest near the city of Chatham. This structural high continues near Windsor, where it is called the Findlay Arch, extending to southwest into Michigan and Ohio. The structural depression shaped between the two Arch sections is the Chatham Sag (Armstrong and Carter, 2006).

The orogenic activity at the eastern margin of North America controlled the geometry of the basins and the separating arches. Basinal subsidence due to sedimentation and thermal contraction with movement of the arch (e.g., uplift)

collectively are the main tectonic elements controlling sedimentation in the two basins (Johnson et al., 1992; Carter et al., 1996).

The Algonquin and Findlay arches formed a broad platform between the differentially subsiding Michigan Basin in the west and Appalachian Basin to the southeast (Fig. 4.1). The arches formed in the Late Precambrian and remained intermittently active throughout the Palaeozoic (Sanford et al., 1985). All the formations in this region are part of a thick, gently westward-dipping Paleozoic sequence that extends from the Precambrian basement and includes Cambrian sandstone, Ordovician shale and carbonate rocks, Silurian carbonates and evaporites, and Devonian carbonates and shales (Fig. 4.2).

4.2.1 Ordovician carbonates (Black River and Trenton Groups)

Sedimentation of Paleozoic cover in the area commenced with a transgression over the Precambrian basement. This transgression represents one of the greatest sea level rises in geological history (Brookfield and Brett, 1988). This transgression was responsible for the sequence of Black River and Trenton facies assemblages that consist of a succession from supratidal and tidal flat clastics/carbonates to lagoonal carbonates and offshore shallow water and deep shelf carbonates (Brookfield and Brett, 1988).

The Middle Ordovician consists of Trenton and Black River groups, which together range up to 280 meters in thickness. The Black River and Trenton groups consist of fossiliferous carbonates underlying the deeper-water shales of the Blue Mountain Formation (Armstrong and Carter, 2006). The Trenton Group represent the upper part of a widespread carbonate platform developed during the Middle Ordovician over a vast area of the North American craton (Wilson and Segupta, 1985).

4.2.2 Silurian carbonates (Guelph Formation)

During Late to Middle Silurian, southern Ontario and Michigan was flooded by warm shallow seas and lay approximately 25° south of the equator (Van der Voo, 1988). This condition was ideal for development of reefal complexes (barrier and patch reef) in the warm shallow waters and for the formation of pinnacle reefs in deeper waters sloping into the Michigan Basin. These reefal carbonates are known as the Guelph Formation in southern Ontario, while they are called Niagaran carbonates in Michigan. Rapid

subsidence in the center of the basin relative to the margin of the basin caused deeper water basinal facies of the Guelph Formation deposited in the middle of the Michigan Basin, while shallower low energy restricted facies, shallow higher energy facies and reef and inter-reef facies were deposited on the margin of the basin and Algonquin Arch (Armstrong and Goodman, 1990).

Guelph Formation facies were deposited over the carbonate ramp deposits of the underlying Goat Island Member of the Lockport Formation and are overlain by Late Silurian Salina Group cyclical evaporites and carbonates (Fig. 4.2). Lateral and vertical development of the reef bank/barrier reef complex ultimately formed a nearly continuous barrier and transformed the Michigan Basin into an isolated evaporative basin, characterized by cyclical evaporite-carbonate deposits for most of the remaining Silurian (Sonnenfeld and Al-Aasm, 1991).

4.2.3 Devonian carbonates (Lucas Formation)

During the Middle Devonian the Michigan Basin experienced extreme aridity and restricted marine conditions as indicated by fauna and evaporative supratidal, mud flat, shallow intertidal and subtidal lithofacies of the Detroit River Group (i.e., Amherstburg and Lucas formations) (Birchard et al., 2004). The Devonian succession in southwestern Ontario mainly consists of limestones, shales with dolostone and sandstones (Armstrong and Carter, 2006).

Throughout most of the region, the Lucas Formation sharply and conformably overlies the Amherstburg Formation. The Lucas Formation of the Michigan Basin in the study area is characterized as a low-energy, shallow-water evaporitic system (Birchard et al., 2004), while in the Appalachian Basin a more open marine, higher energy depositional environment prevailed during deposition of the Lucas Formation (Birchard et al., 2004). In the Michigan Basin, to the north of Algonquin Arch in general, the Lucas Formation consist fine crystalline dolostone with anhydrite interbeds, while south of Algonquin Arch in the Appalachian Basin it is limestone (Birchard et al., 2004). Anhydrite and anhydritic dolostone interbeds are common lithofacies of the Lucas Formation in the Michigan Basin part of the study area. In deeper wells up to 7 cycles of dolomite capped by anhydrite were reported (Birchard et al., 2004).

4.3 Tectonic setting

Following the formation of the Proterozoic metamorphic basement (Grenville Orogen), the region experienced three pulses of tectonic activity (Sanford, 1993): 1) Taconic (Ordovician), 2) Acadian/Caledonian (Devonian), and 3) Alleghanian (Carboniferous). The major phases of basin subsidence and uplift coincide with peaks of these orogenic cycles and had a controlling effect on the sedimentary input into the region (Sanford et al., 1985).

The resulting stresses were substantial to produce local reactivation of basement structures and regional development of fractures in the Paleozoic cover. These basins and their prevailing arches were active over an extended period of time from the Cambrian until the Carboniferous and major uplift of most of the basin fault blocks occurred at the end of the Mississippian Period (320 Ma).

The basement is believed to have a well-developed pattern of joints and faults, similar to the highly fractured Canadian Shield (Sanford et al., 1985; Boyce and Morris, 2002). Reactivation of deep-seated faults and fractures in the basement of the Michigan Basin has been suggested to account for the circulation of hot fluids and formation of hydrothermal dolomite reservoirs (Sanford et al., 1985; Coniglio et al., 1994; Ma et al., 2009).

4.4 Materials and methods

Most parts of southern Ontario are overlain by a relatively thick cover of glacial deposits. Due to the scarcity of outcrops in the western part of study area, most of the samples for this investigation were obtained from subsurface cores from numerous oil and gas wells drilled and stored in the Ontario Oil, Gas and Salt Resources Library in London, Ontario. Rock exposures and natural outcrops were examined in accessible quarries. Approximately four hundred thin sections were prepared and stained with Alizarin red S and potassium ferricyanide and studied using regular conventional petrographic microscopy as well as ultraviolet and cathodoluminescence microscopy.

For $\delta^{18}\text{O}$ and $\delta^{13}\text{C}$ isotope analysis, approximately 5 mg of selected calcite and dolomite were micro-drilled and reacted with 100% pure phosphoric acid at 25°C for calcite and 50°C for dolomite, respectively (Al-Aasm et al., 1990) and the resultant CO_2

was measured for its oxygen and carbon isotopic ratios on a Delta plus mass spectrometer. Isotopic values are given in δ -notation and reported relative to the VPDB standard. Repeatability of isotopic measurements is better than $\pm 0.05\%$.

Thirty doubly-polished, 100 μm -thick wafers of calcite, dolomite, celestine, fluorite, and sphalerite were prepared for fluid inclusion studies. To avoid reequilibration of fluid inclusions a liquid cooled diamond rotary saw was used to cut samples (Goldstein, 2003). Based on the criteria by Roedder (1984) detailed petrography was carried to determine the type of inclusion (i.e. primary or secondary/pseudosecondary) using an Olympus BX51 microscope.

Fluid inclusion microthermometry measurements were carried out using a Linkam THMG 600 heating-freezing stage at the University of Windsor. Calibration with precision of $\pm 1^\circ\text{C}$ at 300°C and $\pm 0.1^\circ\text{C}$ at -56.6°C was conducted using synthetic H_2O and CO_2 fluid inclusion standards. To reduce the risk of stretching or decrepitation during freezing of inclusions, the fluid inclusion heating experiments were conducted prior to cooling experiments.

The $^{87}\text{Sr}/^{86}\text{Sr}$ isotope ratios were analyzed for few selected calcite cements and matrix dolomites using an automated Finnigan 261 mass spectrometer equipped with nine Faraday collectors. Correction for isotopic fractionation was made by normalization to $^{86}\text{Sr}/^{88}\text{Sr} = 0.1194$. The mean standard error of mass spectrometer performance was ± 0.00003 for standard NBS-987.

Rare Earth Element (REE) concentrations were measured using an X series II Thermo Fisher ICP-MS, subsequent to a general leach and digestion procedure. Each sample powder was weighed, reacted with 1% HNO_3 acid, and then diluted with approximately 50 mg laboratory internal standards. Precision is in the range of 3.3% to 17%, and accuracy is in the range of 1.0% to 6.4%. Measured values were normalized to Post-Archean Australian average Shale (PAAS). The REE and strontium isotope analysis were carried out in Commonwealth Scientific and Industrial Research Organisation (CSIRO) of Australia.

4.5 Results

4.5.1 Petrography

Petrographic investigations indicate various diagenetic minerals including calcite, dolomite, anhydrite, fluorite, sphalerite, and celestine in the Devonian to Ordovician carbonate succession of southwestern Ontario (Figs. 4.3A, B, and C). Different types of replacive dolomite and cement are present. Saddle dolomite occurs only in Silurian and Ordovician rocks as vug- and fracture-filling cement. The abundance of saddle dolomite in Ordovician rocks is significantly higher than in Silurian rocks. The major late-stage diagenetic mineral is vug- and fracture-filling calcite.

4.5.1.1 Devonian

Two main types of replacive dolomite have been distinguished based on petrographic observations. The first occurs throughout the study area and is a fine-grained (D1), crystalline, matrix dolomite with non-planar to planar-s crystals ranging in size from 5 to 20 μm that has mainly replaced mudstone facies, and in some samples replaced peloids (Fig. 4.4A).

The second is a less abundant medium-grained crystalline (50 to 150 μm , average size of 100 μm) planar-e dolomite (D2) with cloudy cores and clear rims (Fig. 4.4B). Medium-crystalline dolomite replaced bioclasts and calcite cement and in some samples is associated with solution seams. Both dolomite types exhibit homogeneous dull-red cathodoluminescence.

Non-ferroan late-stage blocky calcite range in size from 500 μm to 3 mm fills fractures. Fracture-filling calcite cement in shows growth zones of bright and dark orange under CL.

4.5.1.2 Silurian

Three types of dolomite fabrics occur as replacive and cement phases in the Middle Silurian Guelph Formation. These are: non-ferroan fabric destructive unimodal tightly packed replacive fine-crystalline dolomite (D1) with non-planar to planar-s crystals (Fig. 4.4C) ranging in size from 10 to 50 μm . It exhibits homogeneous dull red luminescence and its abundance is less than the other type of replacive dolomite (D2).

The other type is fabric destructive replacive dolomite with planar-s to non-planar crystals (D2) ranging in size from 100 to 250 μm (Fig. 4.4D), with homogeneous red luminescence. Larger crystals commonly show zonation with cloudy centers and clear rims. This dolomite is the most abundant dolomite type. In some samples, the coincidence of fine-crystalline dolomite (D1) and coarser inclusion-rich, non-planar crystals (D2) likely is an indication of recrystallization (Fig. 4.4E).

The third type is non-ferroan vug-filling non-planar saddle dolomite cement with curved crystal faces (D3) with cloudy centers and clear rims and sweeping extinction which range in size from 500 μm to 2 mm (Fig. 4.4C). These crystals have wider clear rims than the medium-crystalline replacive dolomite. It exhibits homogeneous dull red luminescence.

Late-stage blocky calcite cement (Fig. 4.4F) ranges in size from 500 μm to 3 mm with homogeneous light orange luminescence and postdates saddle dolomite and generally occurs in vugs.

4.5.1.3 Ordovician

Three principal types of dolomite are recognized, fine crystalline dolomite with crystal size ranging from 25 to 50 μm (D1), replacing skeletal grains, calcite cement and micrite (Fig. 4.4G). D1 dolomite consists of tightly packed planar-e to planar-s, non-luminescent ferroan rhombs (Fig. 4.4B). Volumetrically, this type of dolomite is less than the other types of dolomite.

Replacive matrix dolomite (D2) is fabric destructive and replaces skeletal grains, micrite and calcite cement. The only recognizable replaced bioclasts are echinoderms. D2 dolomite is volumetrically more abundant than other types and is predominantly fracture-related. It includes two sub-populations of replacement (D2a and D2b) (Figs. 4.4H, and I). D2a forms coarse planar-s to non-planar crystals (300-700 μm) and is crosscut by solution seams. D2b forms planar-s to non-planar crystals ranging in size from 50 to 100 μm . Both D2a and D2b are non-luminescent.

Two types of dolomite cement are present. D3a fills open pore spaces as cement, with planar rhombs ranging in size from 250 to 750 μm , showing strong zonation with cloudy centers and clear rims. D3a crystals show sweeping extinction.

The latest dolomite is vug- and fracture-filling saddle dolomite (D3b). Saddle dolomite cement (Fig. 4.4J) is the most abundant porosity occluding phase and it postdates matrix dolomite (D2). It is zoned with cloudy centers and clear rims and has curved crystal faces. Saddle dolomite crystals range in size from 500 μm to 3 mm and also occur as ferroan cement in limestone. Saddle dolomite crystals exhibit a dull red luminescence or non-luminescence with weak zonation.

Non-ferroan translucent, coarse blocky calcite cement fills secondary pores and fractures and postdates saddle dolomite (Fig. 4.4J). Crystals range in size from 500 μm to 5 mm and exhibit a uniform bright orange. Fracture-filling calcite cement occludes remaining fracture porosity.

4.5.2 Geochemistry

4.5.2.1 Oxygen and carbon isotopes

Replacive dolomite and cement and late-stage calcite cement in fractures (Devonian and Ordovician) and replacive dolomite vug-filling saddle dolomite and late-stage calcite cement (Silurian) from three reservoirs were analysed for oxygen and carbon stable isotopes (Table 4.1, Figs. 4.5A, B, and C).

4.5.2.1.1 Devonian

Fine crystalline matrix dolomite has $\delta^{18}\text{O}$ values ranging from -9.4 to -3.9‰ VPDB and $\delta^{13}\text{C}$ values from 0.9 to 3.3‰ VPDB. Medium crystalline matrix dolomite $\delta^{18}\text{O}$ values vary from -9.3 to -5.8‰ VPDB and $\delta^{13}\text{C}$ values vary from 0.8 to 3.2‰ VPDB. Calcite cement occluding fractures has $\delta^{18}\text{O}$ values ranging from -9.4 to -5.5‰ VPDB and $\delta^{13}\text{C}$ values from -0.1 to -7.7‰ VPDB.

4.5.2.1.2 Silurian

Fine crystalline dolomite (D1) $\delta^{18}\text{O}$ values range from -5.1 to -8.6‰ VPDB and $\delta^{13}\text{C}$ values from 0.6 to 4.8‰ VPDB. D2 dolomite $\delta^{18}\text{O}$ values vary from -4.1 to -8.1‰ VPDB and $\delta^{13}\text{C}$ values from -0.2 to 5.9‰ VPDB. Saddle dolomite cement (D3) yields

$\delta^{18}\text{O}$ values of -4.0 to -10.0‰ VPDB and $\delta^{13}\text{C}$ values from 0.1 to 2.1‰ VPDB. Late-stage vug-filling calcite $\delta^{18}\text{O}$ values vary from -6.7 to -9.5‰ VPDB and $\delta^{13}\text{C}$ values vary from -0.9 to -31.8‰ VPDB.

4.5.2.1.3 Ordovician

Samples of D1 micro-sampled from dolomitic limestone display $\delta^{18}\text{O}$ values ranging from -2.6‰ to -8.6‰ and $\delta^{13}\text{C}$ values of 1.3‰ to -0.2‰ VPDB. D2a samples were analyzed giving $\delta^{13}\text{C}$ values of -1.0‰ to 0.8‰ and $\delta^{18}\text{O}$ values of -11.5‰ to -8.0‰ VPDB. Samples of D2b were analyzed giving $\delta^{13}\text{C}$ values of -0.5‰ to 0.4‰ and $\delta^{18}\text{O}$ values of -10.4‰ to -7.8‰ VPDB.

In addition samples were obtained from D3a yielding $\delta^{13}\text{C}$ values of -0.9‰ to 1.3‰ and $\delta^{18}\text{O}$ values of -11.8‰ to -7.1‰ VPDB. Analyses of D3b dolomite gave $\delta^{13}\text{C}$ and $\delta^{18}\text{O}$ values ranging from 1.3‰ to -0.8‰ , and -8.9‰ to -11.8‰ VPDB, respectively. Fracture-filling calcite cement was analyzed and yielded $\delta^{13}\text{C}$ values of 0.4‰ to -1.2‰ VPDB and $\delta^{18}\text{O}$ values of -7.3‰ to -11.5‰ VPDB.

4.5.2.2 Strontium isotopes

Dolomite from all the three reservoirs was analyzed for $^{87}\text{Sr}/^{86}\text{Sr}$ ratios (Table 4.1, Fig. 4.6A). Fine crystalline dolomite samples of the Middle Devonian Lucas Formation yields $^{87}\text{Sr}/^{86}\text{Sr}$ ratios of 0.7080 to 0.7084 . The $^{87}\text{Sr}/^{86}\text{Sr}$ ratios of selected dolomite samples of Middle Silurian Guelph Formation range from 0.7080 to 0.7093 .

Dolomite samples from Middle Ordovician Trenton Group yields $^{87}\text{Sr}/^{86}\text{Sr}$ ratios from 0.7083 to 0.7093 . Samples of matrix dolomite yields $^{87}\text{Sr}/^{86}\text{Sr}$ ratios ranging from 0.7083 to 0.7092 . These ratios are similar to those obtained from matrix dolomite of Trenton Group by McNutt et al., (1987). The range of $^{87}\text{Sr}/^{86}\text{Sr}$ for saddle dolomite is from 0.7087 to 0.7091 .

4.5.2.3 Rare Earth Elements (REE)

Samples of replacive dolomite, saddle dolomite cement, and fracture- and vug-filling calcite from the Devonian, Silurian, and Ordovician were analysed for REE content (Table 4.2). $\text{Ce}_{\text{SN}} = [(\text{Ce}/\text{Ce}^*)_{\text{SN}} = \text{Ce}_{\text{SN}} / (0.5\text{La}_{\text{SN}} + 0.5\text{Pr}_{\text{SN}})]$, $\text{La}_{\text{SN}} = [(\text{Pr}/\text{Pr}^*)_{\text{SN}} = \text{Pr}_{\text{SN}} / (0.5\text{Ce}_{\text{SN}} + 0.5\text{Nd}_{\text{SN}})]$ anomalies were calculated with the equations of Bau and Dulski (1996).

The Σ REE of Ordovician dolomite and calcite is significantly higher than those in Silurian and Devonian strata (Table 4.2). The REE_{SN} content of dolomite and calcite samples from all ages are higher by one to three order of magnitude relative to modern warm water brachiopods (Figs. 4.7A, B, and C). The REE_{SN} pattern of dolomite and calcite from different ages is different; Devonian samples preserved the seawater REE_{SN} pattern but Silurian and specifically Ordovician samples evidently do not (Figs. 4.7A, B, and C). The Devonian samples exhibit a pronounced positive La anomaly, while Silurian and Ordovician samples show a minor negative La anomaly (Figs. 4.8A, B, and C). The Devonian and Ordovician samples exhibit a predominantly negative Ce anomaly, while Silurian dolomite samples exhibit a positive and negative Ce anomaly.

4.5.3 Fluid inclusions

Fluid inclusion microthermometry data from different minerals (i.e. calcite, saddle dolomite, celestine, fluorite, and sphalerite) from Middle Devonian, Silurian and Ordovician strata are presented in Table 4.3 and Fig. 4.9.

4.5.3.1 Devonian

Microthermometric measurements were made on 104 primary fluid inclusions in samples including fracture-filling calcite (n = 19) and celestine (n = 85). The medium crystalline dolomite contains small inclusions (<3 μ m) unsuitable for microthermometric work. Primary fluid inclusions in calcite samples are located along growth zones, while there is no clear growth zonation in celestine. Large (20 to 40 μ m) fluid inclusions in celestine unrelated to fractures are considered to be primary in origin. Smaller inclusions (5 to 10 μ m) located along fractures are considered as secondary.

Fluid inclusions in both calcite and celestine samples have consistent liquid/vapour (L/V) phases. Some of the inclusions in calcite fluoresce under UV light. The hydrocarbon-bearing inclusions neither homogenized nor froze under high or low temperatures, respectively. Homogenization (T_h) temperatures of non-hydrocarbon bearing fluid inclusions in calcite range from 87.1 °C to 171.9 °C, averaging 126 ± 24.5 °C. Ice melting temperatures range from -15.1 °C to -19.3 °C, averaging -19.3 °C, indicating a salinity of 19.7 ± 0.8 wt. % NaCl.

In addition to two phase (LV) inclusions in celestine, some vapour-rich inclusions were also observed. The salinity of fluids responsible for precipitation of celestine is slightly less than calcite. Ice melting temperatures of celestine range from -6.1°C to -16.1°C , averaging -10.4°C , indicating a salinity of 10.3 to 18.4 wt. % NaCl with a mean value of 14.5 ± 2.9 wt. % NaCl. Homogenization temperatures of celestine vary over a wide range of temperatures from 118.2°C to 321.8°C , with an average of $219.5 \pm 52.8^{\circ}\text{C}$.

4.5.3.2 Silurian

The inclusions are two-phase (liquid-rich with vapor bubble) and have irregular shapes. Rare fluid inclusions in matrix and saddle dolomite were very small, ranging in size from 2 to 8 μm , and contain small vapor bubble composing less than 20 vol. %. Due to the small size of fluid inclusions in matrix and saddle dolomite, it was not possible to measure the last ice melting temperature. Matrix dolomite shows a wide range of T_h values from 64.5° to 140°C averaging $103.7 \pm 19.2^{\circ}\text{C}$ ($n = 32$).

Fluid inclusions in saddle dolomite range in size from 3 to 7 μm and contain a vapor bubble constituting 10 vol. % of the inclusion. Fluid inclusions are aligned growth zonation considered primary in origin. Homogenization temperatures (T_h) in saddle dolomite cement show a range from 91.5° to 123.3°C (average = $105.6 \pm 11.1^{\circ}\text{C}$, $n = 9$).

Fluorite fluid inclusions range in size from 10 to 40 μm and contain vapor bubbles composing about 20 vol. % of the inclusion. Thermometric measurements of fluorite shows a range of T_h values from 93.1° to 118.3°C (average = $108.7 \pm 6.1^{\circ}\text{C}$, $n = 75$) with the last ice-melting temperatures ranging from -33.4° to -26.1°C (average = -31.3°C), indicating salinities in the range of 26.6 to 24.1 wt.% NaCl+CaCl₂ equivalent (with average of 25.9 ± 0.6 wt. %, $n = 75$).

Fluid inclusions in sphalerite range in size from 15 to 35 μm and contain vapor bubbles composing less than 10 vol. % of inclusion. Measured T_h values for sphalerite samples range from 61.6 to 96.3°C (average = $75.2 \pm 9.1^{\circ}\text{C}$, $n = 53$) and last ice-melting temperature range from -21.4° to -26.1°C , corresponding to salinities range from 22.1 to 24.1 wt.% NaCl+CaCl₂ equivalent (with average of 23.2 ± 0.5 , $n = 53$). The salinity values slightly decrease from fluorite to sphalerite, with concurrent decrease in homogenization temperature in sphalerite compared to fluorite.

Zheng (1999) reported T_h values for matrix dolomite that were lower than our measurements. The T_h of matrix dolomite ranges from 64.5 to 116.7°C (average = $88 \pm 19^\circ\text{C}$, $n = 12$) with last ice-melting temperatures range from -9.9 to -31.2°C , indicating salinities in the range of 14.1 to 25.9 wt.% NaCl+CaCl₂ equivalent (average = 20.3 ± 4.9). Saddle dolomite T_h range from 95.7 to 116.8°C (average = $114.7 \pm 14.8^\circ\text{C}$, $n = 4$) with ice-melting temperature range from -29.2 to -32.4°C , indicating salinities from 24.6 to 26.3 wt.% NaCl+CaCl₂ equivalent (average = 25.5 ± 0.7).

4.5.3.3 Ordovician

The inclusions are two-phase (liquid-rich with vapor bubble) showing irregular shapes. Matrix dolomite fluid inclusions are very small, ranging from 2 to 8 μm , and contain small vapor bubble composing less than 20 vol. %. Matrix dolomite shows a narrow range of T_h values from 67.6° to 98.9°C averaging $81.8 \pm 9.5^\circ\text{C}$ ($n = 30$). It was not possible to measure the last ice melting temperature due to small size of the inclusions. Fluid inclusions in saddle dolomite range from 15 to 30 μm and contain a vapor bubble constituting 10 vol. % of the inclusion. Homogenization temperatures (T_h) in saddle dolomite cement show a wider range from 96.7° to 143.5° (average = $121.1 \pm 13.3^\circ\text{C}$, $n = 36$), with the last ice-melting temperatures (T_m) ranging from -28.8° to -21.9°C (average = -25.6°C). These values correspond to salinities of 24.4 to 21.5 wt. % NaCl+CaCl₂ equivalent (with average of 23.9 ± 0.7 , $n = 23$).

Fracture-filling calcite fluid inclusions range in size from 10 to 40 μm and contain vapor bubbles composing less than 20 vol. % of the inclusion. Thermometric measurements of late-stage calcite shows a wide range of T_h values from 60.2° to 131.1°C (average = $83 \pm 17.4^\circ\text{C}$, $n = 37$) with the last ice-melting temperatures range from -24.8° to -18.5°C (average = -21.5°C), indicating salinities in the range of 22.8 to 19.8 wt.% NaCl+CaCl₂ equivalent (with average of 21.2 ± 1 , $n = 24$).

Liquid hydrocarbons are detected in the inclusions of saddle dolomite and fracture-filling calcite in few samples, which showing a slight bright greenish-yellow fluorescence under ultra violet light and commonly homogenize to liquid phase. The inclusions containing hydrocarbons are mainly colourless under transmitted light and did not freeze during the measurement.

4.6 Discussion

4.6.1 Dolomitization models

Dolomitization plays a major role in reservoir creation in the Paleozoic carbonates in southwestern Ontario (Hamilton, 1991; Coniglio et al., 1994; Coniglio et al., 2003). The main hydrocarbon reservoir units in southwestern Ontario are: 1) the Middle Devonian Dundee and Lucas formations, 2) the Middle Silurian Guelph Formation reefs, and Upper Silurian A-1 and A-2 carbonate units of the Salina Group, and 3) the Middle Ordovician Trenton and Black River groups carbonates (Fig. 4.2). Different mechanisms with variable patterns of dolomitization have been proposed for dolomitization of Paleozoic carbonates in the region.

4.6.1.1 Ordovician

Middle Ordovician Trenton Group carbonates are fractured and extensively dolomitized along the axis of the Algonquin Arch in southwestern Ontario. Fractures acted as conduits for dolomitizing fluids. The occurrence of dolomite in the vicinity of fractures implies an epigenetic origin for Middle Ordovician dolomites in the study area. Hot basinal brines migrated laterally through basal sandstones and ascended into the network of faults and fractures and precipitated fracture-related dolomite (Coniglio et al., 1994; Haeri-Ardakani et al., 2012b). The low permeability of Trenton Group host limestones and the focussing of dolomitizing fluids along fractures confined dolomitization to the fractures and a limited volume of rock in the vicinity of fractures.

4.6.1.2 Silurian

Pervasive dolomitization of patch and pinnacle reefs of the Guelph Formation in more platformward positions suggests that dolomitizing fluids migrated from the basin margin towards its center through a regional aquifer (Zheng, 1999; Coniglio et al., 2003). A relative sea level drop in the late Wenlockian isolated the Michigan Basin from the Silurian ocean (Warren, 2006 and references therein). The isolation of the Michigan Basin resulted in deposition of thick sequence of Salina Group evaporites in the central part of the basin. A succession of evaporite-carbonate strata of the Salina Group indicates several episodes of drawdown and reconnection to the surrounding Silurian ocean (Warren, 2006).

The drawdown produced a hydraulic head from the basin margin to its center. A continuous topography-driven flow system produced from drawdown in the center of the basin and forced seawater through permeable reefal Guelph limestone (Zheng, 1999; Coniglio et al., 2003). This flow system best explains the pattern of dolomitization in the Guelph Formation.

The lower Mg^{+2}/Ca^{+2} ratio (~ 1.4), SO_4^{-2} concentration and higher Ca^{+2} concentration of fluids extracted from halite-hosted fluid inclusions from Late Silurian A-1, A-2 and F Unit evaporites in the Michigan Basin compared to evaporated modern seawater (Das et al., 1990; Brennan and Lowenstein, 2002) further support contemporaneous dolomitization of the Guelph Formation and deposition of the Salina Evaporites. Dolomitization (e.g., Das et al., 1990) and anhydrite precipitation could explain lower Mg^{+2}/Ca^{+2} ratio and SO_4^{-2} concentration of fluids extracted from the Salina Group evaporites fluid inclusions. Deposition of A-1 anhydrite over the Guelph Formation produced seal and helped dolomitizing fluids to channel through the Guelph limestone.

4.6.1.3 Devonian

Reflux of hypersaline brines during deposition of the Lucas Formation (Middle Devonian) produced cycles of anhydrite and fine-crystalline dolomite (Haeri-Ardakani et al., 2012a). The thickness and abundance of dolomitized beds decreases away from the Michigan Basin toward the Appalachian Basin. The limited depth of fluid flow in a sabkha environment resulted in thin layers of dolomite (0.3 to 5 m; Hamilton, 1991; Birchard et al., 2004) and a limited amount of dolomite in the Lucas Formation.

Stratigraphy, petrography, and dolomitization pattern of the Paleozoic carbonate succession of southwestern Ontario indicates that Devonian and Silurian dolomite formed in the early stages of diagenesis and under surface conditions, while Ordovician dolomite formed in later stages of diagenesis. Thus, it appears that three different dolomitization mechanisms are largely responsible for dolomitization of Paleozoic carbonates in the study area. The paleohydrology and initial porosity and permeability of precursor limestone or carbonate sediments mainly controlled the extent and pattern of dolomitization of Paleozoic carbonates in southwestern Ontario.

4.6.2 Oxygen and carbon isotope geochemistry

The oxygen isotope composition of diagenetic minerals is controlled by temperature as well as the oxygen isotope composition of the fluid and may provide valuable information about conditions of mineral precipitation or recrystallization (Land, 1985). Dolomite recrystallization is a common process during progressive burial (Al-Aasm, 2000 and references therein). The oxygen and carbon isotopic composition of replacive dolomite and cement from Devonian to Ordovician of the Paleozoic carbonate succession in the study area were used to fingerprint the fluids affected these rocks and determine their temporal and spatial relationships.

Figure 4.5A shows $\delta^{18}\text{O}$ versus $\delta^{13}\text{C}$ cross plot of replacive dolomite of these rocks. There is an overlap in $\delta^{18}\text{O}$ and $\delta^{13}\text{C}$ values of Devonian and Silurian replacive dolomite, while the majority of Ordovician dolomite shows more depleted $\delta^{18}\text{O}$ values relative to Devonian and Silurian replacive dolomite. The $\delta^{13}\text{C}$ values of dolomite from each interval well fit in the range of estimated $\delta^{13}\text{C}$ values of marine calcite of corresponding age. The dolomite $\delta^{13}\text{C}$ of Lucas Formation (0.8 to 3.3‰ VPDB), Guelph Formation (-0.2 to 5.9‰ VPDB), and Trenton Group (-0.9 to 1.4‰ VPDB; Geldern et al., 2006) are in the range of Middle Devonian (0 to 3.5‰ VPDB), Middle Silurian (-1 to 7.5‰ VPDB; Azmy et al., 1998), and Middle Ordovician (-1 to 1.5‰ VPDB; Shields et al., 2003), respectively. The $\delta^{13}\text{C}$ values of the dolomite from each interval are interpreted to reflect the carbon isotopic composition of the respective precursor limestone.

4.6.2.1 Replacive Dolomite

4.6.2.1.1 Devonian

Assuming the Lucas Formation dolomite precipitated in a sabkha environment, dolomitizing fluid was likely to be mainly evaporated Middle Devonian seawater. Evaporated seawater at or near gypsum saturation would be $3 \pm 1\%$ (i.e., 2 to 4‰) enriched in ^{18}O relative to contemporaneous seawater (Gonfiantini 1986). Assuming a $\delta^{18}\text{O}$ value of -2‰ (VSMOW) for Middle Devonian normal seawater (Veizer et al., 1999), the $\delta^{18}\text{O}$ value of evaporated seawater would range from 0 to +2‰ (VSMOW). A dolomite precipitated from such evaporated seawater at temperatures typical of a sabkha setting (30 to 40°C, McKenzie, 1981) would have a $\delta^{18}\text{O}$ value in the range -2.3 to +1.4‰ (avg. = -0.5‰ VPDB), using the fractionation equation of Fritz and Smith (1970)

for proto-dolomite. The $\delta^{18}\text{O}$ value of fine-crystalline dolomite varies in wide range from -3.9 to -9.4‰ ($-6.4 \pm 1.2\text{‰}$ VPDB).

Average $\delta^{18}\text{O}$ value of fine-crystalline dolomite (D1) (-6.4‰ VPDB) is -6‰ more negative than estimated average $\delta^{18}\text{O}$ value (-0.5‰ VPDB) of dolomite precipitated in Middle Devonian sabkha environment. Despite uniform petrographic and cathodoluminescence characteristics, $\delta^{18}\text{O}$ values and $^{87}\text{Sr}/^{86}\text{Sr}$ ratios of Lucas Formation dolomite indicates it has been recrystallized. Recrystallization of early dolomite under high temperature resulted in $\delta^{18}\text{O}$ depletion of fine-crystalline dolomite.

Based on $\delta^{18}\text{O}$ values of Lucas Formation dolomite it appears that dolomite experienced higher temperatures than would be possible under a few hundred metres of burial. Assuming a range of dolomite $\delta^{18}\text{O}$ values (-3.9 to -9.4‰ VPDB), and Middle Devonian evaporated seawater ($\delta^{18}\text{O} = 1.0\text{‰}$ VSMOW), indicates precipitation/recrystallization between 60 and 98°C with an average of $76.7 \pm 8.2^\circ\text{C}$, which corresponds to a range of burial depth of 1.6 to 3.1 km, assuming surface temperature is 20°C and a geothermal gradient of $25^\circ\text{C}/\text{km}$.

The inferred maximum burial temperature for Middle Devonian in southwestern Ontario using conodont and acritarch alteration index is 60°C (Legall et al., 1981). This estimate is in accordance with organic maturity studies of Devonian source rocks (Marcellus and Kettle Point shale) which show that Devonian source rocks in Ontario are immature to marginally mature (Powell et al., 1984; Obermajer et al., 1997). The oil window temperature is between 60 and 90°C (Tissot and Welte, 1984).

A higher estimated temperature (76.7°C) than those expected from maximum burial for Devonian rocks (60°C) implies that recrystallization took place in the presence of hydrothermal fluids. High homogenization temperatures (avg. = 126°C , Haeri-Ardakani et al., 2012a) of late-stage fracture filling calcite in the Lucas Formation and the occurrence of fracture-related hydrothermal (120 to 150°C) saddle dolomite of the Middle Devonian Dundee Formation from the central part of the Michigan Basin (Luczaj et al., 2006) further supports the role of hydrothermal fluids in recrystallization of dolomite.

4.6.2.1.2 Silurian

Assuming the Guelph Formation replacive dolomite formed in the early stages of diagenesis from Silurian seawater (Coniglio et al., 2003), the expected $\delta^{18}\text{O}$ value for dolomite precipitated at 20°C using the paleotemperature equation of Land (1985) would be -0.1‰ (VPDB). However, $\delta^{18}\text{O}$ values of replacive dolomite ranging from -4.1 to -8.6‰ VPDB (this study), and from -5.2 to -9.7‰ VPDB (Zheng, 1999; Coniglio et al., 2003), respectively. These values are significantly more depleted than the estimated value (-0.1‰ VPDB) for Middle Silurian dolomite.

Although there is no systematic co-variation between dolomite crystal size and $\delta^{18}\text{O}$ values of replacive dolomite (e.g., Coniglio et al., 2003) the coincidence of fine-crystalline replacive dolomite with coarser non-planar inclusion-rich crystals of dolomite (Fig. 4.4E) could be an indication of dolomite recrystallization during progressive burial or in the presence of hydrothermal fluids.

Based on the burial curve reconstruction of Zheng (1999), the maximum burial temperatures that would have been experienced by the Guelph Formation in southwestern Ontario, assuming geothermal gradient of 25°C/km and surface temperature of 20°C for 1700 m thick sedimentary cover, would be 62.5°C. Preliminary results of fluid inclusions micro-thermometry (Zheng, 1999) and our T_h measurements from a bigger sample collection of dolomite-hosted (67 to 140°C, avg. = $104 \pm 19^\circ\text{C}$) and fluorite-hosted (93 to 118°C, avg. = $109 \pm 6^\circ\text{C}$) fluid inclusions shows temperatures significantly higher than maximum burial temperatures for Silurian strata which is more evidence for recrystallization in presence of hydrothermal fluids.

The results of fluid inclusion micro-thermometry of replacive and saddle dolomite from the Guelph Formation equivalents (Burnt Bluff Group) in the central part of the Michigan Basin (Barnes et al., 2008) shows an increase in homogenization temperatures (140 to 170°C), which readily explains the observed gradual depletion of dolomite $\delta^{18}\text{O}$ values from patch reef on the platform to the lower slope toward the basin center by Coniglio et al. (2003).

Based on calculated and measured temperatures it appears that hydrothermal fluids were involved in recrystallization of Devonian and Silurian dolomite. The ranges of

dolomite $\delta^{18}\text{O}$ values of the Lucas (-3.9 to -9.4% VPDB) and Guelph (-4.1 to -8.6% VPDB) formations are comparable (Fig. 4.5A). Given the lower burial depth and temperature for Devonian rocks relative to those of Silurian, in order to have similar $\delta^{18}\text{O}_{\text{dolomite}}$ values, the $\delta^{18}\text{O}_{\text{fluid}}$ involved in recrystallization of Lucas Formation dolomite would have to be more ^{18}O -depleted than those involved in recrystallization of Guelph Formation dolomite.

Assuming maximum burial temperature of 60°C for Middle Devonian strata in southwestern Ontario (Legall et al., 1981) the $\delta^{18}\text{O}_{\text{fluid}}$ for this temperature and dolomite $\delta^{18}\text{O}$ values of Lucas Formation (-3.9 to -9.4% VPDB) would range between -5 and $+1\%$ (VSMOW), which is more depleted than Middle Devonian seawater (-2% VSMOW, Veizer et al., 1999) while the $\delta^{18}\text{O}_{\text{fluid}}$ of the Guelph Formation dolomite for measured T_h values (67 to 140°C) ranges from -3 to $+11\%$ (VSMOW).

The calculated $\delta^{18}\text{O}_{\text{fluid}}$ varies from values similar to Middle Silurian seawater (-3.5% VSMOW; Azmy et al., 1998) to those significantly more positive ($+11\%$ VSMOW) than estimated Middle Silurian seawater. The $\delta^{18}\text{O}$ values of basinal brines typically shift toward more positive values as temperature and salinity increase (Sheppard, 1986). Dissolution of thick layers of Late Silurian salt contributed significantly to high salinity of fluids and ^{18}O -enrichment of fluids.

High salinity (27.2 to 31.3 wt. % NaCl) of late-stage fracture-related saddle dolomite-hosted fluid inclusions from Middle Devonian Dundee Formation in central part of the basin (Luczaj et al., 2006) suggests that hypersaline fluids were involved in dolomitization. However, late-stage fracture-filling calcite-hosted fluid inclusions of the Lucas Formation show relatively lower salinities (Fig. 4.9; avg. = 19.7 ± 0.8 wt. % NaCl) which could be an indication of dilution of brine in the margin of the basin.

The calculated ^{18}O -depleted fluids responsible for recrystallization of the Lucas Formation dolomite (-5 to $+1\%$ VSMOW) relative to fluids that recrystallized the Guelph Formation dolomite (-3 to $+11\%$ VSMOW) is likely due to mixing of the brines with meteoric water in the margin of the basin. Progressive decreasing salinities of Middle Devonian fracture-filling calcite and celestine-hosted fluid inclusions (19.7 wt. %

NaCl and 14.4 wt. % NaCl, respectively) relative to Middle Devonian saddle dolomite in the center of the basin (27.2 to 31.3 wt. % NaCl) suggests that Middle Devonian brines were possibly diluted due to mixing with fresh water in the margin of the basin.

Studies of major elements and stable isotopes suggest that these basinal brines originated from ancient seawater and have an evolution history involving water-rock interactions, dissolution of evaporites, and possibly mixing with meteoric water (Wilson and Long, 1993a, 1993b; McIntosh et al., 2004).

4.6.2.1.3 Ordovician

The $\delta^{18}\text{O}$ values of Trenton Group replacive dolomite (D2) (-11.5 to -7.1‰ VPDB) is distinct from and more depleted than Lucas and Guelph formations dolomite (Fig. 4.5A). The depleted $\delta^{18}\text{O}$ values could be in response to higher precipitation temperatures or ^{18}O -depleted fluids. Micro-thermometry of primary matrix dolomite-hosted (D2) fluid inclusions of Trenton Group shows a narrow range of T_h values from 67.6 to 98.9°C with an average of $82 \pm 10^\circ\text{C}$.

The average homogenization of Middle Ordovician replacive dolomite (D2) is lower than the average homogenization temperature ($104 \pm 19^\circ\text{C}$) of the Guelph Formation dolomite. Based on dolomite (D2) $\delta^{18}\text{O}$ values and micro-thermometry data (estimate of minimum entrapment temperatures) the $\delta^{18}\text{O}_{\text{fluid}}$ responsible for precipitation of Middle Ordovician replacive dolomite would range from -6 to $+2\text{‰}$ VSMOW (Land, 1985).

Calculated $\delta^{18}\text{O}_{\text{fluid}}$ for Ordovician replacive dolomite varies from values similar to Middle Ordovician seawater (-6.3‰ VSMOW; Shields et al., 2003) to values more positive ($+2\text{‰}$ VSMOW) than estimated Middle Ordovician seawater which resulting from mixing of Ordovician connate waters with ^{18}O -enriched saline water originated from dissolution of Silurian evaporites by younger seawater (Devonian and/or Silurian).

4.6.2.2 Saddle Dolomite

Saddle dolomite occurs only in Middle Silurian and Ordovician rocks of the study area. The $\delta^{18}\text{O}$ values of saddle dolomite from Middle Silurian and Middle Ordovician samples define two distinct populations with minor overlap (Fig. 4.5B). Middle Silurian

saddle dolomite shows significantly more positive $\delta^{18}\text{O}$ values (-4 to -9.3% VPDB) than Middle Ordovician saddle dolomite samples (-8.9 to -11.8% VPDB). The difference in $\delta^{18}\text{O}$ values of Trenton Group and Guelph Formation saddle dolomite is possible if Silurian dolomite precipitated from cooler and ^{18}O -enriched fluids relative to Ordovician dolomite.

Previous microthermometric analyses (Zheng, 1999) and current study measurement (Fig. 4.9) show that Middle Silurian saddle dolomite precipitated at temperatures ranging from 91.5 to 128.2°C ($108 \pm 12^\circ\text{C}$) with salinities ranging from 24.7 to 26.3 wt. % $\text{NaCl}+\text{CaCl}_2$ (25.5 ± 0.6 wt. % $\text{NaCl}+\text{CaCl}_2$). Whereas Middle Ordovician saddle dolomite precipitated from fluids with temperatures ranging from 96.7 to 143.5°C ($121 \pm 13^\circ\text{C}$) and salinities from 22.4 to 25.1 wt. % $\text{NaCl}+\text{CaCl}_2$ (23.9 ± 0.7 wt. % $\text{NaCl}+\text{CaCl}_2$).

Fluids responsible for precipitation of Silurian saddle dolomite are cooler and slightly more saline than those of Ordovician samples. Calculated $\delta^{18}\text{O}_{\text{fluid}}$ of dolomitizing fluids for Ordovician and Silurian is ranging from -2 to $+6$ and from $+3$ to $+10\%$ (VSMOW), respectively. The ^{18}O -enriched saline fluids could explain unexpectedly more positive $\delta^{18}\text{O}$ values of Middle Silurian saddle dolomite (Fig. 4.5B). Fluids resulting from dissolution of Salina Group evaporites in immediate contact with the Guelph Formation are responsible for high salinity and ^{18}O -enriched fluids that precipitated saddle dolomite. Downward migration of these fluids and mixing with Middle Ordovician connate waters resulted in depleted $\delta^{18}\text{O}_{\text{fluid}}$ values and also slightly lower salinities for Middle Ordovician saddle dolomite (Fig. 4.9).

The inferred maximum paleotemperature for the Palaeozoic sequence from Devonian to Ordovician in southwestern Ontario, based on conodont and acritarch alteration index, ranges from 60 to 90°C (Legall et al., 1981). The measured homogenization temperatures for Middle Silurian and Ordovician saddle dolomite as well as Silurian ($104 \pm 19^\circ\text{C}$) and Devonian ($76.7 \pm 8.2^\circ\text{C}$) replacive dolomite are significantly higher than the maximum burial temperatures for the corresponding interval which could be an indication of involvement of hydrothermal fluids in precipitation/recrystallization of dolomite. In contrast, comparable homogenization temperatures of Middle Ordovician

replacive dolomite ($82 \pm 10^\circ\text{C}$) with a maximum burial (90°C) suggest precipitation of matrix dolomite at maximum burial temperature.

4.6.2.3 Late-stage calcite

Despite the fact that $\delta^{13}\text{C}$ range of the dolomite is within the limits of normal for diagenetic carbonates, however the $\delta^{13}\text{C}$ values (Fig. 4.5C) of the late-stage fracture-filling (Devonian and Ordovician) and vug-filling (Silurian) calcite have significantly depleted values approaching -31.8‰ (VPDB), suggesting the presence of considerable petroleum-derived carbonate in subsurface formation waters. The late-stage calcite $\delta^{13}\text{C}$ of Lucas Formation varies from 0 to -7.7‰ (VPDB), while Guelph Formation (1.3 to -31.8‰ VPDB) and Trenton Group (1.6 to -31.2‰ VPDB; Coniglio and Williams-Jones, 1992) calcite cements show more depleted values.

The low $\delta^{13}\text{C}$ values ($<-10\text{‰}$ VPDB) for oil field brines most likely result from sulfate reduction during bacterial or thermal degradation of organic matter (Carothers and Kharaka, 1980; Franks et al., 2001). The negative $\delta^{13}\text{C}$ values of fracture-filling calcite are interpreted to indicate the incorporation of carbon that was produced by the oxidation of hydrocarbons. In such a model, hydrocarbon oxidation via thermal sulfate reduction (TSR) resulted in production of CO_2 that was incorporated into calcite characterized by low $\delta^{13}\text{C}$ values. The presence of native sulfur postdate celestine in Devonian samples (Figs. 2.6C and 4.3A) and anhydrite postdate saddle dolomite in Ordovician samples (Fig. 4.3C) is evidence of thermal sulfate reduction.

Hydrocarbon-bearing fluid inclusions in Middle Devonian, Silurian (Cercione and Lohmann, 1987) and Ordovician fracture-filling calcite further support the presence of hydrocarbon in brines precipitated late-stage calcite. High homogenization temperatures of Middle Devonian ($126 \pm 25^\circ\text{C}$), Middle Silurian ($104.1 \pm 14.5^\circ\text{C}$; Cercione and Lohmann, 1987) and Middle Ordovician ($83 \pm 17^\circ\text{C}$) indicates that hydrothermal fluids responsible for precipitation of late-stage calcite carried hydrocarbons.

4.6.3 Strontium isotopes

$^{87}\text{Sr}/^{86}\text{Sr}$ ratios could provide significant information with respect to the type of fluids involved in the formation of calcite and dolomite cements and are also used as a geochronological tool for marine sediments (McNutt et al., 1987). In addition, they could

indicate changes in fluid chemistry, degree and extent of water/rock interaction, and as a tracer for basinal fluid movement (Barnaby et al., 2004). The potential sources of ^{87}Sr in sedimentary basin brines are: illitization of smectite, alkali feldspar, and also of detrital mica in the deep subsurface (Chaudhuri and Claur, 1992). $^{87}\text{Sr}/^{86}\text{Sr}$ ratios of dolomite from different ages from southwestern Ontario Paleozoic carbonates were used to quantify sources of dolomitizing fluids and degree of water/rock interaction and mixing of brines.

4.6.3.1 Devonian

$^{87}\text{Sr}/^{86}\text{Sr}$ ratios of Lucas Formation dolomite range from 0.70797 to 0.70838 (Fig. 4.6A) which is slightly more radiogenic than Middle Devonian seawater (0.7078 to 0.7079, Geldern et al., 2006), but in the range of Devonian seawater (0.7078 to 0.7087, Veizer et al., 1999; Geldern et al., 2006). Recent study on hydrogeochemistry of brines in Paleozoic succession of southwestern Ontario (Hobbs et al., 2011) shows that $^{87}\text{Sr}/^{86}\text{Sr}$ ratios of the majority of brines in Devonian-aged carbonate formations are in the range of $^{87}\text{Sr}/^{86}\text{Sr}$ ratios of Devonian seawater except for few samples that more radiogenic than coeval seawater (Fig. 4.6B).

The study (Hobbs et al., 2011) suggested that brines hosted by Devonian carbonates had no major water/rock interaction with siliciclastic rocks or ^{87}Sr -bearing rocks. In contrast, $^{87}\text{Sr}/^{86}\text{Sr}$ ratios of brines in Late Devonian Berea sandstone are significantly more radiogenic than coeval seawater (Hobbs et al., 2011). However, few higher $^{87}\text{Sr}/^{86}\text{Sr}$ ratios of Devonian-hosted brines in carbonate rocks could be reflecting the influence of mixing Late Devonian brines with Middle Devonian counterparts. This may suggest that there were connection between two reservoirs (e.g., Barnaby et al., 2004) and the two rock units were hydraulically connected.

4.6.3.2 Silurian

The majority of Guelph Formation dolomite $^{87}\text{Sr}/^{86}\text{Sr}$ ratios (this study and Zheng, 1999) range from 0.70861 to 0.70887 (Fig. 4.6A), which is in the range of $^{87}\text{Sr}/^{86}\text{Sr}$ ratios of Middle Silurian seawater (0.7084 to 0.7088, Cramer et al., 2012). In contrast to dolomite, the majority of the Guelph Formation brines have $^{87}\text{Sr}/^{86}\text{Sr}$ ratios more radiogenic than coeval seawater and range from 0.70889 to 0.70934 (McNutt et al., 1987;

Hobbs et al., 2011). Variation in $^{87}\text{Sr}/^{86}\text{Sr}$ ratios of dolomite and formation waters implies that fluids with higher $^{87}\text{Sr}/^{86}\text{Sr}$ ratios migrated to reservoirs in later stages of diagenesis likely contemporaneous with hydrocarbon migration, as oil filled brines usually have $^{87}\text{Sr}/^{86}\text{Sr}$ ratios more radiogenic than coeval seawater (e.g., Barnaby et al., 2004).

Results of the recent study of Hobbs et al. (2011) indicate that Guelph Formation brines have $^{87}\text{Sr}/^{86}\text{Sr}$ ratios more radiogenic than Phanerozoic seawater (Fig. 4.6B). Brines of Lower Silurian sandstone (Grimsby, Thorold and Whirlpool) showed even more radiogenic values (0.70977 to 0.71112; Hobbs et al., 2011) than the Guelph Formation brines and coeval seawater. Upward migration and mixing of brines from two reservoirs (i.e. Lower Silurian sandstone and Guelph Formation) could have resulted in higher $^{87}\text{Sr}/^{86}\text{Sr}$ ratios of Guelph Formation brines. Dolomite with higher $^{87}\text{Sr}/^{86}\text{Sr}$ ratios than Middle Silurian seawater (Fig. 4.6A) likely precipitated or recrystallized from fluids after mixing.

4.6.3.3 Ordovician

The $^{87}\text{Sr}/^{86}\text{Sr}$ ratios of Middle Ordovician Trenton Group dolomite (our data and McNutt et al., 1987) is variable and vary from values less radiogenic (0.70830 to 0.70858) to values more radiogenic (0.70902 to 0.71066) than Middle Ordovician seawater (0.7086 to 0.7088; Shields et al., 2003), while the rest of samples $^{87}\text{Sr}/^{86}\text{Sr}$ ratios (0.70861 to 0.70873) fall in the range of respective seawater (Fig. 4.6A). The $^{87}\text{Sr}/^{86}\text{Sr}$ ratios of least radiogenic samples are in the range of estimated values of younger seawater (Late Ordovician, Silurian and Devonian, Fig. 4.6B).

The high salinity of Trenton Group saddle dolomite (avg. = 23.1 wt. % NaCl+CaCl₂; Coniglio et al., 1994; Haeri-Ardakani et al., 2012b) suggest mixing of saline fluids from dissolution of younger evaporites (Silurian and Devonian) with Ordovician connate waters. Therefore, the least radiogenic $^{87}\text{Sr}/^{86}\text{Sr}$ ratios of dolomite could be due to involvement of fluids that originated from younger seawater (Devonian and/or Silurian), whereas samples with Sr isotope ratios in the range of Middle Ordovician seawater suggest they were equilibrated with host rock and coeval seawater.

An alternative reason for the least radiogenic values of Ordovician replacive dolomite (D2) (Fig. 4.6A) is possible water/rock interaction with ultra mafic rocks of

buried mid-continent rift (MCR) beneath the Michigan Basin. The mid-continent rift (MCR) of North America comprises ultramafic and intrusive rocks emplaced during Mesoproterozoic (Hollings et al., 2011). The $^{87}\text{Sr}/^{86}\text{Sr}$ ratio of these rocks varies from 0.7037 to 0.7064 (Hollings et al., 2011). Circulation of diagenetic fluids through highly fractured basement rocks in the center of basin is another possible source of less radiogenic values of replacive dolomite in comparison to Middle Ordovician seawater (e.g., Brand et al., 2010).

More radiogenic $^{87}\text{Sr}/^{86}\text{Sr}$ ratios of dolomite are in the range of Cambrian. The wide range of Middle Ordovician dolomite $^{87}\text{Sr}/^{86}\text{Sr}$ ratios (0.70830 to 0.70918) suggests a dynamic paleohydrological system in the Michigan Basin. A density driven fluid flow combined with thermal-driven convection cells circulated dolomitizing fluid while fluids of different reservoirs mixed (Coniglio et al., 1994; Haeri-Ardakani et al., 2012b). In McNutt et al. (1987) dataset there are two saddle dolomite samples that have $^{87}\text{Sr}/^{86}\text{Sr}$ ratios more radiogenic than Phanerozoic seawater (0.71029 and 0.71066) which is comparable with $^{87}\text{Sr}/^{86}\text{Sr}$ ratios of Trenton Group and Cambrian sandstone brines.

The majority of Trenton Group carbonates and all of the Cambrian sandstone brines are significantly more radiogenic than Phanerozoic seawater (Fig. 4.6B), which implies that these fluids have had extensive water/rock interaction with ^{87}Sr -bearing minerals or they were mixed with higher ^{87}Sr -enriched brines. The basal Cambrian sandstone is arkosic sandstone and contains abundant K-feldspar (Armstrong and Carter, 2006). Circulation of diagenetic fluids through those sandstones could be the cause of the radiogenic $^{87}\text{Sr}/^{86}\text{Sr}$ ratios of brines.

An alternative reason for the elevated $^{87}\text{Sr}/^{86}\text{Sr}$ ratios of Trenton Group and Cambrian brines is interaction of fluids with Precambrian basement rocks. The $^{87}\text{Sr}/^{86}\text{Sr}$ ratios of Precambrian shield brines vary over a wide range of values from 0.70421 to 0.75333 with an average of 0.71535 (McNutt et al., 1990) which is significantly higher than Trenton Group (0.70887 to 0.71045; Hobbs et al., 2011) and Cambrian sandstone (0.70923 to 0.71029; Hobbs et al., 2011) brines. Circulation of hot brines in highly fractured basement rock, upward migration of these fluids, and mixing with Middle Ordovician connate waters could be the cause of fluid $^{87}\text{Sr}/^{86}\text{Sr}$ ratios elevation.

Downward migration of Lower Silurian sandstone brines also could be another potential source of ^{87}Sr -enriched fluids.

Regardless the source of the ^{87}Sr , the comparable ranges of $^{87}\text{Sr}/^{86}\text{Sr}$ ratios of Trenton Group, Cambrian sandstone, and Lower Silurian sandstone brines strongly suggest some sort of fluid mixing. Percolation of younger seawater (Devonian and/or Silurian) through the network of fractures in the center of the basin likely caused mixing of fluids with different origins and resulted in precipitation/recrystallization of Trenton Group dolomite with a wide range of Sr isotope ratios.

The $^{87}\text{Sr}/^{86}\text{Sr}$ ratios of dolomite from all ages vary from values in the range of estimated values for corresponding seawater to values more radiogenic than coeval seawater. This implies that the Sr-isotope composition of dolomitizing fluid(s) has been progressively modified by water/rock interaction with ^{87}Sr -enriched minerals prior to dolomite precipitation/recrystallization.

4.6.4 Rare earth elements (REE)

The rare earth element (REE) shale normalized patterns of modern marine carbonates, including scleractinian corals (Wyndham et al., 2004) and microbialites (Webb and Kamber, 2000) resemble those of their ambient seawater (Webb et al., 2009). However, subsequent diagenetic alteration may change these REE patterns and concentrations (Shields and Stille, 2001; Azmy et al., 2011), and therefore REE can be used as potential indicators of diagenetic redistribution of REE in carbonates (Azmy et al., 2011).

Nonetheless, many workers suggest that carbonates preserve their REE composition and/or pattern during diagenesis (Webb et al., 2009; Allwood et al., 2010), specifically dolomitization (Banner et al., 1988; Bau and Alexander, 2006), except in high water/rock ratio diagenetic systems. However, the diagenetic fluid REE composition could be a potential contributing factor in REE concentrations in diagenetic minerals (e.g., Azmy et al., 2011). The REE characteristics of dolomite and late-stage calcite of the Paleozoic carbonate succession were employed to determine any possible genetic relationship between them.

4.6.4.1 Devonian

The Σ REE of Devonian dolomite and late-stage calcite are comparable with Silurian dolomite and late-stage calcite but significantly lower than those of Ordovician (Table 4.2). The REE_{SN} contents of fine- and medium-crystalline dolomite are significantly different (higher) by more than one order of magnitude than those of modern warm water brachiopods (Azmy et al., 2011, Fig. 4.7A), while they have lower REE_{SN} content than Devonian microbialites (Nothdurft et al., 2004).

The fine- (D1) and medium-crystalline (D2) dolomite and calcite exhibit a significant positive La anomaly similar to Holocene reefal carbonates (Webb and Camber, 2000) and Negative Ce anomaly with only a few fine-crystalline (D1) samples with a generally positive Ce anomaly (Fig. 4.8A). The REE_{SN} pattern of all Devonian dolomite and calcite are subparallel to those of modern warm water brachiopods (Azmy et al., 2011) and Devonian microbialites with slight HREE depletion (Fig. 4.7A). This similarity in REE_{SN} trends suggest that Middle Devonian Lucas Formation rocks interacted with seawater dominated brines while they potentially preserved the REE_{SN} seawater signatures.

4.6.4.2 Silurian

The REE_{SN} of saddle dolomite (D3) from the Guelph Formation is higher by one order of magnitude than well-preserved Silurian brachiopods (Azmy et al., 2011), while the REE_{SN} contents of fine- (D1) and medium-crystalline (D2) dolomite and vug-filling calcite fall between them (Fig. 4.7B). An evaluation of Silurian dolomite and calcite Ce_{SN} and La_{SN} anomalies shows that the rocks exhibit a minor negative La anomaly coupled with positive Ce anomaly (Fig. 4.8B).

All of the fine-crystalline (D1) and approximately half of medium-crystalline (D2) dolomite exhibit a positive Ce anomaly (Fig. 4.8B). Furthermore, all of samples show a general slight MREE enrichment and LREE enrichment over HREE. The LREE enrichment is more significant in saddle dolomite (Fig. 4.7B). The REE_{SN} pattern and Ce_{SN} and La_{SN} anomalies indicates that diagenetic fluids masked the general seawater signature of precursor rocks, however, there is a similarity between their REE_{SN} pattern and those of Silurian well-preserved brachiopods. Comparable REE_{SN} pattern of fine- and

medium-crystalline dolomite and vug-filling calcite suggest a common source of fluid while saddle dolomite precipitated from a fluid with different REE composition.

4.6.4.3 Ordovician

The REE_{SN} of Ordovician dolomite and fracture-filling calcite are one order of magnitude higher than that of undolomitized host rock (Fig. 4.7C) and one to two order of magnitude higher than those of Silurian and Devonian dolomite and calcite. Ordovician samples exhibit minor positive Ce anomaly and predominantly positive La anomaly (Fig. 4.8C). Furthermore, dolomite and calcite samples do not exhibit the typical seawater pattern and show a significant MREE enrichment and negative (Eu/Eu*)_{SN} anomaly (Fig. 4.8C), while undolomitized host rock show a smooth REE_{SN} trend with slight MREE enrichment (Fig. 4.7C). This indicates that REE concentration of diagenetic minerals could have changed during dolomitization and may not necessarily preserve the precursor rock REE pattern.

Higher concentrations of Σ REE of dolomite (D2 and D3) and fracture-filling calcite (C3) relative to undolomitized host rocks indicates that dolomitizing fluids were significantly rich in REE. Such a higher concentration of REE is possible where the diagenetic fluids interacted with rocks with elevated REE content. Two possible sources for higher REE contents in the Michigan Basin are the Upper Ordovician Blue Mountain shale and Precambrian basement rocks. Whole rock and organic matter fraction of the Blue Mountain shale Σ REE content are 202.7 ± 86.5 and 343.1 ± 436.6 ppm (Abanda and Hannigan, 2006), respectively where those of matrix and saddle dolomite and fracture-filling calcite are 206.6 ± 185.6 , 352.5 ± 303.4 , and 557.2 ± 430.8 ppm, respectively. The average Σ REE of Precambrian basement are 164.9 ppm (Wedepohl, 1995). Thus, the comparable Σ REE and REE_{SN} pattern of Upper Ordovician shale and those of dolomite and calcite suggest that water/rock interaction with overlying shale likely elevated the REE contents of fluid(s), assuming downward migration of dolomitizing fluids. However, interaction with basement rocks could not be discounted as there is similarity in LREE pattern of dolomite and calcite and those of Precambrian basement rocks.

Devonian to Ordovician dolomite and late-stage calcite exhibit three distinct REE_{SN} patterns, (Figs. 4.7A to C) and (Ce-La)_{SN} anomalies (Figs. 4.8A to C). Devonian

samples preserved a typical seawater REE_{SN} pattern. Although Silurian samples REE_{SN} patterns were masked by diagenetic alteration, however, there is a weak similarity between their REE_{SN} pattern and those of well-preserved Silurian brachiopods, while Silurian saddle dolomite (D3) shows a different REE_{SN} pattern. On the other hand, REE_{SN} patterns of Ordovician samples are distinctly different from seawater pattern and their Σ REE are significantly higher than those of Devonian and Silurian dolomite and calcite. These observations suggest that three different fluids were involved in precipitation and/or alteration of Devonian to Ordovician diagenetic minerals. Furthermore, it indicates that REE can be utilized as potential indicators of diagenetic alteration in carbonate rocks (e.g., Azmy et al., 2011), whether their seawater REE_{SN} is preserved or not.

4.6.5 Fluid flow model

Fluid flow in sedimentary basins transfer heat and mass causing mineral precipitation and facilitate hydrocarbon migration. The main factors in migration of diagenetic fluids, including mineralizing fluids that precipitate MVT minerals, and those involved in dolomitization and hydrocarbon migration are: 1) a permeable aquifer to facilitate lateral migration of brines over tens to hundreds of kilometer from the basin center to its margins; and 2) a driving mechanism for fluid flow.

Three major fluid flow mechanisms are generally recognized for intracratonic sedimentary basins (Garven, 1995): 1) topography-driven fluid flow, 2) compaction-driven fluid flow, and 3) free convection cells driven by temperature or density gradients. Due to the low relief topography of the Michigan Basin topography-driven fluid flow was not likely a driving force for migration of diagenetic fluids. Results of fluid flow modelling show that compaction-driven fluid flow in basins is characterized by fluid velocities of 0.1 mm/yr to 1 mm/yr and very small excess hydraulic potentials. In addition, the slow movement of fluids expelled from the deep basin by compaction causes conductive cooling of fluid to the surface before reaching host rocks at the basin margin (Bjorlykke, 1993; Deming, 1994). Therefore, compaction-driven flow is not a viable mechanism for transporting dolomitizing fluid(s). Furthermore, in carbonate rocks-dominated sedimentary basins like the Michigan Basin, the compaction of existing shale could not produce enough fluid.

Buoyancy-driven fluid flow resulting from temperature or density gradients could transport mass and heat over large distances in significantly shorter time scales than compaction-driven flow (Bethke, 1986; Garven, 1995). Depending on aquifer thickness, permeability and fluid density gradient, flow rates in convection cells approach 1 m/yr (Garven, 1995). Numerical modelling of the Illinois Basin showed density-driven fluids responsible for formation of Upper Mississippi Valley Pb-Zn deposits had fluid velocities up to several m/yr (Bethke, 1986).

In sedimentary basins characterized by alternating sedimentary rocks with variable permeability, faults and fractures can facilitate cross-formational fluid flow (Bjorlykke, 1994). They effectively provide a continuous void space that acts as a conduit for fluid flow. Intermittent reactivation of basement structures was suggested to control the location of Paleozoic fault and fracture systems in the Paleozoic sedimentary cover of southern Ontario (Sanford et al., 1985, Boyce and Morris, 2002). The network of fractures provides a possible conduit for migration of fluids through low permeability strata like shale and evaporite deposits.

The high salinity of Ordovician saddle dolomite and fracture-filling calcite fluid inclusions (20.6 to 25.1 wt. % NaCl+CaCl₂) is significantly higher than seawater salinity assuming Ordovician connate water as the source of fluids. This suggests that connate waters were mixed with higher salinity fluids. Thick layers of Silurian evaporites in the Michigan Basin are potential source of fluids with higher salinity. Therefore, dissolution of evaporites through downward migration of younger seawater (Devonian and/or Silurian) could have produced saline fluids.

The comparable ⁸⁷Sr/⁸⁶Sr ratios of Ordovician dolomite with younger seawater support the downward migration of fluids. In addition, the heavier calculated $\delta^{18}\text{O}_{\text{fluid}}$ for Ordovician matrix (-6 to +2‰ VSMOW) and saddle (-2 to +6‰ VSMOW) dolomite than Ordovician seawater (-6.4‰ VSMOW) indicates that ¹⁸O-enriched fluids were mixed with Ordovician connate waters. Furthermore, the significantly higher ΣREE of matrix and saddle dolomite and fracture-filling calcite relative to limestone host rock, which is comparable with those of overlying shale (Blue Mountain shale), suggests downward migration of dolomitizing fluids.

Dense saline fluids become warm while descending. Assuming a geothermal gradient of 25°C/km and surface temperature of 20°C, the fluid temperature at 3610 m (approximate maximum sediment thickness of the Michigan Basin Paleozoic succession, Cercone, 1984) in the central part of the basin would be 110°C. However, fluid inclusion results of different diagenetic phases from Ordovician to Devonian Paleozoic succession in central part of the basin (Table 4.4) are significantly higher than maximum burial temperature.

The gravity and aeromagnetic maps of mid-continent North America shows generally linear positive anomalies that extend from central Kansas to Lake Superior and then turn southward into central Michigan. The exposed rocks associated with these linear features in the Lake Superior region comprise volcanic, plutonic, and immature clastic sedimentary units of the 1.0-1.2 Gyr old. The axial basins filled with basalt and immature clastic rocks along with evidence of crustal extension suggest an incipient rifting in mid-continent North America during Paleoproterozoic (Van Scums, 1985).

A thermal anomaly over the buried mid-continent rift (MCR) in the center of the Michigan Basin (Fig. 4.10) is attributed to reactivation of MCR (Girard and Barnes, 1995). K-Ar dating of authigenic illite yielded ages ranging from Late Devonian to Mississippian (367 to 322 Ma). The youngest (322 Ma) illite samples have more depleted $\delta^{18}\text{O}$ values and the highest estimated temperatures (~170°C) in vicinity of the rift (Girard and Barnes, 1995). The progressive depletion of illite $\delta^{18}\text{O}$ values could be an indication of increasing heat flux with time. Furthermore, the maximum homogenization temperature (170°C) of quartz overgrowth cements that postdate illite were recorded from samples located over the buried mid-continent rift (MCR).

Simo et al. (1994) also reported high homogenization temperatures ($175 \pm 25^\circ\text{C}$) for late-stage saddle dolomite in the Middle Ordovician Glenwood Formation in central part of the Michigan Basin. In addition, results of numerical modeling have also shown that circulation of hot fluids could originate from the ancient buried rift (MCR) at the base of sedimentary sequence and could be responsible for the high basin temperatures (Nunn, 1994). In a recent study on concentration of noble gases in brines from different ages in the Michigan Basin, depletion of atmospheric noble gases in brines was attributed

to reactivation of the MCR (Ma et al., 2009). They suggested that reactivation of the MCR was likely responsible for release of heat and mantle noble gases into the basin through deep-seated faults.

The potential thermal gradient of fluids due to this thermal flux was a driving force for circulation and movement of diagenetic fluids. The higher temperature of diagenetic minerals in the Paleozoic succession in the center of the Michigan Basin (Simo et al., 1994; Luczaj et al., 2006; Barnes et al., 2008) than those of corresponding rocks at the margin of the basin (Table 4.4) indicates that hydrothermal fluids originated from central part of the basin. Highly radiogenic $^{87}\text{Sr}/^{86}\text{Sr}$ ratios of Ordovician brines (Hobbs et al., 2011) and saddle dolomite and high ΣREE of dolomite suggest water/rock interaction with Precambrian basement rocks.

Cambrian rocks in the subsurface of southwestern Ontario are dominated by quartzose sandstones of the Eau Claire and Mount Simon formations. These units unconformably overlie the Precambrian basement and wedge out towards the east (Armstrong and Carter, 2006). These high permeability sandstones could have acted as a regional aquifer throughout the basin for ascending hot brines from the center of the basin toward its margin (e.g., Harper et al., 1995; Ziegler and Longstaffe, 2000). Uprising hot fluids through network of fractures altered host rock and precipitated replacive and saddle dolomite.

Migration of hydrothermal fluids from deeper parts of the basin through major fault and fracture zones which connected to structures in the Precambrian basement were invoked as a mechanism for hydrothermal dolomitization in Silurian and Devonian rocks in the central part of the basin (e.g., Luczaj et al., 2006; Barnes et al., 2008). However, distinct ΣREE , REE_{SN} patterns and $\delta^{18}\text{O}_{\text{fluid}}$ of selected minerals (Table 4.5) from Devonian to Ordovician carbonate succession indicates that three different fluids were involved in precipitation and/or recrystallization of these minerals. Therefore, geochemical signatures signify changes in pore fluid composition and compartmentalization of diagenetic fluids.

Although the high salinity of Ordovician dolomite fluid inclusions and least radiogenic $^{87}\text{Sr}/^{86}\text{Sr}$ ratios of dolomite suggest involvement of younger seawater (e.g., Simo et al., 1994; Coniglio et al., 1994) in precipitation of Ordovician dolomite, geochemical evidence (ΣREE , REE_{SN} patterns, $\delta^{18}\text{O}_{\text{fluid}}$) suggest that Upper Ordovician shale prevented upward migration of diagenetic fluids and acted as a seal. On the other hand, distinct fluid inclusion salinity, REE_{SN} patterns, and $\delta^{18}\text{O}_{\text{fluid}}$ of selected minerals in the Lucas (Devonian) and Guelph (Silurian) formations (Table 4.5) suggest compartmentalization of fluids involved in precipitation and/or recrystallization of these minerals.

The seawater like REE_{SN} pattern of Devonian diagenetic minerals and $^{87}\text{Sr}/^{86}\text{Sr}$ ratios in the range of Devonian seawater suggest a seawater dominated brine with minimal water/rock interaction affected Devonian rocks. Whereas modified REE_{SN} patterns of Silurian and specifically Ordovician diagenetic minerals suggest a progressive water/rock interaction process. The lower Devonian (Sylvania sandstone) and lower Silurian sandstone layers of the Clinton–Cataract Groups (Grimsby and Whirlpool formations) and the Cambrian sandstone (Eau Claire and Mount Simon formations) acted as regional aquifers for transport of diagenetic fluids from the center toward the margin of the Michigan Basin.

4.6.6 Timing of hydrothermal event

The wide distribution of secondary K-feldspar (453 – 368 Ma) at the Precambrian–Paleozoic boundary and secondary K-feldspar and illite (383 – 299 Ma) in Cambro–Ordovician rocks throughout mid-continental North America suggest a regional fluid flow system with more than one episode of fluid movement in response to Paleozoic orogenies (Harper et al., 1995, Ziegler and Longstaffe, 2000). The results of recent study (Liu et al., 2003) on authigenic K-feldspar in uppermost Precambrian rocks in the North American mid-continent indicates that Late Devonian–Mississippian K-feldspar formed at temperatures of 100°C from saline fluids which may have originated from the Michigan Basin, East-Central Iowa Basin, and/or the Illinois Basin, coincident with the Acadian orogeny.

It seems that reactivation of the mid-continent rift (367 to 322 Ma) and a corresponding thermal anomaly associated with illite formation over it (e.g., Girard and Barnes, 1995; Ma et al., 2009) developed a hydrothermal system in the central part of the basin and diagenetic fluids migrated towards the margin of the basin through a lateral outward flow. The Late Devonian–Mississippian regionally extensive illitization coincides with widespread hydrothermal activity and clay-mineral diagenesis in the continental interior (Liu et al, 2003).

These events are coincident with the time interval between the Acadian (410 to 360 Ma) and Alleghanian orogenies (300 to 250 Ma), where reactivation of basement faults (Sanford et al., 1985) caused opening of fractures that facilitated transport of diagenetic fluids through them. Regardless of the driving force, heated brine would be expected to cool towards basinal margins (Bethke and Marshak 1990) therefore significant decrease in fluid inclusion homogenization temperatures of diagenetic minerals from equivalent formations in the center and margin of the basin (Table 4.4) from Ordovician to Devonian supports outward migration of diagenetic fluids.

On the other hand the significant difference in fluid inclusions salinity of minerals from Devonian strata from the central part of the basin towards its margin (Table 4.4) suggest dilution of diagenetic fluids with local meteoric water over the crest of arch in southwestern Ontario. Furthermore, the decreasing trend in salinity and temperature of Silurian fluorite and sphalerite and Ordovician saddle dolomite and fracture-filling calcite (Fig. 4.9) could be a response of tectonic uplift and introduction of meteoric water to the system. Reactivation of basement arches in response to the Acadian orogeny was suggested as the cause of emergence along the arch crest and introduction of meteoric water to local aquifers (e.g., Ziegler and Longstaffe, 2000).

4.7 Conclusions

Petrographic, isotopic, and fluid inclusion investigations of the Ordovician to Devonian fracture systems and host rocks from southwestern Ontario, Canada suggest that the diagenetic evolution of carbonates in these strata is related to the regional tectonics as summarized below:

- 1) The pattern and extent of dolomitization in combination with stratigraphy and petrography indicate that three different paleohydrologic systems were responsible for dolomitization of the Paleozoic carbonate succession in southwestern Ontario.
- 2) ^{18}O -depleted $\delta^{18}\text{O}$ values of replacive dolomite in the Lucas and Guelph formations relative to estimated values for dolomite precipitated from Middle Devonian and Silurian seawater suggest recrystallization of early formed dolomite, while Middle Ordovician replacive dolomite formed at higher temperature ($\sim 90^\circ\text{C}$).
- 3) Middle Silurian saddle dolomite precipitated from warm (108°C), saline (26 wt. % NaCl) and ^{18}O -enriched fluids ($\delta^{18}\text{O}$ ranges from +3 to +11‰ VSMOW), while Middle Ordovician saddle dolomite precipitated from warmer (121°C), less saline (24 wt. % NaCl) and ^{18}O -depleted ($\delta^{18}\text{O}$ ranges from -2 to +6‰ VSMOW) fluids.
- 4) High salinity of Middle Silurian-hosted fluid inclusions suggests that fluids involved in the dissolution of Silurian evaporites were involved in precipitation of these minerals. Slightly lower salinity of Middle Ordovician saddle dolomite relative to those of Silurian replacive and saddle dolomite suggests mixing of saline fluids with Ordovician connate waters. Significant lower salinity of Devonian samples in the margin of the basin relative to the correlative rocks at the center of the basin suggests mixing of brines with meteoric water at the basin margin.
- 5) The higher than expected homogenization temperatures of replacive and saddle dolomite and late-stage calcite (75 to 145°C) of the Paleozoic carbonate succession of southwestern Ontario than maximum burial temperatures for each interval (60 to 90°C) indicates that hydrothermal fluids were involved in precipitation/recrystallization of dolomite and calcite.
- 6) The presence of hydrocarbon-bearing fluid inclusions with high homogenization temperatures ($>80^\circ\text{C}$) in late-stage calcite cement of all ages from Ordovician to Devonian indicates hydrothermal fluids carried hydrocarbons.
- 7) $^{87}\text{Sr}/^{86}\text{Sr}$ ratios of dolomite from different ages vary from seawater ratios to values that are more radiogenic than coeval seawater. This implies that basinal brines were

involved in precipitation and/or recrystallization of dolomite. Middle Ordovician dolomite has lower $^{87}\text{Sr}/^{86}\text{Sr}$ ratios than coeval seawater, which suggests involvement of younger seawater (Devonian and/or Silurian) in precipitation of dolomite.

- 8) Distinct REE_{SN} content and trend of Paleozoic dolomite from Devonian to Ordovician dolomite imply that different fluids were involved in dolomite precipitation and/or recrystallization. Average REE_{SN} trends of late-stage calcite cements are significantly different and suggest diversity of fluid origins.
- 9) Overall comparison of geochemical characteristics of dolomite and late-stage calcite in the Ordovician to Devonian succession of southwestern Ontario suggests compartmentalization of diagenetic fluids. The decreasing trend in fluid inclusion homogenization temperatures from the center of the basin towards the basin margin suggests that hydrothermal fluids originated from the center of Michigan. Reactivation of the mid-continent rift during Late Devonian-Mississippian is the major source of heat for hydrothermal fluids.

4.8 Acknowledgements

This work was supported by Natural Sciences and Engineering Research Council of Canada (NSERC) to I. Al-Aasm and Mario Coniglio. Special thanks to M. Price for running the samples for stable isotope ratios

4.9 References

- Abanda, P. A., Hannigan, R. E., 2006. Effect of diagenesis on trace element partitioning in shales. *Chemical Geology* 230, 42–59.
- Al-Aasm, I. S., Taylor, B. E., South, B., 1990. Stable isotope analysis of multiple carbonate samples using selective acid extraction. *Chemical Geology* 80, 119-125.
- Al-Aasm, I. S., 2000. Chemical and Isotopic Constraints for Recrystallization of Sedimentary Dolomites from the Western Canada Sedimentary Basin. *Aquatic Geochemistry* 6, 229-250.

- Allwood, A. C., Kamber, B. S., Walter, M. R., Burch, I. W., Kanik, I., 2010. Trace elements record depositional history of an Early Archean stromatolitic carbonate platform. *Chemical Geology* 270, 148–163.
- Armstrong, D. K., Carter, T. R., 2006. An updated guide to subsurface Paleozoic stratigraphy of southern Ontario. Ontario Geological Survey, Open File Report 6191, 214.
- Armstrong, D. K., Goodman, W. R., 1990. Stratigraphy and depositional environments of Niagaran carbonates, Bruce Peninsula, Ontario. American Association of Petroleum Geologists, 1990 Eastern Section Meeting, Ontario Petroleum Institute, Field Trip Guidebook 2, 59 p.
- Azmy, K., Brand, U., Sylvester, P., Gleeson, S. A., Logan, A., Bitner, M. A., 2011. Biogenic and abiogenic low-Mg calcite (bLMC and aLMC): Evaluation of seawater-REE composition, water masses and carbonate diagenesis. *Chemical Geology*, 280, 180–190.
- Azmy, K., Veizer, J., Bassett, M. G., Copper, P., 1998. Oxygen and carbon isotopic composition of Silurian brachiopods: Implications for coeval seawater and glaciations. *Geological Society of America Bulletin* 110, 1499-1512.
- Banner, J. L., Hanson, G. N., Meyers, W. J., 1988. Rare earth element and Nd isotopic variations in regionally extensive dolomites from the Burlington–Keokuk Formation (Mississippian): implications for REE mobility during carbonate diagenesis. *Journal of Sedimentary Petrology* 58, 415–432.
- Barnaby, R. J., Oetting, G. C., Gao, G., 2004. Strontium isotopic signatures of oil-field waters: Applications for reservoir characterization. *American Association of Petroleum Geologists Bulletin* 88, 1677–1704.
- Barnes, D. A., Parris, T. M., Grammer, G. M., 2008. Hydrothermal Dolomitization of Fluid Reservoirs in the Michigan Basin, USA. Search and Discovery Article #50087, Adapted from oral presentation at AAPG Annual Convention, San Antonio, Texas.

- Bau, M., Alexander, M., 2006. Preservation of primary REE patterns without Ce anomaly during dolomitization of Mid-Paleoproterozoic limestone and the potential re-establishment of marine anoxia immediately after the “Great Oxidation Event”. *South African Journal of Geology*, 109, 81-86.
- Bau, M., Dulski, P., 1996. Distribution of yttrium and rare-earth elements in the Penge and Kuruman iron-formations, Transvaal Supergroup, South Africa. *Precambrian Research* 79, 37–55.
- Bethke, C. M., 1986. Hydrologic Constraints on the Genesis of the Upper Mississippi Valley Mineral District from Illinois Basin Brines. *Economic Geology* 81, 233-249.
- Bethke, C. M., Marshak, S., 1990. Brine migrations across North America the plate tectonics of groundwater. *Annual Review of Earth and Planetary Science* 18, 287-315.
- Birchard, M.C., Rutka, M.A., Brunton, F.R., 2004. Lithofacies and geochemistry of the Lucas Formation in the subsurface of Southwestern Ontario: A high purity limestone and Potential high purity dolostone resource. Ontario Geological Survey Open file report 6137, 180 p.
- Bjorlykke, K., 1993. Fluid flow in sedimentary basins. *Sedimentary Geology* 86, 137-158.
- Bjorlykke, K., 1994. Fluid-flow processes and diagenesis in sedimentary basins. In: Parnell, J. (Ed.), *Geofluids: Origin, migration and evolution of fluids in sedimentary basins*. Geological Society special publication 87, 127-140.
- Boyce, J. J., Morris, W. A., 2002. Basement-controlled faulting of Paleozoic strata in southern Ontario, Canada: New evidence from geophysical lineament mapping. *Tectonophysics* 353, 151-171.
- Brand, U., Azmy, K., Tazawa, J., Sano, H., Buhl, D., 2010. Hydrothermal diagenesis of Paleozoic seamount carbonate components. *Chemical Geology* 278, 173-185.

- Brennan, S. T., Lowenstein, T. K., 2002. The major-ion composition of Silurian seawater. *Geochimica et Cosmochimica Acta* 66, 2683-2700.
- Brookfield, M. E., Brett, C. E., 1988. Paleoenvironments of Mid-Ordovician (Upper Caradocian) Trenton limestones of southern Ontario, Canada: Storm sedimentation on a shoal-basin shelf model. *Sedimentary Geology* 57, 75-105.
- Carothers, W. W., Kharaka, Y. K., 1980. Stable carbon isotopes of HCO₃ in oil-field waters-implication for origin of CO₂. *Geochimica et Cosmochimica Acta*, 44, 323-332.
- Carter, T. R., Trevail, R. A., Easton, R. M., 1996. Basement controls on some hydrocarbon traps in southern Ontario, Canada. In: Van der Pluijm, B.A., Catacosinos, P.A. (Eds.), *Basement and Basins of Eastern North America*. Geological Society of America Special Paper 308, 95-107.
- Cercone, K. R., 1984. Thermal history of Michigan Basin. *American Association of Petroleum Geologists Bulletin* 68, 130–136.
- Cercone, K. R., Lohmann, K. C., 1987. Late Burial Diagenesis of Niagaran (Middle Silurian) Pinnacle Reefs in Michigan Basin. *American Association of Petroleum Geologists Bulletin* 71, 156-166.
- Chaudhuri, S., Clauer, N., 1992. In: Clauer, N., Chaudhuri, S. (Eds.), *Isotopic Signatures and Sedimentary Records*. Lecture Notes in Earth Sciences 43, 497-529.
- Coniglio, M., R. Sherlock, Williams-Jones, A. E., Middleton, K., Frappe, S. K., 1994. Burial and hydrothermal diagenesis of Ordovician carbonates from the Michigan Basin, Ontario, Canada. In: Purser, B., Tucker, M., Zenger, D. (Eds.), *Dolomites a volume in honour of Dolomieu*. Special Publications of the International Association of Sedimentologists 21, 231-254.
- Coniglio, M., Williams-Jones, A. E., 1992. Diagenesis of Ordovician carbonates from the northeast Michigan Basin, Manitoulin Island area, Ontario: evidence from petrography, stable isotopes and fluid inclusions. *Sedimentology* 39, 813-836.

- Coniglio, M., Zheng, Q., Carter, T. R., 2003. Dolomitization and recrystallization of middle Silurian reefs and platform carbonates of the Guelph Formation, Michigan Basin, southwestern Ontario. *Bulletin of Canadian Petroleum Geology* 51, 177-199.
- Cramer, B. D., Munnecke, A., Schofield, D. I., Haase, K. M., Hasse-Schramm, A., 2011. A revised $^{87}\text{Sr}/^{86}\text{Sr}$ curve for Silurian; Implication for global ocean chemistry and Silurian Time Scale. *The Journal of Geology* 119, 335-349.
- Deming, D., 1994. Fluid flow and heat transport in the upper continental crust. In: Parnell, J. (Ed.), *Geofluids: Origin, migration and evolution of fluids in sedimentary basins*. Geological Society special publication 87, 27-42.
- Franks, S. G., Dias, R. F., Freeman, K. H., Boles, J. R., Holba, A., Fincannon, A. L., Jordan, E. D., 2001. Carbon isotopic composition of organic acids in oil field waters, San Joaquin Basin, California, USA. *Geochimica et Cosmochimica Acta* 65, 1301-1310.
- Fritz, P. and Smith, D. C. W., 1970. The isotopic composition of secondary dolomites: *Geochimica et Cosmochimica Acta* 34, 1161-1173.
- Garven, G., 1995. Continental-Scale Groundwater Flow and Geologic Processes. *Annual Review of Earth and Planetary Science* 23, 89-117.
- Geldern, R. a, Joachimski, M. M., Day, J., Jansen, U., Alvarez, F., Yolkin, E. A. and Ma, X. P. 2006. Carbon, oxygen and strontium isotope records of Devonian brachiopod shell calcite. *Palaeogeography, Palaeoclimatology, Palaeoecology* 240, 47-67.
- Girard, J. P., Barnes, D. A., 1995. Illitization and paleothermal regimes in the middle Ordovician St. Peter sandstone, central Michigan Basin: K-Ar, oxygen isotope, and fluid inclusion data. *American Association of Petroleum Geologists Bulletin* 79, 49-69.
- Goldstein, R. H., 2003. Petrographic analysis of fluid inclusions, In: Samson, I., Anderson A., and Marshall, D. (Eds.), *Fluid inclusions Analysis and interpretation*. Mineralogical Association of Canada Short Course Series 32, 9-53.

- Gonfiantini, R., 1986. Environmental isotopes in lake studies. In: Fritz, P., Fontes, J. C. (Eds.), *Handbook of Environmental Isotope Geochemistry*. Amsterdam, Elsevier, 113-168.
- Haeri-Ardakani, O., Al-Aasm, I., Coniglio, M., 2012a. (In review) Diagenetic evolution and associated mineralization in Middle Devonian carbonates, southwestern Ontario, Canada. Submitted to the *Bulletin of Canadian Petroleum Geologists*.
- Haeri-Ardakani, O., Al-Aasm, I., Coniglio, M., 2012b. (In review) Petrologic and geochemical attributes of fracture-related dolomitization in Ordovician carbonates and their spatial distribution in southwestern Ontario, Canada. Submitted to the *Journal of Marine and Petroleum Geology*.
- Hamilton, G. D., 1991, Styles of reservoir development in Middle Devonian carbonates of southwestern Ontario. Unpublished MSc thesis.
- Harper D. A., Longstaffe F. J., Wadleigh M. A. McNutt R. H., 1995. Secondary K-feldspar at the Precambrian-Paleozoic unconformity, southwestern Ontario. *Canadian Journal of Earth Science* 32, 1432-1450.
- Hobbs, M. Y., Frappe, S. K., Shouakar-Stash, O., Kennell, L. R., 2011. Regional hydrogeochemistry - Southern Ontario. Nuclear Waste Management Organization Report, 157.
- Hollings, P., Smyk, M., Cousens, B., 2011. The radiogenic isotope characteristics of dikes and sills associated with the Mesoproterozoic Midcontinent Rift near Thunder Bay, Ontario, Canada. *Precambrian Res.* (2011), doi:10.1016/j.precamres.2011.11.006.
- Johnson, M. D., Armstrong, D. K., Sanford, B. V., Telford, P. G., Rutka, M. A., 1992. Paleozoic and Mesozoic geology of Ontario. In: *Geology of Ontario*, Ontario Geological Survey Special Volume 4, Part 2, 907-1008.
- Land, L. S., 1985. The origin of massive dolomite. *Journal of Geological Education* 33, 112-125.

- Legall, F. D., Barnes, C. R., Macqueen, R. W., 1981. Thermal maturation, burial history and hotspot development, Paleozoic strata of southern Ontario-Quebec, from conodont and acritarch colour alteration index. *Bulletin of Canadian Petroleum Geology* 29, 492-539.
- Liu, J., Hay, R. A., Deino, A., Kyser, T. K., 2003. Age and origin of authigenic K-feldspar in uppermost Precambrian rocks in the North American Midcontinent. *GSA Bulletin*, 115, 422-433.
- Luczaj, J. A., Harrison III, W. B., Williams, N. S., 2006. Fractured hydrothermal dolomite reservoirs in the Devonian Dundee Formation of the central Michigan Basin. *American Association of Petroleum Geologists Bulletin* 90, 1787-1801.
- Ma, L., Castro, M. C., and Hall, C. M., 2009, Atmospheric noble gas signatures in deep Michigan Basin brines as indicators of a past thermal event. *Earth and Planetary Science Letters*, v. 277, p. 137-147.
- Ma, L., Castro, M. C., Hall, C. M., Walter, L. M., 2005. Cross-formational flow and salinity sources inferred from a combined study of helium concentrations, isotopic ratios, and major elements in the Marshall aquifer, southern Michigan. *Geochemistry Geophysics Geosystems* 6, 1-21.
- McIntosh, J. C., Walter, L. M., Martini, A. M., 2004. Extensive microbial modification of formation water geochemistry: Case study from a Midcontinent sedimentary basin, United States. *GSA Bulletin* 116, 743-759.
- McKenzie, J. A., 1981, Holocene dolomitization of calcium carbonate sediments from the coastal sabkhas of Abu Dhabi, UAE: a stable isotope study. *The Journal of Geology* 89, 185-198.
- McNutt, R. H., Frappe, S. K., Dollar, P., 1987. A strontium, oxygen and hydrogen isotopic composition of brines, Michigan and Appalachian Basins, Ontario and Michigan. *Applied Geochemistry* 2, 495-505.

- McNutt, R. H., Frape, S. K., Fritz, P., Jones, M. G., MacDonald, I. M., 1990. The $^{87}\text{Sr}/^{86}\text{Sr}$ values of Canadian Shield brines and fracture minerals with applications to groundwater mixing, fracture history, and geochronology. *Geochimica et Cosmochimica Acta* 54, 205-215.
- Melchin, M. J., Brookfield, M. E., Armstrong, D. K., Coniglio, M., 1994. Stratigraphy, sedimentology and biostratigraphy of the Ordovician rocks of the Lake Simcoe area, south-central Ontario. Geological Association of Canada–Mineralogical Association of Canada, Joint Annual Meeting, Waterloo, Ontario, Guidebook for Field Trip A4, 101.
- Middleton, K. 1990, Dolomitization and porosity development in Middle Ordovician carbonate reservoirs, southwestern Ontario. In: Carter, T.R. (Ed.), *Subsurface Geology of Southwestern Ontario; a Core Workshop*, American Association of Petroleum Geologists, 1990 Eastern Section Meeting, p.51-68.
- Nothdurft, L. D., Webb, G. E., Kamber, B. S., 2004. Rare earth element geochemistry of Late Devonian reefal carbonates, Canning Basin, Western Australia: confirmation of a seawater REE proxy in ancient limestones. *Geochimica et Cosmochimica Acta*, v. 68, p. 263–283.
- Nunn, J. A., 1994. Free thermal convection beneath intracratonic basins: thermal and subsidence effects. *Basin Research* 6, 115–130.
- Obermajer, M., Fowler, M. G., Goodarzi, F., Snowdon, L. R., 1997. Organic petrology and organic geochemistry of Devonian black shales in southwestern Ontario, Canada. *Organic Geochemistry* 26, 229-246.
- Powell, T. G., Macqueen, R. W., Barker, J. F. Bree, D. G., 1984. Geochemical character and origin of Ontario oils. *Bulletin of Canadian Petroleum Geology* 32, 289-312.
- Roedder, E., 1984. Fluid inclusions. *Mineralogical Society of America, Review in Mineralogy* 12, 646.

- Sanford, B. V., 1993. St. Lawrence Platform: geology; In: Stott, D.F. and Aitken, J.D. (Eds.), *Sedimentary Cover of the Craton in Canada*, Geological Survey of Canada, *Geology of Canada Series*, 5, 723-786.
- Sanford, B. V., Thomson, F. J., McFall, G. H., 1985. Plate tectonics – a possible controlling mechanism in the development of hydrocarbon traps in southwestern Ontario. *Bulletin of Canadian Petroleum Geology* 33, 52-71.
- Sheppard, S. M. F., 1986. Characterization and isotopic variations in natural waters. In: Valley, J.W., Taylor, H.P. Jr., O'Neil, J.R. (Eds.) *Stable Isotopes in High Temperature Geochemical Processes*, *Reviews in Mineralogy* 16, 165-183.
- Shields, G. A., Carden, G. A. F., Veizer, J., Meidla, T., Rong, J., Li, R. 2003. Sr, C, and O isotope geochemistry of Ordovician brachiopods: A major isotopic event around the Middle-Late Ordovician transition, *Geochimica et Cosmochimica Acta* 67, 2005-2025.
- Shields, G., Stille, P., 2001. Diagenetic constraints on the use of cerium anomalies as paleoseawater redox proxies: an isotopic and REE study of Cambrian phosphorites. *Chemical Geology* 175, 29–48.
- Simo, J. A., Johnson, C. M., Vandrey, M. R., Brown, P. E., Castro Giovanni, E., Drzewiecki, P. E., Valley, J. W., Boyer, J. 1994. Burial dolomitization of the Middle Ordovician Glenwood Formation by evaporitic brines, Michigan Basin. In: Purser, B., Tucker, M., Zenger, D. (Eds.), *Dolomites – A volume in honour of Dolomieu*, *Special Publication IAS* 21, 169-186.
- Sonnenfeld, P. and Al-Aasm, I. 1991. The Salina evaporites in the Michigan Basin. In: Catacosinos, P. A., Daniels, Jr., P. A. (Eds.), *Early sedimentary evolution of the Michigan Basin*. Geological Society of America, *Special Paper* 256, 139-153.
- Van der Voo, R., 1988. Paleozoic paleogeography of North America, Gondwana, and intervening displaced terranes: Comparisons of paleomagnetism with paleoclimatology and biogeographical patterns. *Geological Society of America Bulletin* 100, 311-324.

- Van Schmus, W. R., 1985. The midcontinent rift system. *Annual Review of Earth and Planetary Science* 13, 345-383.
- Veizer, J., Ala, D., Azmy, K., Bruckschen, P., Buhl, D., Bruhn, F., Carden, G.A.F., Diener, A., Ebner, S., Godderis, Y., Jasper, T., Korte, C., Pawellek, F., Podlaha, O. G., Strauss, H., 1999. $^{87}\text{Sr}/^{86}\text{Sr}$ and $\delta^{13}\text{C}$ and $\delta^{18}\text{O}$ evolution of Phanerozoic seawater. *Chemical Geology* 161, 59-88.
- Vogler, E. A., Meyers, P. A., Moore, W. A., 1981. Comparison of Michigan Basin crude oils. *Geochimica et Geochimica Acta* 45, 2287-2293.
- Weaver, T. R., Frapre, S. K., Cherry, J. A., 1995. Recent cross-formational fluid flow and mixing in the shallow Michigan Basin. *GSA Bulletin* 107, 697-707.
- Webb, G. E., Kamber, B. S., 2000. Rare earth elements in Holocene reefal microbialites: a new shallow seawater proxy. *Geochimica et Cosmochimica Acta* 64, 1557–1565.
- Webb, G. E., Nothdurft, L. D., Kamber, B. S., Kloprogge, J. T., Zhao, J.-X., 2009. Rare earth element geochemistry of scleractinian coral skeleton during meteoric diagenesis: a before and-after sequence through neomorphism of aragonite to calcite. *Sedimentology* 56, 1433–1463.
- Wedepohl, K. H., 1995. The composition of continental crust. *Geochimica et Cosmochimica Acta* 59, 1217-1232.
- Wilson, J. A., Sengupta, A., 1985. The Trenton Formation in the Michigan Basin and environs: pertinent questions about its stratigraphy and diagenesis, In: Cercone, K. R., Budai, J. M. (Eds.), *Ordovician and Silurian rocks of Michigan Basin: Michigan Basin Geological Society Special Paper* 4, 1-13.
- Wilson, T. P., Long, D. T., 1993a. Geochemistry and isotope chemistry of Michigan Basin brines: Devonian formations. *Applied Geochemistry* 8, 81-100.
- Wilson, T. P., Long, D. T., 1993b. Geochemistry and isotope chemistry of Ca-Na-Cl brines in Silurian strata, Michigan Basin, U.S.A. *Applied Geochemistry* 8, 507-524.

- Wyndham, T., McCulloch, M., Fallon, S., Alibert, C., 2004. High-resolution coral records of rare earth elements in coastal seawater: biogeochemical cycling and a new environmental proxy. *Geochimica et Cosmochimica Acta* 68, 2067–2080.
- Yoo, C. M., Gregg, J. M., Shelton K. L., 2000. Dolomitization and dolomite neomorphism: Trenton and Black River limestone (Middle Ordovician) Northern Indiana, U.S.A. *Journal of Sedimentary Research* 70, 265-274.
- Zheng, Q., 1999. Carbonate diagenesis and porosity evolution in the Guelph Formation, southwestern Ontario. Ph.D. thesis, University of Waterloo, Waterloo, Ontario, 265p.
- Ziegler, K., and Longstaffe, F. J., 2001. Clay mineral authigenesis along a mid-continental scale fluid conduit in Palaeozoic sedimentary rocks from southern Ontario, Canada. *Clay Minerals* 59, 239-260.

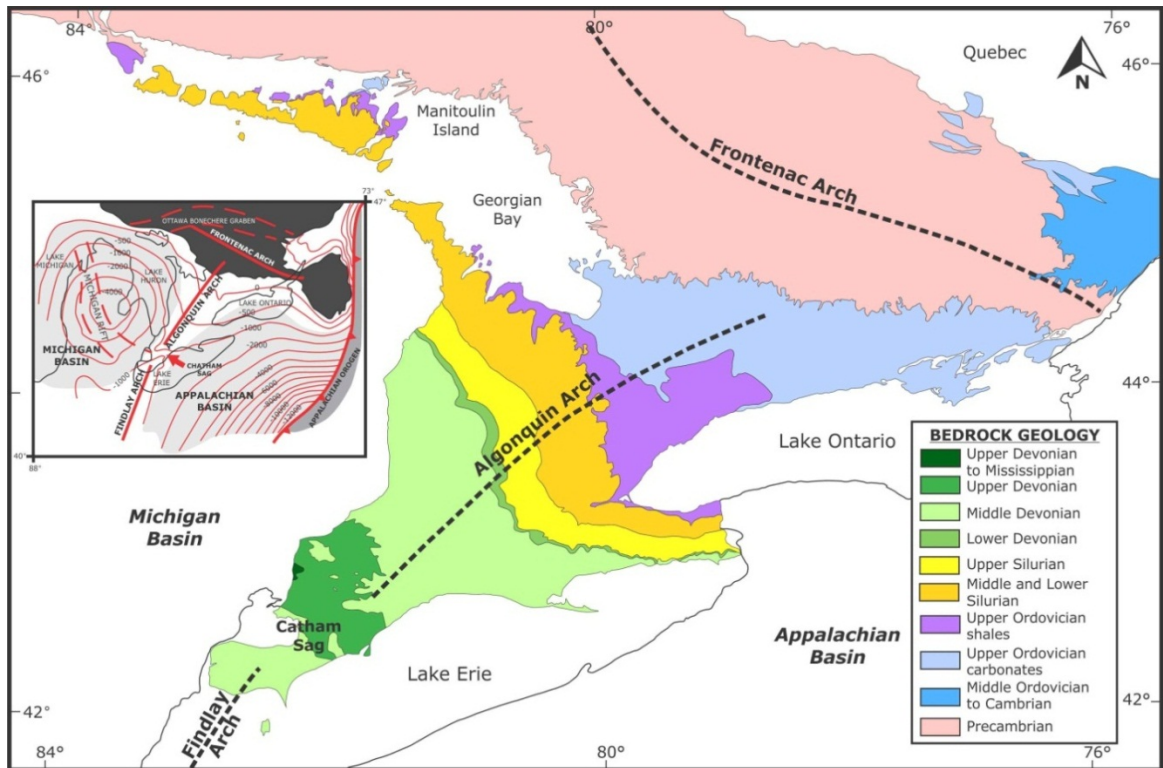


Figure 4.1 Generalized Paleozoic bedrock geology map of southern Ontario (adapted from Armstrong and Carter, 2006). Inset shows generalized basement structural contours (meters above sea level datum) and location of structural arches and basins (adapted from Johnson et al., 1992).

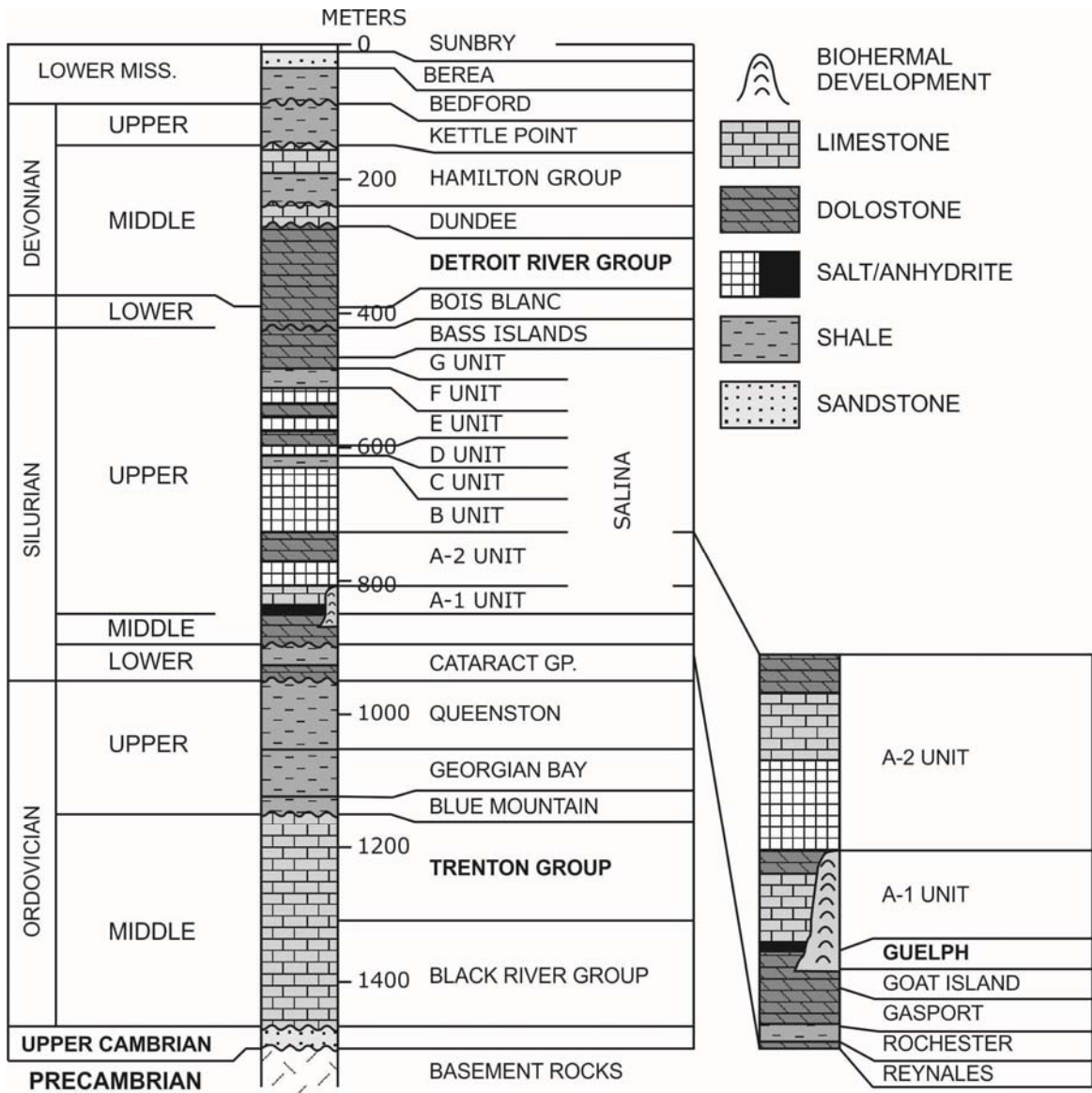


Figure 4.2 Generalized Paleozoic stratigraphic column for southern Ontario (adapted from Sanford et al., 1985). Stratigraphic units in bold font are the focus of this study.

A

Diagenetic events	Early (Marine)	Late (Burial)
Fibrous calcite cement	=====	
Syntaxial calcite cement	=====	
Equant calcite cement		=====
Fine-crystalline dolomite (D1)	=====	
Stylolites		=====
Medium-crystalline dolomite (D2)		=====
Fracturing		=====
Dissolution		=====
Fracture-filling calcite		=====
Hydrocarbon migration		=====
Sulfide mineralization		=====
Celestine		=====
Sulfur		=====
Fluorite		=====

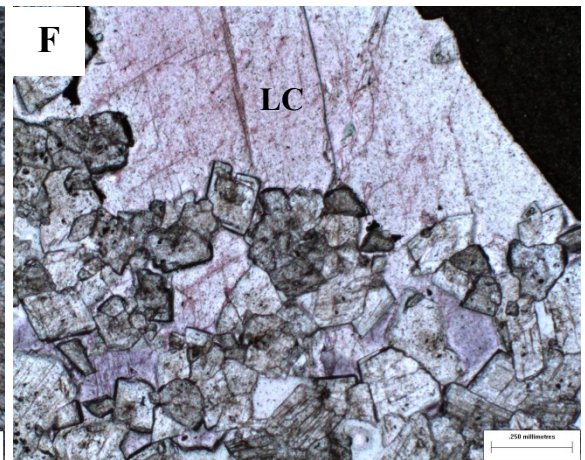
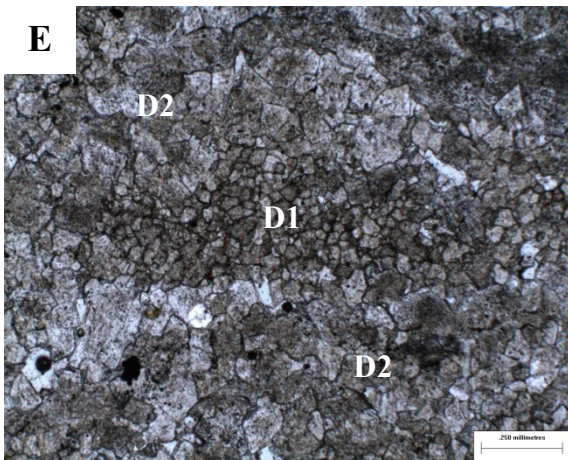
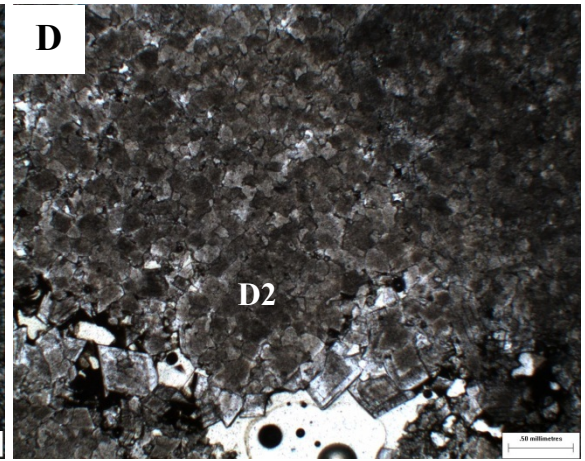
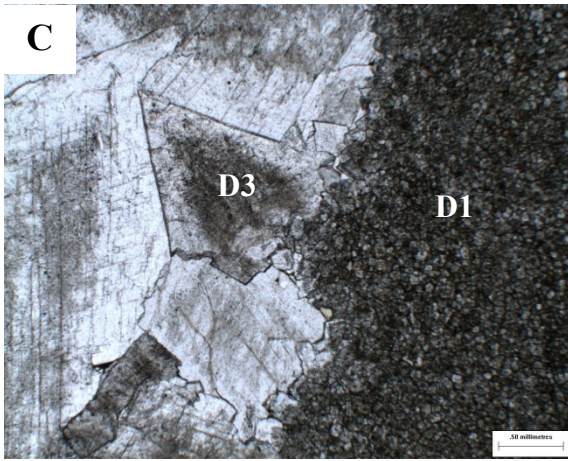
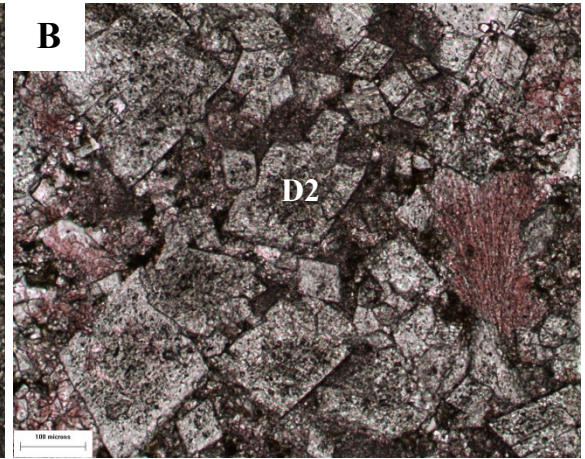
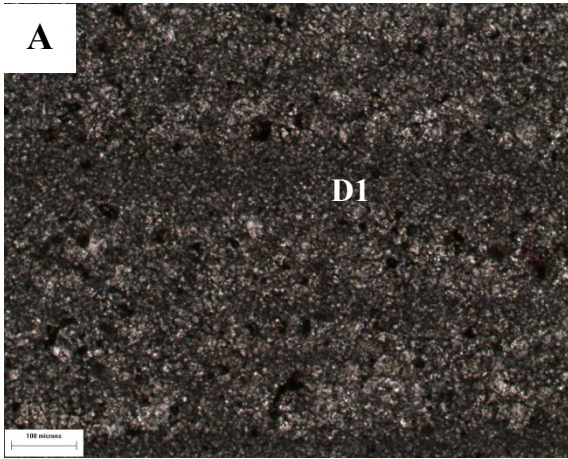
B

Diagenetic events	Early (Marine)	Late (Burial)
Fibrous calcite cement	=====	
Equant cement	=====	
Fine-crystalline dolomite (D1)	=====	
Medium-crystalline dolomite (D2)		=====
Anhydrite		=====
Stylolites		=====
Saddle dolomite (D3)		=====
Fracturing		=====
Dissolution		=====
Late-stage calcite		=====
Hydrocarbon migration		=====
Evaporite dissolution		=====

C

Diagenetic events	Early (Marine)	Late (Burial)
Syntaxial calcite cement (C1)	=====	
Equant calcite cement (C2)	=====	
Fine-crystalline dolomite (D1)	=====	
Stylolites		=====
Fracturing		=====
Dissolution		=====
Medium-crystalline dolomite (D2)		=====
Saddle dolomite (D3)		=====
Fracture-filling calcite (C3)		=====
Hydrocarbon migration		=====
Sulfide mineralization		=====
Anhydrite		=====

Figure 4.3 Paragenetic sequence of the Paleozoic succession in southwestern Ontario, (A) Lucas Formation, (B) Guelph Formation, modified after Zheng (1999) (C) Trenton Group, modified after Middleton (1990).



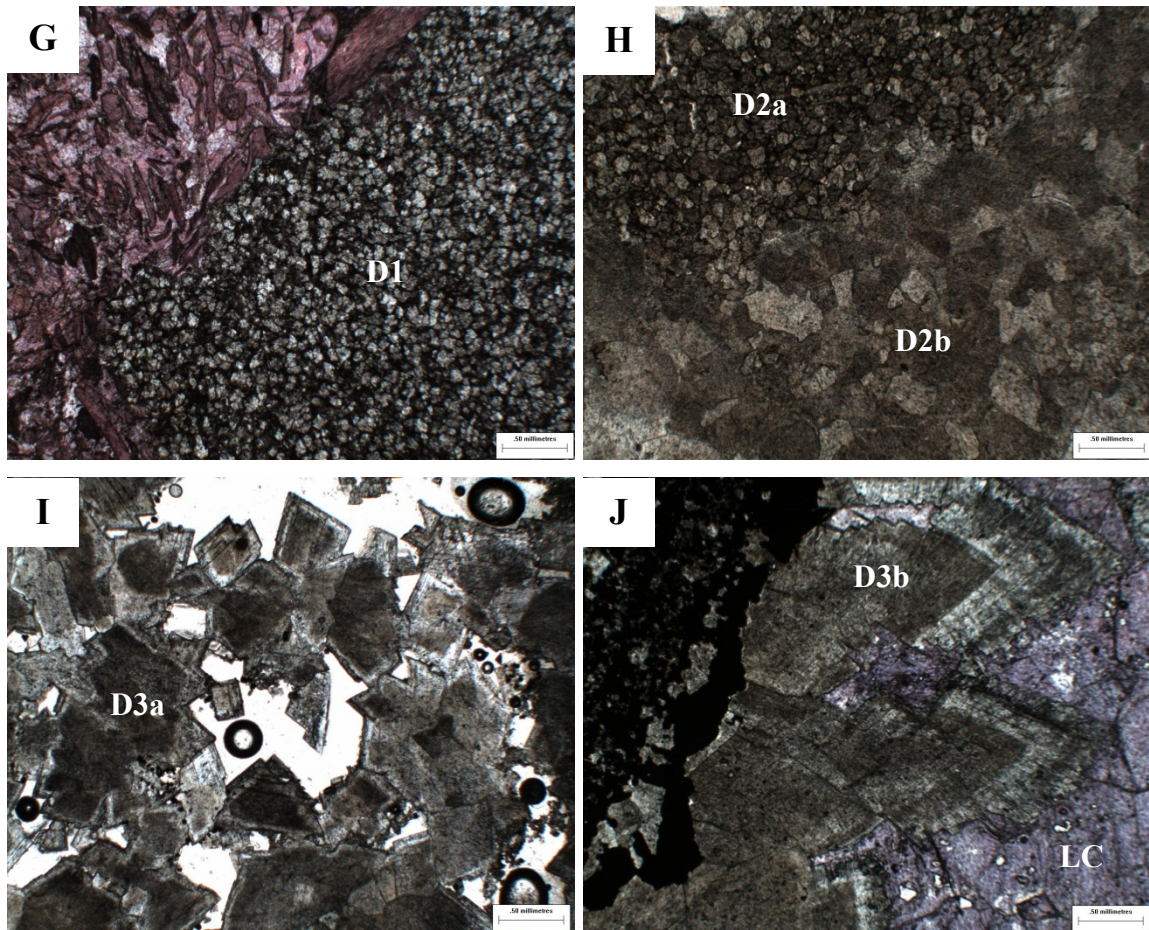


Figure 4.4 Photomicrographs of dolomite and late-stage calcite from the Paleozoic succession of southwestern Ontario; (A) Unimodal fine-crystalline replacive dolomite (D1), Lucas Formation, McGregor quarry, scale bar 100 μm , (B) Medium crystalline dolomite (D2) with cloudy center and clear rim, Lucas Formation, McGregor quarry, scale bar 100 μm , (C) Unimodal fine-crystalline replacive dolomite (D1), and saddle dolomite (D3) with cloudy center and wide clear rim, Guelph Formation, Consumers 13138, Lake Erie 158- H, depth 400.5 m, scale bar 500 μm , (D) Medium-crystalline replacive dolomite shows cloudy center, Guelph Formation, Edys Mills 1, Dawn 3 - 32 - VIII, depth 519.5 m, scale bar 500 μm , (E) Coincidence of fine-crystalline dolomite (D1) and coarser, non-planar, inclusion-rich dolomite (D2), scale bar 250 μm , (F) Vug-filling translucent blocky calcite, Guelph Formation, Geco Eramosa - 1, Eramosa 5 - 28 - VI, depth 50.2, scale bar 250 μm , (G) Ferroan planar-e to planar-s replacive dolomite (D1) replaced precursor grainstone, Picton quarry, scale bar 250 μm , (H) Coarse planar-s to non-planar, cloudy center crystals of D2a dolomite and finer crystals of planar-s D2b, dolomite, Cons et al 34151, depth 835.1 m, scale bar 500 μm , (I) Planar-e to planar-s crystals of D2c dolomite. Crystals have a cloudy center and clear rim, in some cases the outer rim is ferroan, D2c displays undulose extinction, Telesis et al 34336, depth 861.3 m, scale bar 500 μm , (J) Saddle dolomite (D3) filled fracture followed by late-stage calcite. Pyrite and pyrobitumen predate saddle dolomite. Core of saddle dolomite is inclusion-rich, the rim is slightly ferroan and clear.

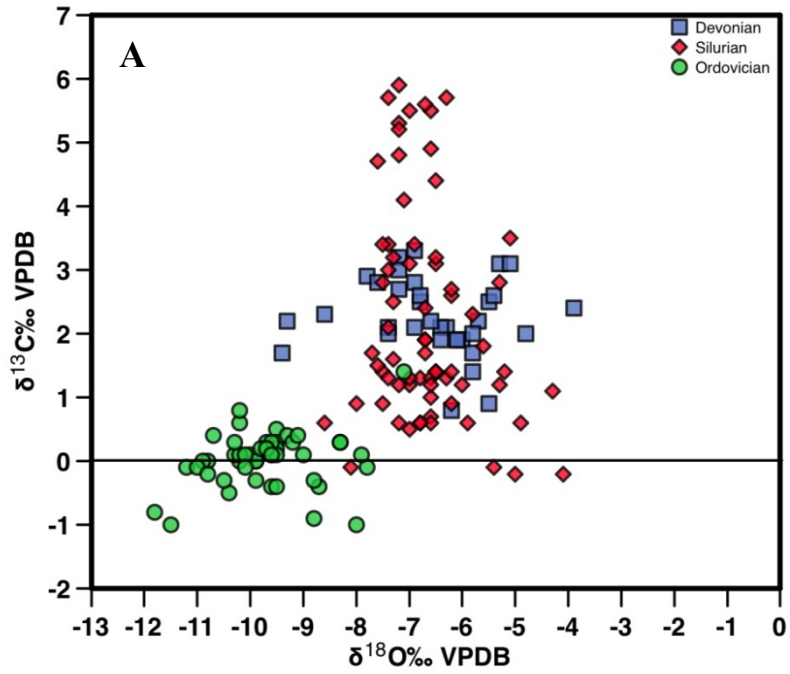


Figure 4.5A $\delta^{18}\text{O}$ and $\delta^{13}\text{C}$ values of replacive dolomite (D1 and D2) of the Paleozoic carbonate succession of southwestern Ontario.

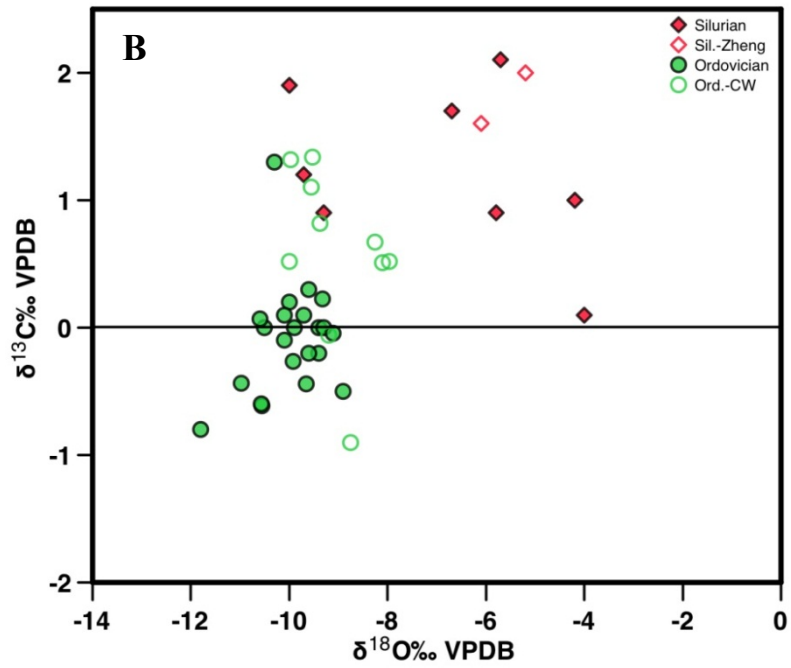


Figure 4.5B $\delta^{18}\text{O}$ and $\delta^{13}\text{C}$ values of saddle dolomite cement (D3) of Silurian and Ordovician rocks.

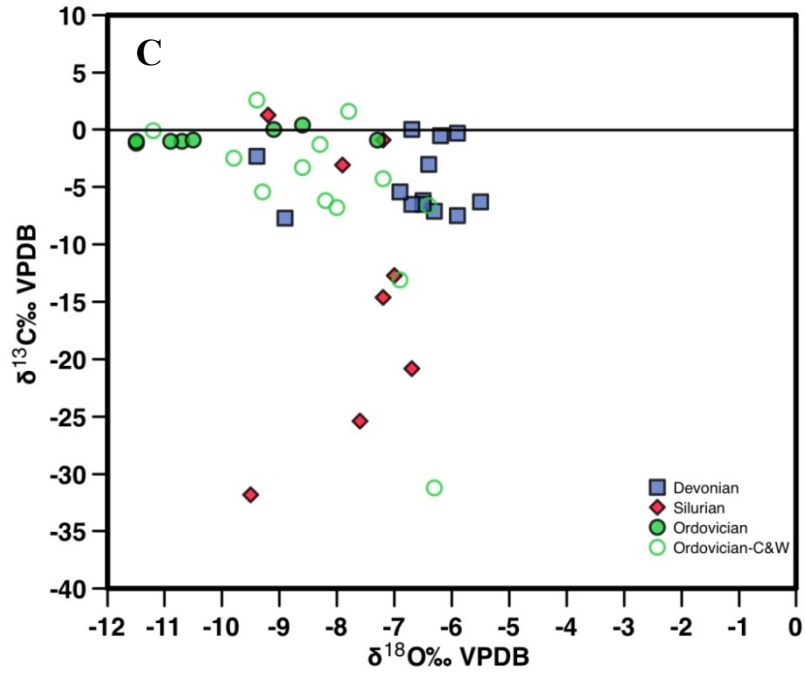


Figure 4.5C $\delta^{18}\text{O}$ and $\delta^{13}\text{C}$ values of late-stage calcite cement of the Paleozoic succession of southwestern Ontario.

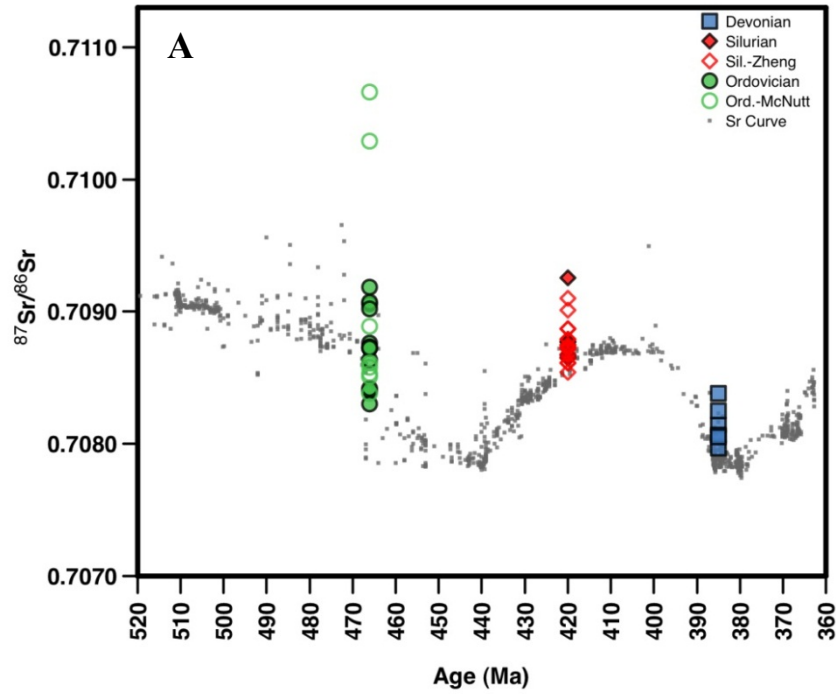


Figure 4.6A Secular $^{87}\text{Sr}/^{86}\text{Sr}$ curve of Devonian to Cambrian seawater and $^{87}\text{Sr}/^{86}\text{Sr}$ ratio of dolomite from Lucas and Guelph formations and Trenton Group. Open circles and diamonds represent results from McNutt et al. (1987) and Zheng, (1999), respectively.

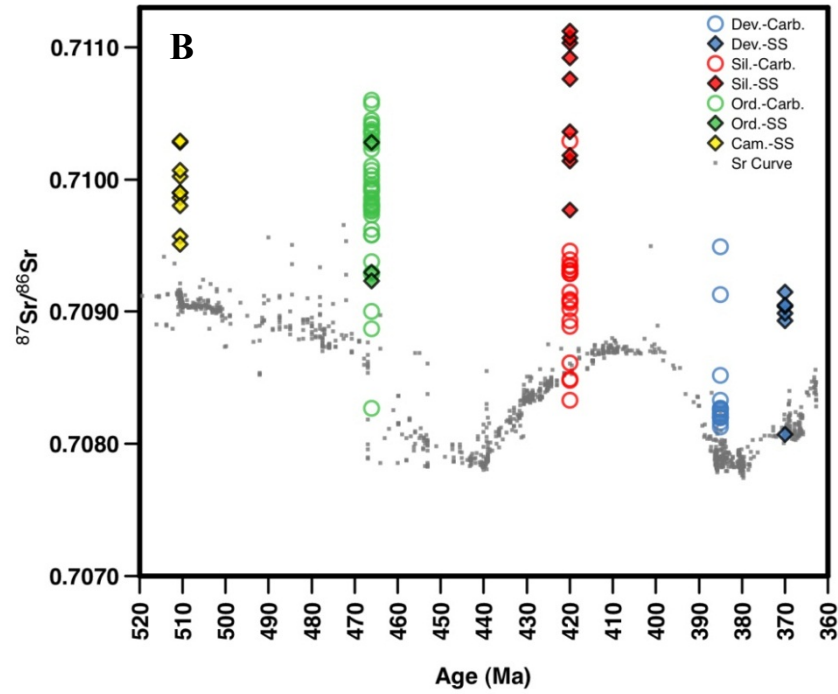


Figure 4.6B Secular $^{87}\text{Sr}/^{86}\text{Sr}$ curve of Devonian to Cambrian sea water and $^{87}\text{Sr}/^{86}\text{Sr}$ ratios variation of brines of sandstone and carbonate reservoirs from Cambrian to Devonian of southwestern Ontario (Hobbs et al., 2011). Secular $^{87}\text{Sr}/^{86}\text{Sr}$ variation is from Veizer et al. (1999).

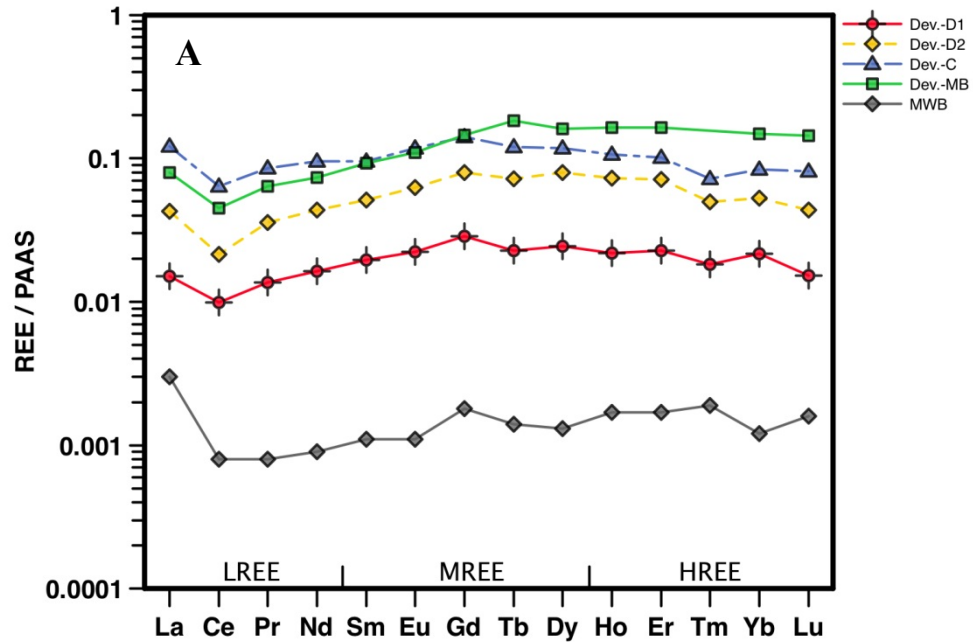


Figure 4.7A Average shale-normalized (PAAS) values of REE concentration in different diagenetic minerals of Devonian samples; fine- (Dev.-D1) and medium-crystalline (Dev.-D2) dolomite, fracture-filling calcite (Dev.-LC), modern warm water brachiopods (MWB, Azmy et al., 2011), and Devonian microbialites (Dev.-MB, Nothdurft et al., 2004). All of the samples exhibit identical REE_{SN} patterns similar to those of seawater, indicative of interaction with seawater dominated brines.

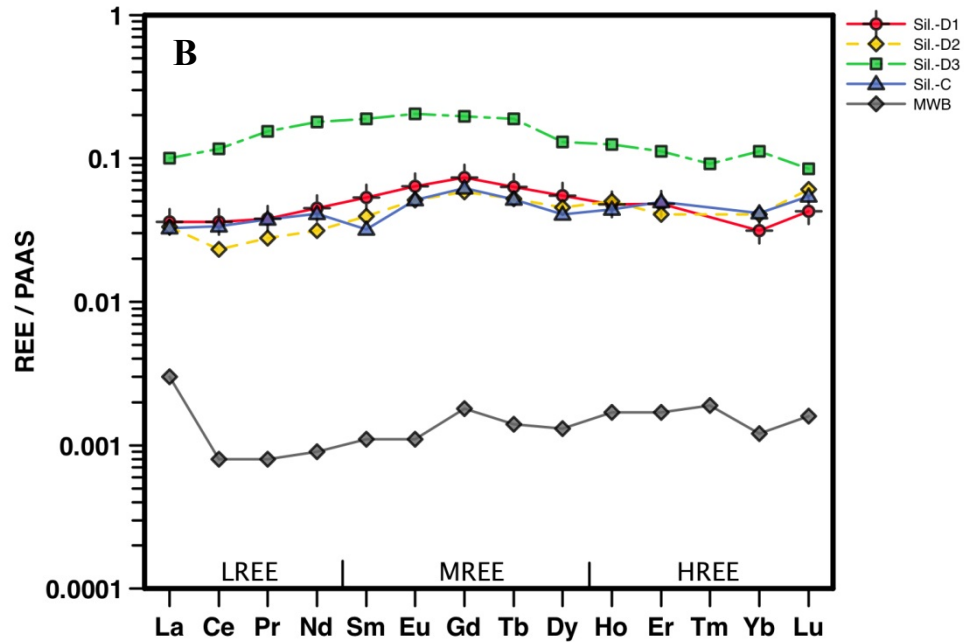


Figure 4.7B Average shale-normalized (PAAS) values of REE concentration in different diagenetic minerals of Silurian samples; fine- (Sil.-D1) and medium-crystalline (Sil.-D2) and saddle dolomite (sil.-D3), vug-filling calcite (Sil.-LC), well-preserved Silurian brachiopod (Sil.-B, Azmy et al., 2011).

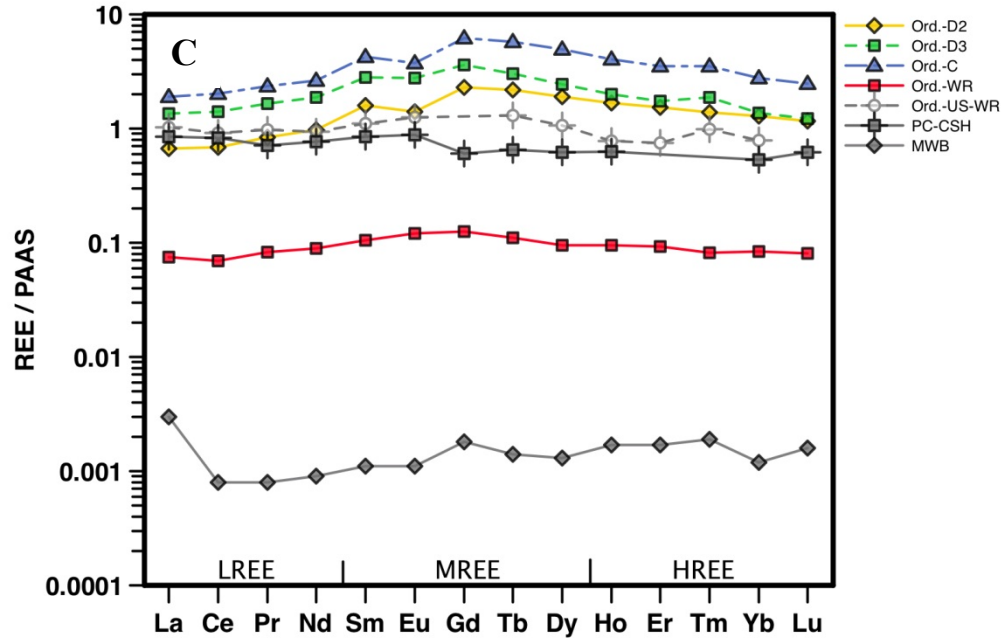


Figure 4.7C Average shale-normalized (PAAS) values of REE concentration in different diagenetic minerals of Ordovician samples; matrix (Ord.-D2) and saddle dolomite (Ord.-D3), fracture-filling calcite (Ord.-LC), undolomitized host rock (Ord.-WR), Utica shale whole rock (Ord.-US-WR, Abanda and Hannigan, 2006), and Precambrian Canadian Shield (PC-CSH, Wedepohl, 1995). Diagenetic minerals do not show the typical seawater pattern and significantly enriched relative to the host rock.

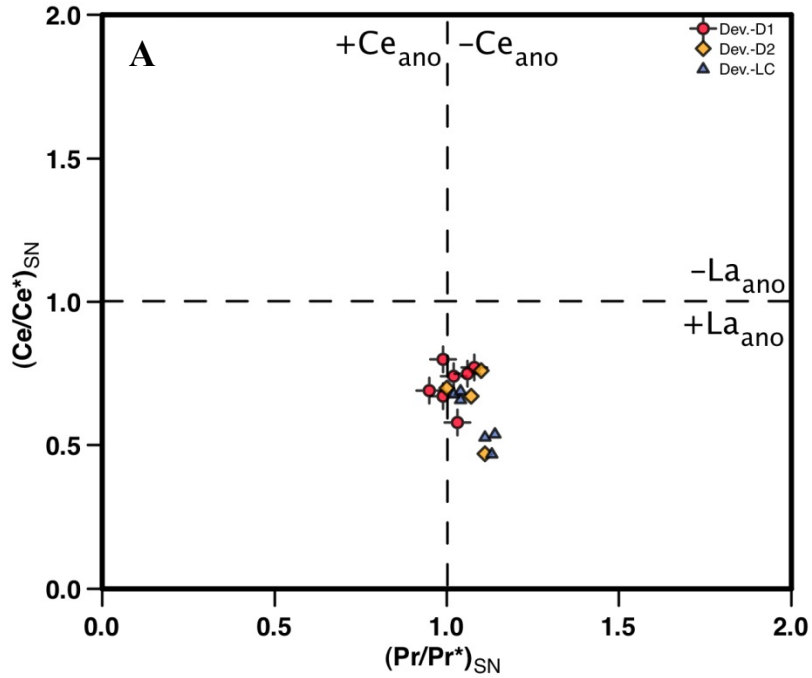


Figure 4.8A Ce $(Ce/Ce^*)_{SN}$ and La $(Pr/Pr^*)_{SN}$ anomaly evaluation of Devonian fine- (D1) and medium-crystalline (D2) dolomite and fracture-filling calcite. All samples exhibit a pronounced positive La anomaly with predominantly negative Ce anomaly.

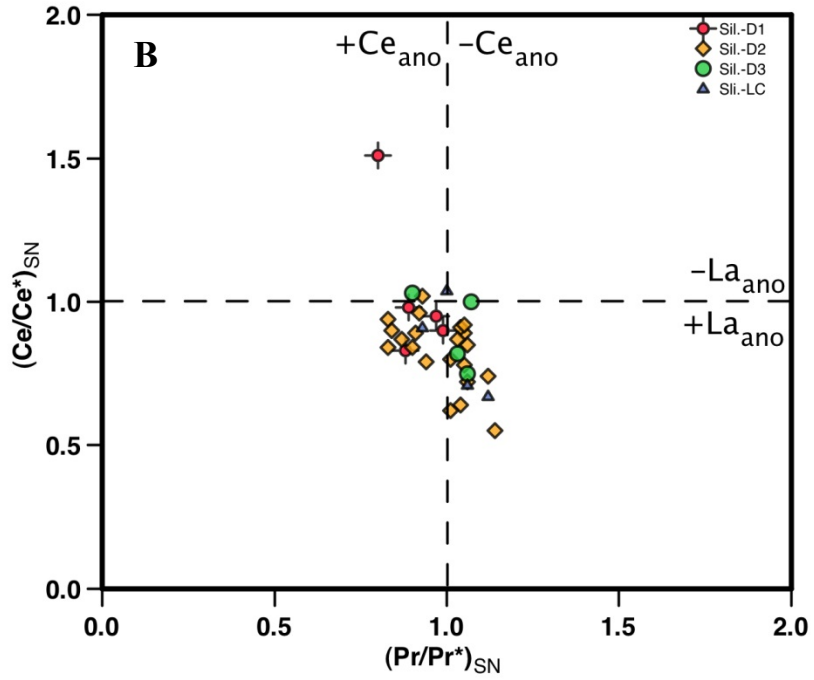


Figure 4.8B Ce $(Ce/Ce^*)_{SN}$ and La $(Pr/Pr^*)_{SN}$ anomaly evaluation of the Silurian fine- (D1) and medium-crystalline (D2) and saddle dolomite (D3) and vug-filling calcite. Samples exhibit a minor negative La anomaly coupled with positive Ce anomaly.

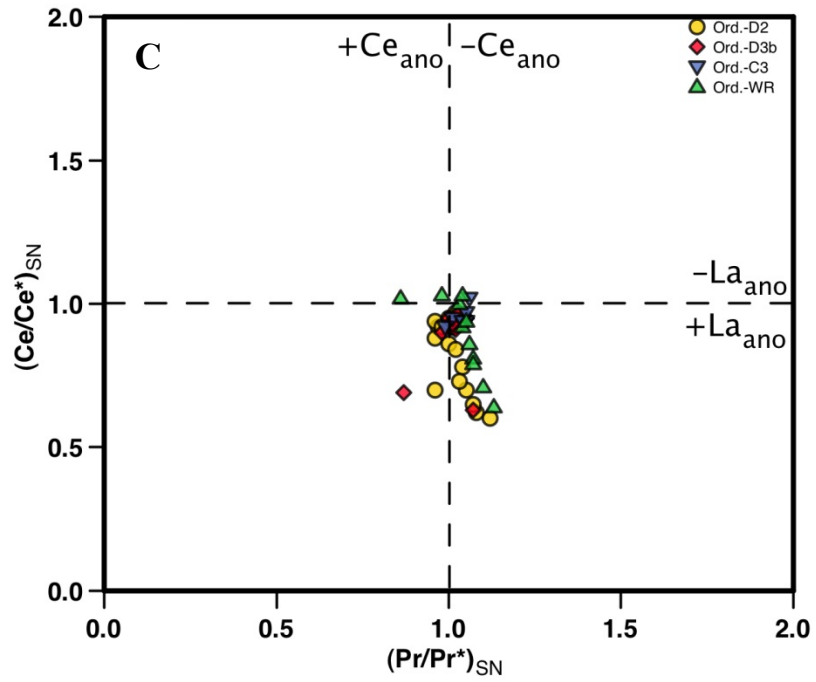


Figure 4.8C Ce $(Ce/Ce^*)_{SN}$ and La $(Pr/Pr^*)_{SN}$ anomaly evaluation of Trenton Group limestone host rock and corresponding diagenetic minerals.

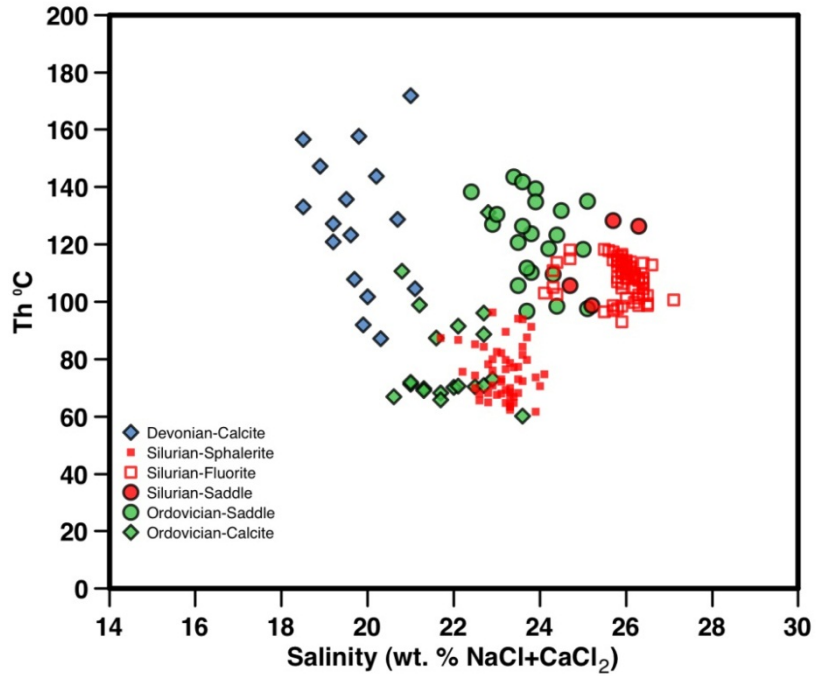


Figure 4.9 Fluid inclusion homogenization temperature and salinity of selected minerals from Paleozoic carbonate succession. Silurian saddle dolomite and fluorite show the highest salinity.

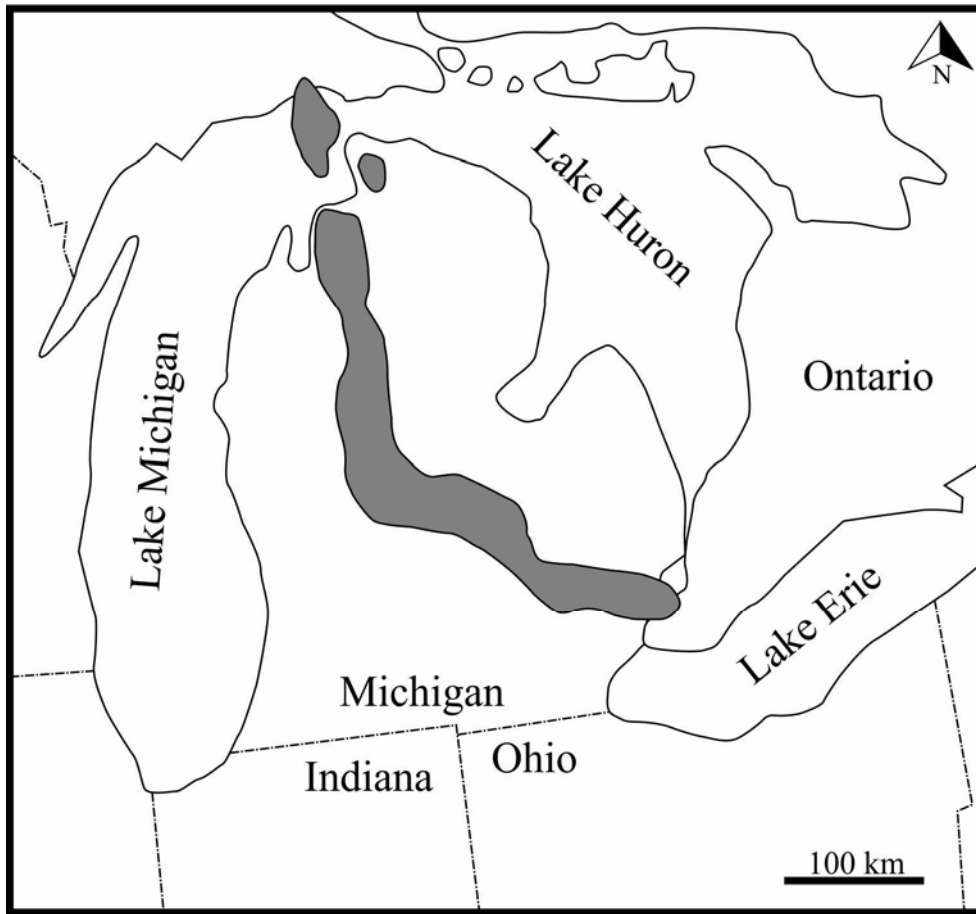


Figure 4.10 The location of buried mid-continent rift (MCR) under the Michigan Basin. A thermal anomaly along this rift produced excess heat in the basin (Adapted from Girard and Barnes, 1995).

Table 4.1 Summary statistics of oxygen, carbon and strontium isotope results of dolomite and late-stage calcite from the Paleozoic succession of southwestern Ontario.

Age	Mineral	$\delta^{13}\text{C}\text{‰ VPDB}$	$\delta^{18}\text{O}\text{‰ VPDB}$	$^{87}\text{Sr}/^{86}\text{Sr}$
Devonian	D1			
Devonian	n	26	26	6
Devonian	Avg.	2.3	-6.4	0.70814
Devonian	Stdev.	0.5	1.2	0.00015
Devonian	Max.	3.3	-3.9	0.70838
Devonian	Min.	0.9	-9.4	0.70797
Devonian	D2			
Devonian	n	8	8	
Devonian	Avg.	2.1	-6.9	
Devonian	Stdev.	0.8	1.1	
Devonian	Max.	3.2	-5.8	
Devonian	Min.	0.8	-9.3	
Devonian	Late Calcite			
Devonian	n	13	13	2
Devonian	Avg.	-4.6	-6.8	0.70807
Devonian	Stdev.	2.9	1.1	0.00012
Devonian	Max.	0.0	-5.5	0.70815
Devonian	Min.	-7.7	-9.4	0.70798
Silurian	D1			
Silurian	n	17	17	2
Silurian	Avg.	2.1	-6.7	0.70870
Silurian	Stdev.	1.3	0.9	0.00004
Silurian	Max.	4.8	-5.1	0.70872
Silurian	Min.	0.6	-8.6	0.70867
Silurian	D2			
Silurian	n	54	54	5
Silurian	Avg.	2.3	-6.7	0.70857
Silurian	Stdev.	1.8	0.9	0.00032
Silurian	Max.	5.9	-4.1	0.70877
Silurian	Min.	-0.2	-8.1	0.70800
Silurian	D3			
Silurian	n	8	8	2
Silurian	Avg.	1.3	-6.7	0.70900
Silurian	Stdev.	0.6	2.2	0.00036
Silurian	Max.	2.1	-4.0	0.70925
Silurian	Min.	0.1	-10.0	0.70875
Silurian	Late Calcite			
Silurian	n	8	8	
Silurian	Avg.	-13.5	-7.8	
Silurian	Stdev.	12.1	1.0	
Silurian	Max.	1.3	-6.7	

Age	Mineral	$\delta^{13}\text{C}\text{‰ VPDB}$	$\delta^{18}\text{O}\text{‰ VPDB}$	$^{87}\text{Sr}/^{86}\text{Sr}$
Silurian	Min.	-31.8	-9.5	
Ordovician	D1			
Ordovician	n	9	9	
Ordovician	Avg.	0.5	-6.1	
Ordovician	Stdev.	0.4	2.0	
Ordovician	Max.	1.3	-2.6	
Ordovician	Min.	-0.2	-8.6	
Ordovician	D2			
Ordovician	n	53	53	12
Ordovician	Avg.	0.0	-9.7	0.70864
Ordovician	Stdev.	0.4	1.0	0.00028
Ordovician	Max.	1.4	-7.1	0.70918
Ordovician	Min.	-1.0	-11.8	0.70830
Ordovician	D3			
Ordovician	n	33	33	8
Ordovician	Avg.	0.1	-9.7	0.70923
Ordovician	Stdev.	0.6	0.8	0.00079
Ordovician	Max.	1.3	-8.0	0.71066
Ordovician	Min.	-0.9	-11.8	0.70861
Ordovician	Late Calcite			
Ordovician	n	21	21	4
Ordovician	Avg.	-3.9	-8.9	0.70864
Ordovician	Stdev.	7.2	1.7	0.00026
Ordovician	Max.	2.6	-6.3	0.70884
Ordovician	Min.	-31.2	11.5	0.70829

Table 4.2 Summary statistics of rare earth elements concentration of various Devonian to Ordovician diagenetic phases (D; various generations of dolomite, WR; undolomitized limestone).

Age	Mineral	La (ppm)	Ce (ppm)	Pr (ppm)	Nd (ppm)	Sm (ppm)	Eu (ppm)	Gd (ppm)	Tb (ppm)	Dy (ppm)	Ho (ppm)	Er (ppm)	Tm (ppm)	Yb (ppm)	Lu (ppm)	ΣREE (ppm)
Devonian	D1															
Devonian	n	7	7	7	7	7	7	7	7	7	7	7	7	7	7	
Devonian	Avg.	0.57	0.79	0.12	0.52	0.11	0.02	0.13	0.02	0.11	0.02	0.07	0.01	0.06	0.01	2.57
Devonian	Stdev.	0.47	0.64	0.10	0.41	0.08	0.02	0.10	0.01	0.08	0.02	0.05	0.01	0.04	0.00	1.98
Devonian	Max.	1.22	1.88	0.27	1.10	0.21	0.05	0.29	0.03	0.23	0.05	0.15	0.02	0.12	0.01	5.34
Devonian	Min.	0.08	0.13	0.02	0.08	0.02	0.00	0.03	0.00	0.01	0.00	0.01	0.00	0.01	0.00	0.38
Devonian	D2															
Devonian	n	4	4		4	4	4	4	4	4	4	4	4	4	4	
Devonian	Avg.	1.62	1.72	0.32	1.39	0.29	0.07	0.37	0.06	0.35	0.07	0.21	0.02	0.15	0.02	6.66
Devonian	Stdev.	2.04	1.72	0.37	1.72	0.33	0.09	0.48	0.08	0.50	0.10	0.28	0.03	0.18	0.02	7.92
Devonian	Max.	4.65	4.17	0.87	3.94	0.78	0.21	1.08	0.17	1.10	0.22	0.62	0.08	0.42	0.05	18.37
Devonian	Min.	0.35	0.45	0.06	0.27	0.07	0.01	0.10	0.01	0.09	0.02	0.06	0.01	0.05	0.01	1.58
Devonian	Late calcite															
Devonian	n	6	6	6	6	6	6	6	6	6	6	6	6	6	6	
Devonian	Avg.	4.61	5.13	0.76	3.06	0.54	0.13	0.66	0.09	0.52	0.11	0.29	0.04	0.23	0.04	16.19
Devonian	Stdev.	4.50	5.48	0.74	2.99	0.51	0.12	0.63	0.08	0.41	0.07	0.18	0.02	0.14	0.02	15.79
Devonian	Max.	13.03	15.52	2.18	8.83	1.53	0.35	1.88	0.25	1.28	0.23	0.57	0.07	0.46	0.07	46.27
Devonian	Min.	0.45	0.65	0.11	0.47	0.09	0.03	0.12	0.02	0.13	0.03	0.09	0.01	0.09	0.01	2.28
Silurian	D1															
Silurian	n	5	5	5	5	5	5	5	5	5	5	5	-	5	5	5
Silurian	Avg.	1.37	2.88	0.34	1.43	0.30	0.07	0.34	0.05	0.24	0.05	0.14	-	0.09	0.02	8.62
Silurian	Stdev.	1.06	2.12	0.30	1.27	0.32	0.05	0.30	0.05	0.31	0.05	0.10	-	0.08	0.01	7.29
Silurian	Max.	3.20	6.50	0.86	3.64	0.82	0.13	0.88	0.13	0.70	0.13	0.31	-	0.23	0.04	21.37
Silurian	Min.	0.52	1.04	0.11	0.50	0.07	0.03	0.16	0.02	0.05	0.01	0.07	-	0.02	0.01	3.25
Silurian	D2a															
Silurian	n	21	21	21	21	21	21	21	21	21	21	21	-	21	21	21
Silurian	Avg.	1.26	1.86	0.25	1.01	0.22	0.06	0.27	0.04	0.20	0.05	0.12	-	0.11	0.03	6.92
Silurian	Stdev.	1.29	1.71	0.27	1.11	0.25	0.07	0.31	0.05	0.30	0.06	0.15	-	0.12	0.02	7.45
Silurian	Max.	5.06	7.53	1.14	4.74	1.07	0.25	1.18	0.18	1.01	0.22	0.56	-	0.45	0.09	31.19
Silurian	Min.	0.12	0.19	0.03	0.11	0.02	0.01	0.03	0.01	0.01	0.01	0.01	-	0.01	0.01	0.70
Silurian	D3															
Silurian	n	4	4	4	4	4	4	4	4	4	4	4	4	4	4	4
Silurian	Avg.	3.83	9.32	1.37	5.72	1.06	0.23	0.92	0.15	0.57	0.13	0.33	0.04	0.31	0.04	27.51
Silurian	Stdev.	2.21	7.71	1.30	5.58	1.04	0.18	0.57	0.09	0.34	0.05	0.14	0.01	0.16	0.02	19.86
Silurian	Max.	6.16	19.82	3.21	13.72	2.57	0.48	1.73	0.27	0.98	0.18	0.51	0.04	0.47	0.05	53.75

Silurian	Min.	1.25	2.89	0.33	1.47	0.25	0.08	0.41	0.07	0.18	0.06	0.18	0.03	0.10	0.01	8.42
Silurian	Late Calcite															
Silurian	n	5	5	5	5	5	5	5	5	5	5	5	-	5	5	5
Silurian	Avg.	1.25	2.68	0.33	1.32	0.18	0.06	0.29	0.04	0.18	0.04	0.14	-	0.12	0.02	8.76
Silurian	Stdev.	1.73	4.28	0.49	1.82	0.24	0.06	0.25	0.04	0.18	0.03	0.10	-	0.08	0.02	10.43
Silurian	Max.	4.32	10.31	1.20	4.54	0.60	0.13	0.71	0.10	0.49	0.10	0.31	-	0.26	0.05	27.19
Silurian	Min.	0.34	0.59	0.07	0.30	0.02	0.02	0.07	0.01	0.05	0.01	0.04	-	0.06	0.01	2.23
Ordovician	D2															
Ordovician	n	24	24	24	24	24	24	24	24	24	24	24	24	24	24	24
Ordovician	Avg.	25.54	54.89	7.39	32.97	8.86	1.52	10.68	1.68	8.85	1.65	4.38	0.56	3.63	0.50	206.6
Ordovician	Stdev.	23.92	51.73	6.69	29.60	8.04	1.33	9.79	1.57	8.47	1.58	4.32	0.61	4.06	0.55	185.5
Ordovician	Max.	93.08	179.7	22.07	97.31	23.09	4.03	29.94	4.38	25.60	5.10	14.70	2.23	15.28	1.99	592.9
Ordovician	Min.	2.12	3.05	0.38	1.69	0.35	0.07	0.58	0.07	0.44	0.09	0.26	0.03	0.20	0.02	13.43
Ordovician	D3															
Ordovician	n	10	10	10	10	10	10	10	10	10	10	10	10	10	10	10
Ordovician	Avg.	51.40	111.6	14.68	63.47	15.59	3.01	16.75	2.33	11.46	1.99	4.97	0.76	3.84	0.53	352.5
Ordovician	Stdev.	44.51	99.59	13.38	59.13	15.03	2.02	13.89	1.96	9.36	1.54	3.76	0.45	3.18	0.44	303.3
Ordovician	Max.	147.8	326.7	43.95	194.7	49.57	7.07	44.19	6.28	29.07	4.77	11.67	1.61	9.98	1.30	991.3
Ordovician	Min.	1.43	1.54	0.22	0.88	0.07	0.71	0.30	0.05	0.11	0.04	0.14	0.20	0.12	0.01	6.70
Ordovician	Late Calcite															
Ordovician	n	6	6	6	6	6	6	6	6	6	6	6	6	6	6	6
Ordovician	Avg.	72.41	160.1	20.87	89.78	23.66	4.05	28.88	4.45	23.25	4.03	9.98	1.23	7.81	1.07	557.2
Ordovician	Stdev.	70.71	135.6	16.76	74.88	17.75	2.94	23.38	3.39	16.55	2.74	6.47	0.71	4.11	0.53	430.8
Ordovician	Max.	212.2	422.9	52.70	230.5	53.31	8.29	60.18	8.98	47.51	8.47	20.92	2.32	12.69	1.72	1352.
Ordovician	Min.	21.40	50.92	7.02	29.59	9.46	1.60	10.65	1.44	7.96	1.55	3.96	0.51	3.11	0.44	217.1
Ordovician	WR															
Ordovician	n	11	11	11	11	11	11	11	11	11	11	11	11	11	11	11
Ordovician	Avg.	2.85	5.50	0.73	3.02	0.58	0.13	0.58	0.08	0.44	0.09	0.26	0.03	0.24	0.03	17.76
Ordovician	Stdev.	1.20	2.30	0.32	1.36	0.27	0.06	0.28	0.04	0.21	0.05	0.12	0.01	0.11	0.01	7.47
Ordovician	Max.	5.40	8.30	1.25	5.32	1.04	0.26	1.15	0.17	0.85	0.18	0.51	0.06	0.48	0.06	31.20
Ordovician	Min.	1.30	2.37	0.26	1.20	0.18	0.04	0.20	0.04	0.13	0.03	0.08	0.02	0.11	0.02	7.02

Table 4.3 Summary statistics of fluid inclusion microthermometry results from selected minerals from Devonian to Ordovician (D; various generations of dolomite).

Age	Mineral	Th °C	Tm °C	Salinity
Devonian	Calcite			
Devonian	n	17	17	17
Devonian	Avg.	126.0	-17.1	19.7
Devonian	Stdev.	24.5	1.3	0.8
Devonian	Max.	171.9	-15.1	21.1
Devonian	Min.	87.1	-19.3	18.5
Devonian	Celestine			
Devonian	n	85	85	85
Devonian	Avg.	218.0	-10.4	14.4
Devonian	Stdev.	52.8	2.1	1.9
Devonian	Max.	321.8	-6.1	19.2
Devonian	Min.	118.2	-16.1	9.7
Silurian	D2			
Silurian	n	44	14	14
Silurian	Avg.	103.7	-20.3	20.5
Silurian	Stdev.	19.2	8.3	4.6
Silurian	Max.	140.0	-9.9	25.9
Silurian	Min.	64.5	-31.2	14.1
Silurian	D3			
Silurian	n	13	4	4
Silurian	Avg.	108.4	-29.9	25.5
Silurian	Stdev.	12.5	2.0	0.7
Silurian	Max.	128.2	-27.6	26.3
Silurian	Min.	91.5	-32.4	24.7
Silurian	Fluorite			
Silurian	n	75	75	75
Silurian	Avg.	108.7	-31.3	25.9
Silurian	Stdev.	6.1	1.7	0.6
Silurian	Max.	118.3	-26.1	27.1
Silurian	Min.	93.1	-35.4	24.1
Silurian	Sphalerite			
Silurian	n	53	53	53
Silurian	Avg.	75.2	-23.7	23.2
Silurian	Stdev.	9.1	1.1	0.5
Silurian	Max.	96.3	-20.5	24.1
Silurian	Min.	61.6	-26.1	21.7
Ordovician	D2			
Ordovician	n	30		
Ordovician	Avg.	81.8		
Ordovician	Stdev.	9.5		
Ordovician	Max.	98.9		
Ordovician	Min.	67.6		
Ordovician	D3			
Ordovician	n	36	23	23
Ordovician	Avg.	121.1	-25.6	23.9
Ordovician	Stdev.	13.3	1.8	0.7
Ordovician	Max.	143.5	-21.9	25.1
Ordovician	Min.	96.7	-28.8	22.4
Ordovician	Calcite			
Ordovician	n	37	24	24
Ordovician	Avg.	82.6	-21.5	22.1
Ordovician	Stdev.	17.5	2.3	1.0

Age	Mineral	T _h °C	T _m °C	Salinity
Ordovician	Max.	131.1	-18.5	24.8
Ordovician	Min.	60.2	-27.9	20.6

Table 4.4 Average T_h and salinity of calcite, dolomite and quartz hosted fluid inclusions of Devonian to Ordovician rocks in the center of the Michigan Basin and its margin.

Age/Mineral	Central part of Michigan Basin	Margin of basin
Dev.-Calcite		T _h = 126°C, S. = 19.7 wt. % NaCl
Dev.-Celestine		T _h = 218°C, S. = 14.1 wt. % NaCl
Dev.-Saddle dolomite	T _h = 140°C, S. = 29.2 wt. % NaCl, Luczaj et al. (2006)	No Saddle Dolomite
Sil.-Matrix dolomite		T _h = 104°C, S. = 20.3 wt. % NaCl+CaCl ₂
Sil.-Saddle dolomite	T _h = 155°C, Barnes et al., (2008)	T _h = 108°C, S. = 25.5 wt. % NaCl+CaCl ₂
Sil.-Fluorite		T _h = 108°C, S. = 25.9 wt. % NaCl+CaCl ₂
Ord.-Matrix dolomite		T _h = 81.8°C
Ord.-Saddle dolomite		
Trenton Group	T _h = 155°C, Barnes et al. (2008)	T _h = 121°C, S. = 24 wt. % NaCl+CaCl ₂
Glenwood Fm.	T _h = 175°C, Simo et al. (1994)	
Ord.-Quartz cement	T _h = 142°C, Girard and Barnes (1995)	
St. Peter Sst.		

Table 4.5 ΣREE of selected minerals from Devonian to Ordovician and δ¹⁸O_{fluid}, and salinity of fluids responsible for their precipitation

Age/Mineral	ΣREE	δ ¹⁸ O _{fluid}	Fluid inclusion salinity
Devonian-replacive dolomite			
D1	2.58 ± 1.98 ppm	-5 to +1‰ VSMOW	
D2	6.66 ± 7.92 ppm		
Devonian-fracture-filling calcite			19.7 wt. % NaCl
Devonian celestine			14.4 wt. % NaCl
Silurian-replacive dolomite			
D1	8.62 ± 7.29 ppm	-3 to +11‰ VSMOW	
D2	6.92 ± 7.45 ppm		20.3 wt. % NaCl+CaCl ₂
Silurian-saddle dolomite	27.51 ± 19.86 ppm	+3 to +11‰ VSMOW	25.9 wt. % NaCl+CaCl ₂
Ordovician-replacive dolomite	206.61 ± 185.56 ppm	-6 to +2‰ VSMOW	
Ordovician-saddle dolomite	352.50 ± 303.37 ppm	-2 to +6‰ VSMOW	24 wt. % NaCl+CaCl ₂

Chapter 5

Conclusions of research

The aim of this thesis was to identify and fingerprint the fluids which affected the Paleozoic succession, and determine their temporal and spatial relationships. To achieve this aim, the following tasks were carried out:

- Identification of diagenetic mineral phases, their relationship to host carbonates, and their environment of formation;
- Characterization of the nature of diagenetic fluids (temperature and composition) during various stages of diagenesis;
- Investigation of the presence or absence of hydrocarbons and their possible role in formation of diagenetic minerals (i.e., carbonate cements); and,
- Development of a general qualitative paleohydrologic model which explains the depth of fluid circulation and how diagenetic fluids moved through the basin.

The above information was used to answer three outstanding questions concerning the diagenesis of the Paleozoic succession in southwestern Ontario listed below:

- What was the nature of the paleohydrologic system(s) that led to partial dolomitization of Devonian and Ordovician sequences and pervasive dolomitization of Silurian sequences?
- Were the diagenetic systems in Ordovician, Silurian and Devonian strata in southwestern Ontario separate or connected?
- What was the source of heat for hydrothermal fluids and driving force for fluid migration?

This thesis was written as a series of 3 related papers (chapters 2-4), and together they address the questions as described below.

5.1 Nature of the paleohydrologic system(s)

To explore the nature of the paleohydrologic systems, chapters 2-4 took into consideration the extent and pattern of dolomitization, dolomite petrography and made conclusions based on the following arguments:

- Relatively thin layers (0.5 to 5 m) of fine-crystalline dolomite associated with evaporite interbeds and shallow water intertidal to supratidal facies suggest replacement of carbonate muds with dolomite from reflux of hypersaline brine in a sabkha setting in early stages of diagenesis.
- The pervasive dolomitization of Silurian patch reefs on the carbonate platform and reefs on the upper basin slope relative to reefs on more basinward parts the slope suggest fluid flow from the basin margin towards its center. The lower Mg^{+2}/Ca^{+2} ratio of fluids extracted from halite-hosted fluid inclusions from the Salina evaporites presented by the other studies support the previous model of dolomitization in response to pumping of seawater through high porosity reefal limestone from the basin margin towards its center. This was the result of hydraulic head due to an evaporative drawdown in the basin center and contemporaneous dolomitization and evaporite precipitation.
- Fracture-related coarse-crystalline Ordovician dolomite with high fluid inclusion homogenization temperatures implies precipitation of this dolomite during the later stages of diagenesis in a burial environment which was influenced by hydrothermal fluids.
- Different patterns and extent of dolomitization and paleohydrologic systems in each stratigraphic interval indicate that dolomitization took place in different diagenetic settings and time frames and there is no genetic relationship between them.

5.2 Connection of the diagenetic systems

To answer this question, Chapter 4 looked at stable oxygen and carbon isotopes, Sr isotopes, and the rare earth elements (REE) composition and fluid inclusion characteristics of different dolomite types and late-stage fracture- and vug-filling calcite cements and came to the following conclusions:

- The $\delta^{13}\text{C}$ values of dolomite from each interval are in the range of expected $\delta^{13}\text{C}$ values of coeval marine calcite, which reflect the carbon isotopic composition of the precursor limestone.
- Calculated $\delta^{18}\text{O}_{\text{fluid}}$ values indicate involvement of fluids with distinct isotopic compositions in precipitation/recrystallization of dolomite from different age intervals. Mixing of Silurian and Ordovician connate waters with ^{18}O -enriched fluids resulted from dissolution of Silurian evaporates, producing fluids with more positive $\delta^{18}\text{O}_{\text{fluid}}$ values relative to corresponding seawater. More ^{18}O -depleted values of Devonian fluids relative to coeval seawater suggest introduction of meteoric water to diagenetic system.
- $^{87}\text{Sr}/^{86}\text{Sr}$ ratios of dolomite from each interval vary from coeval seawater ratios to values that are more radiogenic than coeval seawater. This implies that basinal brines were involved in precipitation and/or recrystallization of dolomite. However, Middle Ordovician dolomite has lower $^{87}\text{Sr}/^{86}\text{Sr}$ ratios than coeval seawater, which suggest involvement of younger seawater (Devonian and/or Silurian) in precipitation of dolomite or water/rock interaction with highly fractured ultramafic rocks of the mid-continent rift (MCR).
- The different ΣREE and REE_{SN} pattern of dolomite from each interval suggest compositional diversity of the diagenetic fluids. The overall depletion or enrichment of diagenetic mineral REE_{SN} trends relative to that of respective host rock indicates that fluid REE composition is an important controlling factor in REE composition of the diagenetic minerals.
- Hydrocarbon-bearing fluid inclusions in late-stage calcite cements of all ages and their significant negative $\delta^{13}\text{C}$ values (approaching -32‰ VPDB) indicate the role of diagenetic fluids in the migration of hydrocarbons. However, the significant difference in ΣREE and REE_{SN} pattern of late-stage calcite cements suggests diversity in fluid composition.
- The overall comparison of dolomite and calcite geochemical data of different ages shows no similarities in geochemical characteristics and suggests compartmentalization of diagenetic fluids in the Paleozoic carbonate succession of southwestern Ontario.

5.3 Source of heat and driving force of hydrothermal fluids

Hydrothermal fluids best explain the higher homogenization temperatures of diagenetic minerals relative to ambient burial-associated temperatures for each interval, high salinity of fluids, and negative $\delta^{18}\text{O}$ values of replacive dolomite and late-stage calcite and dolomite cements. Chapters 2-4 took into consideration fluid inclusion data and paleotemperature estimates for each interval.

The uncertainty in thickness of the Paleozoic sedimentary succession of southwestern Ontario and the paleogeothermal gradient caused ambiguity in estimation of maximum burial temperatures for each interval, however. The maximum burial temperature for the Paleozoic sequence (Devonian to Cambrian) in southwestern Ontario is estimated to be between 60 and 90°C, based on conodont and acritarch alteration index (Legall et al., 1981).

- Assuming this range of temperatures as maximum burial temperatures, the measured homogenization temperatures and calculated temperatures of dolomite, late-stage calcite, and fluorite of each age interval are significantly higher than the expected ambient burial temperatures, suggesting involvement of hydrothermal fluids in precipitation/recrystallization of diagenetic minerals.
- Higher homogenization temperatures of dolomite of each age in the central part of the Michigan Basin than those corresponding to equivalent age at the basin margin suggest hydrothermal fluids migrated and cooled from the basin center towards its margin.
- Reactivation of the buried mid-continent rift during Late Devonian – Mississippian (375–299 Ma) and the associated thermal anomaly over the buried mid-continent rift in the Michigan Basin (~170°C) is likely the source of heat for hydrothermal fluids.
- The timing of the thermal anomaly coincides with the interval between the Acadian (410–360 Ma) and Alleghanian (325–260 Ma) orogenies and the onset of the Alleghanian orogeny. Reactivation of basement faults and faults in the overlying Paleozoic sequence in response to Alleghanian orogeny opened fractures and facilitated migration of hydrothermal fluids.

- Uplift of basement arches in response to the Alleghanian orogeny and resulting emergence and erosion along crest of the arches allowed meteoric water to enter in the Paleozoic succession of the study area. A general decrease in fluid inclusions salinity and temperature of Devonian (calcite and celestine), Silurian (fluorite, dolomite and sphalerite), and Ordovician (saddle dolomite and calcite) is likely due to this event.
- The potential thermal buoyancy produced by excess heat in the basin provided the driving force for hydrothermal fluids. Permeable sandstone layers in the Cambrian (Eau Claire and Mount Simon sandstones), lower Silurian (Grimsby and Whirlpool sandstones), and lower Devonian (Sylvania sandstone) were major regional aquifers for migration of diagenetic fluids from the center of the Michigan Basin towards its margin.

5.4 Recommendation for future studies

The results of this research could serve as a base for future research in the following areas:

- Since the Paleozoic succession of southwestern Ontario is a transition between the Michigan and Appalachian basins, comprehensive diagenetic studies on equivalent strata in both basins could determine the physicochemical conditions of the diagenetic systems in each basin and their possible hydrological connection.
- Results of this study in combination with previous studies on the Paleozoic succession of the Michigan Basin indicate that hydrothermal fluids originated from the center of the basin and migrated outward. However, fluid movement and heat distribution in the basin has not yet been systematically modeled. A systematic review of available data on the nature of fluids involved in dolomitization in the Michigan Basin and neighboring states from different strata could be used to develop a numerical model for fluid movement in the Michigan Basin and its thermal evolution.
- Although a preliminary study (e.g., Barnes et al., 2008) compared fluid inclusion results and oxygen isotopic composition of fracture-filling dolomite in the Paleozoic succession of the central Michigan Basin, results of that study have not been

published. It is recommended that as the next step the textural and geochemical characteristics of diagenetic minerals from the center of the basin be investigated and compared to those of this study to determine the evolution of diagenetic fluids.

Appendices

Appendix 1

Appendix 1 Carbon, oxygen and strontium isotope results of replacive dolomite and cement and fracture-filling calcite of the Paleozoic carbonate succession of southwestern Ontario.

Lab ID	Sample ID	Age	Mineral	$\delta^{13}\text{C}\text{‰ VPDB}$	$\delta^{18}\text{O}\text{‰ VPDB}$	$^{87}\text{Sr}/^{86}\text{Sr}$	Reference
09-583	1010	Devonian	D1	2.5	-5.5	0.70805	
09-580	1011	Devonian	D1	3.1	-5.3		
09-581	1018	Devonian	D1	2.3	-8.6		
09-570	1023	Devonian	D1	2.9	-7.8		
09-582	1024	Devonian	D1	2.6	-5.4		
09-586	1054	Devonian	D1	2.8	-6.9	0.70807	
09-574	1016-1	Devonian	D1	2.2	-5.7		
09-079	AM010	Devonian	D1	2.8	-7.6		
09-080	AM013	Devonian	D1	2.5	-6.8		
09-272	AM014	Devonian	D1	3.3	-6.9		
09-081	AM015-2	Devonian	D1	1.7	-9.4		
09-095	AM016	Devonian	D1	3.1	-5.1		
09-082	AM018	Devonian	D1	2.7	-7.2		
09-270	AM024-1	Devonian	D1	2.6	-6.8		
09-281	AM025-2	Devonian	D1	1.9	-6.0	0.70797	
09-271	MG007	Devonian	D1	2.4	-3.9	0.70814	
09-226	MG017-2	Devonian	D1	2.1	-6.9	0.70838	
09-280	MG021-1	Devonian	D1	2.1	-6.3		
09-273	MG022	Devonian	D1	1.9	-6.1		
09-277	MG023	Devonian	D1	2.0	-4.8		
09-282	MG026	Devonian	D1	2.1	-6.4		
09-279	MG027	Devonian	D1	2.1	-7.4	0.70825	
09-225	MG044	Devonian	D1	1.9	-6.1		
09-278	MG024-2	Devonian	D1	2.0	-5.8		
09-585	SM-2	Devonian	D1	0.9	-5.5		
09-084	AM030-1	Devonian	D1	1.9	-6.4		
09-227	MG032-1	Devonian	D2	1.7	-5.8		
09-576	1056	Devonian	D2	3.2	-7.2		
09-584	1004	Devonian	D2	2.2	-9.3		
09-578	1029	Devonian	D2	1.4	-5.8		
09-269	AM007-1	Devonian	D2	3.0	-7.2		

Lab ID	Sample ID	Age	Mineral	$\delta^{13}\text{C}\text{‰ VPDB}$	$\delta^{18}\text{O}\text{‰ VPDB}$	$^{87}\text{Sr}/^{86}\text{Sr}$	Reference
09-276	MG013	Devonian	D2	2.0	-7.4		
09-275	MG035-2	Devonian	D2	2.2	-6.6		
09-219	MG042-2	Devonian	D2	0.8	-6.2		
09-092	AM014-VUG-6	Devonian	Late Calcite	-6.2	-6.5		
09-074	AM015-1	Devonian	Late Calcite	-2.9	-6.4		
09-077	AM030-3	Devonian	Late Calcite	-7.1	-6.3		
09-090	AM030-2	Devonian	Late Calcite	-7.5	-5.9		
09-558	1012-2	Devonian	Late Calcite	-2.3	-9.4		
09-560	1025-1	Devonian	Late Calcite	-0.5	-6.2		
09-561	1026-1	Devonian	Late Calcite	-0.3	-5.9		
09-565	1053-1	Devonian	Late Calcite	0.0	-6.7		
09-241	AM002	Devonian	Late Calcite	-6.3	-5.5	0.70815	
09-217	MG032-2	Devonian	Late Calcite	-7.7	-8.9	0.70798	
09-242	MG-100	Devonian	Late Calcite	-6.5	-6.5		
09-243	MG-102	Devonian	Late Calcite	-6.5	-6.8		
09-555	SM-1	Devonian	Late Calcite	-5.4	-6.9		
10-024	BV4F	Silurian	D1	2.4	-6.7		
10-028	2130	Silurian	D1	1.2	-6.0		
10-030	BV3	Silurian	D1	2.5	-7.3		
10-042	BV3-1	Silurian	D1	3.5	-5.1		
10-052	2079-2	Silurian	D1	1.4	-6.5		
10-053	2124-1	Silurian	D1	1.2	-5.3		
10-060	2015	Silurian	D1	0.7	-6.6	0.70872	
10-077	2028	Silurian	D1	3.1	-6.5		
10-083	2008	Silurian	D1	2.3	-5.8	0.70867	
10-085	2016	Silurian	D1	1.0	-6.6		
10-088	2078-1	Silurian	D1	1.7	-7.7		
10-128	2039	Silurian	D1	3.4	-7.4		
10-131	2089-2	Silurian	D1	0.6	-8.6		
10-136	2082-2	Silurian	D1	1.3	-6.3		
10-139	2114	Silurian	D1	4.8	-7.2		
10-141	2100	Silurian	D1	0.6	-7.2		
10-142	2012-2	Silurian	D1	4.4	-6.5		
10-021	BP02-2	Silurian	D2	5.5	-7.0		
10-022	2095	Silurian	D2	5.5	-6.6		
10-023	BV4	Silurian	D2	1.4	-7.5		
10-027	TBM	Silurian	D2	0.9	-7.5		
10-029	2079-3	Silurian	D2	1.3	-6.8		
10-031	ADF-1	Silurian	D2	2.1	-7.4	0.70867	
10-032	2054-1	Silurian	D2	1.4	-5.2		

Lab ID	Sample ID	Age	Mineral	$\delta^{13}\text{C}\text{‰ VPDB}$	$\delta^{18}\text{O}\text{‰ VPDB}$	$^{87}\text{Sr}/^{86}\text{Sr}$	Reference
10-033	2115	Silurian	D2	5.3	-7.2		
10-034	BV2	Silurian	D2	3.2	-6.5		
10-035	BV6-1	Silurian	D2	1.1	-4.3		
10-036	2081	Silurian	D2	1.6	-7.3		
10-037	2082-1	Silurian	D2	1.3	-6.6		
10-038	2001-1	Silurian	D2	1.2	-7.0		
10-039	2089-1	Silurian	D2	1.8	-5.6		
10-040	2058	Silurian	D2	1.3	-7.4		
10-041	2094	Silurian	D2	4.7	-7.6		
10-043	2050	Silurian	D2	2.8	-7.5		
10-044	2075	Silurian	D2	1.5	-7.6		
10-045	2112-2	Silurian	D2	2.8	-5.3		
10-046	2014	Silurian	D2	5.2	-7.2		
10-047	2036	Silurian	D2	2.6	-6.2		
10-050	BV7-2-1	Silurian	D2	1.4	-6.5	0.70877	
10-051	2085	Silurian	D2	0.6	-5.9		
10-054	2079-1	Silurian	D2	1.4	-6.2		
10-057	2110A-2	Silurian	D2	-0.2	-4.1		
10-058	2025A	Silurian	D2	2.7	-6.2		
10-059	2087-1	Silurian	D2	0.6	-6.6		
10-062	2092	Silurian	D2	5.6	-6.7		
10-079	2001-2	Silurian	D2	1.2	-6.6		
10-084	2005	Silurian	D2	0.9	-8.0		
10-086	2099	Silurian	D2	0.5	-7.0	0.70865	
10-087	2088	Silurian	D2	1.4	-6.5		
10-089	2029	Silurian	D2	4.1	-7.1		
10-119	2119	Silurian	D2	5.7	-7.4		
10-120	2108-2	Silurian	D2	-0.2	-5.0	0.70800	
10-121	2110A-1	Silurian	D2	-0.1	-5.4		
10-122	2078-2	Silurian	D2	1.9	-6.7		
10-125	2012-1	Silurian	D2	4.9	-6.6		
10-126	2043	Silurian	D2	1.3	-7.0		
10-127	2091	Silurian	D2	5.7	-6.3		
10-129	2022	Silurian	D2	3.4	-7.5		
10-130	2041-2	Silurian	D2	0.6	-6.8		
10-132	2105	Silurian	D2	-0.1	-8.1		
10-134	BV7-1-1	Silurian	D2	1.9	-6.7		
10-135	2116	Silurian	D2	5.9	-7.2		
10-137	2045	Silurian	D2	1.2	-7.2		
10-138	2034	Silurian	D2	3.1	-7.0		

Lab ID	Sample ID	Age	Mineral	$\delta^{13}\text{C}\text{‰ VPDB}$	$\delta^{18}\text{O}\text{‰ VPDB}$	$^{87}\text{Sr}/^{86}\text{Sr}$	Reference
10-143	2112-1	Silurian	D2	3.0	-7.4		
10-265	2056	Silurian	D2	3.2	-7.3		
10-026	BV1	Silurian	D2	3.4	-6.9	0.70877	
10-048	2060-1	Silurian	D2	1.7	-6.7		
10-049	BP04	Silurian	D2	0.6	-4.9		
10-080	2084	Silurian	D2	0.9	-6.2		
10-082	2087-2	Silurian	D2	0.6	-6.8		
10-025	2126-1	Silurian	D3	0.9	-5.8		
10-055	2124-2	Silurian	D3	1.2	-9.7	0.708746	
10-056	2060-2	Silurian	D3	1.9	-10.0		
10-061	BV7-1-2	Silurian	D3	2.1	-5.7		
10-090	2126-2	Silurian	D3	0.9	-9.3		
10-123	2110A-3	Silurian	D3	0.1	-4.0		
10-133	BV7-2-2	Silurian	D3	1.7	-6.7	0.709254	
10-140	BV6-2	Silurian	D3	1.0	-4.2		
	938A	Silurian	D3	1.9	-5.2		Zheng, 1999
	939-D1	Silurian	D3	1.6	-6.1		Zheng, 1999
10-105	2069A-1	Silurian	Late Calcite	1.3	-9.2		
10-106	2079-4	Silurian	Late Calcite	-20.8	-6.7		
10-107	2033	Silurian	Late Calcite	-0.9	-7.2		
10-110	2041	Silurian	Late Calcite	-12.7	-6.9		
10-113	2046	Silurian	Late Calcite	-14.6	-7.2		
10-096	BV6R	Silurian	Late Calcite	-25.4	-7.6		
10-108	BV6	Silurian	Late Calcite	-31.8	-9.5		
10-112	ADF-2	Silurian	Late Calcite	-3.1	-7.9		
10-307	3103	Ordovician	D1	1.3	-8.5		
10-302	3084-1	Ordovician	D1	0.5	-5.3		
10-304	3030	Ordovician	D1	0.6	-7.1		
10-308	3075-1	Ordovician	D1	0.6	-2.6		
10-306	3105	Ordovician	D1	0.6	-6.5		
11-084	3091	Ordovician	D1	0.1	-5.9		
11-085	3070	Ordovician	D1	0.7	-6.2		
11-086	3084	Ordovician	D1	0.3	-4.0		
11-088	3072	Ordovician	D1	-0.2	-8.6		
10-179	3061	Ordovician	D2a	-1.0	-8.0		
10-183	3134-1	Ordovician	D2a	-0.1	-11.2	0.70918	
10-184	3034-1	Ordovician	D2a	-0.4	-8.7	0.70906	
10-185	3046	Ordovician	D2a	-0.3	-8.8		
10-187	3122-1	Ordovician	D2a	-1.0	-11.5		

Lab ID	Sample ID	Age	Mineral	$\delta^{13}\text{C}\text{‰ VPDB}$	$\delta^{18}\text{O}\text{‰ VPDB}$	$^{87}\text{Sr}/^{86}\text{Sr}$	Reference
10-194	3130	Ordovician	D2a	0.6	-10.2		
10-196	3011-1	Ordovician	D2a	0.0	-10.2		
10-198	3128	Ordovician	D2a	0.0	-9.9		
10-200	3007	Ordovician	D2a	0.1	-10.3		
10-202	3161	Ordovician	D2a	0.5	-9.5	0.70840	
10-221	3153	Ordovician	D2a	0.0	-10.8		
10-222	3022-1	Ordovician	D2a	0.3	-9.7		
10-223	3141-1	Ordovician	D2a	0.1	-10.0		
10-225	3002-1	Ordovician	D2a	0.1	-10.2	0.70876	
10-230	3011-2	Ordovician	D2a	0.3	-9.5		
10-262	3157-1	Ordovician	D2a	0.0	-10.9		
10-263	3108	Ordovician	D2a	0.3	-8.3		
10-266	3025	Ordovician	D2a	0.8	-10.2		
10-268	3141-1	Ordovician	D2a	-0.1	-11.0		
10-271	3152	Ordovician	D2a	-0.4	-9.6		
10-273	3124-1	Ordovician	D2a	0.1	-9.6		
10-280	3129	Ordovician	D2a	0.3	-10.3		
10-285	3149-1	Ordovician	D2a	0.4	-10.7		
10-178	3106-1	Ordovician	D2b	-0.4	-9.5		
10-182	3111	Ordovician	D2b	0.1	-9.0		
10-193	3118-1	Ordovician	D2b	0.4	-9.3	0.70864	
10-195	3123-1	Ordovician	D2b	0.0	-9.9		
10-197	3006-1	Ordovician	D2b	0.2	-9.5		
10-201	3120-1	Ordovician	D2b	-0.3	-9.9		
10-218	3004-1	Ordovician	D2b	0.1	-9.5		
10-220	3131	Ordovician	D2b	0.3	-9.6		
10-224	3116	Ordovician	D2b	0.1	-10.1		
10-269	3014-1	Ordovician	D2b	0.2	-9.7		
10-278	3151	Ordovician	D2b	-0.5	-10.4		
10-146	3054	Ordovician	D2b	-0.1	-7.8	0.70830	
10-279	3016-1	Ordovician	D2b	0.2	-9.8		
		Ordovician	D2			0.708580	McNutt et al., 1987
		Ordovician	D2			0.708530	McNutt et al., 1987
		Ordovician	D2			0.708510	McNutt et al., 1987
		Ordovician	D2			0.708890	McNutt et al., 1987
		Ordovician	D2			0.708380	McNutt et al., 1987
10-175	3110	Ordovician	D3a	0.3	-8.3		
10-176	3038-1	Ordovician	D3a	0.2	-9.7		
10-188	3037-1	Ordovician	D3a	0.1	-7.9		
10-199	3136	Ordovician	D3a	-0.2	-10.8		

Lab ID	Sample ID	Age	Mineral	$\delta^{13}\text{C}\text{‰ VPDB}$	$\delta^{18}\text{O}\text{‰ VPDB}$	$^{87}\text{Sr}/^{86}\text{Sr}$	Reference
10-219	3029	Ordovician	D3a	0.3	-9.2		
10-228	3121	Ordovician	D3a	-0.9	-8.8		
10-229	3019	Ordovician	D3a	0.4	-9.1		
10-144	3127-1	Ordovician	D3a	-0.1	-10.1		
10-270	3020	Ordovician	D3a	0.1	-9.6	0.70842	
10-277	3135	Ordovician	D3a	-0.8	-11.8		
10-283	3140	Ordovician	D3a	-0.3	-10.5		
10-293	3103	Ordovician	D3a	1.4	-7.1		
10-177	3114	Ordovician	D3b	1.3	-10.3		
10-286	3141-2	Ordovician	D3b	-0.8	-11.8		
10-180	3123-2	Ordovician	D3b	0.3	-9.6		
10-181	3034-2	Ordovician	D3b	-0.5	-8.9	0.708726	
10-186	3011-3	Ordovician	D3b	0.2	-10.0		
10-189	3118-2	Ordovician	D3b	0.0	-9.9	0.708734	
10-190	3004-2	Ordovician	D3b	-0.2	-9.4		
10-191	3116-2	Ordovician	D3b	-0.1	-10.1		
10-192	3006-2	Ordovician	D3b	0.0	-9.4		
10-217	3122-2	Ordovician	D3b	0.1	-9.7		
10-226	3120-2	Ordovician	D3b	-0.2	-9.6		
10-227	3022-2	Ordovician	D3b	0.0	-10.5		
10-264	3002-2	Ordovician	D3b	0.0	-9.3	0.709074	
10-267	3016-2	Ordovician	D3b	0.1	-10.1		
10-272	3124-2	Ordovician	D3b	0.2	-9.3		
10-274	3149-2	Ordovician	D3b	-0.3	-9.9		
10-275	3014-2	Ordovician	D3b	-0.6	-10.6		
10-281	3154	Ordovician	D3b	-0.6	-10.6		
10-282	3131-2	Ordovician	D3b	-0.4	-11.0		
10-284	3157-2	Ordovician	D3b	-0.4	-9.7	0.709019	
10-145	3134-2	Ordovician	D3b	0.1	-10.6	0.708726	
10-276	3141-2	Ordovician	D3b	-0.4	-10.3		
10-261	3333	Ordovician	D3b	0.0	-9.1		
	87-69	Ordovician	D3	0.5	-10		Coniglio and Williams-Jones, 1992
	87-83A	Ordovician	D3	1.3	-9.9		Coniglio and Williams-Jones, 1992
	87-106	Ordovician	D3	-0.1	-9.2		Coniglio and Williams-Jones, 1992
	87-233BB	Ordovician	D3	0.5	-7.9		Coniglio and Williams-Jones, 1992
	87-233BB	Ordovician	D3	0.5	-8.1		Coniglio and Williams-Jones, 1992
	87-K-5B	Ordovician	D3	0.7	-8.3		Coniglio and Williams-Jones, 1992
	88-32A	Ordovician	D3	0.8	-9.4		Coniglio and Williams-Jones, 1992
	87-85	Ordovician	D3	1.3	-9.5		Coniglio and Williams-Jones, 1992
	89-17A	Ordovician	D3	-0.9	-8.8		Coniglio and Williams-Jones, 1992

Lab ID	Sample ID	Age	Mineral	$\delta^{13}\text{C}\text{‰ VPDB}$	$\delta^{18}\text{O}\text{‰ VPDB}$	$^{87}\text{Sr}/^{86}\text{Sr}$	Reference
	89-36B	Ordovician	D3	1.1	-9.6		Coniglio and Williams-Jones, 1992
		Ordovician	D3			0.70861	McNutt et al., 1987
		Ordovician	D3			0.71066	McNutt et al., 1987
		Ordovician	D3			0.71029	McNutt et al., 1987
10-156	3123-3	Ordovician	Late Calcite	0.0	-9.1		
10-157	3116-3	Ordovician	Late Calcite	0.4	-8.6		
10-158	3037-2	Ordovician	Late Calcite	-1.2	-11.5		
10-159	3126	Ordovician	Late Calcite	-0.9	-11.5		
10-216	3150-2	Ordovician	Late Calcite	-1.0	-10.7		
10-150	3014-3	Ordovician	Late Calcite	-1.0	-10.9		
10-151	3127-2	Ordovician	Late Calcite	-0.9	-10.5		
10-155	3002-3	Ordovician	Late Calcite	-0.9	-7.3		
	87-66	Ordovician	Late Calcite	-6.8	-8.0		Coniglio and Williams-Jones, 1992
	87-76	Ordovician	Late Calcite	-3.3	-8.6		Coniglio and Williams-Jones, 1992
	87-78	Ordovician	Late Calcite	1.6	-7.8		Coniglio and Williams-Jones, 1992
	88-10	Ordovician	Late Calcite	-2.5	-9.8		Coniglio and Williams-Jones, 1992
	89-5	Ordovician	Late Calcite	-0.1	-11.2		Coniglio and Williams-Jones, 1992
	89-7	Ordovician	Late Calcite	2.6	-9.4		Coniglio and Williams-Jones, 1992
	89-10	Ordovician	Late Calcite	-5.4	-9.3		Coniglio and Williams-Jones, 1992
	89-17B	Ordovician	Late Calcite	-4.3	-7.2		Coniglio and Williams-Jones, 1992
	89-21	Ordovician	Late Calcite	-13.1	-6.9		Coniglio and Williams-Jones, 1992
	89-25	Ordovician	Late Calcite	-31.2	-6.3		Coniglio and Williams-Jones, 1992
	89-36A	Ordovician	Late Calcite	-1.3	-8.3		Coniglio and Williams-Jones, 1992
	89-37	Ordovician	Late Calcite	-6.2	-8.2		Coniglio and Williams-Jones, 1992
	90-1	Ordovician	Late Calcite	-6.6	-6.4		Coniglio and Williams-Jones, 1992
		Ordovician	Late Calcite			0.70884	McNutt et al., 1987
		Ordovician	Late Calcite			0.70858	McNutt et al., 1987
		Ordovician	Late Calcite			0.70884	McNutt et al., 1987
		Ordovician	Late Calcite			0.70829	McNutt et al., 1987

Appendix 2

Appendix 2 Results of REE analysis of selected minerals from the Paleozoic succession of southwestern Ontario.

Sample ID	Age	Mineral	La (ppm)	Ce (ppm)	Pr (ppm)	Nd (ppm)	Sm (ppm)	Eu (ppm)	Gd (ppm)	Tb (ppm)	Dy (ppm)	Y (ppm)	Ho (ppm)	Er (ppm)	Tm (ppm)	Yb (ppm)	Lu (ppm)
1011	Devonian	D1	0.318	0.563	0.089	0.362	0.097	0.015	0.081	0.013	0.086		0.015	0.036	0.006	0.038	0.004
1016-1	Devonian	D1	0.156	0.206	0.029	0.141	0.025	0.006	0.038	0.003	0.031		0.005	0.014	0.004	0.014	0.001
1023	Devonian	D1	0.385	0.467	0.065	0.288	0.076	0.015	0.091	0.012	0.087		0.018	0.065	0.009	0.058	0.005
MG-026	Devonian	D1	0.642	1.014	0.155	0.687	0.162	0.042	0.207	0.027	0.149		0.030	0.099	0.014	0.097	0.009
AM-030	Devonian	D1	1.210	1.883	0.273	1.096	0.209	0.040	0.211	0.032	0.163		0.030	0.083	0.012	0.093	0.009
1018	Devonian	D1	1.221	1.302	0.216	0.996	0.182	0.053	0.286	0.034	0.229		0.052	0.153	0.018	0.115	0.015
1012-1	Devonian	D1	0.077	0.129	0.018	0.077	0.015	0.000	0.026	0.001	0.011		0.003	0.011	0.001	0.011	0.002
MG-035-2	Devonian	D2	0.345	0.446	0.062	0.268	0.068	0.014	0.113	0.015	0.085		0.022	0.072	0.007	0.053	0.008
1004	Devonian	D2	0.437	0.614	0.103	0.443	0.108	0.018	0.102	0.013	0.099		0.019	0.056	0.008	0.051	0.007
1029	Devonian	D2	4.651	4.172	0.868	3.936	0.781	0.211	1.084	0.174	1.098		0.223	0.622	0.076	0.424	0.050
1056	Devonian	D2	1.048	1.661	0.241	0.918	0.190	0.033	0.197	0.020	0.125		0.027	0.082	0.009	0.062	0.009
SM-1	Devonian	Late calcite	1.575	1.291	0.245	1.045	0.197	0.048	0.234	0.031	0.188		0.042	0.125	0.016	0.109	0.014
AM002	Devonian	Late calcite	13.031	15.519	2.183	8.828	1.532	0.355	1.884	0.254	1.281		0.234	0.575	0.068	0.463	0.067
AM014	Devonian	Late calcite	5.621	6.432	0.774	2.871	0.451	0.104	0.489	0.071	0.391		0.093	0.303	0.039	0.293	0.052
1025-1	Devonian	Late calcite	3.816	3.585	0.611	2.509	0.443	0.113	0.630	0.084	0.533		0.117	0.310	0.038	0.202	0.032
1026-1	Devonian	Late calcite	3.163	3.295	0.625	2.622	0.510	0.129	0.608	0.099	0.577		0.122	0.366	0.043	0.250	0.034
1016-2	Devonian	Late calcite	0.448	0.653	0.106	0.467	0.091	0.026	0.117	0.017	0.133		0.030	0.089	0.012	0.086	0.011
2008	Silurian	D1	1.190	1.750	0.193	0.870	0.130	0.040	0.180	0.022	0.090	0.670	0.020	0.070	X	0.070	0.020
2015	Silurian	D1	1.160	2.530	0.321	1.360	0.410	0.080	0.230	0.021	0.130	1.100	0.050	0.160	X	0.060	0.008
2114	Silurian	D1	3.200	6.500	0.856	3.640	0.820	0.130	0.880	0.130	0.700	3.760	0.130	0.310	0.040	0.230	0.042
2124-1	Silurian	D1	0.770	2.600	0.204	0.790	0.070	X	0.270	0.053	0.050	0.620	0.030	0.080	X	0.020	0.007
2130	Silurian	D1	0.520	1.040	0.114	0.500	0.070	0.030	0.160	0.018	X	0.630	0.010	0.080	X	0.060	0.015
2001-1	Silurian	D2a	1.770	3.580	0.477	1.850	0.480	0.020	0.490	0.065	0.090	2.020	0.030	0.130	X	0.080	0.094
2012-1	Silurian	D2a	0.600	1.010	0.099	0.450	0.070	0.010	0.140	0.005	X	0.410	0.020	0.070	X	X	0.015
2025 A	Silurian	D2a	1.060	1.940	0.258	0.970	0.200	0.010	0.290	0.060	X	0.970	0.020	X	X	X	0.007
2036	Silurian	D2a	0.490	0.960	0.107	0.450	0.070	0.010	0.110	0.008	0.020	0.430	X	0.020	X	0.010	0.007
2043	Silurian	D2a	0.780	1.080	0.120	0.490	0.140	0.020	0.160	0.014	0.080	1.140	0.030	0.060	X	0.070	0.018
2054-1	Silurian	D2a	0.900	1.610	0.184	0.630	0.150	0.030	0.190	0.014	0.020	0.570	0.020	0.020	X	0.090	X
2056	Silurian	D2a	0.120	0.190	0.029	0.110	0.020	X	0.030	X	X	0.180	X	0.010	X	0.010	X
2079-1	Silurian	D2a	0.560	0.840	0.083	0.350	0.110	X	0.100	0.014	0.020	0.740	X	0.040	X	0.080	0.007
2085	Silurian	D2a	0.590	1.220	0.127	0.490	0.110	X	0.120	0.013	0.040	0.480	0.020	0.040	X	0.020	X
2087-1	Silurian	D2a	0.530	0.890	0.098	0.420	0.070	X	0.070	0.009	0.010	0.400	0.010	0.040	X	0.050	X
2088	Silurian	D2a	0.490	0.780	0.093	0.430	0.090	X	0.090	0.006	0.040	0.690	X	0.030	X	0.060	0.021
2089-1	Silurian	D2a	0.830	1.510	0.169	0.550	0.150	0.030	0.130	0.017	0.080	0.580	0.010	0.040	X	X	0.011
2094	Silurian	D2a	0.910	1.250	0.119	0.530	0.070	0.020	0.150	0.016	0.030	0.530	0.020	0.050	X	0.040	0.007

Sample ID	Age	Mineral	La (ppm)	Ce (ppm)	Pr (ppm)	Nd (ppm)	Sm (ppm)	Eu (ppm)	Gd (ppm)	Tb (ppm)	Dy (ppm)	Y (ppm)	Ho (ppm)	Er (ppm)	Tm (ppm)	Yb (ppm)	Lu (ppm)
2095	Silurian	D2a	0.470	0.770	0.080	0.380	0.080	X	0.080	0.015	0.050	0.350	0.020	0.040	X	0.030	X
2099	Silurian	D2a	1.350	2.030	0.247	0.950	0.200	0.020	0.280	0.038	X	1.610	0.030	0.130	X	0.180	0.017
2112-1	Silurian	D2a	4.520	5.260	0.776	3.260	0.640	0.180	1.020	0.139	0.730	4.810	0.160	0.400	0.050	0.330	0.052
2116	Silurian	D2a	0.710	1.090	0.145	0.560	0.170	0.030	0.130	0.026	0.100	0.880	0.030	0.090	X	0.030	0.014
ADF-1	Silurian	D2a	0.620	1.180	0.156	0.620	0.060	X	0.110	0.022	X	0.450	0.020	0.010	X	0.040	0.014
BV-4	Silurian	D2a	5.060	7.530	1.141	4.740	1.070	0.250	1.180	0.184	1.010	7.660	0.220	0.560	0.070	0.450	0.064
BV-6-1	Silurian	D2a	1.710	1.910	0.282	1.240	0.260	0.060	0.350	0.058	0.400	3.640	0.080	0.260	0.030	0.220	0.026
BV-7-2-1	Silurian	D2a	2.470	2.490	0.427	1.690	0.420	0.100	0.530	0.086	0.480	3.740	0.110	0.320	0.030	0.260	0.043
2124-2	Silurian	D3	5.090	19.820	3.207	13.720	2.570	0.480	1.730	0.265	0.980	4.650	0.180	0.510	0.030	0.470	0.050
2126-1	Silurian	D3	1.250	2.890	0.330	1.470	0.250	0.080	0.410	0.070	0.180	1.140	0.060	0.180	X	0.100	0.014
BV-7-2-2	Silurian	D3	2.810	4.250	0.603	2.390	0.530	0.140	0.760	0.095	0.470	3.930	0.110	0.270	0.040	0.270	0.035
2110A-3	Silurian	D3	6.160	10.320	1.346	5.310	0.900	0.200	0.790	0.151	0.660	4.350	0.150	0.340	0.040	0.410	0.047
2032-2	Silurian	Late Calcite	0.760	1.220	0.204	0.900	0.100	X	0.340	0.042	0.100	2.740	0.040	0.170	X	0.100	X
2033	Silurian	Late Calcite	0.380	0.590	0.108	0.460	0.100	0.020	0.190	0.029	0.160	1.840	0.040	0.100	X	0.080	0.016
2079-4	Silurian	Late Calcite	0.340	0.670	0.085	0.390	0.020	0.020	0.150	0.018	0.100	1.560	0.030	0.100	X	0.080	0.019
ADF-2	Silurian	Late Calcite	4.320	10.310	1.204	4.540	0.600	0.130	0.710	0.101	0.490	4.030	0.100	0.310	0.030	0.260	0.051
BV6	Silurian	Late Calcite	0.430	0.590	0.069	0.300	0.080	X	0.070	0.010	0.050	0.510	0.010	0.040	X	0.060	0.008
3002-1	Ordovician	D2	10.190	22.120	2.909	13.020	2.940	0.550	3.660	0.592	3.660	18.220	0.790	2.450	0.250	1.880	0.283
3006-1	Ordovician	D2	93.080	179.790	22.070	97.310	22.620	4.030	29.940	4.034	17.670	106.210	3.210	7.430	0.850	4.140	0.551
3014-1	Ordovician	D2	69.170	133.230	15.516	67.120	16.160	2.970	24.630	3.400	17.620	109.310	3.180	7.480	0.810	3.660	0.549
3020	Ordovician	D2	5.880	10.710	1.344	6.170	1.590	0.330	2.040	0.309	1.870	12.210	0.390	1.010	0.120	0.840	0.129
3025	Ordovician	D2	2.120	3.900	0.621	2.920	0.720	0.160	0.800	0.114	0.660	5.040	0.140	0.350	0.040	0.300	0.042
3034-1	Ordovician	D2	5.630	6.060	0.881	3.660	0.690	0.140	0.900	0.128	0.710	5.620	0.160	0.490	0.060	0.380	0.055
3046-1	Ordovician	D2	5.630	6.900	1.065	4.700	0.850	0.200	1.080	0.157	0.900	6.550	0.190	0.530	0.050	0.410	0.061
3054	Ordovician	D2	3.310	3.760	0.618	2.620	0.570	0.160	0.830	0.135	0.580	4.800	0.140	0.380	0.040	0.320	0.063
3061	Ordovician	D2	9.140	11.730	1.601	6.720	1.000	0.230	1.930	0.242	1.020	10.370	0.300	0.770	0.060	0.570	0.106
3106-1	Ordovician	D2	27.680	44.380	7.171	34.480	7.820	1.650	8.280	1.072	5.690	41.790	1.030	2.440	0.260	1.400	0.152
3108	Ordovician	D2	2.570	3.050	0.375	1.690	0.350	0.070	0.580	0.074	0.440	3.630	0.090	0.260	0.030	0.200	0.024
3114	Ordovician	D2	24.900	53.580	7.172	31.880	8.650	1.420	9.600	1.513	7.870	40.390	1.510	3.980	0.540	3.400	0.440
3116-1	Ordovician	D2	27.370	68.480	9.688	43.180	13.670	2.160	18.340	3.373	20.070	79.560	3.690	9.960	1.320	9.270	1.353
3116-3	Ordovician	D2	12.750	34.130	5.186	24.300	8.770	1.790	11.810	2.156	11.780	41.210	1.950	5.330	0.740	5.550	0.781
3124-1	Ordovician	D2	29.950	66.230	9.088	41.040	11.270	1.820	12.290	1.955	10.130	49.260	1.910	5.060	0.660	4.060	0.529
3127-1	Ordovician	D2	64.290	144.850	19.497	85.620	23.090	3.720	26.630	4.286	22.200	95.150	3.970	10.420	1.480	9.650	1.294
3129	Ordovician	D2	18.000	33.500	4.432	19.780	4.710	0.740	5.960	0.757	3.910	25.150	0.710	1.730	0.170	0.850	0.124
3134-1	Ordovician	D2	48.870	114.110	15.442	69.130	19.020	2.820	21.780	3.484	20.130	98.510	3.930	11.530	1.370	8.050	1.126
3140	Ordovician	D2	47.370	118.060	15.933	69.460	19.560	3.130	24.000	3.951	21.170	88.450	3.960	10.440	1.470	10.170	1.485
3149-1	Ordovician	D2	10.990	20.910	2.500	10.780	2.250	0.370	2.540	0.319	1.690	14.270	0.330	0.830	0.080	0.480	0.071
3152	Ordovician	D2	35.410	101.880	15.466	70.270	21.810	3.740	23.220	4.384	25.600	108.180	5.100	14.700	2.230	15.280	1.985
3157-1	Ordovician	D2	28.370	69.430	9.876	45.580	13.910	2.230	12.770	1.819	7.500	29.150	1.250	3.060	0.380	2.540	0.339

Sample ID	Age	Mineral	La (ppm)	Ce (ppm)	Pr (ppm)	Nd (ppm)	Sm (ppm)	Eu (ppm)	Gd (ppm)	Tb (ppm)	Dy (ppm)	Y (ppm)	Ho (ppm)	Er (ppm)	Tm (ppm)	Yb (ppm)	Lu (ppm)
3161	Ordovician	D2	6.860	11.760	1.529	6.500	1.560	0.290	1.790	0.237	1.150	9.640	0.220	0.580	0.070	0.390	0.049
3118-1	Ordovician	D2	23.340	54.690	7.360	33.410	8.940	1.670	10.970	1.796	8.470	41.690	1.550	3.860	0.430	3.220	0.454
3002-2	Ordovician	D3	31.500	68.900	8.864	35.460	8.680	1.500	11.490	1.677	9.050	42.390	1.780	4.640	0.490	2.920	0.409
3006-2	Ordovician	D3	68.180	153.260	19.902	88.270	21.410	3.550	21.810	2.928	15.290	85.450	2.640	6.460	0.760	4.230	0.542
3014-2	Ordovician	D3	68.220	143.680	19.335	84.690	21.030	3.380	23.780	2.929	13.500	59.830	2.160	5.050	0.620	3.700	0.583
3034-2	Ordovician	D3	6.720	7.840	0.952	5.100	0.800	X	1.910	0.128	0.470	8.010	0.170	0.730	X	0.580	0.043
3038-1	Ordovician	D3	1.430	1.540	0.215	0.880	0.070	X	0.300	0.051	0.110	1.790	0.040	0.140	X	0.120	0.013
3106-2	Ordovician	D3	23.770	53.040	6.646	27.180	6.220	1.130	7.560	1.147	5.910	25.010	1.090	2.870	0.360	2.240	0.310
3124-2	Ordovician	D3	19.520	35.740	4.336	18.710	4.360	0.710	4.980	0.738	3.520	18.230	0.630	1.530	0.200	1.190	0.155
3134-2	Ordovician	D3	86.210	186.060	24.037	103.120	24.620	3.730	27.510	3.887	19.730	76.780	3.320	8.100	0.940	5.880	0.809
3149-2	Ordovician	D3	60.680	139.370	18.522	76.580	19.090	3.010	23.970	3.494	17.920	78.600	3.250	8.510	1.070	7.590	1.140
3118-2	Ordovician	D3	147.810	326.750	43.947	194.710	49.570	7.070	44.190	6.279	29.070	112.600	4.770	11.670	1.610	9.980	1.301
3002-3	Ordovician	Late Calcite	21.400	50.920	7.016	29.590	9.460	1.840	11.490	1.895	9.710	61.650	1.820	4.730	0.620	4.360	0.606
3014-3	Ordovician	Late Calcite	75.120	183.040	25.548	115.740	37.050	7.170	57.450	8.466	39.320	166.750	5.990	12.860	1.400	8.740	1.166
3123-3	Ordovician	Late Calcite	37.270	109.620	15.281	63.790	18.840	3.370	18.710	3.531	21.920	86.060	4.020	11.370	1.710	12.380	1.640
3127-2	Ordovician	Late Calcite	44.730	97.790	12.625	52.010	12.940	2.040	14.810	2.371	13.050	53.510	2.320	6.020	0.840	5.590	0.845
3150-2	Ordovician	Late Calcite	43.660	96.500	12.029	47.020	10.340	1.600	10.650	1.435	7.960	56.480	1.550	3.960	0.510	3.110	0.440
3126	Ordovician	Late Calcite	212.280	422.990	52.696	230.520	53.310	8.290	60.180	8.983	47.510	209.240	8.470	20.920	2.320	12.690	1.722
3026	Ordovician	WR	2.260	2.700	0.409	1.640	0.320	0.080	0.350	0.057	0.340	3.100	0.080	0.230	0.030	0.210	0.028
3032	Ordovician	WR	1.980	4.030	0.517	2.090	0.400	0.090	0.400	0.053	0.360	2.680	0.070	0.230	0.020	0.190	0.029
3063	Ordovician	WR	5.400	7.970	1.248	5.320	1.040	0.260	1.150	0.166	0.850	6.510	0.180	0.510	0.060	0.480	0.059
3070	Ordovician	WR	1.430	2.370	0.315	1.250	0.250	0.060	0.270	0.047	0.220	1.840	0.050	0.160	0.020	0.130	0.027
3076	Ordovician	WR	3.650	6.060	0.866	3.660	0.760	0.160	0.760	0.121	0.670	4.970	0.150	0.390	0.050	0.370	0.052
3082	Ordovician	WR	3.530	7.530	0.955	3.810	0.720	0.140	0.710	0.092	0.530	3.760	0.110	0.320	0.040	0.250	0.039
3091	Ordovician	WR	3.340	6.320	0.849	3.480	0.690	0.150	0.740	0.102	0.550	4.210	0.120	0.310	0.030	0.260	0.042
3096	Ordovician	WR	2.010	4.880	0.621	2.550	0.500	0.100	0.460	0.064	0.250	1.500	0.050	0.140	0.020	0.170	0.024
3100	Ordovician	WR	1.300	2.580	0.258	1.200	0.180	0.040	0.200	0.037	0.130	0.860	0.030	0.080	X	0.110	0.016
PN-1	Ordovician	WR	3.160	7.770	0.951	3.710	0.740	0.190	0.700	0.094	0.440	2.280	0.080	0.220	0.030	0.180	0.034
PN015	Ordovician	WR	3.320	8.300	1.019	4.480	0.820	0.170	0.650	0.098	0.540	3.290	0.110	0.320	0.030	0.250	0.033

Appendix 3

Appendix 3 Results of fluid inclusions microthermometry of selected minerals from the Paleozoic carbonate succession of southwestern Ontario.

Sample ID	Age	Mineral	Th °C	Tm °C	Salinity	Reference
AMFI-1	Devonian	Calcite	143.7	-17.7	20.2	
	Devonian	Calcite	102.1			
	Devonian	Calcite	156.7	-15.1	18.5	
	Devonian	Calcite	123.4	-16.8	19.6	
	Devonian	Calcite	120.8	-16.2	19.2	
	Devonian	Calcite	157.7	-17.1	19.8	
	Devonian	Calcite	147.2	-15.7	18.9	
	Devonian	Calcite	133.2	-15.1	18.5	
	Devonian	Calcite	127.2	-16.1	19.2	
MGFI-3	Devonian	Calcite	87.1	-17.9	20.3	
	Devonian	Calcite	104.5	-19.3	21.1	
	Devonian	Calcite	128.7	-18.6	20.7	
	Devonian	Calcite	101.7	-17.4	20.0	
	Devonian	Calcite	135.6	-16.7	19.5	
	Devonian	Calcite	91.9	-17.2	19.9	
	Devonian	Calcite	171.9	-19.1	21.0	
	Devonian	Calcite	107.9	-16.9	19.7	
D1-1	Devonian	Celestine	144.2	-16.1	19.2	
	Devonian	Celestine	137.6	-15.9	19.0	
	Devonian	Celestine	121.2	-15.4	18.7	
	Devonian	Celestine		-15.8	19.0	
	Devonian	Celestine	170.8	-10.9	15.0	
	Devonian	Celestine		-6.1	9.7	
	Devonian	Celestine	201.9	-7.5	11.5	
	Devonian	Celestine		-10.4	14.6	
	Devonian	Celestine	197.7	-7.6	11.6	
	Devonian	Celestine	199.2	-7.5	11.5	
	Devonian	Celestine		-10.9	15.0	
	Devonian	Celestine		-16.1	19.2	
	Devonian	Celestine	183.8	-8.2	12.3	
	Devonian	Celestine	174.4	-8.9	13.0	
	Devonian	Celestine	181.8	-8.4	12.5	
	Devonian	Celestine	185.4	-8.9	13.0	
	Devonian	Celestine	219.6	-8.6	12.7	
	Devonian	Celestine		-13.3	17.1	
Devonian	Celestine		-10.6	14.8		
D1-5	Devonian	Celestine	189.8	-8.8	12.9	
	Devonian	Celestine	202.7	-9.1	13.3	
	Devonian	Celestine		-7.8	11.8	
	Devonian	Celestine	187.4	-8.1	12.2	
	Devonian	Celestine	249.8	-7.8	11.8	
	Devonian	Celestine	224.5	-9.2	13.4	
	Devonian	Celestine	216.5	-10.9	15.0	
	Devonian	Celestine	236.6	-8.4	12.5	
	Devonian	Celestine		-12	16.0	
	Devonian	Celestine	198.2	-13.8	17.5	
	Devonian	Celestine	201.4	-8.4	12.5	
	Devonian	Celestine	269.9	-10.8	15.0	
	Devonian	Celestine	223.2	-10.1	14.3	
	Devonian	Celestine	287.7			
	Devonian	Celestine		-8	12.0	

Sample ID	Age	Mineral	Th °C	Tm °C	Salinity	Reference
D1-8	Devonian	Celestine	265.2	-8.9	13.0	
	Devonian	Celestine	291.2	-10.9	15.0	
	Devonian	Celestine	225.1			
	Devonian	Celestine	300.5	-8.9	13.0	
	Devonian	Celestine	297.6	-8.9	13.0	
	Devonian	Celestine	243	-9.1	13.3	
	Devonian	Celestine	252.9	-9.5	13.7	
	Devonian	Celestine	261.7	-8.7	12.8	
	Devonian	Celestine	215.9	-10.1	14.3	
	Devonian	Celestine	130.9	-9.8	14.0	
	Devonian	Celestine	118.2	-8.8	12.9	
	Devonian	Celestine	183.3	-10.9	15.0	
	Devonian	Celestine	179.6	-12.1	16.1	
D2-2	Devonian	Celestine	154.6	-9.7	13.9	
	Devonian	Celestine	215.3	-10.9	15.0	
	Devonian	Celestine	189.4	-10.6	14.8	
	Devonian	Celestine	241.4	-10.8	15.0	
	Devonian	Celestine	251.9	-9.5	13.7	
	Devonian	Celestine	265.4	-8.7	12.8	
	Devonian	Celestine		-13.3	17.1	
	Devonian	Celestine	279.2	-9.9	14.1	
	Devonian	Celestine	277.9	-11.6	15.7	
	Devonian	Celestine	255.7	-9.6	13.8	
	Devonian	Celestine	153.1	-9.8	14.0	
	Devonian	Celestine	215.3	-10.6	14.8	
	Devonian	Celestine	162.7	-10.3	14.5	
	Devonian	Celestine		-10.8	15.0	
	Devonian	Celestine		-10.5	14.7	
	Devonian	Celestine		-10.7	14.9	
	Devonian	Celestine		-12.7	16.6	
	Devonian	Celestine	291.2	-11.6	15.7	
	Devonian	Celestine	321.8	-12.1	16.1	
	Devonian	Celestine	247.1	-10.4	14.6	
	Devonian	Celestine		-9.7	13.9	
	Devonian	Celestine	278.1	-9.5	13.7	
	Devonian	Celestine	226.3	-11	15.1	
Devonian	Celestine	283.4	-9.7	13.9		
D2-4	Devonian	Celestine	288.2	-10.2	14.4	
	Devonian	Celestine		-12.5	16.5	
	Devonian	Celestine		-12.2	16.2	
	Devonian	Celestine	129.7	-9	13.1	
	Devonian	Celestine	132.3	-9.2	13.4	
	Devonian	Celestine	156.4	-9.4	13.6	
	Devonian	Celestine	177	-9.9	14.1	
	Devonian	Celestine	199.7	-10.9	15.0	
	Devonian	Celestine	194.2	-10.2	14.4	
	Devonian	Celestine	315	-11.3	15.4	
	Devonian	Celestine		-9.7	13.9	
	Devonian	Celestine	277.7	-11.9	16.0	
	Devonian	Celestine		-13.8	17.5	
Devonian	Celestine		-8.9	13.0		
Silurian	Matrix dolomite	67	-10.8	15.0	Zheng, 1999	
Silurian	Matrix dolomite	74.3	-12.3	16.3	Zheng, 1999	
Silurian	Matrix dolomite	70.5	-9.9	14.1	Zheng, 1999	
Silurian	Matrix dolomite	74.8	-11.5	15.6	Zheng, 1999	

Sample ID	Age	Mineral	Th °C	Tm °C	Salinity	Reference
	Silurian	Matrix dolomite	64.5	-11.7	15.8	Zheng, 1999
	Silurian	Matrix dolomite	73.4	-13.5	17.3	Zheng, 1999
	Silurian	Matrix dolomite	95.8	-24.7	23.6	Zheng, 1999
	Silurian	Matrix dolomite	108.2	-27.8	24.7	Zheng, 1999
	Silurian	Matrix dolomite	102	-28.7	25.1	Zheng, 1999
	Silurian	Matrix dolomite	109.3	-31.2	25.9	Zheng, 1999
	Silurian	Matrix dolomite	99.6	-27.9	24.8	Zheng, 1999
	Silurian	Matrix dolomite	116.7	-30.7	25.7	Zheng, 1999
W-12	Silurian	D2	108.3			
	Silurian	D2	106			
	Silurian	D2	95.8			
	Silurian	D2	111.1			
	Silurian	D2	107.7			
	Silurian	D2	108.4			
	Silurian	D2	102.6			
W-47	Silurian	D2	116.8			
	Silurian	D2	106.7			
	Silurian	D2	115			
	Silurian	D2	132.2			
W-88	Silurian	D2	102.9			
	Silurian	D2	90.3			
	Silurian	D2	92			
	Silurian	D2	107.2			
	Silurian	D2	116.8			
W-51	Silurian	D2	140	-20	20.6	
W-51	Silurian	D2	95			
W-51	Silurian	D2	140			
W-51	Silurian	D2	140			
W-51	Silurian	D2	118			
W-51	Silurian	D2	118			
W-51	Silurian	D2		-23.5	22.2	
W-51	Silurian	D2	110			
W-51	Silurian	D2	107			
W-51	Silurian	D2	78.3			
W-51	Silurian	D2	133			
W-57	Silurian	D2				
W-60	Silurian	D2	117			
W-60	Silurian	D2	111			
W-60	Silurian	D2	89.8			
W-60	Silurian	D2	88.4			
W-60	Silurian	D2	86.3			
W-60	Silurian	D2	117			
	Silurian	Saddle dolomite	98.7	-29.2	25.2	Zheng, 1999
	Silurian	Saddle dolomite	126.4	-32.4	26.3	Zheng, 1999
	Silurian	Saddle dolomite	105.6	-27.6	24.7	Zheng, 1999
	Silurian	Saddle dolomite	128.2	-30.5	25.7	Zheng, 1999
SD-01	Silurian	D3	98.5			
	Silurian	D3	104.6			
SD-02	Silurian	D3	91.5			
	Silurian	D3	96.5			
	Silurian	D3	106.3			
	Silurian	D3	107.4			
SD-03	Silurian	D3	99.6			
	Silurian	D3	122.8			
	Silurian	D3	123.2			
FL-01	Silurian	Fluorite	93.1	-31.3	25.9	

Sample ID	Age	Mineral	Th °C	Tm °C	Salinity	Reference
	Silurian	Fluorite	98.6	-30.7	25.7	
	Silurian	Fluorite	107	-30.9	25.8	
	Silurian	Fluorite	108	-31.6	26.0	
	Silurian	Fluorite	108.4	-31.1	25.8	
	Silurian	Fluorite	108.6	-32.9	26.4	
	Silurian	Fluorite	108.9	-32.3	26.2	
	Silurian	Fluorite	109.3	-32.1	26.2	
	Silurian	Fluorite	109.6	-31.7	26.0	
	Silurian	Fluorite	110.1	-31.4	25.9	
	Silurian	Fluorite	110.8	-31.2	25.9	
	Silurian	Fluorite	111.4	-31.6	26.0	
	Silurian	Fluorite	112.1	-31.5	26.0	
	Silurian	Fluorite	112.6	-31	25.8	
	Silurian	Fluorite	112.8	-33.4	26.6	
	Silurian	Fluorite	113.4	-33	26.4	
	Silurian	Fluorite	113.9	-31.9	26.1	
	Silurian	Fluorite	114.3	-31.4	25.9	
	Silurian	Fluorite	114.9	-31.2	25.9	
	Silurian	Fluorite	115.8	-31.1	25.8	
FL-04	Silurian	Fluorite	99.4	-33.2	26.5	
	Silurian	Fluorite	98.6	-33.1	26.5	
	Silurian	Fluorite	102.1	-33.1	26.5	
	Silurian	Fluorite	102.6	-33	26.4	
	Silurian	Fluorite	104.6	-32.9	26.4	
	Silurian	Fluorite	106.6	-32.8	26.4	
	Silurian	Fluorite	106.9	-32.8	26.4	
	Silurian	Fluorite	107.3	-32.6	26.3	
	Silurian	Fluorite	107.8	-32.5	26.3	
	Silurian	Fluorite	108.1	-32.2	26.2	
	Silurian	Fluorite	108.7	-32.1	26.2	
	Silurian	Fluorite	110.7	-31.9	26.1	
	Silurian	Fluorite	111.5	-31.7	26.0	
	Silurian	Fluorite	112.4	-31.6	26.0	
	Silurian	Fluorite	112.8	-31.5	26.0	
	Silurian	Fluorite	113.5	-31.2	25.9	
	Silurian	Fluorite	113.9	-31.1	25.8	
	Silurian	Fluorite	114.3	-30.9	25.8	
	Silurian	Fluorite	114.6	-30.6	25.7	
	Silurian	Fluorite	115	-27.8	24.7	
FL-05	Silurian	Fluorite	96.5	-30.1	25.5	
	Silurian	Fluorite	97	-30.6	25.7	
	Silurian	Fluorite	97.7	-31.1	25.8	
	Silurian	Fluorite	98.5	-31.2	25.9	
	Silurian	Fluorite	99.7	-32.3	26.2	
	Silurian	Fluorite	100.6	-35.4	27.1	
	Silurian	Fluorite	101.2	-31.6	26.0	
	Silurian	Fluorite	102.7	-26.9	24.4	
	Silurian	Fluorite	103.1	-26.1	24.1	
	Silurian	Fluorite	104.8	-31.4	25.9	
	Silurian	Fluorite	105.1	-26.6	24.3	
	Silurian	Fluorite	106.3	-31.3	25.9	
	Silurian	Fluorite	108.1	-33	26.4	
	Silurian	Fluorite	110.8	-26.5	24.3	
	Silurian	Fluorite	112.3	-31.7	26.0	
	Silurian	Fluorite	113.7	-31.4	25.9	
FL-07	Silurian	Fluorite	112.1	-31.9	26.1	

Sample ID	Age	Mineral	Th °C	Tm °C	Salinity	Reference
FL-10	Silurian	Fluorite	113.6	-31.7	26.0	
	Silurian	Fluorite	114.4	-31.6	26.0	
	Silurian	Fluorite	114.9	-30.8	25.8	
	Silurian	Fluorite	115.8	-31.4	25.9	
	Silurian	Fluorite	116.5	-31.2	25.9	
	Silurian	Fluorite	117.4	-30.5	25.7	
	Silurian	Fluorite	117.9	-30.2	25.6	
	Silurian	Fluorite	118.1	-27.8	24.7	
	Silurian	Fluorite	98.6	-32.6	26.3	
	Silurian	Fluorite	101.4	-32.5	26.3	
	Silurian	Fluorite	102.3	-32.4	26.3	
	Silurian	Fluorite	104.7	-32.3	26.2	
	Silurian	Fluorite	109.8	-32.1	26.2	
	Silurian	Fluorite	111.8	-31.9	26.1	
	Silurian	Fluorite	112.7	-31.7	26.0	
	Silurian	Fluorite	113.1	-31.2	25.9	
Silurian	Fluorite	113.8	-26.8	24.4		
Silurian	Fluorite	118.3	-30.1	25.5		
SP-01	Silurian	Sphalerite	61.6	-25.4	23.9	
	Silurian	Sphalerite	63.4	-24.1	23.3	
	Silurian	Sphalerite	68.4	-23.9	23.3	
	Silurian	Sphalerite	69.3	-23.7	23.2	
	Silurian	Sphalerite	72.1	-23.5	23.1	
	Silurian	Sphalerite	74.4	-22.1	22.5	
	Silurian	Sphalerite	75.6	-21.6	22.2	
	Silurian	Sphalerite	82.6	-23.4	23.0	
	Silurian	Sphalerite	85.3	-22.1	22.5	
	Silurian	Sphalerite	86.7	-21.4	22.1	
SP-02	Silurian	Sphalerite	87.3	-20.5	21.7	
	Silurian	Sphalerite	64.7	-24.2	23.4	
	Silurian	Sphalerite	64.9	-22.9	22.8	
	Silurian	Sphalerite	65.6	-22.4	22.6	
	Silurian	Sphalerite	66.8	-24.2	23.4	
	Silurian	Sphalerite	67.4	-24.1	23.3	
	Silurian	Sphalerite	69.9	-23.9	23.3	
	Silurian	Sphalerite	73	-23.5	23.1	
	Silurian	Sphalerite	76.1	-23.1	22.9	
	Silurian	Sphalerite	76.4	-23.7	23.2	
SP-03	Silurian	Sphalerite	78.2	-22.8	22.8	
	Silurian	Sphalerite	68.1	-22.5	22.6	
	Silurian	Sphalerite	77.1	-24.3	23.4	
	Silurian	Sphalerite	79.9	-23.1	22.9	
SP-05	Silurian	Sphalerite	82.1	-23.5	23.1	
	Silurian	Sphalerite	64.5	-23.9	23.3	
	Silurian	Sphalerite	64.7	-23.7	23.2	
	Silurian	Sphalerite	67.5	-23.3	23.0	
	Silurian	Sphalerite	68.3	-22.8	22.8	
	Silurian	Sphalerite	69.9	-22.1	22.5	
	Silurian	Sphalerite	70.9	-23	22.9	
	Silurian	Sphalerite	72.3	-24.8	23.6	
	Silurian	Sphalerite	73.1	-24.5	23.5	
	Silurian	Sphalerite	78.6	-24.1	23.3	
SP-06	Silurian	Sphalerite	79.8	-23.8	23.2	
	Silurian	Sphalerite	84.3	-22.7	22.7	
	Silurian	Sphalerite	62.3	-23.9	23.3	
	Silurian	Sphalerite	63.4	-24	23.3	

Sample ID	Age	Mineral	Th °C	Tm °C	Salinity	Reference
SP-07	Silurian	Sphalerite	68	-23.5	23.1	
	Silurian	Sphalerite	68.2	-24.4	23.5	
	Silurian	Sphalerite	74.8	-26.1	24.1	
	Silurian	Sphalerite	79.7	-25	23.7	
	Silurian	Sphalerite	84.3	-24.8	23.6	
	Silurian	Sphalerite	89.5	-23.8	23.2	
SP-08	Silurian	Sphalerite	96.3	-23.1	22.9	
	Silurian	Sphalerite	70.6	-25.8	24.0	
	Silurian	Sphalerite	73.6	-25.6	23.9	
	Silurian	Sphalerite	77.3	-24.5	23.5	
	Silurian	Sphalerite	81.5	-24.8	23.6	
	Silurian	Sphalerite	87.5	-25.1	23.7	
3125	Silurian	Sphalerite	91.2	-25.2	23.8	
	Silurian	Sphalerite	93.9	-24.7	23.6	
	Silurian	Sphalerite	94.2	-24.5	23.5	
	Ordovician	D2	68.5			
	Ordovician	D2	77.8			
	Ordovician	D2	79.1			
	Ordovician	D2	95.4			
	Ordovician	D2	81.6			
	Ordovician	D2	76.9			
	Ordovician	D2	84.8			
	Ordovician	D2	76.1			
	Ordovician	D2	89.6			
3023	Ordovician	D2	67.6			
	Ordovician	D2	71.9			
	Ordovician	D2	91.7			
	Ordovician	D2	90.2			
	Ordovician	D2	93.5			
	Ordovician	D2	98.9			
3005	Ordovician	D2	84.4			
	Ordovician	D2	69.9			
	Ordovician	D2	69.1			
	Ordovician	D2	71.1			
3015	Ordovician	D2	74.8			
	Ordovician	D2	86.1			
	Ordovician	D2	88.3			
3127	Ordovician	D2	91.2			
	Ordovician	D2	95.5			
3127	Ordovician	D2	81.7			
	Ordovician	D2	93.2			
3005	Ordovician	D2	87.6			
	Ordovician	D2	70.1			
	Ordovician	D2	73.2			
3138	Ordovician	D2	75.6			
	Ordovician	D3	118.2	-28.5	25.0	
	Ordovician	D3	120.6	-24.5	23.5	
	Ordovician	D3	110.2	-25.3	23.8	
	Ordovician	D3	99.8			
	Ordovician	D3	98.5	-26.7	24.4	
3125	Ordovician	D3	105.7	-24.6	23.5	
	Ordovician	D3	102.1			
3125	Ordovician	D3	111.7	-24.9	23.7	
	Ordovician	D3	139.4	-25.4	23.9	
3125	Ordovician	D3	122.4			

Sample ID	Age	Mineral	Th °C	Tm °C	Salinity	Reference
3023	Ordovician	D3	109.5	-26.6	24.3	
	Ordovician	D3	107.1			
	Ordovician	D3	140.6			
3118	Ordovician	D3	117.8			
	Ordovician	D3	134.9	-25.6	23.9	
	Ordovician	D3	118.6	-26.2	24.2	
	Ordovician	D3	143.5	-24.2	23.4	
	Ordovician	D3	131.8	-27.1	24.5	
	Ordovician	D3	123.2	-26.9	24.4	
	Ordovician	D3	121.8			
	Ordovician	D3	123.7	-25.3	23.8	
	Ordovician	D3	141.7	-24.7	23.6	
	Ordovician	D3	138.3	-21.9	22.4	
	Ordovician	D3	122.3			
3119	Ordovician	D3	118.9			
	Ordovician	D3	126.9			
	Ordovician	D3	127.1	-23.1	22.9	
	Ordovician	D3	126.4	-24.7	23.6	
	Ordovician	D3	134.3			
	Ordovician	D3	130.4	-23.2	23.0	
	Ordovician	D3	119.9			
	Ordovician	D3	128.3			
3005	Ordovician	D3	96.7	-25	23.7	
	Ordovician	D3		-26.8	24.4	
3023	Ordovician	D3	135.1	-28.8	25.1	
	Ordovician	D3	114.5			
3139	Ordovician	D3	97.6	-28.7	25.1	
3015	Ordovician	C3	93.6			
	Ordovician	C3	91.4	-21.3	22.1	
	Ordovician	C3	88.7	-22.6	22.7	
	Ordovician	C3	87.3	-20.3	21.6	
	Ordovician	C3	69.7	-19.8	21.3	
	Ordovician	C3	92.3			
	Ordovician	C3	70.3	-22.1	22.5	
	Ordovician	C3		-20.2	21.5	
	Ordovician	C3	85.3			
	Ordovician	C3	103.5			
	Ordovician	C3	121.6			
	Ordovician	C3	76.1			
	Ordovician	C3	106.2			
	Ordovician	C3		-27.9	24.8	
	3125	Ordovician	C3	69.1	-19.8	21.3
Ordovician		C3	68.3	-20.5	21.7	
Ordovician		C3	70.9	-22.6	22.7	
Ordovician		C3	71.2	-19.1	21.0	
Ordovician		C3	70.5			
3013	Ordovician	C3	96.1	-22.7	22.7	
	Ordovician	C3	71.5			
	Ordovician	C3	99	-19.5	21.2	
	Ordovician	C3	71.9			
	Ordovician	C3		-20.4	21.6	
	Ordovician	C3	72.1			
	Ordovician	C3	115.1			
	Ordovician	C3	66.8	-18.5	20.6	
	Ordovician	C3		-25.6	23.9	
	Ordovician	C3	110.6	-18.8	20.8	

Sample ID	Age	Mineral	Th °C	Tm °C	Salinity	Reference
3138	Ordovician	C3	65.8	-20.6	21.7	
	Ordovician	C3	72	-19.2	21.0	
	Ordovician	C3	131.1	-22.9	22.8	
	Ordovician	C3	85.5			
	Ordovician	C3	60.2	-24.8	23.6	
	Ordovician	C3	74.7			
	Ordovician	C3	70.6			
	Ordovician	C3	70.2	-21.2	22.0	
	Ordovician	C3	74.5			
	Ordovician	C3	73.1	-23.1	22.9	
	Ordovician	C3	70.7	-21.4	22.1	
	Ordovician	C3	70.3			

Vita Auctoris

Omid Haeri-Ardakani was born in 1970 in Ardakan, Iran. He studied geology at the University of Tehran in Tehran, where he obtained his B.Sc. degree in geology in 1993. He completed his M.Sc. in sedimentology in 1997.

He worked for Iranian National Institute of Oceanography (INIO) from 1997 to 2004. He Joined Keyhan Exploration and Production Services (KEPS) in 2004 till 2007. In September 2007 he attended the University of Windsor in Canada, where he started his Ph.D. degree.